TUM School of Engineering and Design

Optimisation-based design of industrial chemical processes

Anna-Maria Ecker

Vollständiger Abdruck der von der TUM School of Engineering and Design der Technischen Universität München zur Erlangung des akademischen Grades einer

Doktorin der Ingenieurwissenschaften

genehmigten Dissertation.

Vorsitz: Prof. Dr.-Ing. Johannes Fottner

Prüfer der Dissertation:

1. Prof. Dr.-Ing. Harald Klein
2. Prof. Dr.-Ing. Mirko Skiborowski

Die Dissertation wurde am 28.06.2022 bei der Technischen Universität München eingereicht und durch die TUM School of Engineering and Design am 28.09.2022 angenommen.

This thesis originates from research performed by the author. Parts of section 2.4 and chapter 3 have already been published in:

> Ecker et al. 2019
> A.-M. Ecker, I. Thomas, M. Häfele, B. Wunderlich, A. Obermeier, J. Ferstl, H. Klein, A. Peschel:
> *Development of a new column shortcut model and its application in process optimisation*, Chemical Engineering Science 196: 538–551, 2019.

Parts of sections 2.1, 2.2, 2.3, 2.5, 2.6 and chapter 4 have already been published in:

> Ecker et al. 2022
> A.-M. Ecker, H. Klein, A. Peschel:
> *Systematic and efficient optimisation-based design of a process for CO_2 removal from natural gas*, Chemical Engineering Journal 445: 136178, 2022.

Preface

This thesis has been developed during my time as a doctoral candidate with the Linde GmbH (formerly Linde AG) in the Department for Research and Development for Processes of the Engineering Division.

I would like to personally thank my doctoral advisor Prof. Dr.-Ing. Harald Klein for his academic guidance and supervision of my work in the context of this thesis. Further, I would like to express my gratitude for preparing me for the world of industrial process engineering by providing many great in-depth courses during my Bachelor's and Master's studies. I would particularly like to thank Prof. Dr.-Ing. Mirko Skiborowski for taking over the examination of my dissertation.

A sincere 'thank you' goes to my mentor and Linde advisor Dr. Andreas Peschel for academic and personal guidance, for numerous fruitful discussions, and for always providing expert advice when needed. Andreas, I am looking forward to continuing working with you.

I would also like to express my gratitude to Dr. Johann Ferstl, previously Head of the Department for Research and Development for Processes, for letting me travel to multiple sites all over the world so that I was able to gain not just academic but also a very practical insight into plant design and operation.

Further, I am grateful for the support provided by the IT department for Process Design and Control, namely Dr. Martin Häfele, Dr. Ingo Thomas, Dr. Stephania Hokenmaier, Dr. Peter Bose, Dr. Johann-Günter Simon, Dr. Gerhard Lauermann, and Dr. Andreas Kröner. Thank you all for helping with occurring challenges during implementation and sharing your expertise with process simulation and optimisation.

A big 'thank you' goes to Christian Kunz, Michael Siebel, Florian Schliebitz, and Gerhard Zapp from the air separation product line for teaching me about the design and control of air separation units. Moreover, I very much appreciate the fruitful discussions about natural gas processes with Claudia Hugger, Martin Gwinner, and Dr. Heinz Bauer.

I would like to thank Dr. Bernd Wunderlich, Dr. Andreas Obermeier, and Dr. Simon Hill for the friendly and supportive atmosphere in our different shared offices. From the Institute of Plant and Process Technology, I would like to thank Dr. Fabian Höhler, Dr. Johannes Sundberg, and Robert Kender for collegial support with all kinds of things. I would also like to thank my students Andreas Senftl, Dr. Andreas Eschenbacher, and Gordon Hüllen for their great work.

Most importantly, I would like to thank my family for giving me my foundations for life and for their everlasting support.

Gary and Emilia, thank you not only for patiently supporting the development of this thesis. Cheers for everything! My love goes to both of you.

Abstract

Simultaneous optimisation of process structure and design variables is a powerful tool for process synthesis in early phases of development. However, the underlying optimisation problem is usually of large scale and high complexity for industrial processes. Thermodynamic phase equilibrium conditions are included in process models in substantial numbers but are strongly nonlinear making the optimisation problem harder to solve. In case integer variables, such as the number of column stages, are included as degrees of freedom in optimisation, a nonlinear programming optimisation problem is transformed into a harder to solve mixed integer nonlinear programming problem. The goal of this thesis is to facilitate simultaneous optimisation of process structure and design variables by developing robust and computationally efficient yet accurate reduced models.

To enable modelling of entire industrial processes, reduced models for distillation columns, absorption columns, membrane units, multi-stage compression units and multi-stage cooling units are developed. For distillation columns, a new shortcut model for integer-free optimisation of the number of column stages and feed or side draw locations is developed. It is based on the Edmister method and can be applied to any column setup. Hybrid surrogate models including physical equations as well as data information are proposed for an absorption and two distillation columns. The input/output correlation of the data information is approximated by a trained artificial neural network which is tranformed into a system of algebraic equations. Both the shortcut and the hybrid surrogate models for columns are based on aggregation of column stages into groups to reduce the number of equilibrium calculations. For a multi-stage compression unit, a shortcut model is proposed in which the number of compression stages is considered a continuous number enabling continuous space optimisation of the compressor outlet pressure. Further, a shortcut model for hollow-fibre membrane modules and a hybrid surrogate model for multi-stage cooling units are presented. Validation of the listed reduced models shows that they are all accurate, provide sufficient derivative information and are hence suited for gradient-based process optimisation.

In addition, a framework for systematic optimisation-based process design is introduced. It comprises an equation-oriented modelling environment including the developed reduced as well as more detailed models, a gradient-based nonlinear programming optimiser and a task bot for automated handling of process model initialisation, simulation, and optimisation.

The application of the newly developed shortcut model for distillation columns is demonstrated by designing a thermally coupled double column for separation of air into nitrogen and oxygen products based on process optimisation. The number of column stages in the high pressure column, side draw and feed locations of the low pressure column as well as further design variables such as split factors, pressures, and

temperatures are optimised simultaneously in a nonlinear programming problem using the new shortcut model. Optimisation is performed to show the trade-off between the plant's energy efficiency related to liquid oxygen production and the overall number of stages in the double column. Compared to classical nonlinear programming optimisation employing stage-to-stage column models, a two-step approach of optimisation with the new shortcut model and a stage-to-stage model leads to an over 2% better optimum, which is significant for air separation.

With a second example, systematic design of hybrid separation processes for removal of CO_2 from natural gas considering different combinations of distillation, membrane separation, and physical absorption is demonstrated. The influence of a wide range of CO_2 concentrations in the natural gas feed (40 mol% to 80 mol%) combined with varying limits for CO_2 concentrations in the natural gas product (from 3 mol% for pipeline transport to 50 ppm for LNG specification) on different process alternatives is investigated. For this purpose, the presented framework using different shortcut and hybrid surrogate models is applied for automated performance of an extensive series of optimisation calculations minimising operational energy requirements. As a result, an overview for identification which process topology is optimal for which combination of natural gas feed and natural gas product specifications is provided. For lower CO_2 contents in the natural gas feed of 40 mol-%, a process including cryogenic distillation and membrane separation is favourable. For large enough membrane areas, the order of the two separation operations is not critical. However, for higher CO_2 contents of 80 mol-%, it is favourable to separate CO_2 by cryogenic distillation first and obtain sweet natural gas by membrane separation second.

For both process examples, optimisation using the developed reduced models provides very similar results compared to optimisation using detailed models. It is shown that the reduced models and the presented framework enable a systematic and efficient approach to industrial process development by making simultaneous optimisation of process structure and design variables practical.

Kurzfassung

Simultane Optimierung von Prozessstruktur und Designvariablen ist ein leistungsfähiges Instrument für frühe Phasen der Prozessentwicklung. Allerdings ist das sich ergebende, der Optimierung zugrundeliegende mathematische Problem für industrielle Prozesse typischerweise großskalig und sehr komplex. So sind in Prozessmodellen vielfach enthaltene thermodynamische Gleichgewichtsbeziehungen stark nichtlinear und erschweren die Lösung des Optimierungsproblems. Falls ganzzahlige Variablen, wie z.B. Kolonnenstufenzahlen, als Freiheitsgrade im Optimierungsproblem berücksichtigt werden sollen, wird aus einem Nonlinear-Programming-Problem ein Mixed-Integer-Nonlinear-Programming-Problem, das schwerer zu lösen ist. Das Ziel der vorliegenden Arbeit ist es, die simultane Optimierung von Prozessstruktur und Designvariablen durch Entwicklung von robusten, effizienten, aber dennoch genauen reduzierten Modellen zu erleichtern.

Um ganze industrielle Prozesse modellieren zu können, werden reduzierte Modelle für Rektifikationskolonnen, Absorptionskolonnen, Membranmodule, mehrstufige Kompressoren und mehrstufige Kühlprozesse entwickelt. Für Rektifikationskolonnen wird ein neues Shortcut-Modell zur integer-freien Optimierung der Stufenzahlen und der Lage von Einspeise- oder Abzugsstufen entwickelt. Es basiert auf der Edmister-Methode und kann auf beliebige Kolonnenkonfigurationen angewendet werden. Darüber hinaus werden für Absorption und Rektifikation hybride Surrogat-Modelle, in denen physikalische Beziehungen mit Dateninformation kombiniert sind, vorgestellt. Die Input/Output-Korrelation der enthaltenen Dateninformation wird approximiert durch ein trainiertes künstliches neuronales Netz, das in ein System von algebraischen Gleichungen überführt wird. Im Shortcut-Modell und den hybriden Surrogat-Modellen für Kolonnen werden Kolonnenstufen in Segmenten aggregiert, um die Anzahl der Gleichgewichtsberechnungen zu reduzieren. Weiterhin wird ein Shortcut-Modell für mehrstufige Kompressoren eingeführt, das die Anzahl der Kompressorstufen als positive reelle Zahl berücksichtigt und so die schaltungsfreie Optimierung des Drucks am Kompressoraustritt ermöglicht. Für Hohlfaser-Membranmodule wird außerdem ein Shortcut-Modell und für mehrstufige Kühlprozesse ein hybrides Surrogat-Modell vorgestellt. Durch Validierung kann gezeigt werden, dass alle genannten reduzierten Modelle genaue Ergebnisse liefern, Ableitungszusammenhänge adäquat abbilden und daher für gradientenbasierte Prozessoptimierung geeignet sind.

Darüber hinaus wird ein Framework für systematisches optimierungsbasiertes Prozessdesign vorgestellt. Es besteht aus einer gleichungsbasierten Modellierungsumgebung, in der die entwickelten reduzierten sowie detailliertere Modelle zur Verfügung stehen, aus einem gradientenbasierten Nonlinear-Programming-Optimierer und aus einem Task-Bot. Der Task-Bot ermöglicht die Automatisierung von Modellinitialisierung, Simulation und Optimierung.

Das neue Shortcut-Modell für Kolonnen wird in einem Prozessbeispiel angewendet, in dem eine thermisch gekoppelte Doppelsäule für Zerlegung von Luft in Stickstoff- und Sauerstoffprodukte optimiert wird. Dabei werden die Anzahl der Kolonnenstufen in der Hochdrucksäule, Einspeise- und Abzugsstufen in der Niederdrucksäule und Prozessvariablen wie Splitfaktoren, Drücke und Temperaturen simultan und integer-frei mit Hilfe des neuen Shortcut-Modells optimiert. Die Optimierung ermöglicht eine Abwägung zwischen der energetischen Effizienz der Anlage im Bezug auf die Produktion von Flüssigsauerstoff und der Gesamtanzahl an Kolonnenstufen in der Doppelsäule. Im Vergleich zur klassischen Nonlinear-Programming-Optimierung mit Gleichgewichtsstufenmodellen liefert ein Zwei-Schritt-Ansatz zur Optimierung mit Hilfe des neuen Shortcut-Modells und eines Gleichgewichtsstufenmodells ein über 2% besseres Optimum, was für Luftzerlegung signifikant ist.

In einem zweiten Beispiel werden hybride Prozesse zur Abtrennung von CO_2 aus Erdgas systematisch synthetisiert. Als Trennoperationen werden unterschiedliche Kombinationen von Rektifikation, Membranabtrennung und Absorption berücksichtigt. Der Einfluss eines großen Bereichs von CO_2-Konzentrationen im Erdgas-Feed (40 mol% bis 80 mol%) zusammen mit variierenden Grenzwerten für CO_2-Konzentrationen im Erdgasprodukt (von 3 mol% für Pipelinetransport bis 50 ppm für LNG Spezifikation) auf unterschiedliche Prozessalternativen wird untersucht. Hierfür werden das vorgestellte Framework und unterschiedliche Shortcut- und Surrogat-Modelle verwendet, um eine umfangreiche Serie von Optimierungsberechnungen zur Minimierung des Energiebedarfs im Betrieb automatisiert durchzuführen. Als Ergebnis wird eine Übersicht erstellt, aus der hervorgeht, welche Prozesstopologie für welche Kombination aus Erdgaszufuhr- und Erdgasproduktspezifikationen optimal ist. Für niedrigere CO_2-Konzentrationen von 40 mol% im Erdgas-Feed ist eine Kombination aus kryogener Rektifikation und Membranabtrennung zu bevorzugen. Ist die Membranfläche groß genug, ist die Reihenfolge der beiden Trennoperationen unkritisch. Für höhere CO_2-Konzentrationen von 80 mol% ist jedoch die kryogene Rektifikation als erste Trennoperation günstiger.

Anhand beider Prozessbeispiele wird deutlich, dass die Optimierung mit Hilfe der neuen reduzierten Modelle im Vergleich zur Optimierung mit detaillierten Modellen sehr ähnliche Ergebnisse liefert. Es wird gezeigt, dass die reduzierten Modelle und das vorgestellte Framework systematische und effiziente optimierungsbasierte Entwicklung industrieller Prozesse ermöglichen und die simultane Optimierung von Prozessstruktur und Designvariablen deutlich erleichtern.

Contents

Nomenclature and abbreviations

Latin symbols

Symbol	Description	Unit
A	Area	m^2
Ae	Absorption factor	-
B	Estimation of Hessian matrix	-
b	Scalar for correction of performance factor	-
b_j	Bias for neuron j	-
c	Scalar for correction of performance factor	-
d_{inner}	Inner diameter	m
d_{outer}	Outer diameter	m
E	Error measure in backpropagation	-
f	Function	-
f_{SPL}	Split factor	$^{\text{mol}}/_{\text{mol}}$
$f(v_{\Sigma,j})$	Activation function	-
g	Inequality constraint	-
g_{a}	Active inequality constraint	-
$\dot{H}$	Enthalpy stream	W
$\Delta\dot{H}_{\text{err}}$	Error in energy balance	W
h	Equality constraint	-
i	Discrete counting variable	-
j	Discrete counting variable	-
K	Equilibrium ratio	-
k	Discrete counting variable	-
L	Lagrange function	-
L_{fibres}	Length of hollow fibres in membrane module	m
l	Discrete counting variable	-
$\dot{N}$	Molar flow	$^{\text{mol}}/_{\text{s}}$
n	Polytropic coefficient	-
n_{c}	Number of components	-
n_{cool}	Number of cooling stages	-
n_{cs}	Number of compression stages	-
n_{fibres}	Number of hollow fibres in membrane module	-
n_{fv}	Number of finite volumes	-

n_{out}	Number of output variables	-
n_{s}	Number of column stages	-
n_{DS}	Size of data set	-
n_{TDS}	Size of training data set	-
n_{EDS}	Size of evaluation data set	-
obj	Objective function	-
P	Power	W
P_i	Permeance of component i	$^{\text{mol}}/_{\text{sm}^2\text{bar}}$
P_{sh}	Shaft power	W
p	Pressure	bar
Δp_{s}	Pressure drop per column stage	bar
$\dot{Q}$	Heat flow	W
q	Constraint	-
R	Recovery	$^{\text{mol}}/_{\text{mol}}$
r	Actual compression ratio of one compression stage	$^{\text{bar}}/_{\text{bar}}$
r_{rf}	Reflux ratio	$^{\text{mol}}/_{\text{mol}}$
r_{rb}	Reboil ratio	$^{\text{mol}}/_{\text{mol}}$
S	Stripping factor	-
Se	Effective stripping factor	-
$\vec{s}$	Direction vector	-
T	Temperature	K
T_{CW}	Process temperature after cooling with cooling water	K
t	Counting variable for training epochs	-
t_∞	Number epochs at training end	-
u	Flow velocity	$^{\text{m}}/_{\text{s}}$
V	Volume	m^3
v	Specific volume	$^{\text{m}^3}/_{\text{kg}}$
$\vec{v}$	Vector in artificial neural network	-
$v_{\Sigma,j}$	Transfer function	-
vf	Vapour fraction	$^{\text{mol}}/_{\text{mol}}$
W	Work	J
$w_{i,j}$	Connection parameter / weights	-
w_x	Continuous optimisation variable	-
w_x^*	Optimal solution for continuous optimisation variable	-
w_y	Discrete optimisation variable	-
w_z	Optimisation variable	-

$w_{z\mathrm{b}}$	Basic optimisation variable	-
$w_{z\mathrm{n}}$	Non-basic optimisation variable	-
$w_{z\mathrm{s}}$	Super-basic optimisation variable	-
x	Component mole fraction in liquid phase	-
y	Component mole fraction in gaseous phase	-
z	z-coordinate	-
z_{c}	Compressibility	-
z_i	Mole fraction of component i in multi-phase mixture	-

Greek Symbols

Symbol	Description	Unit
α	Momentum	-
δ	Deviation	-
δ_{net}	Network error	-
ε	Small number	-
ζ	Ratio of heat flow to molar flow	$^{\mathrm{J}}/_{\mathrm{mol}}$
η_{adia}	Adiabatic efficiency	-
η_{is}	Isentropic efficiency	-
η	Learning rate	-
η_0	Learning rate at start of training	-
η_∞	Learning rate at end of training	-
η_{dec}	Learning rate decay	-
Θ	Membrane stage cut	$^{\mathrm{mol}}/_{\mathrm{mol}}$
κ	Isentropic coefficient	-
λ	Kuhn-Tucker multiplier	-
μ	Dynamic viscosity	$\mathrm{Pa} \cdot \mathrm{s}$
ν	Kuhn-Tucker multiplier	-
ξ	Split fraction, ratio of molar flows	-
Π	Product term	-
Σ	Progression term	-
φ	Fugacity coefficient	-
ϕ	Performance factor	-
ϕ^{corr}	Corrected performance factor	-

Superscripts

Index	Description
bub	At bubble point
dew	At dew point
F	Feed stream / side of membrane
L	Liquid
P	Permeate stream /side of membrane
R	Residue stream of membrane
S	Sweep stream of membrane
T	Transfer stream through membrane
V	Vapour

Subscripts

Index	Description
A	Based on absorption factors
abs	Absolute
av	Average
bot	Bottom of column segment
cond	Condensing
conti	Continuous
feed	Referring to the feed stream
in	Referring to inlet or input
is	Isentropic change of state
max	Maximum
min	Minimum
ms	Multi-stage
out	Referring to outlet or output
perm	Referring to the membrane permeate stream
PSA	Pressure swing adsorption
rel	Relative
rTSA	Rapid temperature swing adsorption
S	Based on stripping factors
subcool	Subcooled state
top	Top of column segment
TSA	Temperature swing adsorption

Constants

Symbol	Description and value
$\bar{R}$	Ideal gas constant $\bar{R} = 8.3145\,\frac{\mathrm{J}}{\mathrm{mol\,K}}$

Abbreviations

Abbreviation	Description
AEM	Adapted Edmister Model
AI	Artificial intelligence
ANN	Artificial neural network
BVM	Boundary value method
DEB	Dynamic equation block
GAN	Gaseous nitrogen
FUG	Fenske-Underwood-Gilliland
GM	Group methods
HYSU	Hybrid surrogate model
IP	Integer programming
IPN	Impure nitrogen
KKT	Karush-Kuhn-Tucker
LIN	Liquid nitrogen
LOX	Liquid oxygen
LP	Linear programming
MESH	Stage-to-stage column model based on material balances, equilibrium conditions, summation rules, and heat balances
MILP	Mixed integer linear programming
MINLP	Mixed integer nonlinear programming
ML	Machine learning
NG	Natural gas
NLP	Nonlinear programming
QP	Quadratic programming
RBM	Rectification body method
RG	Reduced gradient
RM	Reduced model
SEG	Segment
SEN	State equipment network
SQP	Successive quadratic programming
STN	State task network

TCA	Temperature collocation algorithm
USP	Upstream processing

1 Introduction

Process optimisation is a powerful tool to identify promising process alternatives in early phases of process development. In the context of this thesis, methods and models facilitating optimisation-based design of industrial chemical processes have been developed. The following introduction outlines the motivation, provides a brief theoretical background, and defines the scope of this thesis.

1.1 Motivation

Process synthesis in industrial process development often relies on sequential optimisation of process subsystems following the logic of the onion model by Smith & Linnhoff (1988) as shown in Figure 1.1. After the reactor is designed, a separation and recycle system, heat integration systems and needed utilities are determined layer by layer. Since previously designed subsystems are typically reconsidered after all subsystems are optimised, sequential optimisation practically is an iterative approach. It is time consuming and relies on engineering experience.

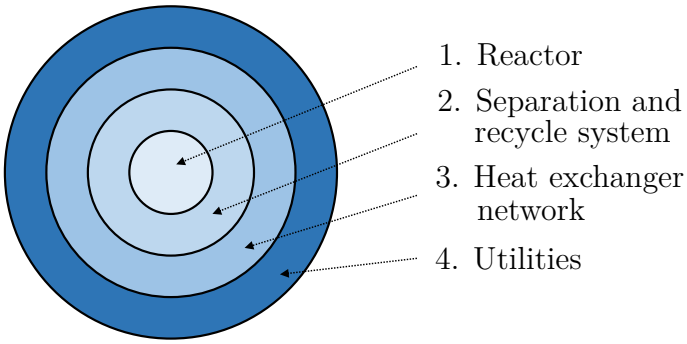

Figure 1.1: Onion model for process synthesis according to Smith & Linnhoff (1988).

Iterative subsystem optimisation is avoided by simulatenously optimising the reaction section, separation sequences, recycle and heat integration options as well as process design variables. Further, simultaneous optimisation of all process subsystems provides a better optimum than iterative sequential optimisation (Biegler et al. 1999). It is enabled by applying mathematical algorithms to optimise process flowsheets or superstructures. Process superstructures are subordinate flowsheets which consolidate different process alternatives in terms of different separation sequences combined with different recycle and heat integration options. Superstructure optimisation including process topology as well as process design variables as degrees of freedom is a systematic and practical approach to simultaneous optimisation.

However, industrial process optimisation usually results in large-scale optimisation problems which can become very complex. In addition, thermodynamic phase equilibrium conditions are essential in process modelling but also strongly nonlinear making the optimisation problem even harder to solve. In case integer variables, such as numbers of column stages, are included as degrees of freedom, a nonlinear programming (NLP) optimisation problem is transformed into a harder to solve mixed integer nonlinear programming (MINLP) optimisation problem. As a consequence, issues with convergence and long calculation times are likely to occur rendering simultaneous process optimisation difficult and time consuming.

The goal of this thesis is to facilitate simultaneous optimisation of process structure and design variables in the early phase of process development during which many process alternatives still need to be considered. Especially for industrial process development, problem scale and complexity have to be reduced to overcome the resulting high computational effort and probably occurring issues with convergence. A methodology for systematic and efficient process optimisation shall be developed. Further, a framework to implement the developed methodology shall be provided. The framework includes a set of newly developed reduced models for different unit operations which are used to reduce the complexity of underlying process optimisation problems. The reduced models are designed to overcome modelling challenges increasing model complexity such as a large number of thermodynamic equilibrium conditions and integer type degrees of freedom.

1.2 Background

After addressing basic terms and concepts with regard to model reduction, a brief introduction to process optimisation is given. Further, existing frameworks for optimisation-based process design are presented.

1.2.1 Terms and definitions: detailed and reduced models

Detailed models The term 'detailed models' refers to models for unit operations which consider physical effects in detail. In the context of this thesis, thermodynamic models for unit operations are referred to as detailed models, if they provide enough modelling detail to be used in equipment design. This typically applies to standard models for unit operations which are available in commerical simulation environments such as UniSim® Design or Linde OPTISIM® (Eich-Soellner et al. 1997). For example, a stage-to-stage column model with equations for mass and energy balances as well as thermodynamic equilibria on each stage is considered a detailed model. Models including CFD simulation or forces applied to equipment material, for example, are not considered in the context of this thesis. Detailed models are often referred to as 'rigorous models' in scientific literature (e. g., Caballero 2008, Beneke & Linninger 2011 and Dowling & Biegler 2015).

Reduced models The term 'reduced models' refers to models for unit operations which are reduced regarding the degree of modelling detail. Reduced models are classified in different ways in literature. Biegler (2017) distinguishes two general approaches to develop reduced models: data-driven model reduction which results in surrogate models and physics-based model reduction by applying simplified assumptions for physical phenomena. Reduced order modelling also includes systematic techniques such as multi-grid methods, i. e., dicretisation by finite differences, volumes, or elements.

The differentiation of white box, black box and grey box models is another common classification in systems and control theory (von Stosch et al. 2014). With white box models, the model's functional principles are comprehensible. With black box models, only the model's external behaviour is observed. Grey box models are a combination of white box and black box submodels.

In this thesis, 'reduced models' is the generic term for shortcut models, surrogate models and hybrid surrogate models. Figure 1.2 provides an overview over these three types of reduced models including their setup and advantages or disadvantages, respectively.

Reduced models		
Shortcut models (white box models)	**Hybrid surrogate models (grey box models)**	**Surrogate models (black box models)**
Based on physically substantiated assumptions applied to detailed models	Combination of shortcut models and surrogate models	Based on limited sets of data obtained from, e.g., calculations with detailed models, experiments, or plant operation
Include • Physical equations • Theoretically derived simplifications	Include • Physical equations • Theoretically derived simplifications • Approximated input/output correlations of data information	Include • Approximated input/output correlations of data information
Advantages / disadvantages • Valid for entire physical operating range of model • Offset between shortcut and detailed model to be expected	Advantages / disadvantages • Basic physical equations such as mass and energy balances are respected • Potential for higher accuracy than shortcut models • Limitation of operating range, extrapolation partially possible	Advantages / disadvantages • Potential for very high accuracy • Limitation to operating range covered by data set, extrapolation only with significant uncertainty

Figure 1.2: Overview over types of reduced models used in the context of this thesis.

Shortcut models are developed by applying physically substantiated assumptions and simplifications to detailed models. Therefore, shortcut models approximate a detailed model's output based on physical principles and theoretically derived simplifications.

Shortcut models – like detailed models – can also be called white box models. Surrogate models are based on limited sets of data which can be collected from calculations with detailed and computationally expensive models, from experiments, or from plant operation. Within surrogate models, the input/output correlation of the underlying data set is approximated. Physical principles are not applied. Surrogate models can also be called black box models. Hybrid surrogate models are reduced models which include physical equations as well as data set information. Hybrid surrogate models can also be called grey box models.

Shortcut models usually implicate a mismatch between modelling results and reality. By including data information in reduced models, accuracy can be enhanced. However, as a general rule, data-based models cannot be used to extrapolate the range of the included data. Surrogate or hybrid surrogate models are of advantage, if data is available or can be generated but mathematical models are difficult to develop (Fernandes 2006, Peer et al. 2008). Further, they are typically used to replace models which are too complex or simply not suited for the desired application (Pirrung et al. 2017). The input/output correlation of the included data information can be approximated, for example, by common fit functions such as polynomials, Kriging interpolation, artificial neural networks, or support vector regression.

1.2.2 Process optimisation

The objective of process optimisation is to minimise a function f with respect to certain degrees of freedom under the limitation of equality constraints h and inequality constraints g. The objective function often quantifies optimisation criteria such as energy requirements or cost. Maximising the objective function f is equivalent to minimising $-f$. Typical constraints are process or product specifications. Further, physical limits such as mass fraction values between zero and one must be respected. The objective function f is minimised by optimising selected degrees of freedom of the process. These degrees of freedom can be continuous optimisation variables w_x or discrete optimisation variables w_y.

Continuous variable optimisation problems If the optimisation problem only includes continuous optimisation variables, NLP problems are the most general case. If objective and constraints are differentiable and the optimisation problem is non-convex, NLP problems can have multiple local optima. Local and global optimisation methods are available in this case but global methods are far more computationally expensive. Convex NLP problems can be, for example, linear programming (LP) or quadratic programming (QP) problems. If objective or constraints are not differentiable, derivative-free optimisation methods are applied (Biegler 2014). Optimisation with continuous optimisation variables w_x is described by Biegler et al. (1999):

$$\min_{w_x} \quad f(w_x) \tag{1.1}$$
$$\text{s.t.} \quad g(w_x) \leq 0 \tag{1.2}$$
$$h(w_x) = 0 \tag{1.3}$$
$$w_x \in \mathbb{R}^{n_{w_x}}. \tag{1.4}$$

Mixed-integer variable optimisation problems Discrete optimisation variables are included in mixed-integer problems. MINLP, mixed-integer linear programming (MILP) and integer programming (IP) are distinguished. A general formulation of an optimisation problem with continuous and discrete optimisation variables w_x and w_y is (Biegler et al. 1999, Biegler et al. 2014):

$$\min_{w_x, w_y} \quad f(w_x, w_y) \tag{1.5}$$
$$\text{s.t.} \quad g(w_x, w_y) \leq 0 \tag{1.6}$$
$$h(w_x, w_y) = 0 \tag{1.7}$$
$$w_x \in \mathbb{R}^{n_{w_x}},\ w_y \in \{0,1\}^{n_{w_y}}. \tag{1.8}$$

Without loss of generality, discrete variables w_y are typically defined to represent binary values 0 and 1 (Biegler et al. 1999). Process systems engineering applications are often modelled using MINLP. MINLP problems can be solved, for instance, with NLP Branch and Bound, Generalised Benders Decomposition, Outer Approximation, or Generalised Disjunctive Programming approaches (Grossmann et al. 2005). MINLP problems are harder to solve than corresponding NLP problems since discrete variable sets have to be optimised in addition to handling nonlinear functions.

Local optimality conditions for NLP problems A common approach is to define the optimisation problem as a Lagrange function. The vectors ν and λ are known as dual variables, shadow prices, or Kuhn-Tucker multipliers (Kuhn & Tucker 1951):

$$L(w_x, \lambda, \nu) = f(w_x) + g(w_x)^{\mathrm{T}}\nu + h(w_x)^{\mathrm{T}}\lambda\ . \tag{1.9}$$

Based on the Lagrange function in eq. (1.9), the optimality conditions are established:

$$\text{Stationarity:} \quad \nabla L(w_x^*, \lambda, \nu) = \nabla f(w_x^*) + \nabla h(w_x^*)^{\mathrm{T}}\lambda + \nabla g(w_x^*)^{\mathrm{T}}\nu = 0 \tag{1.10}$$
$$\text{Feasibility:} \quad g(w_x^*) \leq 0,\ h(w_x^*) = 0 \tag{1.11}$$
$$\text{Complementarity:} \quad g(w_x^*)^{\mathrm{T}}\nu = 0,\ \nu \geq 0 \tag{1.12}$$
$$\text{Constr. qualific.:} \quad [\nabla g_{\mathrm{a}}(w_x^*) | \nabla h(w_x^*)] \text{ is matrix of full column rank} \tag{1.13}$$
$$\text{Curvature:} \quad \begin{aligned} &s^{\mathrm{T}}\nabla_{w_x w_x} L(w_x^*, \lambda, \nu) s \geq 0 \\ &\forall\ s \neq 0,\ \nabla h(w_x^*)^{\mathrm{T}} s = 0,\ \nabla g_{\mathrm{a}}(w_x^*)^{\mathrm{T}} s = 0. \end{aligned} \tag{1.14}$$

Eqs. (1.10) to (1.14) are referred to as Karush-Kuhn-Tucker (KKT) conditions (Karush 1939, Kuhn & Tucker 1951). They are used to identify local solutions. Eqs. (1.10) to (1.13) are first order conditions. They are necessary for optimality. At the optimal solution w_x^*, the gradient of the Lagrange function is zero and the constraints must be satisfied. Inequality constraints are either inactive ($g_i(w_x^*) < 0$) or active ($g_{\mathrm{a},i}(w_x^*) = 0$). In case constraint $g_i(w_x^*)$ is inactive, multiplier ν_i is zero so that the constraint is not relevant to the solution. In case $g_i(w_x^*)$ is active, multiplier ν_i can be positive. Constraint qualifications have to be met to satisfy the KKT conditions in local solutions w_x^*. A common constraint qualification is linear independence of the gradients of active constraints $g_{\mathrm{a},i}(w_x^*) = 0$ and $h_i(w_x^*) = 0$ (Biegler et al. 1999).

Eq. (1.14) is a second order condition. It is needed to confirm a minimum in w_x^*. Curvature is evaluated using the Hessian matrix of the Lagrange function $\nabla_{w_x w_x} L(w_x^*, \lambda, \nu)$. Positive curvature of the Lagrange function for all non-zero allowable directions s (positive definite Hessian with $s^{\mathrm{T}} \nabla_{w_x w_x} L(w_x^*, \lambda, \nu) s > 0$) is a sufficient condition for a minimum in w_x^*. Non-negative curvature of the Lagrange function for all non-zero allowable directions s (positive semidefinite Hessian with $s^{\mathrm{T}} \nabla_{w_x w_x} L(w_x^*, \lambda, \nu) s \geq 0$) is a necessary condition for a minimum in w_x^*. Non-zero allowable directions s for the optimisation variables are defined based on active constraints $\nabla h(w_x^*)^{\mathrm{T}} s = 0$ and $\nabla g_{\mathrm{a}}(w_x^*)^{\mathrm{T}} s = 0$. Some modern algorithms allow to calculate the Hessian. This is viable, especially if automatic differentiation engines are used (Kawajir & Laird 2015). Instead of calculating second order derivatives in process optimisation, the Hessian can be approximated (Biegler et al. 1999).

Solving NLP problems According to Biegler et al. (1999) and Biegler (2014), two major approaches to solve NLP problems are the reduced gradient (RG) method and successive quadratic programming (SQP). The principle of the RG method is solving a sequence of subproblems by partitioning optimisation variables into a set of super-basic variables $w_{z\mathrm{s}}$ driving the optimisation (between bounds), non-basic variables $w_{z\mathrm{n}}$ (fixed at their bounds) and basic variables $w_{z\mathrm{b}}$ (solved from equality constraints). By adding slack variables and redefining optimisation variables and constraints, the optimisation problem can reformulated (Biegler 2014):

$$\min_{w_z} \quad f(w_z) \tag{1.15}$$

$$\text{s.t.} \quad q(w_z) = 0 \tag{1.16}$$

$$w_{z,\min} \leq w_z \leq w_{z,\max} \tag{1.17}$$

$$w_z^{\mathrm{T}} = [w_{z\mathrm{s}}^{\mathrm{T}}, w_{z\mathrm{n}}^{\mathrm{T}}, w_{z\mathrm{b}}^{\mathrm{T}}]. \tag{1.18}$$

$w_{z\mathrm{b}}$ is solved for fixed values of $w_{z\mathrm{s}}$ and $w_{z\mathrm{n}}$ in each iteration. If the bounds of variables $w_{z\mathrm{b}}$ or $w_{z\mathrm{s}}$ are violated during iteration, variable partition is modified. RG methods are included in GRG2 (Lasdon & Waren 1981) and CONOPT codes (Drud 1994). Also, extended RG methods are used for large-scale reduced-space SQP algorithms in

SNOPT (Biegler 2014). In an SQP algorithm, a QP subproblem is solved in every iteration (Biegler et al. 1999):

$$\min_{w_x} \quad \nabla f(w_{x,k})^{\mathrm{T}} s + \frac{1}{2} s^{\mathrm{T}} B_k s \tag{1.19}$$

$$\text{s.t.} \quad g(w_{x,k}) + \nabla g(w_{x,k})^{\mathrm{T}} s \leq 0 \tag{1.20}$$

$$h(w_{x,k}) + \nabla h(w_{x,k})^{\mathrm{T}} s = 0. \tag{1.21}$$

$w_{x,k}$ is the current point, B_k is an estimation of the Hessian matrix $\nabla_{w_x w_x} L(w_{x,k}, \nu_k, \lambda_k)$ and s is a predicted search direction. Point $w_{x,k}$ can be infeasible. Hence, the successive point is determined by $w_{x,k} = w_{x,k+1} + \tau s$ and size τ is calculated so that the objective is improved, while the violation of constraints is reduced. With SQP algorithms, fast convergence is possible since solving the QP with the exact Hessian of the Lagrangian is equivalent to applying Newton's method to the KKT conditions (Biegler et al. 1999, Biegler 2014).

Process optimisation with reduced models For reduced models to be applicable in gradient-based process optimisation, they have to match results and derivative information of the corresponding detailed models to enable convergence to correct optimised solutions. The KKT conditions in the optimum must be similar for the reduced and the corresponding detailed model (Biegler et al. 2014).

1.2.3 Frameworks for optimisation-based process design

Different types of frameworks for optimisation-based process design can be found in literature. Some frameworks are focused on systematic modelling to simplify superstructure optimisation. Yeomans & Grossmann (1999) present a systematic modelling framework which is used to represent superstructures and mathematically derive process optimisation problems in three steps. First, the representation of the design alternatives is determined. Superstructures can be respresented by two complementary concepts for process systhesis: the state task network (STN) and the state equipment network (SEN). States are physical and chemical properties describing process streams. Tasks are physical and chemical transformations between cohesive states. Equipments are devices executing a specific task. Second, the STN or SEN is transferred to a mathematical programming problem by generalised disjunctive programming (Raman & Grossmann 1994) and, third, reformulated as an MILP or MINLP problem. The framework allows for systematic model derivation for process synthesis problems.

Another systematic superstructure representation method is presented by Proios et al. (2005). It is based on the principles of the generalised modular framework introduced by Papalexandri & Pistikopoulos (1996). Main elements are building blocks such as modules for simultaneous mass and heat transfer (e.g., column section) or pure heat transfer (e.g., cooler, heater). Further elements are structural sets providing structural information such as number and topology of building blocks, desired

products and available feeds. Structural constraints are binary variables which are mathematically modelling the superstructure problem. Once this method is implemented, superstructures can be generated systematically and automatically. Hence, the approach can be seen as a valid balance between rigorous and shortcut methods (Proios et al. 2005).

Biegler et al. (2014) introduce a multi-scale optimisation framework using reduced models as a substitute for detailed models. To ensure convergence of optimisation with the reduced model to the optimum of the detailed model, reduced and corresponding detailed models must be consistent. Further, optimisation with reduced models must include iterations providing sufficient improvement towards the optimum. Three trust region algorithms are part of the reduced model based optimisation framework. In the first algorithm, trust region problems are solved using reduced models, but function and gradient information from detailed models is required. In the second algorithm, derivative-free optimisaiton methods are used so that no gradient information is needed, but the detailed model still has to be evaluated in each iteration. By using reduced models, which are validated prior to optimisation and approximate the detailed model sufficiently, the third algorithm requires minimal recourse to the evaluation of the detailed model during optimisation.

Kossack et al. (2006), Marquardt et al. (2008) and Kraemer et al. (2009) present a systematic framework for separation sequence synthesis based on a three-step approach. First, flowsheets for different separation sequences are generated. Second, these flowsheets are evaluated using shortcut models. Feasibility checks are performed and promising process alternatives are identified. Third, an MINLP superstructure optimisation problem is solved using detailed models to determine the optimal process alternative. The shortcut results from the second step are used as a starting point, for initialisation and for bounding of optimisation variables in the MINLP optimisation with detailed models. Also, since a significant number of process alternatives can be eliminated after the second step, only a few optimisation runs are needed in the third step.

Dowling & Biegler (2015) present a framework for large-scale flowsheet optimisation. The framework is based on two principles. First, it is designed to be modular. Specific units (e.g., heat exchanger, flash drum) inherit model equations from generalised parent models (e.g., general heat exchanger, general thermodynamic equipment). This makes the framework easy to extend. Second, models are constructed from simple to complex meaning that a flowsheet is first optimised applying reduced models. The results from this first optimisation are used to initialise harder-to-solve optimisation with more detailed models.

While Kossack et al. (2006), Marquardt et al. (2008), Kraemer et al. (2009), and Dowling & Biegler (2015) apply shortcut models, hybrid surrogate models or surrogate models can also be used. Henao & Maravelias (2011) propose a superstructure-based optimisation strategy with hybrid surrogate models replacing detailed models for unit operations. Pirrung et al. (2017) use surrogate models

in a superstructure to optimise biopurification sequences including different forms of chromatography.

A framework for a hybrid approach to process optimisation has been developed by Sundberg et al. (2017). The process model, which is subjected to optimisation, can be set up in a sequential simulation environment. Sundberg et al. (2017) perform process optimisation combining a process model in Aspen HYSYS®, a reactor model in MATLAB® and an external MATLAB® optimiser. The framework is also applied by Cardella et al. (2017) who perform process optimisation with a process model in UniSim® Design which is coupled to an external MATLAB® optimiser.

1.3 Scope and content of the thesis

Scope The goal of this work is to facilitate simultaneous optimisation of process structure and design variables of industrial processes. For this purpose, a new framework for systematic optimisation-based process design is presented. As described in section 1.2.3, process optimisation can be simplified by applying systematic modelling methods for superstructure representation (Yeomans & Grossmann 1999, Raman & Grossmann 1994, Papalexandri & Pistikopoulos 1996, Proios et al. 2005) or by applying reduced models instead of detailed models once the superstructure or process model is available (Kossack et al. 2006, Marquardt et al. 2008, Kraemer et al. 2009, Biegler et al. 2014, Dowling & Biegler 2015). While systematic modelling is useful to identify possible process topologies, it does not focus on simplifying the optimisation process after a superstructure is available. For industrial applications, however, reducing the complexity of optimisation problems arising from available superstructures or process models is more critical. Hence, in agreement with Kossack et al. (2006), Marquardt et al. (2008), Kraemer et al. (2009), Biegler et al. (2014) and Dowling & Biegler (2015), the presented framework includes reduced models for unit operations to be used in process optimisation. New reduced models are developed. Further, in the developed reduced models, typical integer type design variables, such as the number of column stages, are considered as continuous variables so that MINLP optimisation is avoided and NLP optimisation can be performed, even if these variables are used as optimisation variables.

The new framework comprises an equation-oriented modelling environment with detailed models and the developed reduced models, a gradient-based NLP optimiser and a task bot for automated handling of process model initialisation, calculation, and optimisation. Since the process model, which is subjected to optimisation, and the optimiser exist in the same equation-oriented environment, a hybrid approach as presented by Sundberg et al. (2017) is not necessary.

Robust and computationally efficient reduced models, which are suited for gradient-based NLP optimisation, are provided. The developed reduced models include shortcut models for multi-stage compression units, distillation columns and membrane operations as well as hybrid surrogate models for multi-stage cooling units, distillation and

absorption columns. Combining these separation techniques allows for optimisation-based design of hybrid separation processes. Although the developed reduced models are extensively evaluated, accurate and provide sufficient derivative information to an NLP optimiser, subsequent optimisation using detailed models is beneficial to ensure results accuracy as required by industrial standards.

The framework is developed based on and for the Linde proprietary simulation and optimisation software OPTISIM® (Eich-Soellner et al. 1997) but can be implemented in any other equation-oriented modelling and optimisation environment. The proposed approach to process design is demonstrated by application to two industrial process examples: a double column for air separation and a hybrid separation process for removal of CO_2 from natural gas.

Content After a brief introduction regarding motivation, general background, scope and content of this thesis is provided, the developed reduced models for multi-stage cooling units, multi-stage compression units, membranes and columns are introduced in chapter 2. The current state of the art for the reduced models is outlined. Each reduced model is validated in comparison to a corresponding detailed model or experimental data. It is evaluated, whether the reduced model is accurate and whether it provides sufficient gradient information.

In chapter 3 and chapter 4, the proposed approach to optimisation-based process synthesis is demonstrated by application to two different industrial process examples. As a first process example, a thermally coupled double column for separation of air into nitrogen and oxygen products is designed. Feed and side draw locations of the double column as well as process variables such as pressures, temperatures and split factors are optimised simultaneously. Integer-free optimisation of the number of column stages is enabled by applying a new column shortcut model. As a second example, a process for removal of CO_2 from natural gas is synthesised. Depending on varying natural gas feed pressures, CO_2 contents and natural gas product purities, optimal hybrid separation sequences are determined. Shortcut models for multi-stage compression and membrane separation as well as hybrid surrogate models for multi-stage cooling, distillation and absorption are used for process optimisation. In chapter 5 a summary and a conclusion of the thesis as well as an outlook are outlined.

2 Modelling, model evaluation and optimisation framework

The newly developed reduced models for multi-stage compression units, multi-stage cooling units, membranes, and columns are introduced in this chapter. Literature overviews, modelling equations as well as validation results for the models are provided. Model reduction was performed with respect to three main guidelines:

1.) The number of equations introducing nonlinearties into the models, i.e., equations for equilibirum conditions, is reduced.

2.) Integer variables, i.e., the number of compression stages or the number of column stages, are included as continuous variables in the reduced models. This enables continuous space optimisation, even if compression and column stage numbers are considered optimised variables.

3.) Differential equations are transferred to integral algebraic forms.

For a reduced model to be applicable in process optimisation, the Karush-Kuhn-Tucker conditions have to be similar for the reduced and the corresponding detailed model (Biegler et al. 2014). Explicitly evaluating and comparing the KKT conditions is difficult. Hence, the reduced models are validated with respect to accuracy. Further, it is evaluated, if systematically varying independent model variables leads to similar changes in the results of reduced and detailed models as this indicates whether the models' derivative information is sufficient. General modelling specifications are given in Table A.1 in the appendix.

For model validation, relative deviations $\delta_{i,\mathrm{rel}}$ are defined by (exemplarily given for component molar flows):

$$\delta_{i,\mathrm{rel}} = \frac{\dot{N}_{i,\mathrm{reduced}} - \dot{N}_{i,\mathrm{detailed}}}{\dot{N}_{i,\mathrm{detailed}}}. \tag{2.1}$$

Further, relative component molar flows are defined by:

$$\dot{N}_{i,\mathrm{rel,detailed}} = \frac{\dot{N}_{i,\mathrm{detailed}}}{\dot{N}_{i,\mathrm{detailed,max}}} \tag{2.2}$$

$$\dot{N}_{i,\mathrm{rel,reduced}} = \frac{\dot{N}_{i,\mathrm{reduced}}}{\dot{N}_{i,\mathrm{detailed,max}}}. \tag{2.3}$$

2.1 Shortcut model for multi-stage compression units

A shortcut model for intercooled multi-stage compressors for use in gradient-based process optimisation has been developed.

2.1.1 Literature

As a starting point for the developed shortcut model, equations for multi-stage compressor sizing provided by Biegler et al. (1999) are used. Biegler et al. (1999) assume equal inlet temperatures for each compression stage. Within the context of this thesis, however, the multi-stage compression unit is used for cryogenic gases potentially making intercoolers partly unnecessary. Hence, the inlet temperatures for each compression stage are not equal in every case. In the context of his Master's Thesis, Eschenbacher (2016) has implemented a shortcut model based on the equations provided by Biegler et al. (1999). Extensions such as temperature corrections have not been considered.

2.1.2 Modelling

If a maximum compression ratio is exceeded, multi-stage compression is necessary. Figure 2.1 shows a multi-stage compression unit with intercooling. The cooling water operated intercoolers achieve an outlet temperature of T_{CW}. In case inlet temperature T_0 or the outlet temperature of the previous compression stage T_k is lower than T_{CW}, the intercooler is inactive with $\tilde{T}_0 = T_0$ or $\tilde{T}_k = T_k$, respectively. The intercooler is active, if $T_0 > T_{\mathrm{CW}}$ or $T_k > T_{\mathrm{CW}}$ so that $\tilde{T}_0 = T_{\mathrm{CW}}$ or $\tilde{T}_k = T_{\mathrm{CW}}$. Pressure drops of intercoolers are neglected leading to $\tilde{p}_k = p_k \; \forall k = 0, ..., n_{\mathrm{cs}}$.

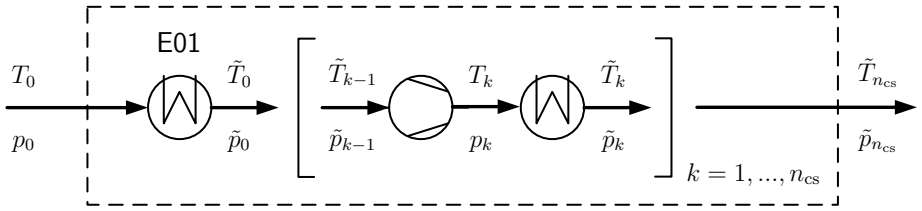

Figure 2.1: Layout of multi-stage compression shortcut model with intercooling.

The number of compression stages n_{cs} in a multi-stage compressor depends on the overall compression ratio and varies during optimisation. As continuous space optimisation of the outlet pressure shall be enabled, the number of compression stages is included as a continuous number in the developed shortcut model. In general, the change of state is defined by:

$$p \cdot v^n = \text{const.} \tag{2.4}$$

Depending on an inlet pressure p_{in} and an outlet pressure p_{out}, compression work defined by:

$$W = \int_{p_{\text{in}}}^{p_{\text{out}}} V dp \ . \tag{2.5}$$

In Figure 2.2, the compression work is equal to the area below the different plots. Isentropic compression with $n = \kappa$ requires maximum and isothermal compression minimum work. Isothermal compression would imply heat removal during compression, which is not realistic. Isentropic compression is assumed for the multi-stage compression unit. Intercoolers reduce the overall compression work for multi-stage compression.

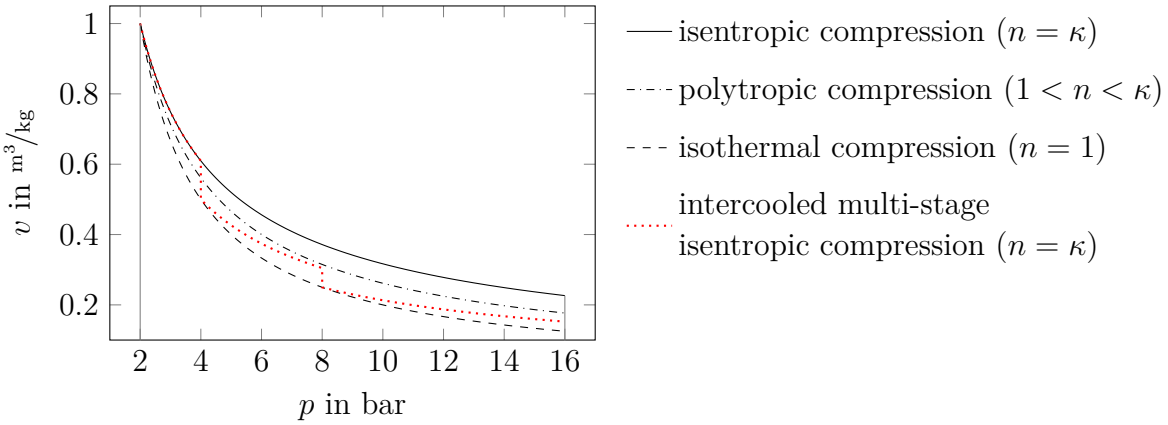

Figure 2.2: Exemplary plot for single-stage and multi-stage air compression from $p_{\text{in}} = 2\,\text{bar}$ to $p_{\text{out}} = 16\,\text{bar}$.

For multi-stage compressors with a certain number of compression stages, minimum work occurs for equal compression ratios (Biegler et al. 1999). Hence, equal compression ratios are assumed. While Seider et al. (2004) recommend a maximum compression ratio per stage of 4, Biegler et al. (1999) suggest 2.5. The latter is preferred because it relates to a lower compression effort.

$$\frac{p_1}{p_0} = \frac{p_2}{p_1} = \cdots = \frac{p_{n_{\text{cs}}}}{p_{n_{\text{cs}}-1}} = \left(\frac{p_{n_{\text{cs}}}}{p_0}\right)^{\frac{1}{n_{\text{cs}}}} \leq 2.5 \tag{2.6}$$

$$\left(\frac{p_{n_{\text{cs}}}}{p_0}\right)^{\frac{1}{n_{\text{cs,conti}}}} = 2.5 \tag{2.7}$$

The number of compression stages $n_{\text{cs,conti}}$ is a continuous number. Rounding up to the next integer provides the number of compression stages n_{cs}. The actual compression ratio per stage r is determined using n_{cs}:

$$\left(\frac{p_{n_{\text{cs}}}}{p_0}\right)^{\frac{1}{n_{\text{cs}}}} = r. \tag{2.8}$$

According to Couper et al. (2010), the required compression work for a compression stage k is calculated by:

$$W_k = \frac{\dot{N} \cdot z_c \cdot \bar{R}}{\eta_{is}} \cdot \frac{\kappa_k}{\kappa_k - 1} \cdot \tilde{T}_{k-1} \cdot \left(r^{\frac{\kappa_k - 1}{\kappa_k}} - 1 \right). \tag{2.9}$$

The compressor outlet temperatures T_k can be determined assuming compression as an isentropic change of state for ideal gases:

$$T_k = \tilde{T}_{k-1} \cdot r^{\frac{\kappa_k - 1}{\kappa_k}}. \tag{2.10}$$

However, due to $\eta_{is} < 1$, the compressor outlet temperatures T_k are higher than considered by an isentropic change of state. Carroll (2010), for example, includes the isentropic efficiency:

$$T_k = \tilde{T}_{k-1} \cdot r^{\frac{\kappa_k - 1}{\kappa_k \cdot \eta_{is}}}. \tag{2.11}$$

Considering compression of natural gas, eq. (2.11) was found to be inaccurate. The approach given in eqs. (2.12) to (2.14) is better suited. It is provided by Couper et al. (2010) and is used in the developed multi-stage compression module:

$$\Delta T_{actual} = T_k - \tilde{T}_{k-1} = \Delta T_{is} \cdot \frac{1}{\eta_{is}} \tag{2.12}$$

$$T_k = \tilde{T}_{k-1} + \frac{\Delta T_{is}}{\eta_{is}} \tag{2.13}$$

$$T_k = \tilde{T}_{k-1} \left(1 + \frac{1}{\eta_{is}} \left(\left(\frac{p_k}{p_{k-1}} \right)^{\frac{\kappa_k - 1}{\kappa_k}} - 1 \right) \right). \tag{2.14}$$

Depending on the specified inlet and outlet pressures, the shortcut model provides results for outlet temperature $T_{out} = \tilde{T}_{n_{cs}}$ and the compression work for the whole unit. In the following, shaft power requirements P_{sh} of units are considered.

$$P_{sh,sum} = W_{sum} = \sum_{k=1}^{n_{cs}} W_k. \tag{2.15}$$

2.1.3 Validation

The multi-stage compression shortcut model as shown in Figure 2.1 and described in section 2.1.2 is compared to a detailed multi-stage compression unit. The detailed unit is modelled in UniSim® Design using the available compressor and cooler models. The

compression ratios of the compression stages are equal. A natural gas stream at 2 bar is compressed to varying pressures p_{out}. The natural gas stream is specified by:

$$p_{\text{in}} = 2\,\text{bar},\ T_{\text{in}} = T_{\text{in}}^{\text{dew}},\ \dot{N}_{\text{in,N}_2} = 10\,\text{mol/s},\ \dot{N}_{\text{in,CO}_2} = 20\,\text{mol/s},$$
$$\dot{N}_{\text{in,CH}_4} = 60\,\text{mol/s},\ \dot{N}_{\text{in,C}_2\text{H}_6} = 5\,\text{mol/s},\ \dot{N}_{\text{in,C}_3\text{H}_8} = 5\,\text{mol/s}.$$

The outlet temperature of the cooling water intercoolers is assumed with $T_{\text{CW}} = 313.15\,\text{K}$. Pressure drops in the intercoolers are neglected. The maximum compression ratio is defined by $\left(\frac{p_{\text{out}}}{p_{\text{in}}}\right)^{\frac{1}{n_{\text{CS}}}} = \left(\frac{p_{n_{\text{CS}}}}{p_0}\right)^{\frac{1}{n_{\text{CS}}}} \leq 2.5$. The isentropic compressor efficiencies are $\eta_{\text{is}} = 0.8$. The required shaft power $P_{\text{sh,sum}}$ and the outlet temperature T_{out} of the multi-stage compression unit are important variables in process optimisation. In Figure 2.3, they are plotted for varying outlet pressures p_{out}.

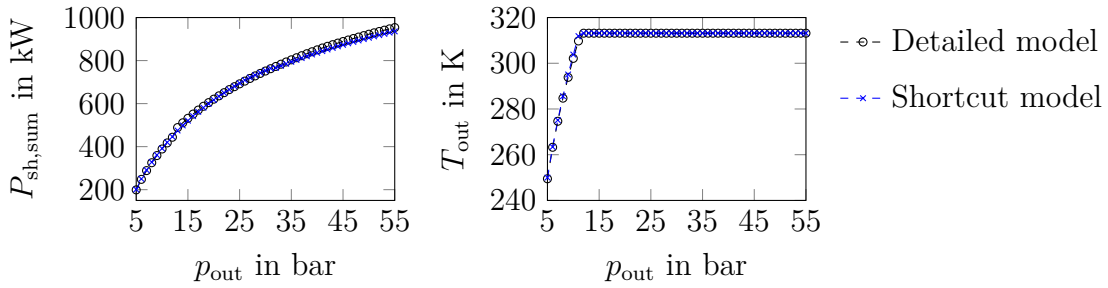

Figure 2.3: Shaft power $P_{\text{sh,sum}}$ and outlet temperature T_{out} of the multi-stage compression unit depending on the specified outlet pressure p_{out}.

The shortcut model is very accurate for an outlet pressure range of $5\,\text{bar} \leq p_{\text{out}} \leq 55\,\text{bar}$. This is equivalent to a multi-stage compressor with one stage to four stages. The outlet temperature T_{out} remains constant for $p_{\text{out}} > 11\,\text{bar}$ since the last compression stage is followed by a cooling water cooler. Relative deviations δ_{rel} are between -2.8% and 1.0%. The correct dependence between the varied outlet pressure p_{out} (independent variable), the required shaft power $P_{\text{sh,sum}}$ and the outlet temperature T_{out} (dependent variables) suggests that the shortcut model provides sufficient derivative information and can be applied in gradient-based process optimisation.

2.2 Hybrid surrogate model for multi-stage cooling unit

A hybrid surrogate model for multi-stage cooling units for use in process optimisation is developed. The model includes coolers at different temperature levels. Since compression work is needed for refrigeration, the cooling duties of the single coolers can be converted to shaft power by a fit function which is derived from simulation of a CO_2 refrigeration system.

2.2.1 Literature

Refrigeration systems are important elements of cryogenic processes. The compressors in refrigeration systems can cause high capital and operating cost. Systematic procedures and frameworks are proposed for the synthesis and design of integrated cascade refrigeration systems. Different approaches to superstructure modelling including different design alternatives and optimisation problem formulations are possible. Shelton & Grossmann (1986) propose an MILP model approach. Colmenares & Seider (1989) propose an NLP model for refrigeration system synthesis and simultaneous selection of alternative refrigerants. Vaidyaraman & Maranas (1999) and Wu & Zhu (2002) propose MINLP models which can be relaxed to MILP models. Zhang & Xu (2011) propose a framework based on an MINLP model.

These publications share the goal to provide a methodology for determining key design specifications concerning optimal refrigeration cycle topology as well as optimal operating conditions and refrigerants. In particular, the number of cooling stages, their temperature levels, and participating refrigerants are determined. Optimisation objectives are mostly aimed at minimising capital and operating cost caused by compressors. Zhang & Xu (2011) include exergies in the objective function to maximise energy efficiency. However, the before mentioned publications are based on detailed modelling approaches.

Shortcut or surrogate models for the design of refrigeration systems for cryogenic processes are difficult to find in literature. Shelton & Grossmann (1985) propose a shortcut model which is expressed in terms of temperature and can be evaluated with saturated refrigerant data only. Further, they introduce the coefficient of performance as the quotient of evaporator duty and power requirement. Biegler et al. (1999) also provide shortcut equations for multi-stage refrigeration systems. They assume equal coefficients of performance for each cooling stage as well as equal temperature differences between the cooling stages to estimate power requirements. In the context of his Master's Thesis, Eschenbacher (2016) has implemented a reduced model for a multi-stage refrigerant cycle which correlates the dissipated heat, the required shaft power of the refrigerant cycle and the refrigerant temperature levels.

2.2.2 Modelling

Refrigeration cycle The multi-stage cooling unit is based on a five-stage CO_2 refrigeration cycle as shown in Figure 2.4. It is assumed that a process side temperature of $T_{CW} = 30\,°C$ can be achieved with available cooling water at 20 °C. The refrigeration cycle is necessary, if process stream cooling below $T_{CW} = 30\,°C$ is needed. The multi-stage cooling unit is used for optimisation-based process design of a natural gas sweeting process. CO_2 is chosen as a refrigerant because it is separated from sour natural gas within the sweetening process and is therefore available in large quantities on site.

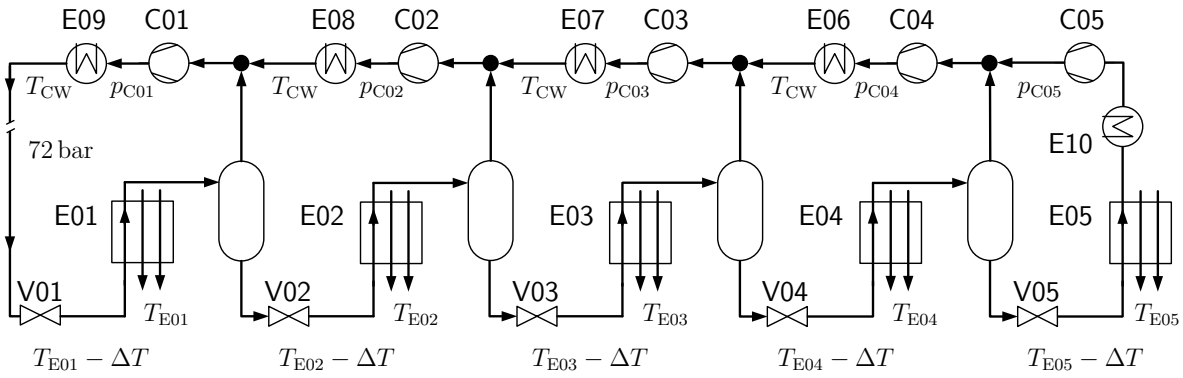

Figure 2.4: Carbon dioxide refrigeration cycle for multi-stage cooling unit.

Upstream of the first cooling stage, CO_2 is assumed to be just below the critical point: $T_{CW} = 303.15\,\mathrm{K}$ and $p_{CO_2} = 72\,\mathrm{bar}$. The cooling temperatures on the process side are assumed with

$$T_{E01} = 296.15\,\mathrm{K} \tag{2.16}$$
$$T_{E02} = 276.15\,\mathrm{K} \tag{2.17}$$
$$T_{E03} = 256.15\,\mathrm{K} \tag{2.18}$$
$$T_{E04} = 236.15\,\mathrm{K} \tag{2.19}$$
$$T_{E05} = 221.15\,\mathrm{K}. \tag{2.20}$$

The corresponding refrigerant temperatures are assumed to be 3 K colder. CO_2 pressures p_{C01} to p_{C05} are determined so that the refrigerant temperatures $T_{E01} - 3\,\mathrm{K}$ to $T_{E05} - 3\,\mathrm{K}$ are achieved. Expansion in valves V01 to V05 leads to cooling but also to higher vapour fractions and hence increases the shaft power consumption of compressors C01 to C05. Cooling water coolers E06 to E10 are only active, if their inlet streams are above temperature T_{CW}.

Hybrid surrogate model for refrigeration cycles For the purpose of process optimisation, the five stage CO_2 refrigeration cycle in Figure 2.4 is reduced to a hybrid surrogate model. A scheme for the hybrid surrogate model is given in Figure 2.5. Figure 2.4 refers to the CO_2 refrigerant side, while Figure 2.5 refers to the process side.

The hybrid surrogate model comprises a flowsheet as shown in Figure 2.5, in which temperatures T_0 to T_5 are determined depending on the given inlet temperature T_{in} and the specified outlet temperature T_{out}. Corresponding cooling duties of the single heat exchangers are calculated:

$$T_k = \begin{cases} T_{E0k} & T_{in} \geq T_{E0k} \wedge T_{out} \leq T_{E0k} \\ T_{out} & T_{in} \geq T_{E0k} \wedge T_{out} > T_{E0k} \\ T_{in} & T_{in} < T_{E0k} \end{cases} \qquad \text{for } \; k = 0, ..., 5. \tag{2.21}$$

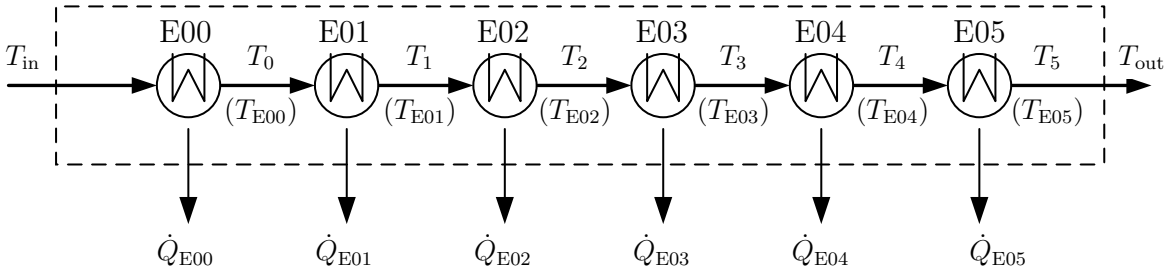

Figure 2.5: Layout of the hybrid surrogate model for the multi-stage cooling unit (process side).

The first heat exchanger E00 in the hybrid surrogate model is a cooling water cooler with $T_{\text{E00}} = T_{\text{CW}}$ which is only active, if $T_{\text{in}} > T_{\text{CW}}$. Heat exchangers E01 to E05 cool the process stream to temperature levels T_{E01} to T_{E05} or T_{out}. If the inlet and outlet temperature of one heat exchanger are equal, the heat exchanger is inactive and the pressure drop is set to zero. Otherwise, the heat exchanger is active and a pressure drop of 0.1 bar is assumed.

In the hybrid surrogate, the duty of each cooling stage is converted to shaft power. This is possible using a correlation between temperature $T_{\text{E0}k}$, cooling duty $\dot{Q}_{\text{E0}k}$ and required shaft power $P_{\text{sh,E0}k}$. In analogy to Figure 2.4 and Figure 2.5, a nine stage refrigeration cycle is also considered. The temperature stages on the process side are arranged from 296.15 K to 226.15 K in steps of 10 K. 221.15 K is the lowest possible temperature.

Nine stages $\left(\text{for } P_{\text{sh,E0}k},\ \dot{Q}_{\text{E0}k} \text{ in W and } T_{\text{E0}k} \text{ in K}\right)$:

$$P_{\text{sh,E0}k} = \dot{Q}_{\text{E0}k}\left(2.7937 \cdot 10^{-5} \cdot (T_{\text{E0}k} - 3\,\text{K})^2 - 2.1096 \cdot 10^{-2} \cdot (T_{\text{E0}k} - 3\,\text{K}) + 4.0360\right) \quad \text{for } k = 1, ..., 9. \tag{2.22}$$

Five stages $\left(\text{for } P_{\text{sh,E0}k},\ \dot{Q}_{\text{E0}k} \text{ in W and } T_{\text{E0}k} \text{ in K}\right)$:

$$P_{\text{sh,E0}k} = \dot{Q}_{\text{E0}k}\left(2.8842 \cdot 10^{-5} \cdot (T_{\text{E0}k} - 3\,\text{K})^2 - 2.1941 \cdot 10^{-2} \cdot (T_{\text{E0}k} - 3\,\text{K}) + 4.2066\right) \quad \text{for } k = 1, ..., 5. \tag{2.23}$$

For a five-stage refrigerant cycle, the shaft power equivalent to a specified cooling task is calculated as given in eq. (2.24):

$$P_{\text{sh,sum}} = \sum_{k=1}^{5} P_{\text{sh,E0}k}. \tag{2.24}$$

The duty for cooling water cooling is not included. The correlations in eqs. (2.22) and (2.23) are fit functions. Figure 2.6 is determined by case studies with a CO_2 refrigeration cycle as shown in Figure 2.4. In these case studies, heat exchangers E01 to E05 in Figure 2.4 are assumed as heaters. This is equivalent to cooling on the process side. The heaters of the cooling stages are only defined to introduce a heat flow of 100 kW into the CO_2 system:

$$\dot{Q}_{\mathrm{E0}k} = 100\,\mathrm{kW} \qquad \text{for } k = 1, 2, ..., n_{\mathrm{cool}} \tag{2.25}$$

$$\Delta p_{\mathrm{E0}k} = 0.1\,\mathrm{bar} \qquad \text{for } k = 1, 2, ..., n_{\mathrm{cool}} \tag{2.26}$$

$$\dot{Q}_{\mathrm{E0}j} = 0 \qquad \text{for } j = \{1, 2, ..., n_{\mathrm{cool}}\} \setminus \{k\} \tag{2.27}$$

$$\Delta p_{\mathrm{E0}j} = 0 \qquad \text{for } j = \{1, 2, ..., n_{\mathrm{cool}}\} \setminus \{k\} \tag{2.28}$$

$$P_{\mathrm{sh,sum}} = \sum_{k=1}^{n_{\mathrm{cool}}} P_{\mathrm{C0}k}. \tag{2.29}$$

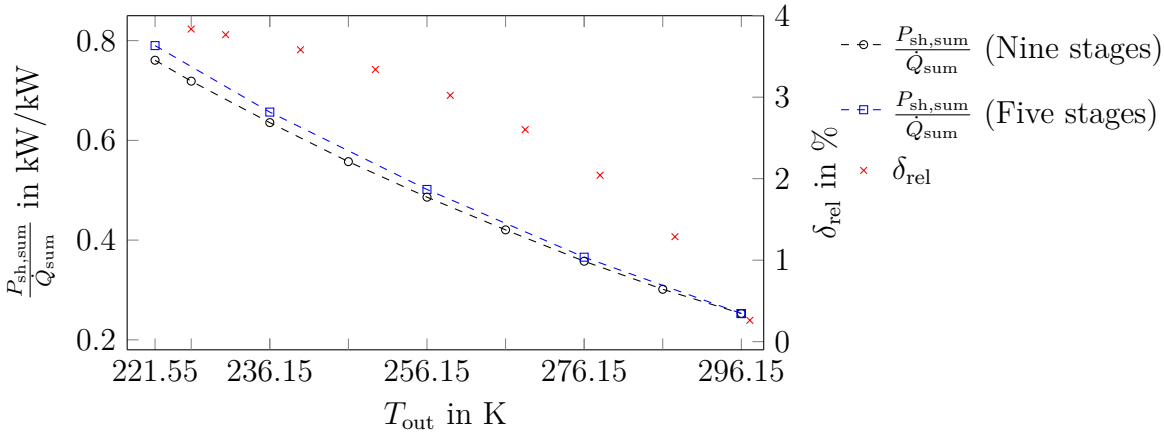

Figure 2.6: Required shaft power $P_{\mathrm{sh,sum}}$ in relation to cooling duty $\dot{Q}_{\mathrm{sum}}$ depending on the specified process temperature T_{out}.

According to Figure 2.6, the ratio $\frac{P_{\mathrm{sh,sum}}}{\dot{Q}_{\mathrm{sum}}}$ for a nine-stage refrigeration cycle is lower compared to a five-stage refrigeration cycle. The relative difference δ_{rel} for $\frac{P_{\mathrm{sh,sum}}}{\dot{Q}_{\mathrm{sum}}}$ between a nine-stage and five-stage cycle increases for lower cooling temperatures does not exceed $\delta_{\mathrm{rel}} = 4\%$. Since four additional compression stages causing captial investment cost are necessary for a nine-stage cycle, the five-stage cycle is chosen for optimisation-based process design in chapter 4.

2.2.3 Validation

The five-stage hybrid surrogate model is evaluated in comparison to the detailed model as shown in Figure 2.4. A sour natural gas process stream is cooled to varying temperatures T_{out}. The stream is specified by:

$$T_{\text{in}} = 303.15\,\text{K},\ p_{\text{in}} = 40\,\text{bar},\ \dot{N}_{\text{in,N}_2} = 0.5\,\text{mol/s},\ \dot{N}_{\text{in,CO}_2} = 2.0\,\text{mol/s},$$
$$\dot{N}_{\text{in,CH}_4} = 6.0\,\text{mol/s},\ \dot{N}_{\text{in,C}_2\text{H}_6} = 1.0\,\text{mol/s},\ \dot{N}_{\text{in,C}_3\text{H}_8} = 0.5\,\text{mol/s}.$$

Using the detailed model, the molar flow of CO_2 refrigerant $\dot{N}_{\text{CO}_2}$ is adjusted so that a minimum delta temperature in the heat exchangers is respected. The evaluation results are plotted in Figure 2.7.

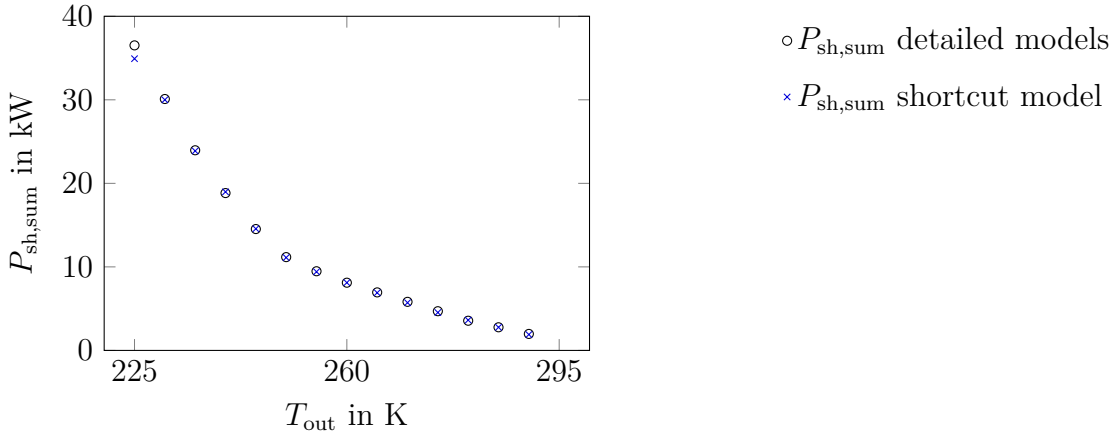

Figure 2.7: Required shaft power $P_{\text{sh,sum}}$ for cooling one process stream from 303.15 K to T_{out} in a five stage CO_2 refrigeration cycle.

The shaft power needed for cooling the sour natural gas stream from $T_{\text{in}} = 303.15\,\text{K}$ to T_{out} is similar for the detailed and the hybrid surrogate model. Relative deviations between detailed and hybrid surrogate model shaft power vary between -3% and 4%. The accurate relation between shaft power $P_{\text{sh,sum}}$ (dependent variable) and T_{out} (independent variable) shows that the hybrid surrogate model provides sufficient derivative information and is hence applicable in process optimisation.

2.3 Shortcut model for membranes

A shortcut model for counterflow hollow fibre membrane modules, which can be used in process optimisaton, is presented.

2.3.1 Literature

An overview over different types of membrane modules, flow patterns and membrane models in literature is provided.

Types of membrane modules Without considering construction details, membrane modules can be divided into two classes and six module types according to Melin & Rautenbach (2004):

- flat-sheet membranes: plate-and-frame modules, pillow modules, spiral-wound modules;
- tubular membranes: tube modules, capillary modules, hollow fibre modules.

The module types are listed in order of increasing area to volume ratio. Hence, spiral-wound and hollow fibre membrane modules are most relevant for industrial purposes. In spiral-wound membrane modules, a spacer with permeate flow channels is enclosed between two flat membrane sheets which are sealed on three edges. Several combined flat sheets with spacers are attached to a slotted mandrel with their open side and rolled around the mandrel forming a spiral arrangement which is placed in a pressure vessel. The feed gas is passed axially through the gaps created by the spacers between the spiraled membrane sheets. The permeate passes the spiral permeate channels to the mandrel collection pipe (Stookey 2006).

Hollow fibre membrane modules are fibre bundels in a shell with tubesheets to separate the feed and the permeate stream. High pressure feed gases are usually passed to the shell side of a hollow fibre module, the permeate is withdrawn at the open end of the fibre tube sheet (Pan 1986, Kovvali et al. 1994). However, significant pressure drops of the permeate stream in the fibres have to be considered. Since the membrane selectivity depends on the ratio of feed to permeate pressure, lower pressure drops on the permeate side are often favourable with gas permeation. In case of moderate feed pressures ($< 15\,\text{bar}$), the feed gas is passed through the fibres. Then, the permeate stream pressure drop on the shell-side of the hollow fibre module is negligible (Melin & Rautenbach 2004).

While hollow fibre modules realise larger membrane areas in compact module sizes, flat sheet membranes in spiral-wound modules show higher permeances in general (Baker & Lokhandwala 2008). Further, hollow fibre modules enable sustantially higher operating pressures and higher pressure differences between the feed and the permeate side of the membrane (Stookey 2006).

Commercial membrane units for CO_2 separation from natural gas An overview over companies selling membrane technology with commercial module types and commercial materials is given in Table 2.1. Cellulose acetate membranes are widely used to separate CO_2 from natural gas. They are challenged by newer materials such as polyimide membranes and perfluoro polymer membranes. For natural gas separation

applications, membranes are produced as hollow fibre modules or flat sheets packaged as spiral-wound modules (Baker & Lokhandwala 2008).

Table 2.1: Suppliers of membrane technology to separate CO_2 from natural gas (partly taken from Baker & Lokhandwala (2008) and Maqsood et al. (2014))

Company	Membrane module type	Membrane material
Air Liquide Medal	hollow fibre	polyimide
W.R. Grace	spiral-wound	cellulose acetate
Honeywell UOP Separex	spiral-wound	cellulose acetate
NATCO Cynara	hollow fibre	cellulose acetate
ABB/MTR	spiral-wound	perfluoro polymers silicone rubber
Linde/Evonik	hollow fibre	Sepuran®

Membrane flow patterns While mass balances and basic transport equations are similar in membrane models, the assumed membrane flow patterns determine the definition of the model's boundary values. Several idealised membrane flow patterns can be found in literature. Figure 2.8 shows five flow patterns which are theoretically possible according to Melin & Rautenbach (2004): co-current, counter-current, cross flow, free permeate flow, and complete mixing.

The feed stream is assumed to be in plug flow in case of co-current, counter-current, cross flow, and free permeate flow. The permeate side is in plug flow in case of co-current and counter-current. Ideal cross flow is characterised by the permeate stream flowing in a collinear direction to the membrane, while free permeate flow means that the permeate stream is withdrawn in a normal direction to the membrane. In literature, free permeate flow is often referred to as cross flow (e.g., Geankoplis 2003, Bounaceur et al. 2006). Some flow patterns are determined by the membrane module type. In spiral-wound membrane modules, cross flow is the governing flow pattern. With other module types, the flow pattern can be chosen. Hollow fibre membrane modules, for example, can be operated in co-current, counter-current, or cross flow (Melin & Rautenbach 2004, Stookey 2006).

Membrane models in literature In the context of this work, a shortcut model for hollow fibre membrane modules is implemented. In contrast to more detailed modelling approaches, detailed information about membrane module geometries is not needed in most shortcut models (Pettersen & Lien 1994). Several mathematical models describing separation of multi-component mixtures in hollow fibre membrane modules are available in literature.

In most publications, the rates of permeation are assumed to obey Fick's law. Fick's law is applied in its differential form (Pan 1986), in an integrated form (Shindo et al. 1985), or in the form of a logarithmic mean driving force (Pettersen & Lien 1994).

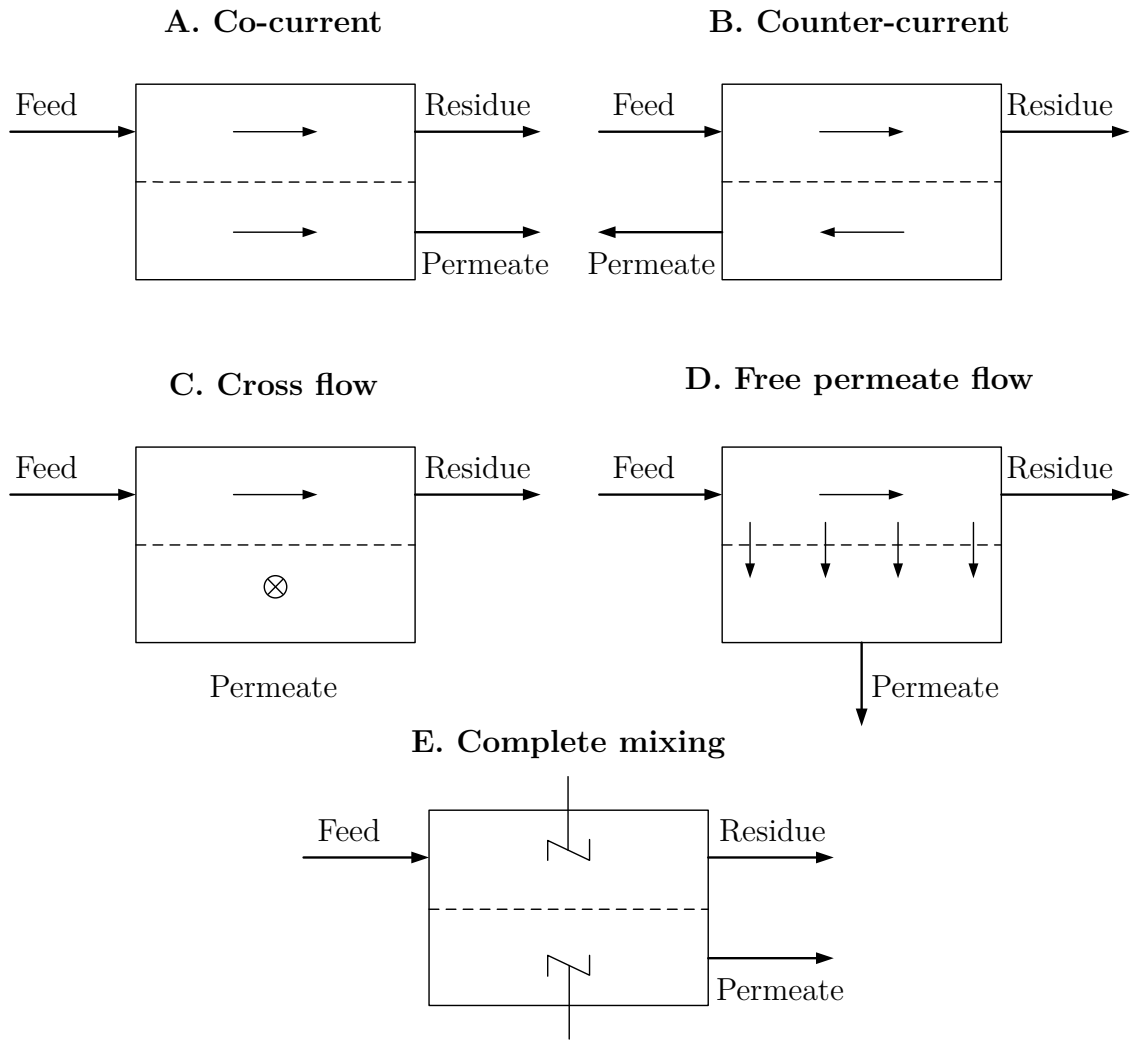

Figure 2.8: Idealised flow patterns in membrane units (Melin & Rautenbach 2004).

If considered, the pressure drop on the membrane side is mostly calculated by the Hagen-Poiseuille equation (e.g., Pan 1986, Pettersen & Lien 1994).

Shindo et al. (1985) provide calculation methods for five flow patterns: co-current flow, counter-current flow, cross flow, perfect mixing, and one-side mixing. Concentrations in the permeation direction and pressure gradients on the feed and on the permeate side are assumed to be negligible.

Pan (1986) has published a more general and widely accepted model for high-flux asymmetric hollow fibre membranes. It includes nonlinear differential equations for local feed and permeate side concentrations as well as for the permeate pressure drop (Hagen-Poiseuille). The solution of this model requires a trial-and-error shooting method to solve the boundary values problem or initial estimates, e.g., for the pressure profile on the permeate side.

Later publications are based on the model described by Pan (1986) and make suggestions to simplify the model and the calculation procedure. Kovvali et al. (1994) assume a linear relationship between permeate and feed stream compositions. For counter-current flow, they provide analytical algebraic equations for flow rates, permeate pressure, and compositions along the permeator length coordinate. Tessendorf et al. (1999) and Kaldis et al. (2000) solve differential equations in membrane models by orthogonal collocation. Chowdhury et al. (2005) provide modelling simplifications allowing to numerically solve the model equations as an inital value problem. Apart from these solving strategies, finite element methods (e.g., by Thundyil & Koros 1997) or finite difference methods (e.g., by Coker et al. 1998, Ahsan & Hussain 2016) are successfully applied in membrane modelling. The advantage of these methods is that algebraic equations are used instead of differential equations. In the context of his Master's Thesis, Senftl (2016) has implemented a membrane shortcut model based on the one-dimensional discretisation of the membrane area in Python. Pressure drops and aspects of convergence have not been considered.

2.3.2 Modelling

A shortcut model for the calculation of a hollow fibre membrane module is developed. Hollow fibre membrane modules can be operated co-current or counter-current (Melin & Rautenbach 2004). Free permeate flow is also possible under the assumption of small permeate flows related to the available membrane area (Ohlrogge & Ebert 2006) but shall not be regarded within this work.

The driving force for gas permeation along the membrane module is determined by local fugacity differences of the permeating components between the feed and the permeate side of the membrane. If ideal gas conditions are assumed on the permeate and the feed side, the driving force is described by the local partial pressure differences instead of local fugacity differences. With the pressure profiles on the feed and on the permeate side being considered negligible or non-dominant, the driving force is simply determined by the difference in composition of the permeating components. In this case, counter-current operation is of advantage in comparison to co-current operation due to a higher driving force along the membrane area. In Figure 2.9, the layout of the implemented counter-current membrane shortcut model is shown. An optional sweep stream can be considered.

In a hollow fibre membrane module, either the feed side or the permeate side can be inside the hollow fibres. The implemented membrane shortcut offers a choice between the two cases:

1.) feed stream passed inside the hollow fibres: $p^{\mathrm{F}} = \text{const.}$, $p^{\mathrm{P}} = \text{const.}$,

2.) permeate stream passed inside the hollow fibres: $p^{\mathrm{F}} = \text{const.}$, $p^{\mathrm{P}} = p^{\mathrm{P}}(z)$.

In the first case, the feed pressure is limited because of limited fibre resilience against internal pressure. For higher feed pressures, the pressure drop on the fibre inside can be neglected. Further, independent of the permeate pressure, pressure drops on the

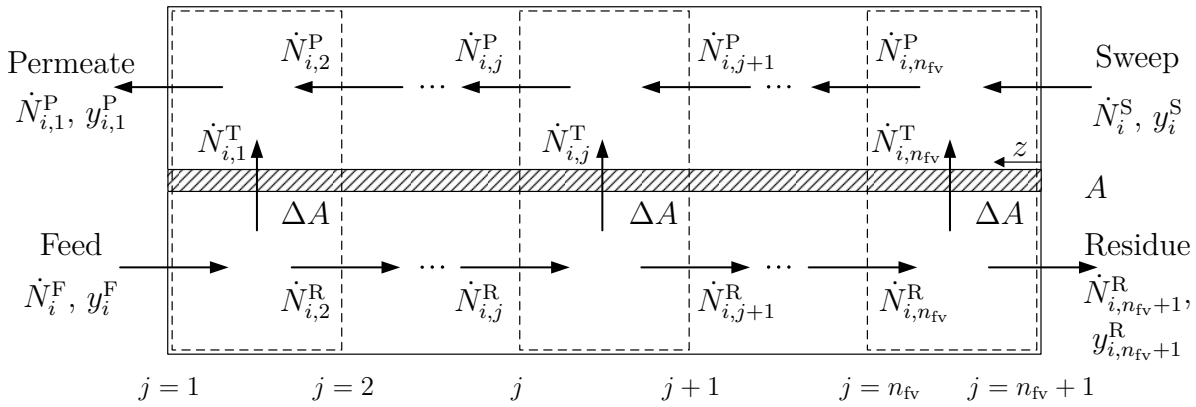

Figure 2.9: Layout of the implemented membrane shortcut model.

shell side of the membrane module can be assumed to be negligible.
In the second case, higher feed pressures are possible since the feed is passed on the shell side of the membrane module and the fibres are more resilient against external pressure. Pressure drops on the feed side can be neglected. However, due to the small inner diameter of the fibres and their length in combination with low pressures, pressure drops must be taken into account on the permeate side of the membrane.

Modelling assumptions For the mathematical formulation of the counter-current membrane shortcut, the following simplifying modelling assumptions are made:

- The feed side and permeate side of the membrane are in plug flow.
- Ideal gas laws apply to the feed and the permeate side of the membrane.
- The membrane module is isothermal. Hence, temperature drops caused by the Joule-Thomson effect due to permeation are not considered.
- The membrane permeances only depend on temperature by an Arrhenius type equation and are independent of pressure and composition.
- The rates of permeation obey Fick's law.
- The effect of back-diffusion is negligible meaning that the composition of the permeate leaving the membrane surface is equal to the bulk permeate composition.
- The hollow fibres do not deform in operation.

The membrane area A has to be specified within the implemented membrane shortcut model. The membrane area, the feed side and the permeate side of the membrane are discretised into n_{fv} equal finite volumes as show in Figure 2.9. Within the finite

volumes, linear concentration profiles and linear pressure profiles are assumed. The finite membrane area is defined by

$$\Delta A = \frac{A}{n_{\mathrm{fv}}} \, . \tag{2.30}$$

Using the finite volume method is computationally efficient since algebraic equations are solved instead of differential equations. Further, mass balance errors due to discretisation are avoided.

Mass balances For each finite volume, a component mass balance for the feed and the permeate side as given in eqs. (2.31) and (2.32) is formulated:

$$0 = \dot{N}^{\mathrm{R}}_{i,j+1} - \dot{N}^{\mathrm{R}}_{i,j} + \dot{N}^{\mathrm{T}}_{i,j} \qquad \text{for } i = 1, ..., n_{\mathrm{c}}; j = 1, ..., n_{\mathrm{fv}} \tag{2.31}$$

$$0 = \dot{N}^{\mathrm{P}}_{i,j} - \dot{N}^{\mathrm{P}}_{i,j+1} - \dot{N}^{\mathrm{T}}_{i,j} \qquad \text{for } i = 1, ..., n_{\mathrm{c}}; j = 1, ..., n_{\mathrm{fv}}. \tag{2.32}$$

The boundary values of the membrane model depend on the assumed flow pattern. Due to the assumption of counter-current operation, the boundary values for the component molar flows on the feed and on the permeate side are determined by:

$$0 = \dot{N}^{\mathrm{R}}_{i,1} - \dot{N}^{\mathrm{F}}_{i} \qquad \text{for } i = 1, ..., n_{\mathrm{c}} \tag{2.33}$$

$$0 = \dot{N}^{\mathrm{P}}_{i,n_{\mathrm{fv}}+1} - \dot{N}^{\mathrm{S}}_{i} \qquad \text{for } i = 1, ..., n_{\mathrm{c}}. \tag{2.34}$$

The composition on the feed side in each finite volume is determined by eq. (2.35) and the composition on the permeate side is determined by eq. (2.36):

$$y^{\mathrm{R}}_{i,j} := \begin{cases} 0 & \text{for } \sum_{i=1}^{n_{\mathrm{c}}} \dot{N}^{\mathrm{R}}_{i,j} \leq \varepsilon \\ \dfrac{\dot{N}^{\mathrm{R}}_{i,j}}{\sum_{i=1}^{n_{\mathrm{c}}} \dot{N}^{\mathrm{R}}_{i,j}}, & \text{for } \sum_{i=1}^{n_{\mathrm{c}}} \dot{N}^{\mathrm{R}}_{i,j} > \varepsilon \end{cases} \qquad \text{for } i = 1, ..., n_{\mathrm{c}}; j = 1, ..., n_{\mathrm{fv}} \tag{2.35}$$

$$y^{\mathrm{P}}_{i,j} := \begin{cases} 0, & \text{for } \sum_{i=1}^{n_{\mathrm{c}}} \dot{N}^{\mathrm{P}}_{i,j} \leq \varepsilon \\ \dfrac{\dot{N}^{\mathrm{P}}_{i,j}}{\sum_{i=1}^{n_{\mathrm{c}}} \dot{N}^{\mathrm{P}}_{i,j}}, & \text{for } \sum_{i=1}^{n_{\mathrm{c}}} \dot{N}^{\mathrm{P}}_{i,j} > \varepsilon \end{cases} \qquad \text{for } i = 1, ..., n_{\mathrm{c}}; j = 1, ..., n_{\mathrm{fv}}. \tag{2.36}$$

In order to improve convergence, the component mole fraction arrays $y^{\mathrm{R}}_{i,j}$ and $y^{\mathrm{P}}_{i,j}$ are not determined explicitly during the solution of the shortcut model. Hence, initialisation of these arrays is not necessary. Convergence is further improved by introducing a very small number $\varepsilon = 10^{-8}$. The mole fraction of each component is considered to be a hard zero instead of a numerical zero, if the total molar flow $\sum_{i=1}^{n_{\mathrm{c}}} \dot{N}^{\mathrm{R}}_{i,j}$ or $\sum_{i=1}^{n_{\mathrm{c}}} \dot{N}^{\mathrm{P}}_{i,j}$ in the corresponding finite volume is smaller than $\varepsilon = 10^{-8}$.

Mass transfer through the membrane Within one finite volume, the component mole fractions are assumed as linear profiles along the membrane length on the feed and

on the permeate side. Hence, according to Fick's law, the trans-membrane component molar flows are calculated by eq. (2.37).

$$0 = \dot{N}^{\mathrm{T}}_{i,j} - 0.5 \cdot \Delta A \cdot P_i \cdot \left(p^{\mathrm{F}} \left(y^{\mathrm{R}}_{i,j} + y^{\mathrm{R}}_{i,j+1}\right) - \left(p^{\mathrm{P}}_j y^{\mathrm{P}}_{i,j} + p^{\mathrm{P}}_{j+1} y^{\mathrm{P}}_{i,j+1}\right)\right) \quad \text{for } i = 1, ..., n_{\mathrm{c}}; j = 1, ..., n_{\mathrm{fv}} \tag{2.37}$$

While the permeances P_i are assumed independent of pressure and composition, the dependence on temperature is considered by the Arrhenius type equation given in eq. (2.38). Since the membrane shortcut is assumed isothermal, the permeances are calculated in dependence of the feed temperature T^{F}. If a sweep stream is used, it should have a similar temperature to minimise the enthalpy error. The parameters a_i and b_i have to be determined with experimental data for the used type of membrane.

$$P_i = e^{\frac{a_i}{T^{\mathrm{F}}} + b_i} \tag{2.38}$$

Pressure drop on the permeate side If the feed stream is introduced into the hollow fibres, pressure drops in the hollow fibres are neglected.

$$p^{\mathrm{P}}_j = p^{\mathrm{P}}_{j+1} = p_{\mathrm{perm}} \qquad \text{for } j = 1, ..., n_{\mathrm{fv}} \tag{2.39}$$

However, if the permeate stream is directed through the hollow fibres, the pressure drop in the hollow fibres is calculated using the Hagen-Poiseuille approach. Hagen-Poiseuille equations describe laminar flow through a pipe of uniform cross section and relate the pressure drop along the length of a pipe to the average flow velocity in the pipe. Inner diameter d_{inner}, length L_{fibres}, and number n_{fibres} of the fibres in the membrane module have to be specified:

$$\Delta A = n_{\mathrm{fibres}} \cdot d_{\mathrm{inner}} \cdot \pi \cdot \Delta z = n_{\mathrm{fibres}} \cdot d_{\mathrm{inner}} \cdot \pi \cdot \frac{L_{\mathrm{fibres}}}{n_{\mathrm{fv}}}. \tag{2.40}$$

The pressure drop $p^{\mathrm{P}}_j - p^{\mathrm{P}}_{j+1}$ in each finite volume is determined by eq. (2.41). The derivation of eq. (2.41) can be found in section A.5 in the appendix.

$$0 = p^{\mathrm{P}}_{j+1} - \frac{1}{2}\left(p^{\mathrm{P}}_j + \sqrt{(p^{\mathrm{P}}_j)^2 + 4 \cdot \frac{128 \mu^{\mathrm{P}} \bar{R} T^{\mathrm{P}} \dot{N}^{\mathrm{P}}_j (L_{\mathrm{fibres}})^2}{(d_{\mathrm{inner}})^3 \cdot A \cdot n_{\mathrm{fv}}}}\right) \quad \text{for } j = 1, ..., n_{\mathrm{fv}} \tag{2.41}$$

The start value for the pressure calculation on the permeate side is given by the specified permeate pressure. Due to isothermal conditions in the membrane module, the temperature on the permeate side equals the temperature of the feed. Further, the

dynamic viscosity μ^{P} is determined for the permeate product and assumed constant on the permeate side:

$$p^{\mathrm{P}}_{j=1} = p_{\mathrm{perm}} \tag{2.42}$$
$$T^{\mathrm{P}} = T^{\mathrm{F}} \tag{2.43}$$
$$\mu^{\mathrm{P}} = \mu^{\mathrm{P}}_{j=1}. \tag{2.44}$$

2.3.3 Validation

Comparison of model results with experimental data In order to evaluate the accuracy of the developed shortcut model for membranes, it is used to reproduce experimental data given by Pan (1986). Carbon dioxide is separated by permeation from a feed stream containing carbon dioxide, methane, ethane, and propane using an asymmetric cellulose acetate hollow fibre membrane. The experiments were performed with a miniature fibre module consisting of ten 36 cm long fibres in a U-loop set-up. The open fibre ends are embedded in a 3 cm long tube sheet. A steel module housing shall reduce void spaces around the fibres. The feed stream is on the outside of the hollow fibres, the permeate is directed in counter-current to the feed inside the fibres. Pan (1986) has provided experimental data for permeate concentrations in dependence of the membrane stage cut which is defined by

$$\Theta = \frac{\dot{N}_{\mathrm{perm}}}{\dot{N}_{\mathrm{feed}}}. \tag{2.45}$$

Figure 2.10 includes experimental data for permeate mole fractions given by Pan (1986) and corresponding simulation results obtained with the membrane shortcut model. For the shortcut calculations, the stage cut Θ is varied by varying the feed molar flow.

In Table 2.2, the specifications for the data plotted in Figure 2.10 are listed. The membrane area used for shortcut simulation is calculated by

$$A = n_{\mathrm{fibres}} L_{\mathrm{fibres}} \cdot 0.5(d_{\mathrm{outer}} + d_{\mathrm{inner}})\pi. \tag{2.46}$$

The experimental data in Figure 2.10 was taken from a plot given by Pan (1986) using the open-source program Engauge Digitizer (Mitchell et al. 2018) to recover the data points. Although this procedure ensures highest possible precision, the accuracy of the recovered data depends on the axis scaling of the original plot. Hence, the axes in Figure 2.10 are scaled similar to the axes of the original plot given by Pan (1986).

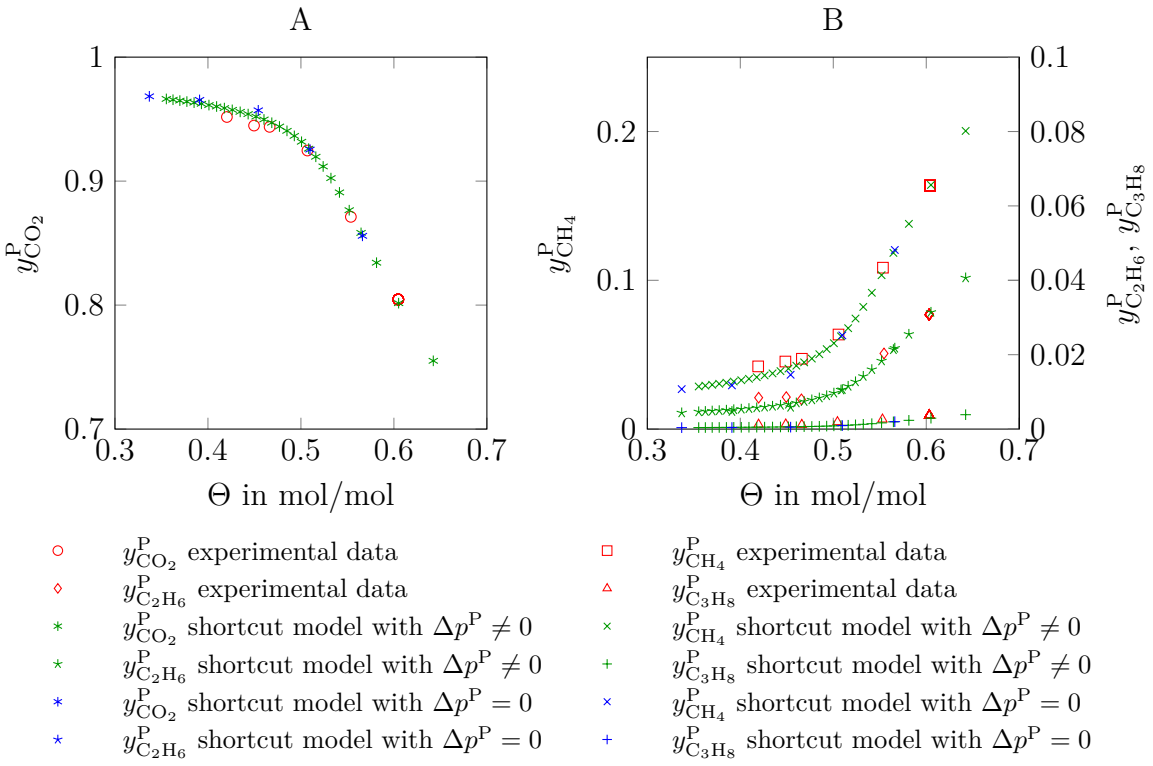

Figure 2.10: Performance of CO_2 separation from a hydrocarbon mixture with a cellulose acetate membrane: comparison of results obtained with the membrane shortcut with experimental data given by Pan 1986.

Table 2.2: Specifications for Figure 2.10 to Figure 2.13.

Specification	**Fig. 2.10 to Fig. 2.13**			
Feed conditions	$p_{\mathrm{feed}} = 35.28\,\mathrm{bar}$, $T_{\mathrm{feed}} = 10\,^{\circ}\mathrm{C}$, $y_{\mathrm{CO_2}} = 0.4850$, $y_{\mathrm{CH_4}} = 0.2790$, $y_{\mathrm{C_2H_6}} = 0.1626$, $y_{\mathrm{C_3H_8}} = 0.0734$			
CO_2 permeability (at 10 °C)	$P_{\mathrm{CO_2}} = 1.34 \cdot 10^{-8}\,\mathrm{mol/(m^2 s Pa)}$			
Selectivities (at 10 °C)	$\frac{P_{\mathrm{CO_2}}}{P_{\mathrm{CH_4}}} = 36.0$, $\frac{P_{\mathrm{C_2H_6}}}{P_{\mathrm{CH_4}}} = 0.275$, $\frac{P_{\mathrm{C_3H_8}}}{P_{\mathrm{CH_4}}} = 0.0536$			
Fibre diameters	$d_{\mathrm{inner}} = 80\,\mu\mathrm{m}$, $d_{\mathrm{outer}} = 200\,\mu\mathrm{m}$			
	Fig. 2.10	**Fig. 2.11**	**Fig. 2.12**	**Fig. 2.13**
Feed molar flow $\dot{N}_{\mathrm{feed}}$	varied	$10\,\mathrm{mol/s}$	$10\,\mathrm{mol/s}$	$10\,\mathrm{mol/s}$
Permeate pressure p_{perm}	0.928 bar	1.2 bar	varied	varied
Membrane area A	-	$1000\,\mathrm{m}^2$	varied	varied
Active fibre length L_{fibres}	15 cm	50 cm	50 cm	50 cm
Number of fibres n_{fibres}	20	-	-	-
Number of finite volumes n_{fv}	50	varied	50	50

Figure 2.10 shows that the results calculated with the membrane shortcut model are in very good agreement with the experimental data provided by Pan (1986). Considering the permeate pressure drop on the fibre inside does not have a significant influence on the accuracy of the shortcut results. This can be explained by the experimental data being obtained with a miniature membrane module consisting of hollow fibres with a short active length of $L_{\text{fibres}} = 15\,\text{cm}$.

Influence of the degree of discretisation For the membrane shortcut model, the membrane area as well as the residue and permeate side of the membrane are discretised into n_{fv} equal finite volumes. A hollow fibre membrane module with the permeate side on the fibre inside and the feed directed in counter-current is assumed. Figure 2.11 is used to evaluate the influence of the degree of discretisation on concentration and pressure profiles over the active fibre length L_{fibres}. In Figure 2.11A, the profile of the CO_2 mole fraction $y^{\text{R}}_{\text{CO}_2}$ on the feed side is plotted. In Figure 2.11B, the absolute pressure p^{P} on the permeate side is plotted. The specifications given in Table 2.2 are applied. In comparison to the specifications for Figure 2.10, a higher membrane area, a longer active fibre length and a corresponding feed molar flow are assumed to provide evaluation results for a larger hollow fibre membrane module. The permeate outlet pressure $p_{\text{perm}} = 1.2\,\text{bar}$ is chosen to be higher than atmospheric pressure so that the permeate can exit the membrane module without a vaccum device.

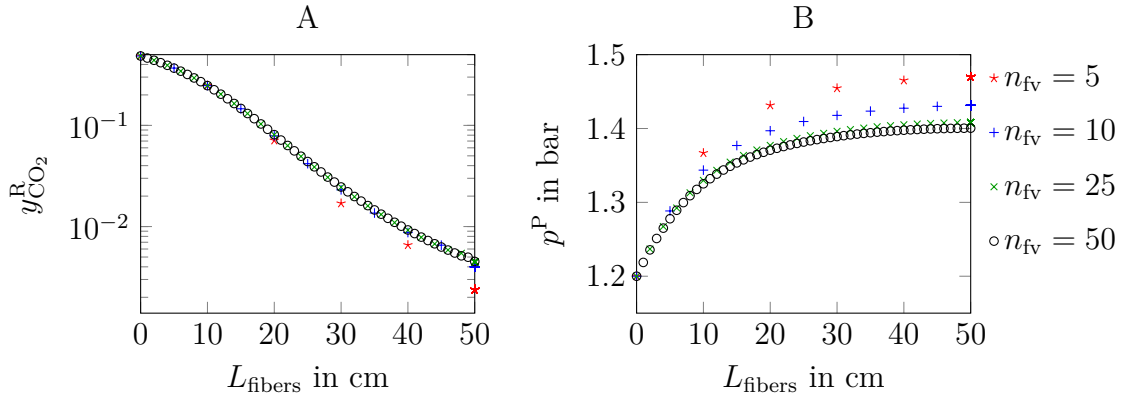

Figure 2.11: CO_2 mole fraction profile on the feed side (A) and pressure profile on the permeate side (B) of a membrane in dependence of the number of finite volumes for discretisation.

The feed inlet and the permeate outlet are located at $L_{\text{fibres}} = 0$, the residue outlet is located at $L_{\text{fibres}} = 50\,\text{cm}$. Regarding the CO_2 mole fraction profile on the feed side, the influence of the number of finite volumes n_{fv} is negligible above $n_{\text{fv}} = 10$ (Figure 2.11A). While the pressure on the feed side is assumed constant, the calculated pressure drop on the permeate side is higher for lower degrees of discretisation (Figure 2.11B).

In Table 2.3, shortcut results for the component molar flows of the permeate and the residue outlet stream are listed depending on the degree of discretisation and in case of

neglected and considered pressure drops on the permeate side. Table 2.3 corresponds to Figure 2.11.

Table 2.3: Influence of the pressure drop on the permeate side on the membrane shortcut results

		$\Delta p^{\mathrm{P}} = \Delta p^{\mathrm{P}}_{\mathrm{n_{fv}}} \neq 0$				$\Delta p^{\mathrm{P}} = 0$			
n_{fv}	$\Delta p^{\mathrm{P}}_{\mathrm{n_{fv}}}$	$\dot{N}^{\mathrm{P}}_{\mathrm{CO_2}}$	$\dot{N}^{\mathrm{R}}_{\mathrm{CH_4}}$	$\dot{N}^{\mathrm{R}}_{\mathrm{C_2H_6}}$	$\dot{N}^{\mathrm{R}}_{\mathrm{C_3H_8}}$	$\dot{N}^{\mathrm{P}}_{\mathrm{CO_2}}$	$\dot{N}^{\mathrm{R}}_{\mathrm{CH_4}}$	$\dot{N}^{\mathrm{R}}_{\mathrm{C_2H_6}}$	$\dot{N}^{\mathrm{R}}_{\mathrm{C_3H_8}}$
-	bar	mol/s	mol/s	mol/s	mol/s	mol/s	mol/s	mol/s	mol/s
5	0.2700	4.8393	2.2110	1.5224	0.7246	4.8440	2.2063	1.5219	0.7245
10	0.2312	4.8321	2.2118	1.5226	0.7246	4.8374	2.2077	1.5221	0.7245
25	0.2081	4.8299	2.2126	1.5226	0.7246	4.8353	2.2084	1.5221	0.7245
50	0.2004	4.8297	2.2128	1.5226	0.7246	4.8347	2.2089	1.5222	0.7245

While the pressure on the permeate side drops off at least 15% (for $n_{\mathrm{fv}} = 50$) along the active length of the fibre, the difference between the shortcut results for the component molar flows with and without permeate pressure drop are not significant in the examined cases. However, the permeate pressure drop on the fibre inside depends on several factors such as inner fibre diameter, active length of the fibre, and permeate flow. In order to ensure accurate results in case of more dominant pressure drop effects, the pressure drop for the permeate on the fibre inside is considered by default in the developed membrane shortcut.

With the pressure drop on the permeate side considered, the outlet component molar flows $\dot{N}^{\mathrm{P}}_i$ and $\dot{N}^{\mathrm{R}}_i$ are very similar for $n_{\mathrm{fv}} = 25$ and $n_{\mathrm{fv}} = 50$. Hence, $n_{\mathrm{fv}} = 50$ finite volumes can be assumed to be sufficient for the discretisation within the membrane shortcut model, even if longer fibres are used.

Dependencies between results and main model variables Separation of CO_2 from natural gas with a cellulose acetate membrane is driven by the relation of CO_2 permeation to CH_4, C_2H_6, and C_3H_8 permeation over the membrane. The design goal is to achieve the CO_2 impurity specification in the natural gas residue stream whilst minimising the natural gas loss in the permeate stream by finding an optimal combination of feed temperature T_{feed}, membrane area A, and the pressure ratio $\frac{p_{\mathrm{perm}}}{p_{\mathrm{feed}}}$.

The temperature influence on the component permeabilites is described by an Arrhenius type equation as given in eq. (2.38). Since the parameters a_i and b_i are fitted to describe experimental data, the dependence between permeability and temperature can be assumed to be sufficiently accurate. In case of pre-specified feed temperatures and pressures, the remaining main model variables to be optimised are the permeate pressure p_{perm} and membrane area A. In Figure 2.12 and Figure 2.13, the influence of p_{perm} and membrane area A on the shortcut model results is shown.

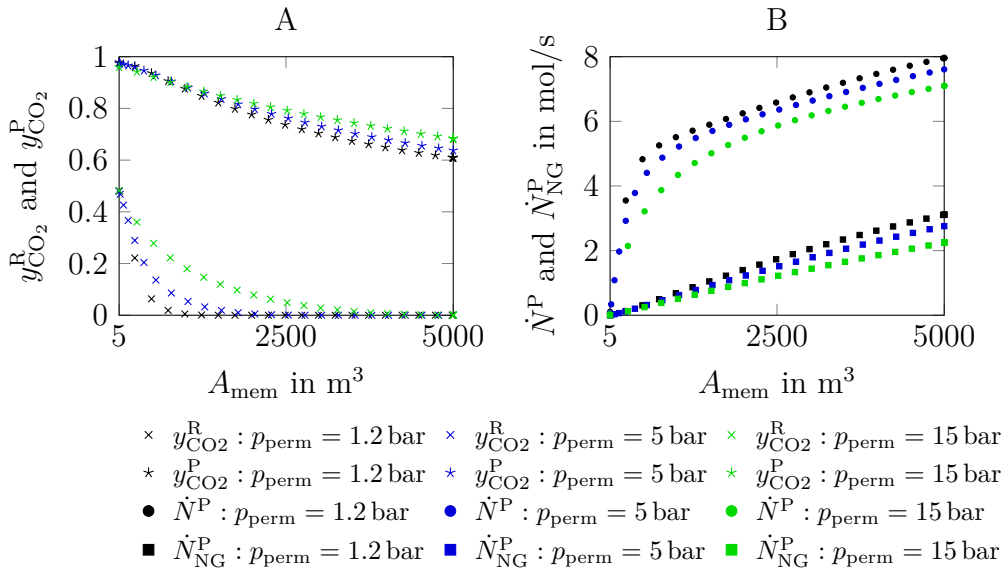

Figure 2.12: CO_2 mole fraction in the residue (A) and permeate molar flow (B) in dependence of increasing membrane areas.

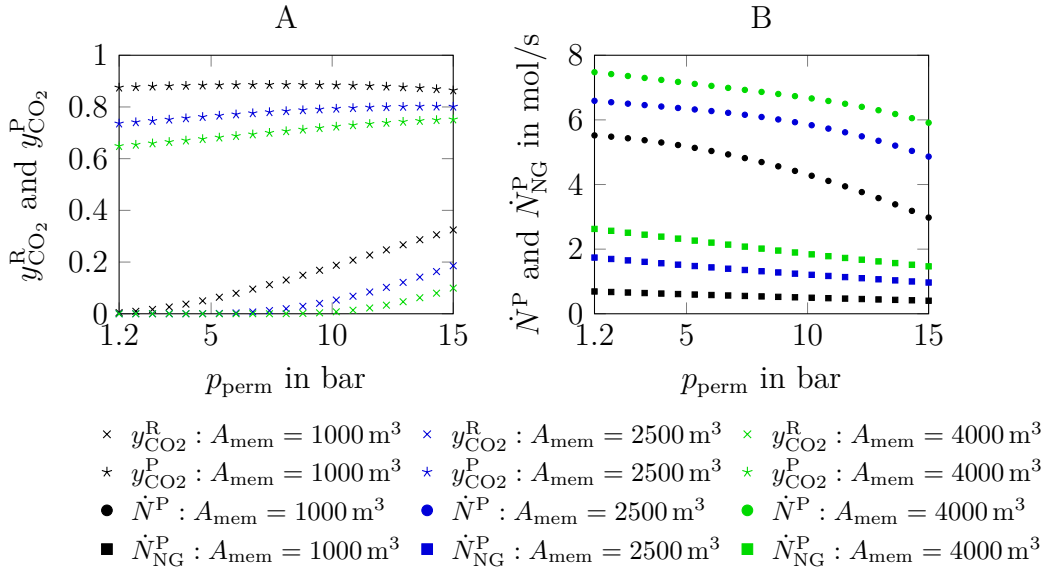

Figure 2.13: CO_2 mole fraction in the residue (A) and permeate molar flow (B) in dependence of increasing permeate pressures.

Figure 2.12 and Figure 2.13 show that higher membrane areas A and lower permeate pressures p_{perm} result in more permeation over the membrane. More permeation over the membrane leads to lower CO_2 contents $y^{\mathrm{R}}_{\mathrm{CO_2}}$ in the residue stream and higher natural gas losses in the permeate stream. Also, Figure 2.12 and Figure 2.13 illustrate that – with the same celluose actetate membrane – an enriched CO_2 permeate product stream is possible as well as a high purity natural gas residue product stream, if a suitable combination of A and p_{perm} is chosen.

Evaluation of the membrane shortcut model has shown that the model is sufficiently accurate in reproducing experimental data. The number of finite volumes does not influence the shortcut results, if enough finite volumes are used. Further, the dependencies between important independent model variables such as the membrane area and the permeate pressure and the model results are in line with theoretical expectations and smooth. This means that the shortcut model provides sufficient derivative information. As a consequence, the presented shortcut model is applicable in process optimisation.

2.4 Shortcut model for columns

A new column shortcut model for use in gradient-based process optimisation is developed. It is based on a method proposed by Edmister (1943) and Edmister (1957) and is called Adapted Edmister Model (AEM). It can be used to model arbitrary column configurations and allows to optimise the number of column stages by NLP optimisation.

2.4.1 Literature

Fenske-Underwood-Gilliland (FUG) The FUG method can be used for sharp and unsharp separations of ideal mixtures in distillation columns with a condenser and reboiler. In case of multicomponent mixtures, a light and heavy key component have to be specified. Depending on light and heavy key concentrations in the column top and bottom, the distribution of non-key components is calculated. The FUG method provides a correlation of the minimum number of stages (from Fenske method), the minimum reflux (from Underwood method), the actual number of stages and the actual reflux (Fenske 1932, Underwood 1932, Underwood 1946a, Underwood 1946b, Gilliland 1940).

Boundary value method (BVM) The BVM was originally proposed to assess the feasibility and minimum energy demand of single-feed distillation columns including a condenser and reboiler. It applies to sharp as well as unsharp separation of ideal, non-ideal, and homogeneous azeotropic distillations (Van Dongen & Doherty 1985, Levy et al. 1985, Fidkowski et al. 1993). The BVM is used for calculation of distillation columns with side streams and several feeds in later publications (Rooks et al. 1996, Barbosa & Doherty 1988b, Barbosa & Doherty 1988a). However, its underlying principle is to specify top and bottom product stream conditions and calculate stage-to-stage column composition profiles starting from condenser and reboiler (Julka & Doherty 1990). Since the necessary intersection of a manifold of calculated profiles has to be checked visually, it is limited to ternary or quaternary mixtures (Marquardt et al. 2008).

Pinch-based methods are based on the BVM and have been developed to overcome the sensitivity of BVM results regarding trace component specifications in the column products (Kraemer 2012). Well-known examples for pinch-based methods are the zero volume method (Julka & Doherty 1990), the minimum angle method (Koehler et al. 1991), eigenvalue methods (Poellmann et al. 1994), the shortest stripping line method (Lucia et al. 2008), and the rectification body method (RBM). With the RBM, for example, the manifold of all possible liquid phase composition profiles for pre-specified column products is approximated by one rectification body (area spanned between certain pinch points) for the stripping and one for the rectifying section. Feasible separations are characterised by overlapping rectification bodies while the minimum energy requirements are indicated by the rectification bodies touching in single points. However, if the column products are specified to contain each feed component (unsharp separation), the rectification bodies turn into finite straight lines approximating curved column profiles. The RBM assumes an infinite number of stages and provides information about minimum reflux. The RBM has been extended to complex column set-ups, but is mostly used for columns with a condenser and reboiler (Kraemer 2012, Bausa et al. 1998, von Watzdorf et al. 1999, Brüggemann & Marquardt 2004, Kraemer et al. 2009).

Temperature collocation algorithm (TCA) In order to reduce problem size and computational effort, a temperature collocation algorithm based on the BVM was developed. Stage-to-stage calculation of column composition profiles is replaced by a bubble point temperature distance function and orthogonal collocation on finite elements resulting in dimensionless temperature profiles for the rectifying and stripping section. The TCA applies to unsharp as well as sharp separations of ideal and non-ideal multicomponent mixtures. It yields finite results for the number of column stages and the reflux. The TCA can be used to design thermally coupled sidestream columns and generate complex distillation networks for column sequencing. However, the columns mostly include condensers and reboilers to provide boundary values (Zhang & Linninger 2004, Linninger 2009, Ruiz et al. 2010, Beneke & Linninger 2011).

∞/∞-Analysis is based on the assumption of infinite reflux and an infinite number of stages in a column. Thus, it describes the thermodynamic limits of distillative separation tasks. It applies to ideal, non-ideal, and even azeotropic multicomponent mixtures and can model sharp as well as unsharp separations. In case of infinite reflux, liquid phase composition profiles are represented by residue curves or distillation lines. With the ∞/∞-analysis, feasible distillate and bottom products for any given feed stream can be located with the help of material balances and either residue curves or distillation lines. Due to assuming infinite reflux, the ∞/∞-analysis is particulary applied to columns with a condenser and reboiler (Petlyuk & Aventyan 1971, Bekiaris et al. 1993, Bekiaris et al. 1996, Bekiaris & Morari 1996, Burger & Hasse 2013, Ryll et al. 2012, Ryll et al. 2014).

Group methods (GM) With group methods, column outlet stream conditions are approximated from given inlet streams as well as the number of stages by grouping the column stages into segments. Detailed changes of composition or temperature along the individual column stages are not considered (Kamath et al. 2010). Kremser (1930) originated the group methods by providing an estimated material balance for absorbers. The estimation is based on constant component absorption factors. Sounders & Brown (1932) introduced stripping factors in addition to absorption factors to make calculations more convenient. Horton & Franklin (1940), Edmister (1943), and Landes & Bell (1960) did not consider absorption and stripping factors as constant but varying along the column height and derived methods to determine effective absorption and stripping factors. Edmister (1957) demonstrated that group methods can be used to model arbitrary column configurations by appling them to, for example, a refluxed absorber, a reboiled stripper, and a distillation column. However, the shortcut method proposed by Edmister (1957) only includes estimations for component flows leaving a column segment.

Owens & Maddox (1968), Kamath et al. (2010), and Dowling & Biegler (2015) have developed shortcut models based on group methods which also include temperature calculations and energy balances.

Applications of column shortcut models Column shortcut methods can be used for separation problem feasibility assessment (e.g., ∞/∞-analysis), for estimations (e.g., FUG and GM), and for the calculation of minimum energy requirements (e.g., BVM and RBM). Further, they are used for generating and evaluating separation networks and sequences (e.g., Ruiz et al. 2010, Beneke & Linninger 2011, Agrawal 1996, Agrawal 2003, Caballero & Grossmann 2001). Karuppiah et al. (2008) apply the FUG method in flowsheet optimisation. Peschel et al. (2012) use the Kremser method – which is a group method – to model absorption columns in the optimisation of an ethylene oxide process.

Criteria for use in industrial process optimisation In Table 2.4, the described column shortcut models are summarised and evaluated regarding criteria for column shortcut models arising from flowsheet optimisation in equation oriented frameworks. Complex column set-ups have to be modelled, hence column shortcut models requiring a condenser and reboiler, for example, are not sufficient for general use. A column shortcut model has to be applicable to sharp (e.g., separation of mixture a, b, c into a product containing a and a product containing b, c) and unsharp separations (e.g., separation of mixture a, b, c into a product containing a, b and a product containing b, c) of ideal and non-ideal multi-component mixtures. A finite column reflux and finite column number of stages are needed since these are typical optimisation variables. Only group methods meet all of the given criteria.

Table 2.4: Selection of column shortcut models for industrial process optimisation (✓... applies; - ... does not apply) (published in Ecker et al. (2019))

Method and short description	Arbitrary column set-ups	Multi-comp. mixtures	Non-ideal mixtures	Sharp separations	Unsharp separations	Finite reflux	Finite number of stages
Fenske-Underwood-Gilliland Determination of min. number of stages (at infinite reflux), min. reflux (at infinite number of stages) and system independent correlation between these variables, actual number of stages and actual reflux.	-	✓	-	✓	✓	✓	✓
Boundary value method After top and bottom product specification, calculation of stage-to-stage liquid phase composition profiles starting from condenser and reboiler based on differential equations for residue curves. Due to intersection check of composition profiles limited to ternary/quaternary mixtures.	-	-	✓	✓	✓	✓	✓
Rectification body method To overcome BVM limitations, all possible liquid phase composition profiles for pre-specified column products are approximated by rectification bodies. Check for overlapping (feasible separation) or touching (min. energy requirement) of the rectification body for the rectifying and stripping section.	-	✓	✓	✓	✓	✓	-
Temperature collocation algorithtm To reduce problem size and computational effort with BVM, composition profiles are replaced by dimensionless temperature profiles.	-	✓	✓	✓	✓	✓	✓
∞/∞ - Analysis Assuming infinite reflux and number of stages, thermodynamic limits of distillation tasks are described based on residue curves or distillation lines.	-	✓	✓	✓	✓	-	-
Group methods Column outlet streams approximated from given inlet streams based on group treatment of the column stages. Detailed changes of, e.g. composition or temperature along the stages not considered.	✓	✓	✓	✓	✓	✓	✓

2.4.2 Modelling

Original Edmister method Edmister applied the group methods to different column configurations (e.g., refluxed absorber, reboiled stripper, distillation column) and showed that arbitrary column configurations can be modelled based on five zones: condensing, absorbing, feed flash, stripping, and reboiling. The condensing, feed flash, and the reboiling zone are each modelled by single-stage flash operations. The absorbing and the stripping zone represent column segments in which both absorptive and stripping effects occur simultaneously but one effect is predominating. Figure 2.14 shows the Edmister model for a column segment in comparison to a stage-to-stage model based on material balances, equilibrium conditions, summation rules, and heat balances (MESH).

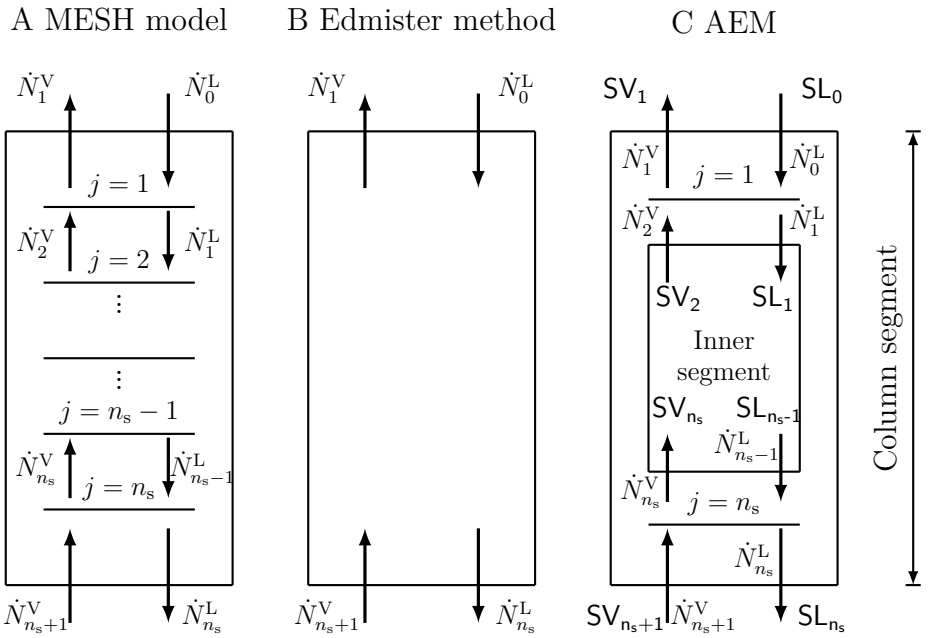

Figure 2.14: Column segments according to MESH model, Edmister method, and AEM.

The Edmister method is based on absorption factors A_i and stripping factors S_i for one equilibrium stage as defined by:

$$A_i = \frac{\dot{N}^{\mathrm{L}}}{K_i \cdot \dot{N}^{\mathrm{V}}} = \frac{\dot{N}_i^{\mathrm{L}}}{\dot{N}_i^{\mathrm{V}}} \tag{2.47}$$

$$S_i = \frac{K_i \cdot \dot{N}^{\mathrm{V}}}{\dot{N}^{\mathrm{L}}} = \frac{\dot{N}_i^{\mathrm{V}}}{\dot{N}_i^{\mathrm{L}}} = \frac{1}{A_i}. \tag{2.48}$$

Absorption and stripping factors are quotients characterising the molar flows and the equilibrium concentrations of a vapour and a liquid stream leaving an equilibrium stage. A_i and/or S_i can be determined on each column stage which would be consistent with stage-to-stage calculations in equilibrium stage models for columns. In order to avoid stage-to-stage calculations, an effective absorption factor Ae_i and an effective stripping

factor Se_i are applied. Instead of calculating A_i and S_i, $A_i = Ae_i$ and $S_i = Se_i$ is assumed on every stage. Thereby, the performance factors $\phi_{\mathrm{A},i}$ and $\phi_{\mathrm{S},i}$ can be determined by:

$$\Pi_{\mathrm{A},i} := A_{i,1}A_{i,2}A_{i,3}\cdots A_{i,n_\mathrm{s}} \tag{2.49}$$

$$\Sigma_{\mathrm{A},i} := A_{i,1}A_{i,2}A_{i,3}\cdots A_{i,n_\mathrm{s}} + A_{i,2}A_{i,3}\cdots A_{i,n_\mathrm{s}} + \cdots + A_{i,n_\mathrm{s}} \tag{2.50}$$

$$\phi_{\mathrm{A},i} = \frac{1}{\Sigma_{\mathrm{A},i}+1} \tag{2.51}$$

$$\phi_{\mathrm{A},i} = \frac{Ae_i - 1}{Ae_i^{n_\mathrm{s}+1} - 1} \tag{2.52}$$

$$\phi_{\mathrm{S},i} = \frac{\Pi_{\mathrm{A},i}}{\Sigma_{\mathrm{A},i}+1} \tag{2.53}$$

$$\phi_{\mathrm{S},i} = \frac{Se_i - 1}{Se_i^{n_\mathrm{s}+1} - 1}. \tag{2.54}$$

The performance factor $\phi_{\mathrm{A},i}$ describes the fraction of a component's molar flow entering the column segment in the vapour inlet which is still present in the vapour outlet. The performance factor $\phi_{\mathrm{S},i}$ describes the fraction of a component's molar flow entering the column segment in the liquid inlet which is contained in the liquid outlet. If correct values for Ae_i and Se_i are found, the Edmister method is equivalent to a stage-to-stage column model. However, finding the correct values for Ae_i and Se_i is challenging. Edmister proposed an approximation for Ae_i and Se_i which is actually valid for two column stages (Edmister 1943):

$$Ae_i = \sqrt{A_{i,\mathrm{bot}}(A_{i,\mathrm{top}}+1)+0.25} - 0.5 \tag{2.55}$$

$$Se_i = \sqrt{S_{i,\mathrm{top}}(S_{i,\mathrm{bot}}+1)+0.25} - 0.5. \tag{2.56}$$

The indices 'top' and 'bot' refer to boundary conditions and can also be determined by a condenser or reboiler, for example. Eqs. (2.57) and (2.58) are used to approximate the material balance of a column segment as shown in Figure 2.14:

$$\dot{N}^{\mathrm{V}}_{i,1} = \dot{N}^{\mathrm{V}}_{i,n_\mathrm{s}+1}\cdot\phi_{\mathrm{A},i} + \dot{N}^{\mathrm{L}}_{i,0}\cdot(1-\phi_{\mathrm{S},i}) \qquad \text{for } i = 1,...,n_\mathrm{c} \tag{2.57}$$

$$\dot{N}^{\mathrm{L}}_{i,n_\mathrm{s}} = \dot{N}^{\mathrm{L}}_{i,0}\cdot\phi_{\mathrm{S},i} + \dot{N}^{\mathrm{V}}_{i,n_\mathrm{s}+1}\cdot(1-\phi_{\mathrm{A},i}) \qquad \text{for } i = 1,...,n_\mathrm{c}. \tag{2.58}$$

According to Edmister, eq. (2.57) is used, if the column segment is classed as an absorbing section, while eq. (2.58) is used, if the column segment is classed as a stripping section. The Edmister equation for a stripping section in eq. (2.58) is linearly dependent on the Edmister equation for an absorbing section in eq. (2.57) and on the component material balance around the segment in eq. (2.59):

$$0 = \dot{N}^{\mathrm{V}}_{i,n_\mathrm{s}+1} + \dot{N}^{\mathrm{L}}_{i,0} - \dot{N}^{\mathrm{V}}_{i,1} - \dot{N}^{\mathrm{L}}_{i,n_\mathrm{s}} \qquad \text{for } i = 1,...,n_\mathrm{c}. \tag{2.59}$$

Hence, it is not necessary to distinguish, whether absorptive or stripping effects are dominating in a column segment. Eq. (2.57) or eq. (2.58) can be combined with

the component material balance around the segment in eq. (2.59) without distinction between absorbing and stripping sections.

According to Edmister, the performance factor $\phi_{\mathrm{S},i}$ is defined as given in eq. (2.53) and (2.54). Hence, $\phi_{\mathrm{S},i}$ can also be expressed by:

$$\phi_{\mathrm{S},i} = \Pi_{\mathrm{A},i} \cdot \phi_{\mathrm{A},i} = Ae_i^{n_\mathrm{s}} \cdot \frac{Ae_i - 1}{Ae_i^{n_\mathrm{s}+1} - 1}. \tag{2.60}$$

Therefore, modelling a general column segment with the Edmister method is possible using effective absorption factors Ae_i only.

Adapted Edmister model To avoid stage-to-stage calculations of phase equilibria as necessary with MESH-based column models, a new column shortcut model is introduced. The presented shortcut model is based on the Edmister method (Edmister 1943, Edmister 1957) and a consequent development of the models presented by Kamath et al. (2010) and Dowling & Biegler (2015). While the original Edmister method is limited to material balances and equilibrium conditions, the presented shortcut model includes energy balances, temperature calculations as well as a pressure profile within the column segment. The top and bottom equilibrium stage are explicitly calculated as boundary values of the modelled column segment. The remaining equilibrium stages of the MESH-based column segment are grouped to an inner segment. This model set-up is referred to as Adapted Edmister Model (AEM).

The AEM allows to model complex column setups. The shortcut column segments can be used in a set of modules including, for example, a reboiler, a condenser, and a flash stage. By combining these modules as needed, any column setup can be represented. An example how arbitrary column setups can be modelled is shown in Figure 2.15.

The inlet streams $\mathsf{SV}_{\mathsf{n_s+1}}$ and SL_{0} as well as the number of stages in the inner segment ($n_\mathrm{s}-2$), the column segment top pressure $p_{j=1}$, and the pressure drop per column stage Δp_s have to be specified. Streams SV_{1}, SV_{2}, $\mathsf{SV}_{\mathsf{n_s}}$, SL_{1}, $\mathsf{SL}_{\mathsf{n_s\text{-}1}}$, and $\mathsf{SL}_{\mathsf{n_s}}$ must be determined. Streams $\mathsf{SV}_{\mathsf{n_s}}$ and $\mathsf{SL}_{\mathsf{n_s}}$ are determined by calculation of the bottom equilibrium stage, while streams SV_{1} and SL_{1} are determined by calculation of the top equilibrium stage. The two equilibrium stages are calculated by:

$$0 = p_j^\mathrm{V} - p_j \qquad \text{for } j = 1, n_\mathrm{s} \tag{2.61}$$

$$0 = p_j^\mathrm{L} - p_j \qquad \text{for } j = 1, n_\mathrm{s} \tag{2.62}$$

$$0 = T_j^\mathrm{V} - T_j^\mathrm{L} \qquad \text{for } j = 1, n_\mathrm{s} \tag{2.63}$$

$$0 = \dot{H}_{j+1}^\mathrm{V} + \dot{H}_{j-1}^\mathrm{L} - \dot{H}_j^\mathrm{V} - \dot{H}_j^\mathrm{L} \qquad \text{for } j = 1, n_\mathrm{s} \tag{2.64}$$

$$0 = \dot{N}_{i,j+1}^\mathrm{V} + \dot{N}_{i,j-1}^\mathrm{L} - \dot{N}_{i,j}^\mathrm{V} - \dot{N}_{i,j}^\mathrm{L} \qquad \text{for } j = 1, n_\mathrm{s},\ i = 1, ..., n_\mathrm{c} \tag{2.65}$$

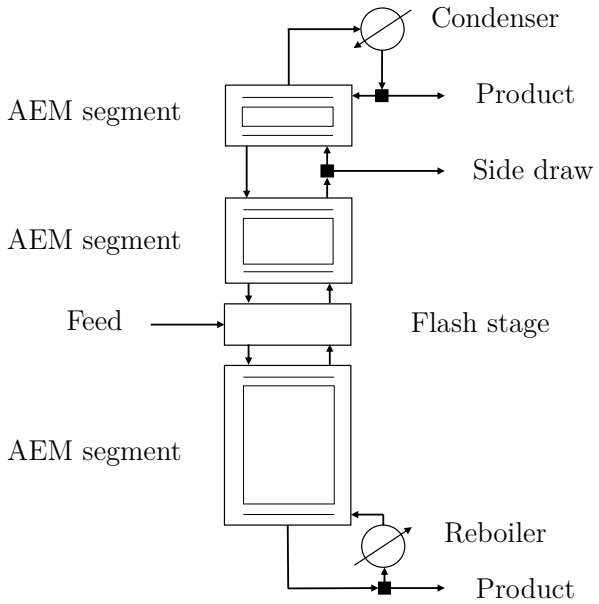

Figure 2.15: Example for column setup modelled with AEM segments.

$$0 = \varphi^{\mathrm{V}}_{i,j} \cdot \dot{N}^{\mathrm{V}}_{i,j} \cdot \sum_{i=1}^{n_\mathrm{c}} \dot{N}^{\mathrm{L}}_{i,j} - \varphi^{\mathrm{L}}_{i,j} \cdot \dot{N}^{\mathrm{L}}_{i,j} \cdot \sum_{i=1}^{n_\mathrm{c}} \dot{N}^{\mathrm{V}}_{i,j} \qquad \text{for } j = 1, n_\mathrm{s},\ i = 1, ..., n_\mathrm{c}. \tag{2.66}$$

With the streams leaving the equilibrium stages being determined, absorption and stripping factors for the top and bottom stage can be calculated:

$$0 = A_{i,j} \cdot \dot{N}^{\mathrm{V}}_{i,j} - \dot{N}^{\mathrm{L}}_{i,j} \qquad \text{for } j = 1, n_\mathrm{s},\ i = 1, ..., n_\mathrm{c} \tag{2.67}$$

$$0 = S_{i,j} \cdot \dot{N}^{\mathrm{L}}_{i,j} - \dot{N}^{\mathrm{V}}_{i,j} \qquad \text{for } j = 1, n_\mathrm{s},\ i = 1, ..., n_\mathrm{c}. \tag{2.68}$$

The component molar flows of streams SV_2 and $\mathsf{SL}_{\mathsf{n_s\text{-}1}}$ are calculated using the Edmister approximation in eq. (2.73) as well as the component material balance of the inner segment in eq. (2.74). Dew or bubble point conditions, respectively, are assumed for streams SV_2 and $\mathsf{SL}_{\mathsf{n_s\text{-}1}}$. Theoretically, if only one of these two streams was set to saturation temperature and the other stream was determined by the energy balance around the inner segment, even small inaccuracies in the component molar flow approximation in eq. (2.73) could lead to incorrect phase states of the other stream. Hence, streams SV_2 and $\mathsf{SL}_{\mathsf{n_s\text{-}1}}$ are determined by eqs. (2.69) to (2.74):

$$0 = p^{\mathrm{V}}_2 - p_{j=1} + \Delta p_\mathrm{s} \tag{2.69}$$

$$0 = p^{\mathrm{L}}_{n_\mathrm{s}-1} - p_{j=1} + (n_\mathrm{s} - 2) \cdot \Delta p_\mathrm{s} \tag{2.70}$$

$$0 = T^{\mathrm{V}}_2 - T^{\mathrm{V,dew}}_2 \tag{2.71}$$

$$0 = T^{\mathrm{L}}_{n_\mathrm{s}-1} - T^{\mathrm{L,bub}}_{n_\mathrm{s}-1} \tag{2.72}$$

$$0 = \dot{N}^{\mathrm{V}}_{i,2} - \phi_{\mathrm{A},i} \cdot \dot{N}^{\mathrm{V}}_{i,n_\mathrm{s}} - (1 - \phi_{\mathrm{S},i}) \cdot \dot{N}^{\mathrm{L}}_{i,1} \qquad \text{for } i = 1, ..., n_\mathrm{c} \tag{2.73}$$

$$0 = \dot{N}^{\mathrm{V}}_{i,n_\mathrm{s}} + \dot{N}^{\mathrm{L}}_{i,1} - \dot{N}^{\mathrm{V}}_{i,2} - \dot{N}^{\mathrm{L}}_{i,n_\mathrm{s}-1} \qquad \text{for } i = 1, ..., n_\mathrm{c}. \tag{2.74}$$

The correct determination or approximation of the performance factors $\phi_{\mathrm{A},i}$ and $\phi_{\mathrm{S},i}$ is not obvious. Two different ways to determine $\phi_{\mathrm{A},i}$ and $\phi_{\mathrm{S},i}$ based on effective absorption and/or effective stripping factors are considered.

AEM without performance factor correction (AEM1) The approximation of the effective factors Ae_i and Se_i which has been proposed by Edmister (Edmister 1957, Edmister 1943) is shown in eqs. (2.75) and (2.76). These equations are derived for a column segment comprising two equilibrium stages. They are applicable to column segments with several stages, if the effective factors are functions of the top and bottom conditions only and do not depend on the number of stages. Performance factors $\phi_{\mathrm{A},i}$ and $\phi_{\mathrm{S},i}$ are determined as given in eqs. (2.77) and (2.78):

$$Ae_i = \sqrt{A_{i,n_\mathrm{s}}(A_{i,1} + 1) + 0.25} - 0.5 \qquad \text{for } i = 1, ..., n_\mathrm{c} \tag{2.75}$$

$$Se_i = \sqrt{S_{i,1}(S_{i,n_\mathrm{s}} + 1) + 0.25} - 0.5 \qquad \text{for } i = 1, ..., n_\mathrm{c} \tag{2.76}$$

$$\phi_{\mathrm{A},i} = \frac{Ae_i - 1}{Ae_i^{(n_\mathrm{s}-2)+1} - 1} \qquad \text{for } i = 1, ..., n_\mathrm{c} \tag{2.77}$$

$$\phi_{\mathrm{S},i} = \frac{Se_i - 1}{Se_i^{(n_\mathrm{s}-2)+1} - 1} \qquad \text{for } i = 1, ..., n_\mathrm{c}. \tag{2.78}$$

AEM with performance factor correction (AEM2) As described above, stream $\mathsf{SV_2}$ is assumed to be at its dew point and stream $\mathsf{SL_{n_s\text{-}1}}$ is assumed to be at its bubble point. This guarantees correct phase states in terms of stream $\mathsf{SV_2}$ being gaseous and stream $\mathsf{SL_{n_s\text{-}1}}$ being liquid. However, an error in the energy balance $\Delta\dot{H}_\mathrm{err}$ around the inner segment occurs in case of an inaccurate approximation of the component molar flows of streams $\mathsf{SV_2}$ and/or $\mathsf{SL_{n_s\text{-}1}}$:

$$\Delta\dot{H}_\mathrm{err} = \dot{H}^{\mathrm{V}}_{n_\mathrm{s}} + \dot{H}^{\mathrm{L}}_{1} - \dot{H}^{\mathrm{V}}_{2} - \dot{H}^{\mathrm{L}}_{n_\mathrm{s}-1}. \tag{2.79}$$

The value of $\Delta\dot{H}_\mathrm{err}$ can be related to the deviation between MESH model and shortcut model. Hence, $|\Delta\dot{H}_\mathrm{err}|$ is minimised by correcting either performance factors $\phi_{\mathrm{A},i}$ to $\phi^{\mathrm{corr}}_{\mathrm{A},i}$ as given in eqs. (2.80) to (2.83) (option 1) or performance factors $\phi_{\mathrm{S},i}$ to $\phi^{\mathrm{corr}}_{\mathrm{S},i}$ as given in eqs. (2.84) to (2.87) (option 2). The choice between correcting $\phi_{\mathrm{A},i}$ or $\phi_{\mathrm{S},i}$ is based on numerical considerations. The performance factors with fewer values at the limits of definition range $0 \leq \phi_{\mathrm{A},i}, \phi_{\mathrm{S},i} \leq 1$ are favoured for correction since they can be corrected to lower values (≥ 0) and higher values (≤ 1) equally.

Option 1:

$$\phi_{\mathrm{A},i}^{\mathrm{corr}} = \phi_{\mathrm{A},i} \cdot b_{\mathrm{A}} \left(\frac{T_i^{\mathrm{sat}}}{T_{\mathrm{av}}^{\mathrm{sat}}} \right)^{(c_{\mathrm{A}} \cdot n_{\mathrm{s}})} \qquad \text{with } b_{\mathrm{A}} \in \mathbb{R}_0^+, c_{\mathrm{A}} \in \mathbb{R}, \text{ for } i = 1, ..., n_{\mathrm{c}} \tag{2.80}$$

$$\min_{b_{\mathrm{A}} \in \mathbb{R}_0^+, c_{\mathrm{A}} \in \mathbb{R}} |\Delta \dot{H}_{\mathrm{err}}| \tag{2.81}$$

$$\text{s. t. } 0 \leq \phi_{\mathrm{A},i}^{\mathrm{corr}} \leq 1 \qquad \text{for } i = 1, ..., n_{\mathrm{c}} \tag{2.82}$$

$$0 \leq \phi_{\mathrm{S},i} \leq 1 \qquad \text{for } i = 1, ..., n_{\mathrm{c}}. \tag{2.83}$$

Option 2:

$$\phi_{\mathrm{S},i}^{\mathrm{corr}} = \phi_{\mathrm{S},i} \cdot b_{\mathrm{S}} \left(\frac{T_i^{\mathrm{sat}}}{T_{\mathrm{av}}^{\mathrm{sat}}} \right)^{(c_{\mathrm{S}} \cdot n_{\mathrm{s}})} \qquad \text{with } b_{\mathrm{S}} \in \mathbb{R}_0^+, c_{\mathrm{S}} \in \mathbb{R}, \text{ for } i = 1, ..., n_{\mathrm{c}} \tag{2.84}$$

$$\min_{b_{\mathrm{S}} \in \mathbb{R}_0^+, c_{\mathrm{S}} \in \mathbb{R}} |\Delta \dot{H}_{\mathrm{err}}| \tag{2.85}$$

$$\text{s. t. } 0 \leq \phi_{\mathrm{A},i} \leq 1 \qquad \text{for } i = 1, ..., n_{\mathrm{c}} \tag{2.86}$$

$$0 \leq \phi_{\mathrm{S},i}^{\mathrm{corr}} \leq 1 \qquad \text{for } i = 1, ..., n_{\mathrm{c}}. \tag{2.87}$$

Scalar b_{A} in eq. (2.80) or b_{S} in eq. (2.84) is determined so that $|\Delta \dot{H}_{\mathrm{err}}|$ is minimised. Quotient $\frac{T_i^{\mathrm{sat}}}{T_{\mathrm{av}}^{\mathrm{sat}}}$ is a weighting term and takes the components' relative volatilities into account. Exponents $(c_{\mathrm{A}} \cdot n_{\mathrm{s}})$ and $(c_{\mathrm{S}} \cdot n_{\mathrm{s}})$ are used to specify the influence of quotient $\frac{T_i^{\mathrm{sat}}}{T_{\mathrm{av}}^{\mathrm{sat}}}$ on the corrected performance factors. They include the number of column stages n_{s} because n_{s} is not considered in the determination of the effective factors Ae_i and Se_i. The influence of n_{s} is damped by factor c_{A} or c_{S}, respectively. The forms $\left(\frac{T_i^{\mathrm{sat}}}{T_{\mathrm{av}}^{\mathrm{sat}}}\right)^{(c_{\mathrm{A}} \cdot n_{\mathrm{s}})}$ and $\left(\frac{T_i^{\mathrm{sat}}}{T_{\mathrm{av}}^{\mathrm{sat}}}\right)^{(c_{\mathrm{S}} \cdot n_{\mathrm{s}})}$ represent general increasing product purification with increasing numbers of stages n_{s}. Exponent $(c_{\mathrm{A}} \cdot n_{\mathrm{s}})$ in eq. (2.80) or exponent $(c_{\mathrm{S}} \cdot n_{\mathrm{s}})$ in eq. (2.84) can be – but does not have to be – tailored to a separation problem.

AEM with simplified performance factor correction for air separation (AEM2-AS)
Option 1 for performance factor correction is applied to an air separation example and simplified with respect to the separation task. Factor c_{A} can be expressed by:

$$c_{\mathrm{A}} = -y_{i,\mathrm{in}}. \tag{2.88}$$

The optimisation problem of minimising the absolute enthalpy error $|\Delta \dot{H}_{\mathrm{err}}|$ with $n_{\mathrm{c}}+1$ degrees of freedom is reduced to a problem with one degree of freedom. Hence, simpler adjusting algorithms can be used to determine b_{A} instead of optimisation solvers.

2.4.3 Validation

The AEM is validated with the help of two simple industrial process examples which are shown in Figure 2.16. The influence of the column number of stages n_s, the column top pressure p_{top}, reflux ratio r_{rf} and reboil ratio r_{rb} on the AEM results is evaluated by systematic variation and comparison to corresponding MESH results. The processes are modelled using the AEM in analogy to Figure 2.15.

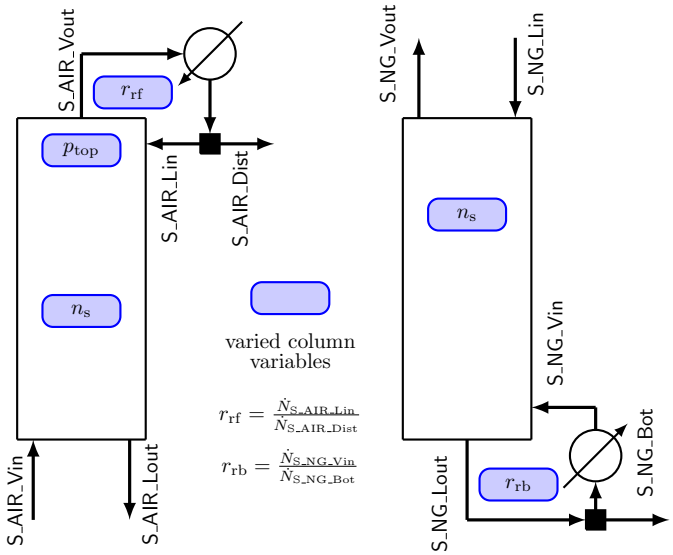

Figure 2.16: Air separation (left) and natural gas (right) process example for the evaluation of the AEM.

The feed to the air separation and the feed to the natural gas process example are specified by:

$$\text{S\_AIR\_Vin}: \quad T = 100\,\text{K},\ p = p_{bot},$$

$$y_{N_2} = 0.7812,\ y_{Ar} = 0.0093,\ y_{O_2} = 0.2095.$$

$$\text{S\_NG\_Lin}: \quad T = T^{bub},\ p = 55\,\text{bar},$$

$$y_{N_2} = 0.014,\ y_{CO_2} = 0.716,\ y_{CH_4} = 0.265,\ y_{C_2H_6} = 0.005.$$

Model validation: AEM with effective absorption factors fitted to MESH results
In theory, the AEM provides correct results, if correct effective factors are included. To validate the AEM, effective absorption factors Ae_i are defined by correlations fitted to MESH-based results and included in the AEM. For the air separation process example as shown in Figure 2.16, the fit functions $Ae_{i,fit}(v_1, v_2, v_3)$ contain 48 simultaneously fitted parameters $c_{jkl,i}$ with $i = 1, ..., n_c$, $j = 1, ..., 4$, $k = 1, ..., 4$, and $l = 1, ..., 4$:

$$Ae_{i,fit} = c_{1,i} \cdot v_1^3 + c_{2,i} \cdot v_1^2 + c_{3,i} \cdot v_1 + c_{4,i} \tag{2.89}$$

$$c_{j,i} = c_{j1,i} \cdot v_2^3 + c_{j2,i} \cdot v_2^2 + c_{j3,i} \cdot v_2 + c_{j4,i} \tag{2.90}$$

$$c_{jk,i} = c_{jk1,i} \cdot v_3^3 + c_{jk2,i} \cdot v_3^2 + c_{jk3,i} \cdot v_3 + c_{jk4,i}. \tag{2.91}$$

Based on these fit functions, the performance factors are determined by:

$$\phi_{\mathrm{A},i} = \frac{Ae_{i,\mathrm{fit}} - 1}{Ae_{i,\mathrm{fit}}^{(n_\mathrm{s}-2)+1} - 1} \qquad \text{for } i = 1, ..., n_\mathrm{c} \tag{2.92}$$

$$\phi_{\mathrm{S},i} = \Pi_{\mathrm{A},i} \cdot \phi_{\mathrm{A},i} = Ae_{i,\mathrm{fit}}^{n_\mathrm{s}-2} \cdot \frac{Ae_{i,\mathrm{fit}} - 1}{Ae_{i,\mathrm{fit}}^{(n_\mathrm{s}-2)+1} - 1} \qquad \text{for } i = 1, ..., n_\mathrm{c}. \tag{2.93}$$

The fit functions $Ae_{\mathrm{i,fit}}(n_\mathrm{s}, p_\mathrm{top}, r_\mathrm{rf})$ for $i = \mathrm{N_2}$, Ar, $\mathrm{O_2}$ represent the effective absorption factors Ae_i from the MESH solution with an accuracy of ±1%. The resulting parity plots in Figure 2.17 compare component molar flows in product stream S_AIR_Dist as calculated by the MESH model ($\dot{N}_{i,\mathrm{MESH}}$) and by the AEM including the fit functions $Ae_{\mathrm{i,fit}}(n_\mathrm{s}, p_\mathrm{top}, r_\mathrm{rf})$ ($\dot{N}_{i,\mathrm{AEM}}$). Relative deviations between $\dot{N}_{i,\mathrm{MESH}}$ and $\dot{N}_{i,\mathrm{AEM}}$ are plotted on the second axis.

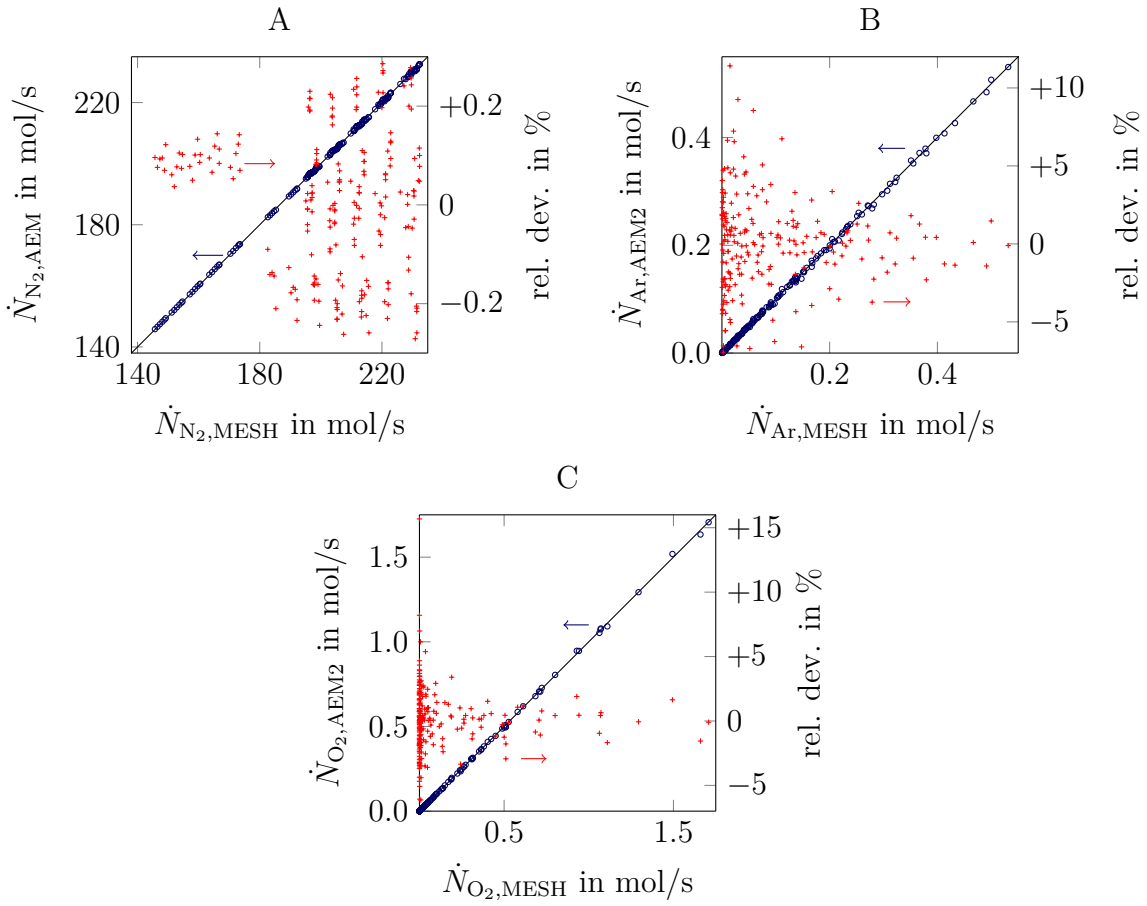

Figure 2.17: Results for AEM with effective absorption factors fitted to MESH solution in relation to MESH results (stream S_AIR_Dist).

Relative deviations vary between 2% and −2% for the nitrogen molar flow in the column top product S_AIR_Dist. For argon and oxygen, relative deviations vary between 15% and −5%. Relative deviations are largest for very small component molar flows. Hence, the accuracy of the AEM with fitted effective absorption factors is sufficient.

In Figure 2.18, trends for the relative component molar flows $\dot{N}_{\mathrm{N_2,rel}}$ and $\dot{N}_{\mathrm{O_2,rel}}$ in stream S_AIR_Dist for the AEM with fitted $Ae_{\mathrm{i,fit}}(n_{\mathrm{s}}, p_{\mathrm{top}}, r_{\mathrm{rf}})$ are plotted against the column variables n_{s}, p_{top}, and r_{rf}. The relative molar flows are defined by eqs. (2.2) and (2.3).

If correct values for the effective absorption performance factors Ae_i are included, AEM results are accurate over a wide operating range (see Figure 2.17) and depend on the column variables in exactly the same way as MESH-based results (see Figure 2.18). Hence, the AEM is applicable in process optimisation as a shortcut model, if the approximation of the effective factors is suitable. Since fitting the effective absorption factors is inefficient, new approaches are developed. This means that the AEM provides sufficient derivative information making it applicable in gradient-based process optimisation.

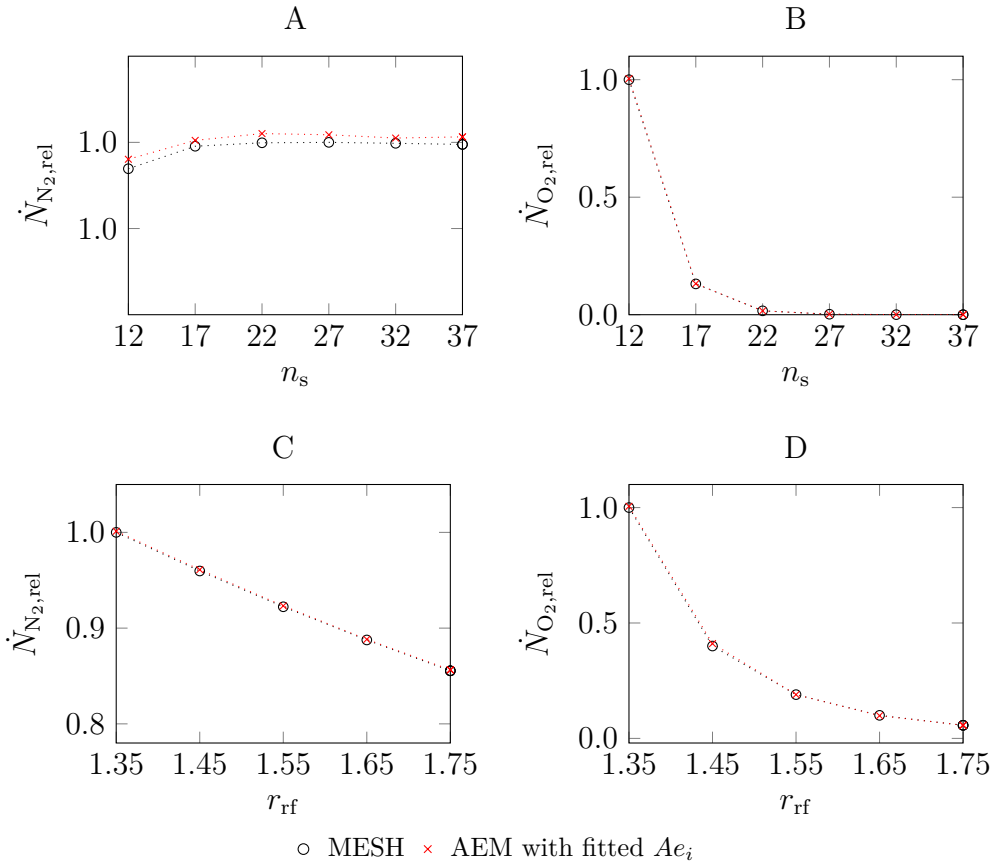

Figure 2.18: AEM with fit functions for Ae_i: $\dot{N}_{\mathrm{N_2,rel}}$ and $\dot{N}_{\mathrm{O_2,rel}}$ in stream S_AIR_Dist in dependence of n_{s} and r_{rf}. Plots A, B: $p_{\mathrm{top}} = 4.5\,\mathrm{bar}$, $r_{\mathrm{rf}} = 1.55$; plots C, D: $n_{\mathrm{s}} = 22$, $p_{\mathrm{top}} = 4.5\,\mathrm{bar}$.

AEM1 and AEM2 In Figure 2.19, three-dimensional plots for $n_s = 17$ give an overview of absolute and relative deviations of the AEM1 results from the MESH results for the component molar flows of N_2, Ar, and O_2 in stream S_AIR_Dist. The AEM1 meets the MESH results for certain combinations of p_{top} and r_{rf}. However, relative deviations for Ar and O_2 can increase up to +967% and +1 501% for low pressures and high reflux ratios. The relative deviations become more severe for higher stage numbers n_s.

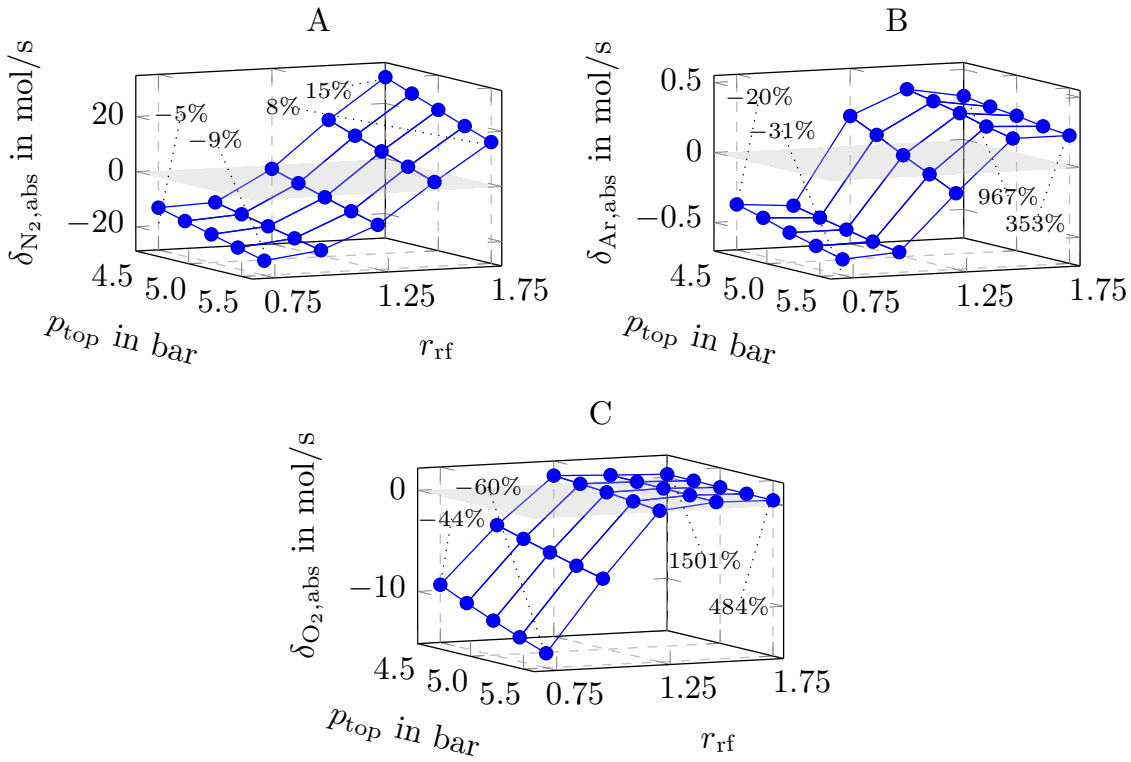

Figure 2.19: AEM1: absolute and relative deviations for stream S_AIR_Dist ($n_s = 17$).

For the air separation process example, Figure 2.20 shows AEM1, AEM2, AEM2-AS and MESH results for the N_2 and O_2 relative molar flows $\dot{N}_{N_2,rel}$ and $\dot{N}_{O_2,rel}$ in stream S_AIR_Dist in dependence of the variables n_s, p_{top}, and r_{rf}. Significantly different trends for the AEM1 and MESH model are shown in the plots of $\dot{N}_{N_2,rel}$ against n_s and $\dot{N}_{O_2,rel}$ against p_{top}. The AEM1 describes a contrary influence of n_s on $\dot{N}_{N_2,rel}$ and of p_{top} on $\dot{N}_{O_2,rel}$. In the remaining plots, similar trends between MESH and AEM1 results are observed. However, slopes and values for the $\dot{N}_{N_2,rel}$ and $\dot{N}_{O_2,rel}$ data point series are different for the AEM1 and MESH model in several cases.

In contrast to the AEM1, the AEM2 and the MESH-based model feature similar dependencies between results and column variables. Plots for AEM2-AS refer to the semi-empirical air separation correction approach as given in eq. (2.88) and plots the AEM2 to the general correction approach as given in eqs. (2.80) to (2.83). The AEM2 with the semi-empirical correction approach provides more accurate trends depending

on the number of stages n_s and the column pressure p_{top}. The AEM2 with the general correction approach provides more accurate results depending on the reflux ratio r_{rf}.

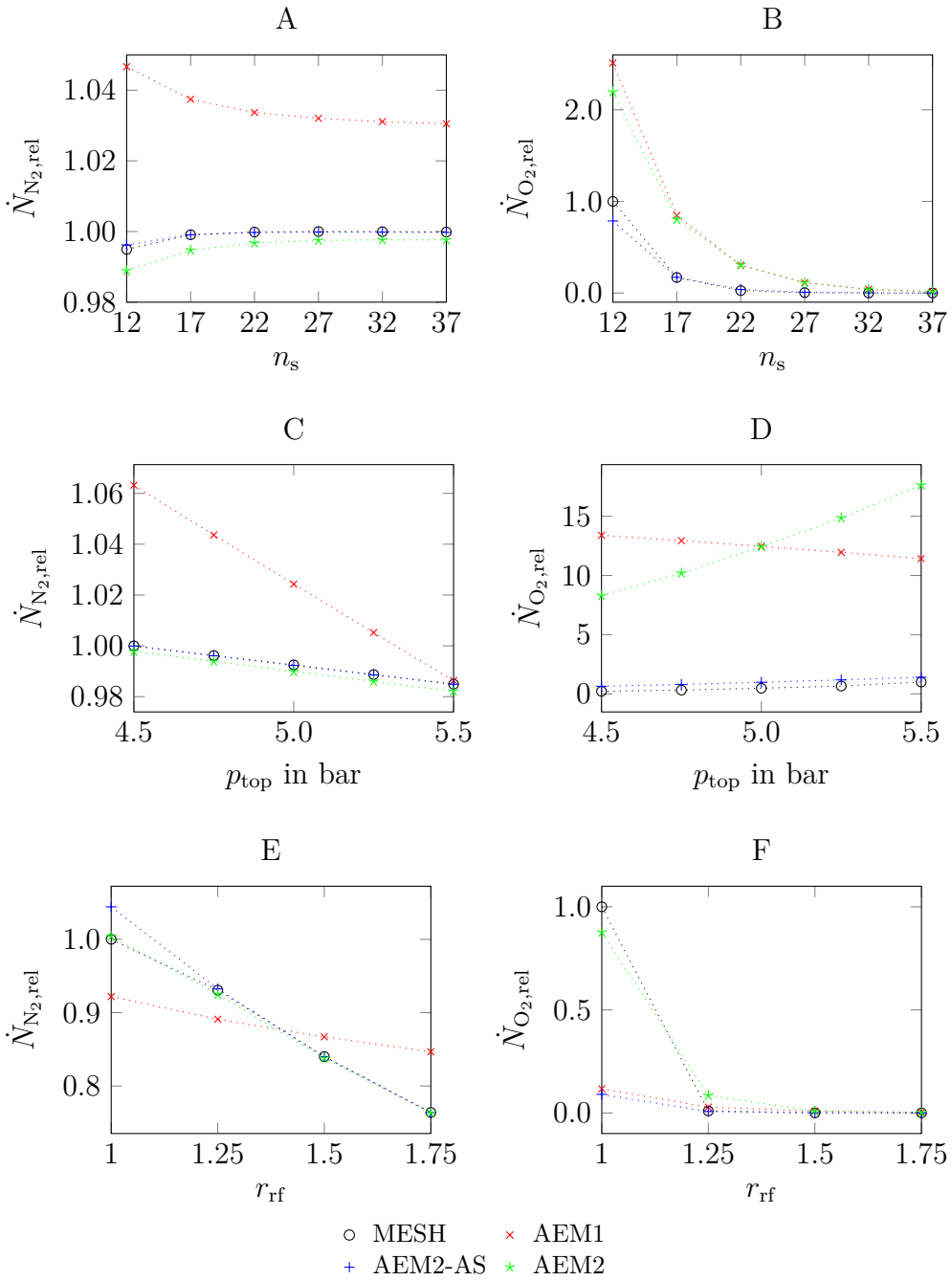

Figure 2.20: AEM1 and AEM2: $\dot{N}_{N_2,rel}$ and $\dot{N}_{O_2,rel}$ in stream S_AIR_Dist in dependence of n_s, p_{top}, and r_{rf}. Plots A, B: $p_{top} = 5.0\,bar$, $r_{rf} = 1.5$; plots C, D: $n_s = 27$, $r_{rf} = 1.5$; plots E, F: $n_s = 27$, $p_{top} = 5.0\,bar$.

For the natural gas process exmaple, dependencies of MESH, AEM1, and AEM2 results for the bottom product S_NG_Bot on column variables n_s and r_{rb} are compared in Figure 2.21. First, variable $c_S = 0.1$ is kept constant while b_S is optimised to minimise $|\Delta\dot{H}_{err}|$. Second, b_S and c_S are both simultaneously optimised to minimise $|\Delta\dot{H}_{err}|$.

Similar to the air separation process example, the AEM1 provides partly wrong dependencies between column variables and process results. While increasing the number of stages n_s increases the CO_2 molar flow in bottom product S_NG_Bot according to the MESH model, the AEM1 predicts less CO_2 molar flow for higher numbers of stages. The AEM2, however, is more accurate and provide correct dependencies. Using b_S and c_S to minimise $|\Delta\dot{H}_{err}|$ provides results for bottom product S_NG_Bot which are close to MESH-based results.

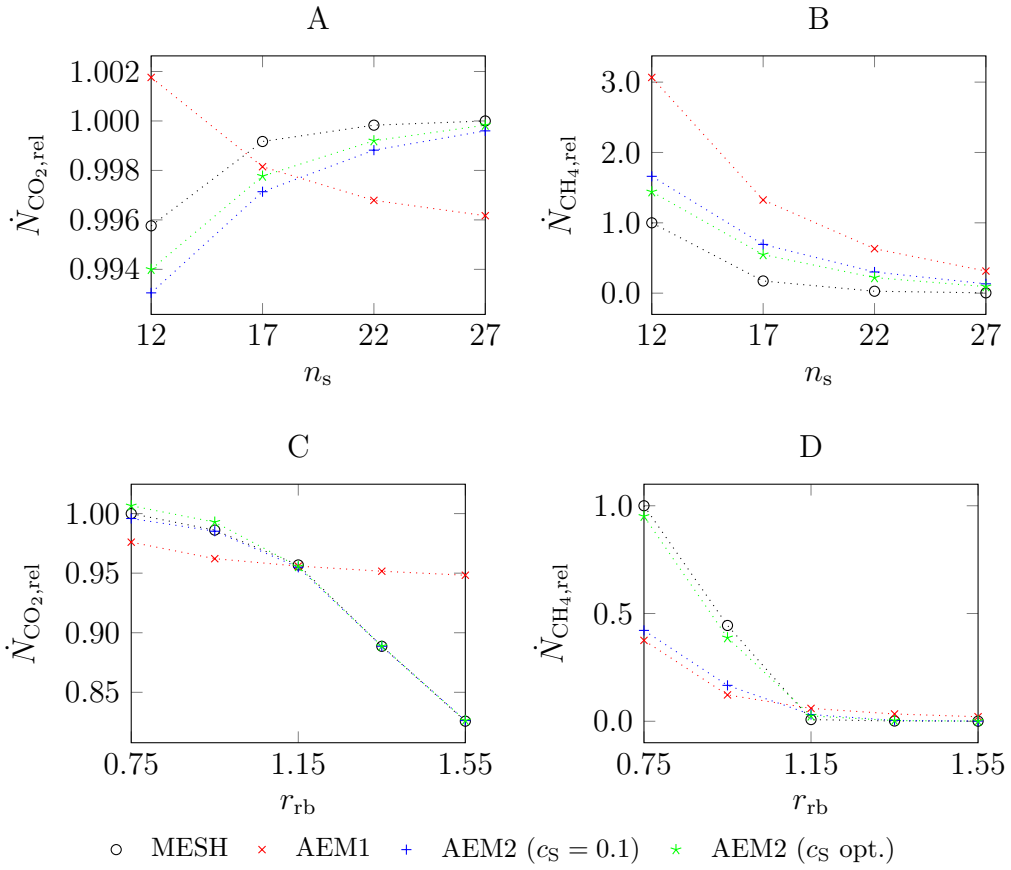

Figure 2.21: AEM1 and AEM2: $\dot{N}_{CO_2,rel}$ and $\dot{N}_{CH_4,rel}$ in stream S_NG_Bot in dependence of n_s and r_{rb}. Plots A, B: $p_{top} = 55\,bar$, $r_{rb} = 1.15$; plots C, D: $p_{top} = 55\,bar$, $n_s = 17$.

The AEM provides accurate results, if correct effective factors are used. This is shown by the model validation provided in Figures 2.17 and 2.18. Hence, the AEM is applicable in process optimisation, if a sufficiently accurate approximation for the effective performance factors can be found.

Application to two different process examples shows that the AEM1 without performance factor correction is not applicable in process optimisation because of two reasons. First, the relative deviations between the AEM1 and MESH results can become very large for certain column variable ranges. Very large relative deviations, however, are partly caused by numeric effects since they occur for low molar flows of

impurity components in pure product streams. Second, the dependencies of AEM1-based and MESH-based results on the model variables were found to be contrary in some cases. Above all, this is problematic in process optimisation when using gradient-based optimisation solvers.

Significant deviations and wrong trends of the AEM1 without performance factor correction are a result of the approximations for Ae_i and Se_i in eqs. (2.55) and (2.56) which are derived for a column segment with two stages originally by Edmister (1943). They are applicable to column segments with several stages, if the effective factors are functions of the top and bottom conditions only and do not depend on the number of stages (Edmister 1957). Occuring deviations can be explained considering these falsely made assumptions.

Performance factor correction in the AEM2 leads to very accurate results. Dependencies between column variables and AEM2 results are modelled correctly. The general approach for performance factor correction was proven to be successful for both the air separation and the natural gas process example. Further, the chosen correction approach can be tailored to the separation problem to maximise accuracy and simplify the optimisation problem as shown for the AEM-AS. In the semi-empirical correction approach, the influence of the number of stages on the correction is dampened differently for components with high and low concentrations in the system. However, the semi-empirical approach has to be determined by systematic variation and observation. In summary, the AEM2 with both general and semi-empirical performance factor correction satisfies all criterial for use in gradient-based process optimisation.

2.5 Hybrid surrogate models for columns

In the context of this thesis, hybrid surrogate models are used to represent stage-to-stage column models in process optimisation in order to save computational effort and simplify the optimisation problem. The hybrid surrogate models include physical equations such as mass and energy balances as well as simplifying assumptions and correlations based on data information. In the context of this thesis, input/output correlations of data information for column design are modelled by artifical neural networks (ANNs). Hybrid surrogate models for different columns are developed, validated, and finally used in process optimisation.

2.5.1 Literature

Data information can be used in different ways to facilitate process design. Bubel et al. (2021) use surrogate models based on artifical intelligence (AI) for unit operations in a flowsheet to avoid issues with convergence and to identify a starting solution. Schöneberger et al. (2021) suggest a workflow for building and validating machine learning (ML) models which are setup with data from flowsheet simulation with commercial software. The resulting hybrid models have shorter calculation times than

the detailed models of the commerical simulation software. Janus & Engell (2021) propose an extension of a global flowsheet optimisation framework with mechanisms for generation and rejection of process candidates. They describe an iterative workflow for process design which is coupled to the framework. Villarrubia et al. (2018) use ANNs to approximate the objective function in process optimisation. They use polynomials for the derivatives. Since ANNs are more commonly used in process engineering, Schweidtmann & Mitsos (2019) have developed an efficient method for deterministic global optimisation of problems with embedded ANNs to improve calculation times.

If data shall be included in a hybrid surrogate model for unit operations, equations to correlate the relation between input and output variables are needed. These equations can be obtained by applying different concepts. For simpler input/output correlations, fit functions such as linear, exponential, or polynomial expressions can be used. For more complex input/output correlations, two commonly used approaches for the development of surrogate models are Kriging interpolation and artificial neural networks.

According to Palmer & Realff (2002), both ordinary polynomials as well as the Kriging form can be used for fits based on small data sets. While ordinary polynomial fits provide non-interpolating smooth curves, the Kriging approach is used to interpolate data resulting in continuous curves passing through single values. Quirante et al. (2015), for example, replace distillation columns, divided wall columns, and extractive distillation columns by Kriging-based surrogate models in order to facilitate MINLP optimisation-based design of distillation columns and distillation sequences. However, according to Quirante et al. (2015), large sets of sampling points help improve the accuracy of a Kriging-based surrogate but result in large CPU times for calibrating the Kriging interpolation.

Exemplary publications discussing artificial neural networks being used in surrogate models for process design are given in the following. Fernandes (2006) applies ANNs to model Fischer-Tropsch synthesis. Since the Fischer-Tropsch reaction mechanism is still not fully understood, an artificial neural network was derived from experimental data and used as a surrogate model for a slurry reactor. Operating conditions are inputs while conversion and product weight fractions are outputs of the ANN. Optimisation of hydrocarbon (diesel and gasoline) production was performed in terms of searching optimal operating conditions of the slurry reactor.

Peer et al. (2008) use ANNs to model membrane gas separation. They compare experimental data, results obtained with an ANN, which was trained to the experimental data, and results obtained with a first principles membrane model. In case of hard-to-model effects such as concentration polarisation and competitive sorption being more significant, simulation results obtained with the ANN were found to be more consistent with the experimental data than simulation results obtained with the first principles membrane model.

Henao & Maravelias (2011) propose a superstructure-based optimisation strategy with hybrid surrogate models replacing detailed models for unit operations. The

data-based part of the hybrid surrogate models is derived from simulation data with detailed models. Taking advantage of the partial linearity of the detailed models, linear equations such as mass balances and hydraulics from the detailed models are included in the hybrid surrogate models. Finally, the hybrid surrogate models can be incorporated in equation oriented simulation and optimisation frameworks. This approach can provide model formulations including only one type of nonlinearity giving rise to the development of special-purpose solution algorithms.

Pirrung et al. (2017) use surrogate models in a superstructure to optimise biopurification sequences including three distinct forms of chromatography: anion exchange chromatography, cation exchange chromatography, and hydrophobic interaction chromatography. Computationally expensive mechanistic models are used to generate data. The ANN is trained to that data so that it can predict the yield and concentration of all proteins (outputs) based on operating conditions (inputs). The ANNs are used in global optimisation to provide starting points for subsequent local optimisation with mechanistic models.

2.5.2 Artificial neural network modelling

ANNs are used for approximating input/output correlations of data sets in the context of this thesis since the available data is extensive and finding fit functions to sufficiently represent the data information is challenging. Further, ANN training is automatable and potentially very accurate.

Artificial neurons Artifical neurons as shown in Figure 2.22 are inspired by biological neurons. They can receive, process, and transmit signals. Inputs $v_{\text{in},i}$ are weighted with connection parameters $w_{i,j}$ and added up to transfer function $v_{\Sigma,j}$ as given by eq. (2.94). Connections may be excitatory ($w_{i,j} > 0$), inhibitory ($w_{i,j} < 0$), or irrelevant ($w_{i,j} = 0$). The neuron bias b_j for the neuron is considered by an additional input $v_{\text{in},n_{\text{in}}+1} = +1$ and connection parameter $w_{n_{\text{in}}+1,j}$. The bias provides the neuron with a trainable constant value which acts like a threshold for the neuron being of positive or of negative weight:

$$v_{\Sigma,j} = \sum_{i=1}^{n_{\text{in}}} w_{i,j} \cdot v_{\text{in},i} + b_j = \sum_{i=1}^{n_{\text{in}}+1} w_{i,j} \cdot v_{\text{in},i}. \tag{2.94}$$

As shown in eq. (2.95), the neuron output v_j is obtained by processing transfer function $v_{\Sigma,j}$ with an appropriate activation function f (Graupe 2013, Mehrotra et al. 2000, Hertz et al. 1991):

$$v_j = f(v_{\Sigma,j}). \tag{2.95}$$

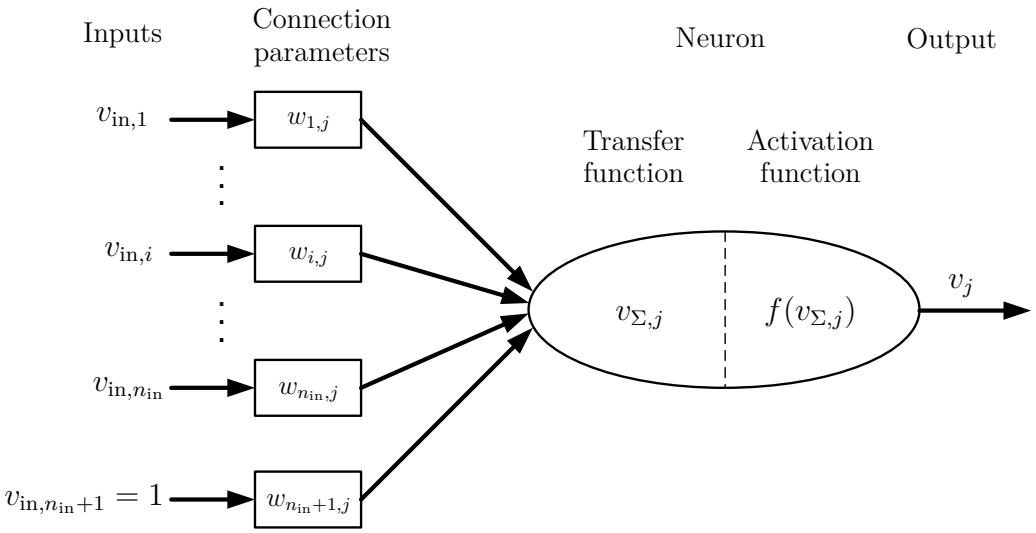

Figure 2.22: Artificial neuron.

Activation function Activation functions describe how the neuron output v_j is calculated based on the summarised neuron input $v_{\Sigma,j}$. The bias included in $v_{\Sigma,j}$ allows to shift the activation function towards smaller or larger values of $v_{\Sigma,j}$. In Figure 2.23, common activation functions are shown. The corresponding equations are given in eqs. (2.96) to (2.101). With regard to biological neurons, activation functions can be step functions (e.g., eq. (2.96) and eq. (2.97)), linear functions (e.g., eq. (2.98)), sigmoid functions (e.g., eq. (2.99) and eq. (2.100)), or radial basis functions (e.g., eq. (2.101)) (LeCun et al. 1998, Graupe 2013, Duch & Jankowski 2001). An ANN can be based on activation functions which are only of one type (homogeneous function networks) or on mixed activation functions (heterogeneous function networks) (Duch & Jankowski 2001). Apart from the activation functions given in eqs. (2.96) to (2.101), numerous alternative approaches can be found in literature. Duch & Jankowski (2001) provide a broad overview of known activation functions as well as guidelines for the choice of activation functions.

Binary step function A: $$f(v_{\Sigma,j}) = \begin{cases} 0 & \text{for } v_{\Sigma,j} \leq 0 \\ 1 & \text{for } v_{\Sigma,j} > 1 \end{cases} \tag{2.96}$$

Sign function B: $$f(v_{\Sigma,j}) = \begin{cases} +1 & \text{for } v_{\Sigma,j} > 0 \\ 0 & \text{for } v_{\Sigma,j} = 0 \\ -1 & \text{for } v_{\Sigma,j} < 0 \end{cases} \tag{2.97}$$

Identity function C: $$f(v_{\Sigma,j}) = v_{\Sigma,j} \tag{2.98}$$

Logistic function D: $f(v_{\Sigma,j}) = \dfrac{1}{1+\mathrm{e}^{-v_{\Sigma,j}}}$ (2.99)

Hypbolic tangent E: $f(v_{\Sigma,j}) = \tanh(v_{\Sigma,j})$ (2.100)

Gaussian function F: $f(v_{\Sigma,j}) = \mathrm{e}^{-{v_{\Sigma,j}}^2}$ (2.101)

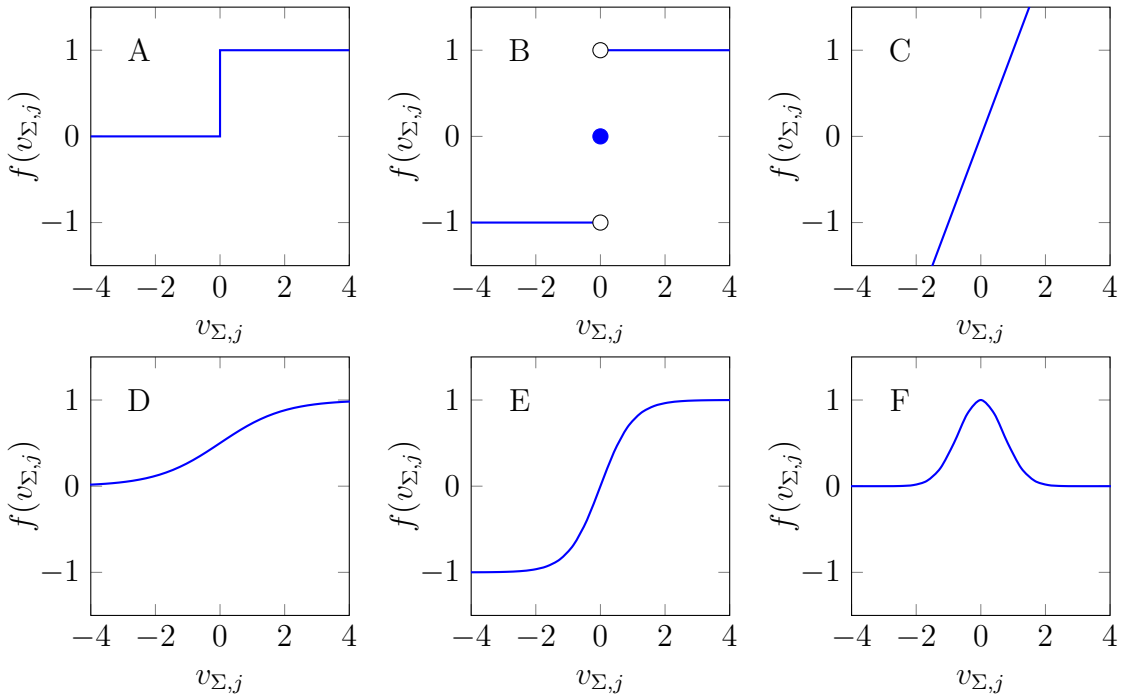

Figure 2.23: Activation functions in artificial neurons

Step functions allow high speed computation and easy realisation in the hardware but have discontinuous derivatives preventing the use of gradient-based training algorithms. Sigmoid activation functions, however, are contiuously differentiable and introduce non-linear properties into neural networks. Sigmoid functions like the hyperbolic tangent, which are symmetric about the origin, offer better convergence properties since their outputs (inputs for the subsequent layer) are more likely to average around zero. Also, it is important for the neural networks capabilities that the sigmoid function is bounded. Further, radial basis functions such as the Gaussian function are commonly used in multi-layer feed forward networks. They are radially symmetric and provide a localised response to the input (Chen & Chen 1995, LeCun et al. 1998, Duch & Jankowski 2001). With regard to the practice of multi-layer neural network backpropagation training, choosing a hyperbolic tangent function is recommended by LeCun et al. (1998).

Artificial neural network architectures Artificial neurons with appropriate activation functions are arranged into network architectures which are inspired by biological neural systems. Different network architectures serve different purposes and are trained

differently. Main architectures can be divided into single-layer feed forward networks, multi-layer feed forward networks, recurrent networks, and mesh networks. Further information to these network architectures is provided in Table A.2 in the appendix.

In Figure 2.24, a multi-layer feed forward neural network with two hidden layers and an output layer is pictured. Two conventions for counting the number of layers can be found in literature. Some authors consider the input terminals as an additional layer (e.g., DA SILVA ET AL. 2017). Some authors do not count the inputs as a network layer (e.g., HERTZ ET AL. 1991). Within this thesis, the inputs are not counted as a network layer. The connections between the neurons in a feed forward network are unidirectional.

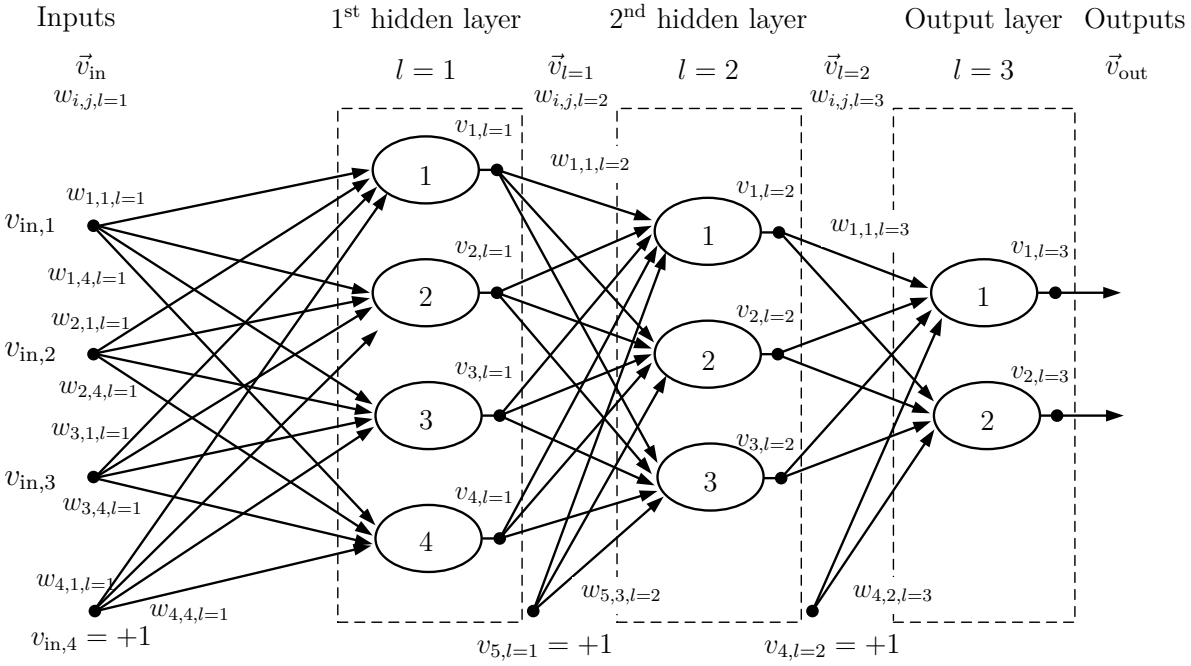

Figure 2.24: Feed forward neural network with inputs, connection weights, bias, and outputs.

$\vec{v}_{\text{in}}$ is the input vector. $\vec{v}_l$ is the output vector of hidden layer l. $\vec{v}_{\text{out}}$ is the output vector of the network.

$$\vec{v}_{\text{in}} = (v_{\text{in},1},\ v_{\text{in},2},\ v_{\text{in},3},\ 1)^{\text{T}} \tag{2.102}$$

$$\vec{v}_{l=1} = (f(\sum_{i=1}^{4} w_{i,1,l=1} \cdot v_{\text{in},i}),\ f(\sum_{i=1}^{4} w_{i,2,l=1} \cdot v_{\text{in},i}) \tag{2.103}$$

$$f(\sum_{i=1}^{4} w_{i,3,l=1} \cdot v_{\text{in},i}), f(\sum_{i=1}^{4} w_{i,4,l=1} \cdot v_{\text{in},i}), 1)^{\text{T}} \tag{2.104}$$

$$\vec{v}_{l=2} = (f(\sum_{i=1}^{5} w_{i,1,l=2} \cdot v_{i,l=1}),\ f(\sum_{i=1}^{5} w_{i,2,l=2} \cdot v_{i,l=1}),\ f(\sum_{i=1}^{5} w_{i,3,l=2} \cdot v_{i,l=1}), 1)^{\text{T}} \tag{2.105}$$

$$\vec{v}_{l=3} = (f(\sum_{i=1}^{4} w_{i,1,l=3} \cdot v_{i,l=2}),\ f(\sum_{i=1}^{5} w_{i,2,l=3} \cdot v_{i,l=2}))^{\text{T}} = \vec{v}_{\text{out}} \tag{2.106}$$

Multi-layer feed forward neural networks are universal approximators. Cybenko (1989), Hornik et al. (1989), as well as Funahashi (1989) independently provide rigorous mathematical proof that a feed forward neural network with one hidden layer employing an arbitrary continuous sigmoidal activation function can approximate any multivariate continuous function. They state that any desired degree of approximation accuracy can be achieved, if a sufficient number of neurons is considered in the hidden layer.

Cybenko (1989), however, concedes that the required number of neurons in the hidden layer might be very large for many approximation problems. Lapedes & Farber (1988) show that two hidden layers are enough to solve most problems and that the approximation accuracy is determined by the number of neurons in each hidden layer.

Hertz et al. (1991) argue that modelling a feed forward network with more than two hidden layers can be of advantage and result in fewer needed neurons and speed up learning. Further, according to Hertz et al. (1991), some functions might not be learnable with two hidden layers, for example in case of occurring local minima. The number of hidden layers and the number of neurons included in these hidden layers depends on the complexity of the problem and on the quantity and quality of the available data set (da Silva et al. 2017).

2.5.3 Artificial neural network training

In the context of this thesis, the connection weights of feed forward neural networks are adapted so that the network output matches a given data set as well as possible. This training approach is known as supervised learning.

Procedure of backpropagation Single-layer and multi-layer feed forward neural networks as shown in Figure 2.24 are often trained with a backpropagation algorithm. The backprogation algorithm has been derived independently by Bryson & Ho (1969), Werbos (1974), Parker (1985), and Rumelhart et al. (1985). Extensive work on backpropagation has been done by LeCun (e.g., LeCun 1985, LeCun 1986, LeCun 1988, LeCun et al. 1998).

The goal of backpropagation is to minimise the error measure E between the j-th data set output variable $v^k_{\mathrm{DS,out},j}$ and the corresponding j-th network output $v^k_{\mathrm{out},j}$:

$$E = \frac{1}{2} \sum_{k=1}^{n_{\mathrm{DS}}} \sum_{j=1}^{n_{\mathrm{out}}} \left(v^k_{\mathrm{DS,out},j} - v^k_{\mathrm{out},j} \right)^2 . \tag{2.107}$$

k is referring to one data set pattern, n_{DS} is the number of patterns in the data set. Minimisation of the error measure E by tuning the connection parameters $w_{i,j,l}$ is performed by gradient descent:

$$\Delta w_{i,j,l}(t) = -\eta \cdot \frac{\partial E}{\partial w_{i,j,l}}. \tag{2.108}$$

η is the learning rate (Riedmiller 1994). First, one data set pattern k is applied to the network input. If the connection parameters $w_{i,j,l}$ do not have values yet, they are randomly initialised. The input is propagated through the network in forward direction and the error for each neuron j in the output layer is determined. The errors for the neurons in the preceding layers are then determined in backwards direction. Finally, using the errors for the neurons in the network, the connection parameters $w_{i,j,l}$ are updated. The procedure is repeated for other data set patterns until training is stopped. Hertz et al. (1991) provide detailed information about the backpropagation procedure as described.

Adaptive approaches in backpropagation As given by eq. (2.108), the learning rate η scales the update of the connection parameters depending on the gradient of the error measure E. Smaller learning rates mean longer calculation times for the minimisation of error measure E. Larger learning rates possibly result in oscillations of the error measure E so that it does not converge to a desired minimum (LeCun et al. 1998, Riedmiller 1994). In Figure A.1 in the appendix, exemplary plots for different constant learning rates are shown.

According to LeCun et al. (1998), it is benefitial for convergence to give each connection weight its own learning rate and to have larger connection weights in lower layers compared to higher layers. While some training algorithms adapt learning rates automatically, the global dynamic learning rate can also be scheduled. The adapted learning rate is used to scale the weight step (Riedmiller 1994). One possibility is to define a start learning rate η_0 and decrease it based on a defined learning rate decay η_{dec}. The effective learning rate is defined by recursion:

$$\eta(t+1) = \eta(t) \cdot \eta_{\text{dec}} \tag{2.109}$$

$$\eta(t) = \eta_0 \cdot \eta_{\text{dec}}^t. \tag{2.110}$$

The learning rate decay η_{dec} is defined by the learning rate at the beginning of the training η_0, by the learning rate at the end of the training η_∞, and by the number of training epochs t_∞:

$$\eta_{\text{dec}} = \left(\frac{\eta_\infty}{\eta_0}\right)^{\frac{1}{t_\infty}}. \tag{2.111}$$

In Figure A.2 in the appendix, exemplary plots for different dynamic learning rates are shown. Further, the effective learning rate can be set to larger values without divergent oscillation in the gradient descent, if a momentum parameter $0 \leq \alpha \leq 1$ is applied (Plaut & Hinton 1987):

$$\Delta w_{i,j,l}(t+1) = -\eta \cdot \frac{\partial E}{\partial w_{i,j,l}} + \alpha \cdot \Delta w_{i,j,l}(t). \tag{2.112}$$

The momentum parameter is often defined by $\alpha = 0.9$. The derivative $\frac{\partial E}{\partial w_{i,j,l}}$ does not change significantly, if a plateau of the network error measure is reached and eq. (2.112) is reduced to (Hertz et al. 1991):

$$\Delta w_{i,j,l}(t+1) \approx \Delta w_{i,j,l}(t) = -\frac{\eta}{1-\alpha} \cdot \frac{\partial E}{\partial w_{i,j,l}}. \tag{2.113}$$

Hence, the idea is to accelarte the training progress by $\frac{1}{1-\alpha}$ without enhancing oscillations.

Data set preprocessing for backpropagation Thoughtful data set generation and preprocessing can improve training results considerably. According to LeCun et al. (1998), input variables should be independent since correlated inputs make the training problem harder to solve. Normalising inputs is of advantage since backpropagation convergence is likely to be faster, if the average of each input variable (over the whole data set) is close to zero. Further, it is advantageous, if the training set is shuffled for stochastic learning so that successive training examples are not similar (LeCun et al. 1998).

The data set is randomly divided into a training set and an evaluation data set. While the training set is used for neural network training, the evaluation set is used for error evaluation to estimate the generalisation capability (LeCun et al. 1998).

Assessment of training success Training success is evaluated for the training and the evaluation data set. The maximum error $\delta_{\max}$ and the network error δ_{net} are assessed. They are defined by:

$$\delta_{\max} = \max_k(E(k)) \tag{2.114}$$

$$\delta_{\text{net}} = \frac{E}{n_{\text{DS}} \cdot n_{\text{out}}}. \tag{2.115}$$

The definition of the error measure E is given in eq. (2.107). The network error δ_{net} is set in relation to the size of the data set and the number of output variables to make it comparable for the evaluation of different data sets.

2.5.4 Modelling: distillation column

In a natural gas sweetening process, CO_2 can be removed from natural gas by cryogenic distillation. In Figure 2.25, reboiled column T01 for cryogenic removal of CO_2 from a natural gas feed containing CO_2, N_2, CH_4, C_2H_6, and C_3H_8 is shown. While the column bottom product S_CO2 is CO_2 at specified grade, the column top product S_VAP2 is natural gas with significant remainings of CO_2. The process in Figure 2.25 is going to be integrated in a superstructure which is used to design a natural gas sweetening process. In the context of his internship, Huellen (2017) has trained different feed

forward networks to approximate the black box part of the column. The model has not been extended to a hybrid surrogate model.

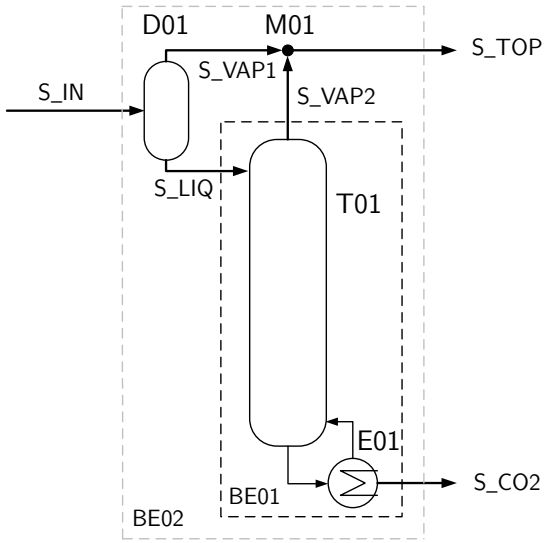

Figure 2.25: Flowsheet for the hybrid surrogate model of a reboiled distillation column for CO_2 separation.

Balance envelope There are two options to draw the balance envelope for a hybrid surrogate model representing the separation task in Figure 2.25. First, separator D01, column T01 and mixer M01 can be surrogated in one hybrid model (BE02). Second, the balance envelope of the hybrid surrogate model can be drawn around column T01 only (BE01). In this case, separator D01 and mixer M01 are modelled individually and connected to the hybrid surrogate model. Balance envelope BE01 is selected. This decision is based on advantages in data set generation explained in the paragraph for data set generation and preprocessing.

Input and output variables Input variables are pressure, temperature, and component molar flows of feed S_LIQ as well as the methane purity specification for CO_2 product S_CO2. Pressure $p_{\mathrm{S\_LIQ}}$ determines the column pressure. Output variables are pressure, temperature, and component molar flows of products S_VAP2 and S_CO2 as well as reboiler duty $\dot{Q}_{\mathrm{E01}}$. It is assumed that the complete N_2 molar flow entering the column in stream S_LIQ leaves the column in top product S_VAP2. Consequently, with a data set comprising the four output variables $\dot{N}_{\mathrm{CO_2,S\_VAP2}}$, $\dot{N}_{\mathrm{CH_4,S\_CO2}}$, $\dot{N}_{\mathrm{C_2H_6,S\_CO2}}$, $\dot{N}_{\mathrm{C_3H_8,S\_CO2}}$, and the component mass balance around column T01, all component molar flows of streams S_VAP2 and S_CO2 are determined.

Data set generation and preprocessing For the generation of the data set to be integrated in the hybrid surrogate model, pressure, temperature, and component molar

flows of stream S_IN are varied as listed in Table 2.5. Calculations are performed in UniSim® Design R451 using the provided detailed models for flash drums, mixers, and columns as well as Linde proprietary physical property data. The column is assumed to have 20 equilibrium stages since this was found to be sufficient in every operation point during the case study.

Table 2.5: Systematic variation of the process variables to create a data set including an input/output correlation of column T01 ($\dot{N}_{\mathrm{S\_IN}} = 100\,\mathrm{mol/s} = \mathrm{const}$, pressure drop in reboiler $\Delta p_{\mathrm{E01}} = 0.1\,\mathrm{bar}$, pressure drop per column stage $\Delta p_{\mathrm{s}} = 0.001\,\mathrm{bar}$).

Varied variable	Min	Max	Points	Spacing
$p_{\mathrm{S\_IN}}$	40 bar	55 bar	5	linear
$T_{\mathrm{S\_IN}}$	225 K	240 K	5	linear
$x_{\mathrm{CH_4,S\_CO2}}$	0.01	0.0001	5	logarithmic
$x_{\mathrm{N_2,S\_IN}}$	0.01	0.05	3	linear
$x_{\mathrm{C_2H_6,S\_IN}}$	0.01	0.05	3	linear
$x_{\mathrm{C_3H_8,S\_IN}}$	0.01	0.05	3	linear
$x_{\mathrm{CO_2,S\_IN}}$	0.40	0.80	4	linear

The systematic process variable variation as shown in Table 2.5 yields a data set with $n_{\mathrm{DS}} = 13500$ data set patterns. The obtained data set contains a correlation between the model's input variables and the output variables $\dot{N}_{\mathrm{CO_2,S\_VAP2}}$, $\dot{N}_{\mathrm{CH_4,S\_CO2}}$, $\dot{N}_{\mathrm{C_2H_6,S\_CO2}}$, and $\dot{N}_{\mathrm{C_3H_8,S\_CO2}}$. While pressure and temperature of stream S_IN and stream S_LIQ are equal, the component molar flows of stream S_LIQ are determined by the combination of pressure, temperature, and component molar flows of stream S_IN. Hence, the component molar flows of S_LIQ are varied over a wide range and can theoretically attain 13500 different values. This is the reason why the balance envelope of the hybrid surrogate model only includes column T01 and does not include separator D01 and mixer M01.

To eliminate the influence of the feed molar flow into the column, the feed component molar flows are transferred into molar fractions. Output component molar flows are expressed by split fractions given by:

$$\xi_{i,\mathrm{product}} = \frac{\dot{N}_{i,\mathrm{product}}}{\dot{N}_{i,\mathrm{feed}}}. \tag{2.116}$$

Further, input and output variables are logarithmised if necessary and normalised so that their values are within a range of -1 to 1. Normalised values are marked with

a tilde. The resulting preprocessed input and output variable vectors are given in eqs. (2.117) and (2.118).

$$\vec{v}_{\text{input}} = (\tilde{x}_{\text{CH}_4\text{,S\_CO2,log}},\ \tilde{p}_{\text{S\_LIQ}},\ \tilde{T}_{\text{S\_LIQ}},\ \tilde{x}_{\text{N}_2\text{,S\_LIQ}},\ \tilde{x}_{\text{CO}_2\text{,S\_LIQ}},\ \tilde{x}_{\text{CH}_4\text{,S\_LIQ}},\ \tilde{x}_{\text{C}_2\text{H}_6\text{,S\_LIQ}},\ \tilde{x}_{\text{C}_3\text{H}_8\text{,S\_LIQ}})^{\text{T}} \tag{2.117}$$

$$\vec{v}_{\text{output}} = \left(\tilde{\xi}_{\text{CO}_2\text{,S\_VAP2}},\ \tilde{\xi}_{\text{CH}_4\text{,S\_VAP2,log}},\ \tilde{\xi}_{\text{C}_2\text{H}_6\text{,S\_VAP2}},\ \tilde{\xi}_{\text{C}_3\text{H}_8\text{,S\_VAP2}}\right)^{\text{T}}. \tag{2.118}$$

ANN modelling and training As shown in eqs. (2.117) and (2.118), the data set includes eight input and four output variables. The structure of the used feed forward network and the selected activation functions are given in Table 2.6. The number of neurons in the first hidden layer is chosen to be 2.5 times the number of the input variables. The number of neurons in the second hidden layer is chosen to be 2.5 times the number of output variables. A feed forward network structure of 8-20-10-4 results in 434 connection parameters w_{ji} which have to be determined in the ANN training.

Table 2.6: Hybrid surrogate model for distillation column to separate CO_2 from sour natural gas: ANN modelling

n_{in}	Network	$l = 1$	$l = 2$	$l = 3$
8	Neurons $n_{\text{n},l}$	20	10	4
	Activation function $f(v_{\Sigma,j})$	$\tanh(v_{\Sigma,j})$	$\tanh(v_{\Sigma,j})$	$\text{lin}(v_{\Sigma,j})$

In Table 2.7, the training parameters are summarised. The training is performed in PyBrain (Schaul et al. 2010) using the provided backpropagation algorithm. It is divided into two training steps. The goal of the first training step is to get the ANN to learn the functional input/output correlation of the data set roughly and fast. In the second training step, the ANN is meant to learn the data set input/output correlation accurately.

Before the first training step, the data set (size $n_{\text{TDS}} = 13500$) is randomly split into a training data set and an evaluation data set in relation of 3:1 ($n_{\text{DS}} = 10125$, $n_{\text{EDS}} = 3375$). Data set elements which are assigned to either the training or the evaluation data set, remain in the assigned data set for both training steps. Hence, the evaluation data set is identical for both training steps. In the first training step, a reduced training data set is used. 20% of the data set elements of the actual training data set are randomly chosen so that $n_{\text{TDS}} = 2025$. In the second training step, the whole training data set with $n_{\text{TDS}} = 10125$ is used. The momentum is specified by $\alpha = 0.9$ in the first training step in order to achieve higher effective learning rates η_{eff} and hence speed up the training progress. For the second training step, the momentum is reduced to $\alpha = 0.1$ rendering the effective learning rate η_{eff} low enough to obtain

an accurate solution for the trained ANN. Training is performed several times and the best solution is selected to be integrated into the hybrid surrogate model.

Table 2.7: Hybrid surrogate model for distillation column to separate CO_2 from sour natural gas: ANN training parameters

	n_{TDS}	t_{start}	t_{end}	η_{start}	η_{end}	α
1st	2025	$t_0 = 0$	$t_1 = 20000$	$\eta(t_0) = 0.01$	$\eta(t_1) = 0.0031623$	0.9
2nd	10125	$t_2 = 20001$	$t_\infty = 40000$	$\eta(t_2) = 0.0031621$	$\eta(t_\infty) = 0.001$	0.1

Equations of the hybrid surrogate model The trained feed forward network is transferred into an algebraic set of equations as exemplarily shown in eqs. (2.102) to (2.106). The input vector $\vec{v}_{\mathrm{input}}$ into the feed forward network is given by eq. (2.117). The output vector $\vec{v}_{\mathrm{output}}$ contains the normalised variables as given in eq. (2.118).

After denormalising the output split variables $\tilde{\xi}_i$ to ξ_i and subsequently applying eq. (2.119) to the methane split fraction $\xi_{\mathrm{CH_4,S\_VAP2}}$, the component molar flows can be calculated as given by eq. (2.120):

$$\xi_{\mathrm{CH_4,S\_VAP2}} = 10^{\xi_{\mathrm{CH_4,S\_VAP2,log}}} \tag{2.119}$$

$$\dot{N}_{i,\mathrm{S\_VAP2}} = \xi_{i,\mathrm{S\_VAP2}} \cdot \dot{N}_{i,\mathrm{S\_LIQ}} \qquad \text{for } i = \mathrm{CO_2},\ \mathrm{CH_4},\ \mathrm{C_2H_6},\ \mathrm{C_3H_8}. \tag{2.120}$$

The component molar flows $\dot{N}_{i,\mathrm{S\_LIQ}}$ are known since they are part of the inlet into the hybrid surrogate model S_LIQ. With eq. (2.120) from the black box part of the hybrid surrogate model, eq. (2.121), and eq. (2.122), the component molar flows of both product streams S_VAP2 and S_CO2 are determined:

$$0 = \dot{N}_{\mathrm{N_2,S\_CO2}} \tag{2.121}$$

$$0 = \dot{N}_{i,\mathrm{S\_LIQ}} - \dot{N}_{i,\mathrm{S\_VAP2}} - \dot{N}_{i,\mathrm{S\_CO2}} \qquad \text{for } i = 1, ..., n_{\mathrm{c}}. \tag{2.122}$$

A linear pressure profile inside the column is assumed as given in eqs. (2.123) and (2.124). As shown in eqs. (2.125) and (2.126), the temperatures of the outlet streams S_VAP2 and S_CO2 are determined by dew and bubble point calculations, respectively. The reboiler duty $\dot{Q}_{\mathrm{E01}}$ is calculated by an energy balance around the column according to eq. (2.127):

$$0 = p_{\mathrm{S\_VAP2}} - p_{\mathrm{S\_LIQ}} \tag{2.123}$$

$$0 = p_{\mathrm{S\_CO2}} - p_{\mathrm{S\_LIQ}} + (n_{\mathrm{T01}} - 1) \cdot \Delta p_{\mathrm{s}} \tag{2.124}$$

$$0 = T_{\mathrm{S\_VAP2}} - T^{\mathrm{dew}}_{\mathrm{S\_VAP2}} \tag{2.125}$$

$$0 = T_{\mathrm{S\_CO2}} - T^{\mathrm{bub}}_{\mathrm{S\_CO2}} \tag{2.126}$$

$$0 = \dot{Q}_{\mathrm{E01}} + \dot{H}_{\mathrm{S\_LIQ}} - \dot{H}_{\mathrm{S\_VAP2}} - \dot{H}_{\mathrm{S\_CO2}}. \tag{2.127}$$

To sum up, the implemented hybrid surrogate model includes

- algebraic equations which model the trained feed forward artificial neural network (black box part), and
- physical equations for mass balances, a linear pressure profile along the column height, dew and bubble point calculations for the outlet streams, and an energy balance as given in eqs. (2.121) to (2.127) (white box part).

2.5.5 Validation: distillation column

The hybrid surrogate model as described in section 2.5.4 is evaluated with respect to its applicability in process optimisation. Results obtained with the hybrid surrogate model as implemented in OPTISIM® are compared to results obtained with a detailed stage-to-stage column model in UniSim® Design R451 which is referred to as a MESH-based model (based on material balances, equilibrium conditions, summation rules, and heat balances) in the following. The hybrid surrogate model is referred to as HYSU. Linde physical property data is used in both simulation environments.

Figure 2.26 includes parity plots for component molar flows in stream S_TOP as obtained by calculation with the hybrid surrogate and with a MESH-based model. Comparing detailed and reduced model, absolute deviations are very small and relative deviations range between -2% and $+2\%$.

Figures 2.27 and 2.28 show trend plots for component molar flows in stream S_TOP depending on varying column top pressures p_{top} and CO_2 concentrations in feed stream S_IN. The vertical grey lines mark the limits of the data set which was used for ANN training and evaluation. The trend plots calculated with the hybrid surrogate model are identical to the corresponding trend plots obtained with the MESH model. This is even true, if the hybrid surrogate is used for extrapolation beyond the range of the underlying data set for ANN training. Trend plots for the temperature of feed stream S_IN are not shown but exhibit similar accuracies.

The hybrid surrogate model comprises physical equations as well as data set information which has been generated using the MESH model. An ANN has been trained to represent the data set information and successively reformulated to be included in the hybrid surrogate model. Several training runs have been performed and the best obtained solution has been selected. Since the hybrid surrogate models provides accurate results, the ANN modelling, training, and reformulating has been successful. Neither underfitting nor overfitting can be oberserved. The ANN can generalise the input/output correlation of the considered data set as extrapolation of the range of the hybrid surrogate model is possible to a certain extent. Dependencies between model results and independent model variables are accurate indicating that the hybrid

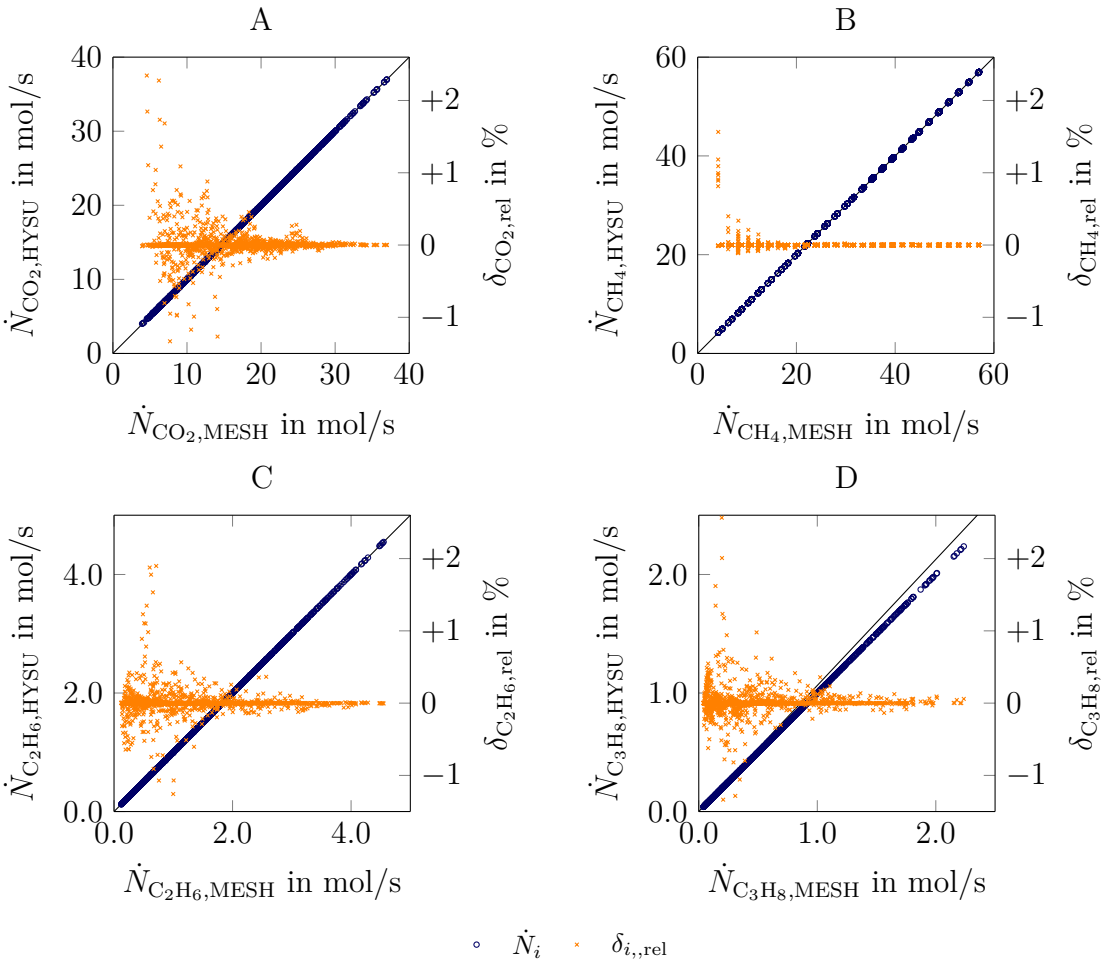

Figure 2.26: Parity plots for component molar flows in stream S_TOP as calculated by a MESH-based column and the hybrid surrogate model for the reboiled column.

surrogate model provides suffient derivative information. The hybrid surrogate model can be applied for gradient-based process optimisation within an extended range of the included data set.

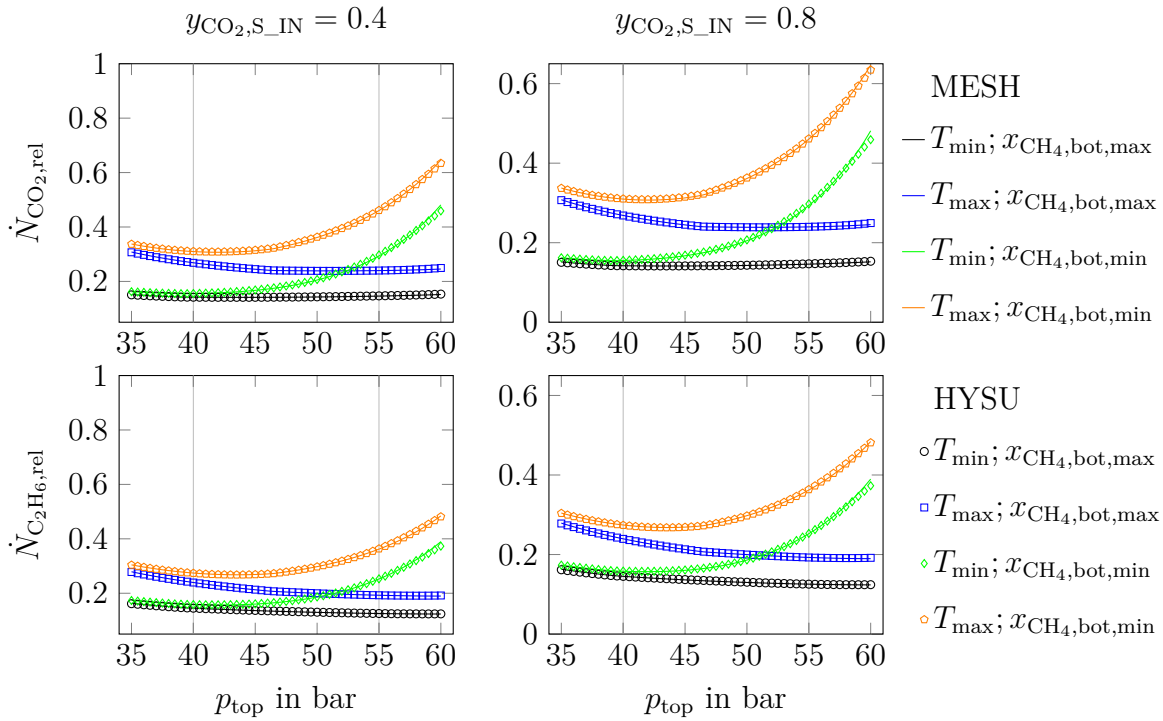

Figure 2.27: Trends in dependence of p_{top} for the MESH-based and the hybrid surrogate model; $T_{min} = 225\,K$, $T_{max} = 240\,K$, $x_{CH_4,bot,min} = 0.0001$, $x_{CH_4,bot,max} = 0.01$

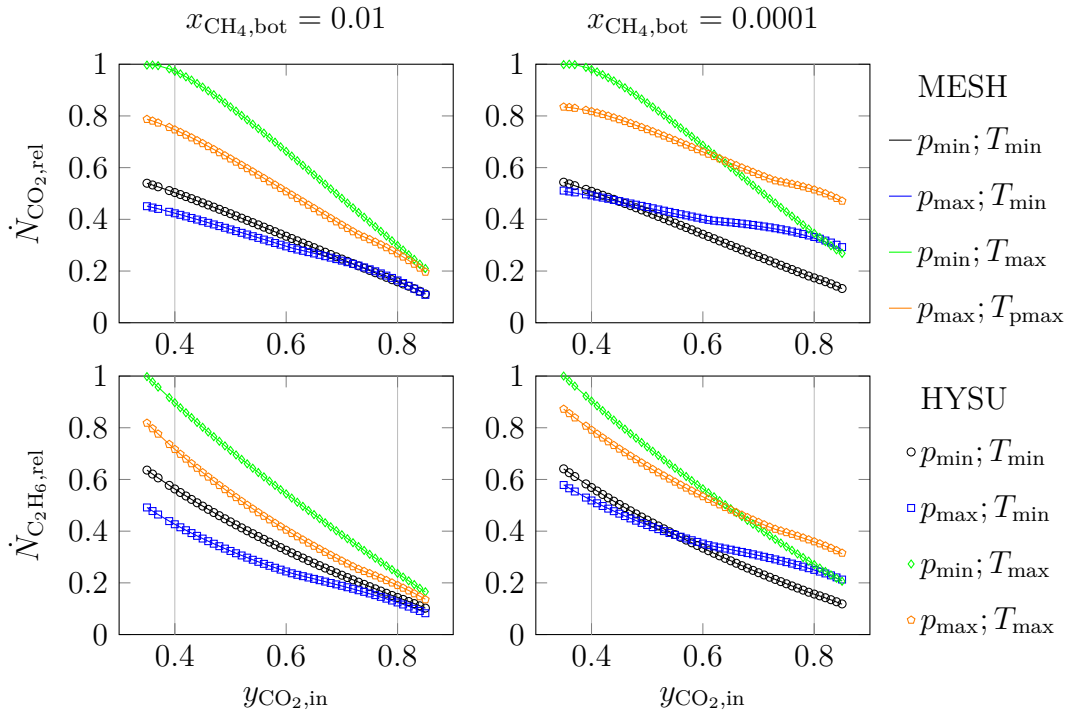

Figure 2.28: Trends in dependence of y_{CO_2,S_IN} for the MESH-based and the hybrid surrogate model; $p_{min} = 40\,bar$, $p_{max} = 55\,bar$, $T_{min} = 225\,K$, $T_{max} = 240\,K$

2.5.6 Modelling: absorption/desorption process

Apart from cryogenic distillation, CO_2 can be separated from natural gas in an absorption/desorption process. A simplified physical absorption process with methanol as a solvent is shown in Figure 2.29. The sour natural gas S_IN contains N_2, CO_2, CH_4, C_2H_6, and C_3H_8. In column T02, CO_2 is absorbed by methanol stream S_ABS1 which has a temperature of T_{abs}. In order to compensate temperature increases due to released absorption enthalpy, internal column liquid is fully withdrawn, cooled to T_{abs} in coolers E02 and E03, and fed back into the column. At the column top, a sweetened natural gas stream S_NG with a specified CO_2 impurity of $50\,\text{ppm} \leq y_{\text{CO}_2,\text{S\_NG}} \leq 0.03$ is obtained. The loaded methanol S_ABS2 is depressurised in valve V01, warmed up in heat exchanger E04, and regenerated in desorption column T03. Regenerated methanol S_ABS5 is mixed with a pure methanol make-up stream S_MEOH compensating the methanol loss $y_{\text{MeOH,S\_CO2}}$ in the CO_2-enriched column top stream S_CO2. The regenerated methanol is pre-cooled in heat exchanger in E04, pressurised in pump P01 and cooled in multi-stage cooling shortcut MSCL01. The process in Figure 2.29 is going to be integrated into a superstructure which is used to design a natural gas sweetening process by optimisation.

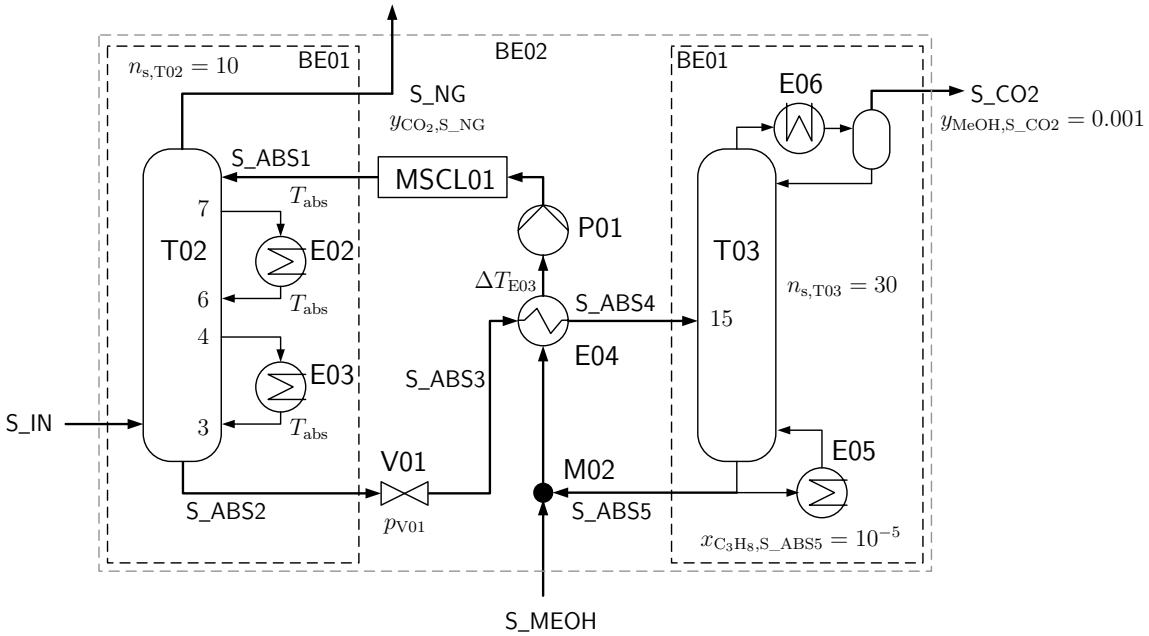

Figure 2.29: Flowsheet for hybrid surrogate model for absorption/desorption module.

Balance envelope There are two main options to define the balance envelope for a hybrid surrogate model which represents the process shown in Figure 2.29. First, the whole process can be included in one single hybrid surrogate model (BE02). In this case, columns T02 and T03 are included in the hybrid surrogate model as well as valve V01, heat exchanger E04, mixer M02, pump P01, and multi-stage cooling unit MSCL01.

The second option is to develop one hybrid surrogate model for column T02 and one hybrid surrogate model for column T03 (BE01). Valve V01, heat exchanger E04, mixer M02, pump P01, and multi-stage cooling unit MSCL01 are then modelled as single units which connect the two hybrid surrogate models for columns T02 and T03. While the number of required data set output variables is equal for both options, the states of the streams between columns T02 and T03 are accessible, if the operations between the two columns are modelled as single units. Also, the specifications for these units between the hybrid surrogate models for T02 and T03 are flexible. Hence, representing columns T02 and T03 with two separate hybrid surrogate models is preferred.

Input and output variables Input variables to the hybrid surrogate models for both columns are temperature, pressure, and component molar flows of the feed streams. Output variables for both hybrid surrogate models are temperature, pressure, and component molar flows of their product streams as well as the heat flows in coolers E02 and E03 or condenser E06 and reboiler E05, respectively. The heat flows of coolers E02 and E03 and of reboiler E05 are determined by data set information. Regarding coolers E02 and E03, this is especially convenient because the energy balance around column T02 is not trivial due to released absorption enthalpy. Further, for each component entering column T02 and column T03, the smaller one of the two product component molar flows is calculated from data set information. Thus, in the ANN training, higher sensitivities towards small deviations between data set and network output are achieved. However, the bottom product leaving column T03 is assumed to be free of N_2, CH_4, and C_2H_6.

Data set generation and preprocessing To generate the data sets, which are incorporated in the hybrid surrogate models for columns T02 and T03, independent process variables are systematically varied as given in Table 2.8. Calculations are performed in UniSim® Design R451 using the provided detailed models for flash drums, mixers, valves, pumps, heat exchangers, and columns. For all calculations, Linde proprietary physical property data is used. The column numbers of stages $n_{\mathrm{s,T02}}$ and $n_{\mathrm{s,T03}}$ as well as feed and side draw locations remain constant and are selected so that they are appropriate in each point of the generated data set. In multi-stage cooling unit MSCL01, only needed coolers are active and cause a pressure drop of $\Delta p_{\mathrm{E0X}} = 0.2\,\mathrm{bar}$.

Table 2.8: Systematic variation of the process variables to create a data set including an input/output correlation of column T02 and T03 ($\dot{N}_{\mathrm{S\_IN}} = 100\,\mathrm{mol/s} = \mathrm{const}$, $\Delta p_{\mathrm{E02}} = \Delta p_{\mathrm{E03}} = 0$, $p_{\mathrm{E04}} = 0.2\,\mathrm{bar}$, $\Delta p_{\mathrm{E05}} = \Delta p_{\mathrm{E06}} = 0.1\,\mathrm{bar}$, $\Delta p_{\mathrm{s}} = 0.001\,\mathrm{bar}$).

Varied variable	Min	Max	Points	Spacing
$p_{\mathrm{S\_IN}}$	30 bar	55 bar	6	linear
T_{abs}	226.15 K	236.15 K	3	linear
r_{abs}	0.50	1.25	4	linear
$y_{\mathrm{N_2,S\_IN}}$	0.01	0.1367	3	linear
$y_{\mathrm{CO_2,S\_IN}}$	0.175	0.325	3	linear
$y_{\mathrm{C_2H_6,S\_IN}}$	0.001	0.10	4	logarithmic
$y_{\mathrm{C_3H_8,S\_IN}}$	0.0005	0.05	4	logarithmic

Systematic process variable variation as given in Table 2.8 provides a data set with $n_{\mathrm{DS}} = 10368$ data set patterns. In order to reduce the number of process variables to be varied, meaningful process assumptions are made. Linear pressure profiles based on a specifed pressure drop per column stage Δp_{s} are assumed inside the columns. The pressure on an inlet stage is assumed to be equal to the corresponding inlet stream. Pressure $p_{\mathrm{S\_IN}}$ determines the pressure in column T02, while p_{V01} specifies the pressure in column T03. As given by eq. (2.128), the inlet temperature of sour natural gas stream S_IN is assumed to be 10 K above the cold absorbens. Further, as shown in eq. (2.129), the outlet pressure of valve V01 is specified so that stream S_CO2 can potentially be recycled and repressurised to $p_{\mathrm{S\_IN}}$ by a compressor with two compression stages and a compression ratio of $r = 2.5$ per stage. The temperature difference ΔT_{E04} between stream S_ABS3 and the pre-cooled absorbens stream entering pump P01 is defined so that a minimum temperature difference in E04 is maintained in each point of the generated data set:

$$T_{\mathrm{S\_IN}} = T_{\mathrm{abs}} + 10\,\mathrm{K} \tag{2.128}$$

$$p_{\mathrm{V01}} = \frac{p_{\mathrm{S\_IN}}}{r^2} + \Delta p_{\mathrm{E04}} + \Delta p_{\mathrm{T03}} \tag{2.129}$$

$$\Delta T_{\mathrm{E04}} = 10\,\mathrm{K}. \tag{2.130}$$

In order to eliminate the influence of the feed molar flows into the columns, input component molar flows are transferred to molar fractions. Output component molar flows are reformulated into split fractions as given by:

$$\xi_{i,\mathrm{product}} = \frac{\dot{N}_{i,\mathrm{product}}}{\dot{N}_{i,\mathrm{feed}}}. \tag{2.131}$$

However, since the nitrogen, methane, ethane, propane component molar flows in absorbens S_ABS1 vary in a range of very small numbers, their split fractions into

the products of column T02 are determined by eq. (2.132). Since the feed S_IN is free of methanol, the split fraction for methanol is calculated by eq. (2.133):

$$\xi_{i,\mathrm{S\_ABS2}} = \frac{\dot{N}_{i,\mathrm{S\_ABS2}}}{\dot{N}_{i,\mathrm{S\_IN}}}, \quad \text{for } i = \mathrm{N_2},\ \mathrm{CH_4},\ \mathrm{C_2H_6},\ \mathrm{C_3H_8} \tag{2.132}$$

$$\xi_{i,\mathrm{S\_NG}} = \frac{\dot{N}_{i,\mathrm{S\_NG}}}{\dot{N}_{i,\mathrm{S\_ABS1}}}, \quad \text{for } i = \mathrm{MeOH}. \tag{2.133}$$

The heat flows of coolers E02 and E03 and reboiler E05 are set in relation with the CO_2 component molar flow in the corresponding column feed:

$$\zeta_{\mathrm{E02}} = \frac{\dot{Q}_{\mathrm{E02}}}{\dot{N}_{\mathrm{CO_2,S\_IN}}} \tag{2.134}$$

$$\zeta_{\mathrm{E03}} = \frac{\dot{Q}_{\mathrm{E03}}}{\dot{N}_{\mathrm{CO_2,S\_IN}}} \tag{2.135}$$

$$\zeta_{\mathrm{E05}} = \frac{\dot{Q}_{\mathrm{E05}}}{\dot{N}_{\mathrm{CO_2,S\_ABS4}}}. \tag{2.136}$$

The data set input and output vectors for the hybrid surrogate models for column T02 and T03 are defined as given in eqs. (2.137) to (2.140):

$$\begin{aligned}\vec{v}_{\mathrm{input,T02}} = (&\tilde{p}_{\mathrm{S\_IN}},\ \tilde{T}_{\mathrm{abs}},\ \tilde{r}_{\mathrm{abs}},\ \tilde{y}_{\mathrm{N_2,S\_IN,log}},\ \tilde{y}_{\mathrm{CO_2,S\_IN}},\\ &\tilde{y}_{\mathrm{C_2H_6,S\_IN,log}},\ \tilde{y}_{\mathrm{C_3H_8,S\_IN,log}},\ \tilde{x}_{\mathrm{CO_2,S\_ABS1,log}})^{\mathrm{T}}\end{aligned} \tag{2.137}$$

$$\begin{aligned}\vec{v}_{\mathrm{output,T02}} = (&\tilde{\xi}_{\mathrm{N_2,S\_ABS2,log}},\ \tilde{\xi}_{\mathrm{CO_2,S\_NG,log}},\ \tilde{\xi}_{\mathrm{CH_4,S\_ABS2,log}},\ \tilde{\xi}_{\mathrm{C_2H_6,S\_ABS2}},\\ &\tilde{\xi}_{\mathrm{C_3H_8,S\_ABS2}},\ \tilde{\xi}_{\mathrm{MeOH,S\_NG,log}},\ \tilde{\zeta}_{\mathrm{E02}},\ \tilde{\zeta}_{\mathrm{E03}})^{\mathrm{T}}\end{aligned} \tag{2.138}$$

$$\begin{aligned}\vec{v}_{\mathrm{input,T03}} = (&\tilde{p}_{\mathrm{S\_ABS4}},\ \tilde{T}_{\mathrm{S\_ABS4}},\ \tilde{y}_{\mathrm{N_2,S\_ABS4,log}},\ \tilde{y}_{\mathrm{CO_2,S\_ABS4}},\\ &\tilde{y}_{\mathrm{CH_4,S\_ABS4}},\ \tilde{y}_{\mathrm{C_2H_6,S\_ABS4,log}},\ \tilde{y}_{\mathrm{C_3H_8,S\_ABS4,log}})^{\mathrm{T}}\end{aligned} \tag{2.139}$$

$$\vec{v}_{\mathrm{output,T03}} = (\tilde{\xi}_{\mathrm{CO_2,S\_ABS5,log}},\ \tilde{\xi}_{\mathrm{C_3H_8,S\_ABS5,log}},\ \tilde{\xi}_{\mathrm{MeOH,S\_CO2,log}},\ \tilde{\zeta}_{\mathrm{E05}})^{\mathrm{T}}. \tag{2.140}$$

The tilde indicates that the variables are normalised so that they have values between -1 and 1. Before normalisation, a logarithm is applied to certain variables if needed. In the last step, the preprocessed data set is randomly split into a training and evaluation data set in relation of 3:1.

ANN modelling and training For each of the two columns T02 and T03, two self-contained feed forward networks are used to model the component distribution between the column products and the columns energy requirements. In Table 2.9, the network structures for HYSU1 and HYSU2 are given. The hybrid surrogate model for column T02 is referred to as HYSU1. The hybrid surrogate model for column T03 is referred to as HYSU2. The number of neurons in the first hidden layers is 2.5 times the number of input variables. The number of neurons in the second hidden layers is two times the number of output variables.

Table 2.9: Hybrid surrogate models for columns T02 and T03: ANN modelling

	n_{in}	Network	$l = 1$	$l = 2$	$l = 3$
T02	8	Neurons $n_{\text{n},l}$	20	16	8
		Activation function $f(v_{\Sigma,j})$	$\tanh(v_{\Sigma,j})$	$\tanh(v_{\Sigma,j})$	$\text{lin}(v_{\Sigma,j})$
T03	7	Neurons $n_{\text{n},l}$	18	8	4
		Activation function $f(v_{\Sigma,j})$	$\tanh(v_{\Sigma,j})$	$\tanh(v_{\Sigma,j})$	$\text{lin}(v_{\Sigma,j})$

Hence, 652 connection parameters w_{ij} are determined by training the network for the hybrid surrogate model for column T02. For the hybrid surrogate model for column T03, 332 connection parameter w_{ij} are determined.

In Table 2.10, the applied training parameters are listed. $t_\infty = 75000$ training epochs were found to be sufficient in combination with a start learning rate of $\eta_0 = 0.1$ and an end learning rate of $\eta_\infty = 0.001$. The training is performed in one step. However, training is performed several times. The best obtained solution is selected to be integrated into the hybrid surrogate model.

Table 2.10: Hybrid surrogate models for columns T02 and T03: ANN training parameters

	n_{DS}	n_{TDS}	t_0	t_∞	η_0	η_∞	α
T02	10368	7776	0	75000	0.1	0.001	0
T03	10368	7776	0	75000	0.1	0.001	0

Equations of the hybrid surrogate model The trained feed forward neural network is transferred into an algebraic set of equations as exemplarily shown in eqs. (2.102) to (2.106). Applying this set of equations, the output vectors as given in eqs. (2.138) and (2.140) are calculated from the input vectors in eqs. (2.137) and (2.139), respectively. After reversing normalisation, delogarithmising if needed, and applying eqs. (2.132) and (2.133), output vectors $\vec{v}_{\text{output,T02}}$ and $\vec{v}_{\text{output,T03}}$ include component molar flows as before data set preprocessing. With the output vector from the black box part, the component mass balances in eqs. (2.141) and (2.142) as well as the assumptions in

eq. (2.143), all component molar flows in streams S_NG, S_ABS2, S_CO2, and S_ABS5 are determined:

$$0 = \dot{N}_{i,\text{S\_IN}} + \dot{N}_{i,\text{S\_ABS1}} - \dot{N}_{i,\text{S\_NG}} - \dot{N}_{i,\text{S\_ABS2}}, \qquad \text{for } i = 1, ..., n_\text{c} \tag{2.141}$$

$$0 = \dot{N}_{i,\text{S\_ABS4}} - \dot{N}_{i,\text{S\_CO2}} - \dot{N}_{i,\text{S\_ABS5}}, \qquad \text{for } i = 1, ..., n_\text{c} \tag{2.142}$$

$$0 = \dot{N}_{\text{N}_2,\text{S\_ABS5}} = \dot{N}_{\text{CH}_4,\text{S\_ABS5}} = \dot{N}_{\text{C}_2\text{H}_6,\text{S\_ABS5}}. \tag{2.143}$$

Stream pressures are calculated by assuming a linear pressure profile in the columns. Stream temperatures are determined by dew point and bubble point calculations, respectively:

$$0 = p_\text{S\_NG} - p_\text{S\_IN} + (n_\text{s,T02} - 1) \cdot \Delta p_\text{s} \tag{2.144}$$

$$0 = p_\text{S\_ABS2} - p_\text{S\_IN} + \Delta p_\text{s} \tag{2.145}$$

$$0 = T_\text{S\_NG} - T^\text{dew}_\text{S\_NG} \tag{2.146}$$

$$0 = T_\text{S\_ABS2} - T^\text{bub}_\text{S\_ABS2} \tag{2.147}$$

$$0 = p_\text{S\_CO2} - p_\text{S\_ABS4} - (n_\text{s,T03} - n_\text{T03,in}) \cdot \Delta p_\text{s} \tag{2.148}$$

$$0 = p_\text{S\_ABS5} - p_\text{S\_ABS4} + (n_\text{T03,in} - 1) \cdot \Delta p_\text{s} \tag{2.149}$$

$$0 = T_\text{S\_CO2} - T^\text{dew}_\text{S\_CO2} \tag{2.150}$$

$$0 = T_\text{S\_ABS5} - T^\text{bub}_\text{S\_ABS5}. \tag{2.151}$$

The heat flows of E02 and E03 are both determined by output vector $\vec{v}_\text{output,T02}$ since an energy balance around column T02 is not trivial due to release of absorption enthalpy. After transferring $\tilde{\zeta}_\text{E05}$ to $\dot{Q}_\text{E05}$ in output vector $\vec{v}_\text{output,T03}$, the energy balance around column T03 provides the heat flow of E06:

$$0 = -\dot{Q}_\text{E06} + \dot{H}_\text{S\_ABS4} - \dot{H}_\text{S\_CO2} - \dot{H}_\text{S\_ABS5} + \zeta_\text{E05} \cdot \dot{N}_{\text{CO}_2,\text{S\_ABS4}}. \tag{2.152}$$

Hence, the hybrid surrogate models for columns T02 and T03 include equations for

- algebraic equations which model the trained feed forward artificial neural network (black box part),
- physical equations for mass balances, a linear pressure profile inside the column as well as dew and bubble point calculations as given in eqs. (2.141) and (2.144) to (2.147) (T02) or eqs. (2.142), (2.143), and (2.148) to (2.152) (T03), respectively (white box part).

2.5.7 Validation: absorption/desorption process

The ANN training is performed five times for both the absorption and the desorption column hybrid surrogate model. The number of epochs is set to 75000 so that the minimum possible network errors are achieved. Further, overfitting is avoided due to early stopping. The best training result out of five is selected to be integrated in the corresponding hybrid surrogate model. In Figure 2.30, the maximum occuring error for one data set element δ_{max} is plotted against the network error δ_{net} for the training and the evaluation data set. Please note that the plotted errors are absolute and refer to normalised and partly logarithmised process variable values as they are used for neural network training.

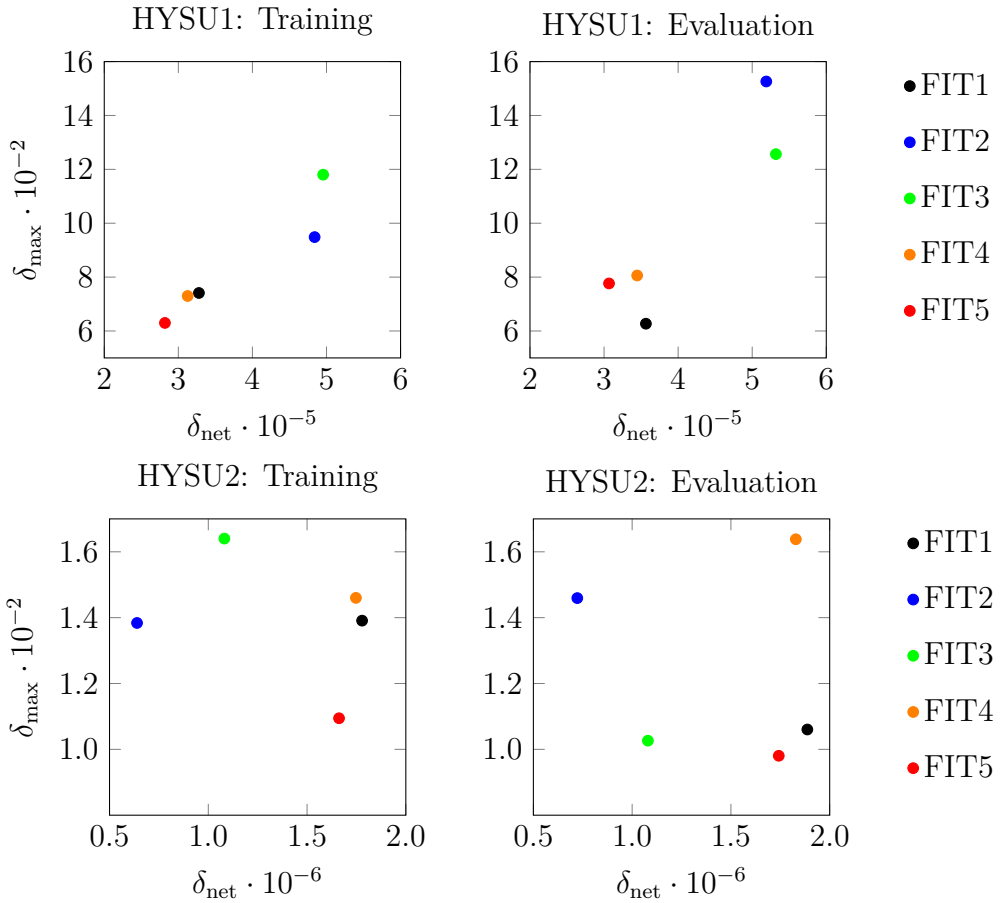

Figure 2.30: Training errors of neural networks for HYSU1 and HYSU2.

For HYSU1, FIT1 and FIT5 are favourable due to low errors δ_{net} and δ_{max}. For HYSU2, FIT2 and FIT5 are favourable due to a low network error δ_{net} and low maximum occuring error for one data set element δ_{max}, respectively. For FIT3, δ_{max} is too high for the training data set. Only considering absolute errors can be of disadvantage with respect to accuracy, for example, if small concentrations occur. Hence, the best training result is selected considering maximum relative errors for actual process results (neither normalised, nor logarithmised). This allows for evaluation of the fit quality with respect to each data set element. Figure 2.31 shows maximum relative errors

$\delta_{\mathrm{max,rel}}$ for every output variable. The points in the diagrams refer to different data set patterns.

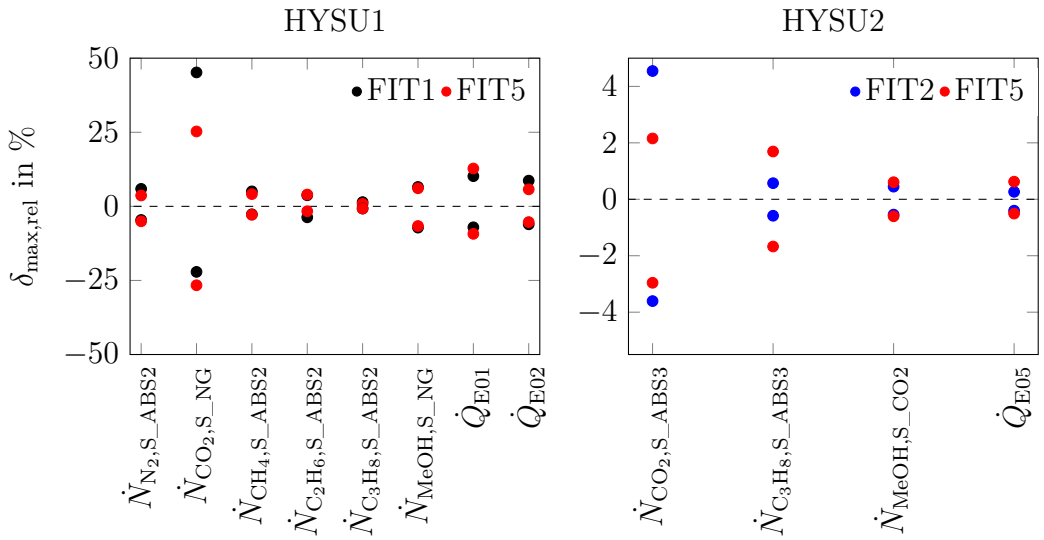

Figure 2.31: Relative maximum and minimum error occurring in the data set target variable values

The trained artificial neural networks for HYSU1 and HYSU2 can represent the target data sets with a network error δ_{net} in the order of magitude of 10^{-5} and 10^{-6}, respectively, for the training and evaluation data sets. For both HYSU1 and HYSU2, the maximum relative deviations are moderate with one exception: the component molar flow of CO_2 in sweet natural gas leaving the absorption column. Single high relative deviations occur since a large interval of 10^{-6} to 0.55 for the split fraction $\xi_{\mathrm{CO_2,S\_NG}}$ is covered by the data set. Maximum relative deviations correlate with small target values of $\dot{N}_{\mathrm{CO_2,S\_NG}}$ in very few cases. Since FIT5 exhibits a smaller positive maximum relative deviation, it is preferred over FIT1 for HYSU1. For HYSU2, FIT5 is preferred since the maximum relative deviations are more equally distributed.

HYSU1 and HYSU2 are both combined in the absorption/desorption module as shown in Figure 2.29. In Figure 2.32, parity plots for component molar flows resulting from calculations with a MESH model and the hybrid surrogate models are shown. Deviations range between −6% and +5% for the component molar flows of nitrogen, methane, ethane, and propane in the sweet natural gas product S_NG and methanol in stream S_CO2. For the component molar flow of CO_2 in the sweet natural gas product, larger realtive deviations occur for very small absolute values.

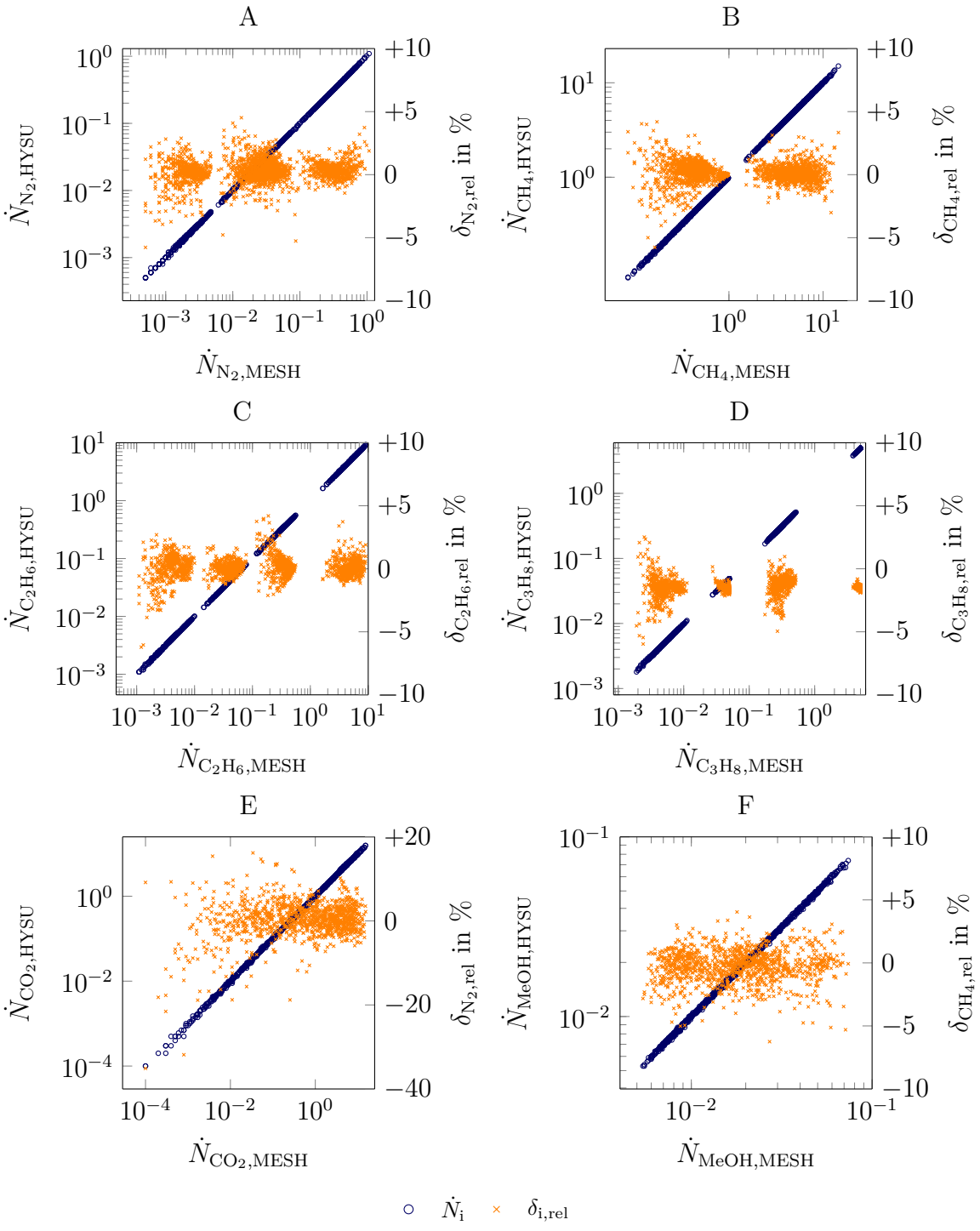

Figure 2.32: Parity plots for component molar flows $\dot{N}_{N_2,HYSU}$, $\dot{N}_{CH_4,HYSU}$, $\dot{N}_{C_2H_6,HYSU}$, $\dot{N}_{C_3H_8,HYSU}$ in stream S_CO2 and $\dot{N}_{CO_2,HYSU}$, $\dot{N}_{MeOH,HYSU}$ in stream S_NG as calculated by a MESH-based column and the hybrid surrogate model for the absorption/desorption unit.

In Figure 2.33, the relative component molar flow $\dot{N}_{CO_2,rel}$ in sweet natural gas S_NG and the required shaft power P_{sh} for the complete absorption/desorption module are plotted in dependence of inlet pressure p_{S_IN}, absorbens temperature T_{abs} and ratio r_{abs}.

Dependencies of $\dot{N}_{CO_2,rel}$ and P_{sh} on p_{S_IN}, T_{abs}, and r_{abs} are similar for the MESH and the hybrid surrogate model.

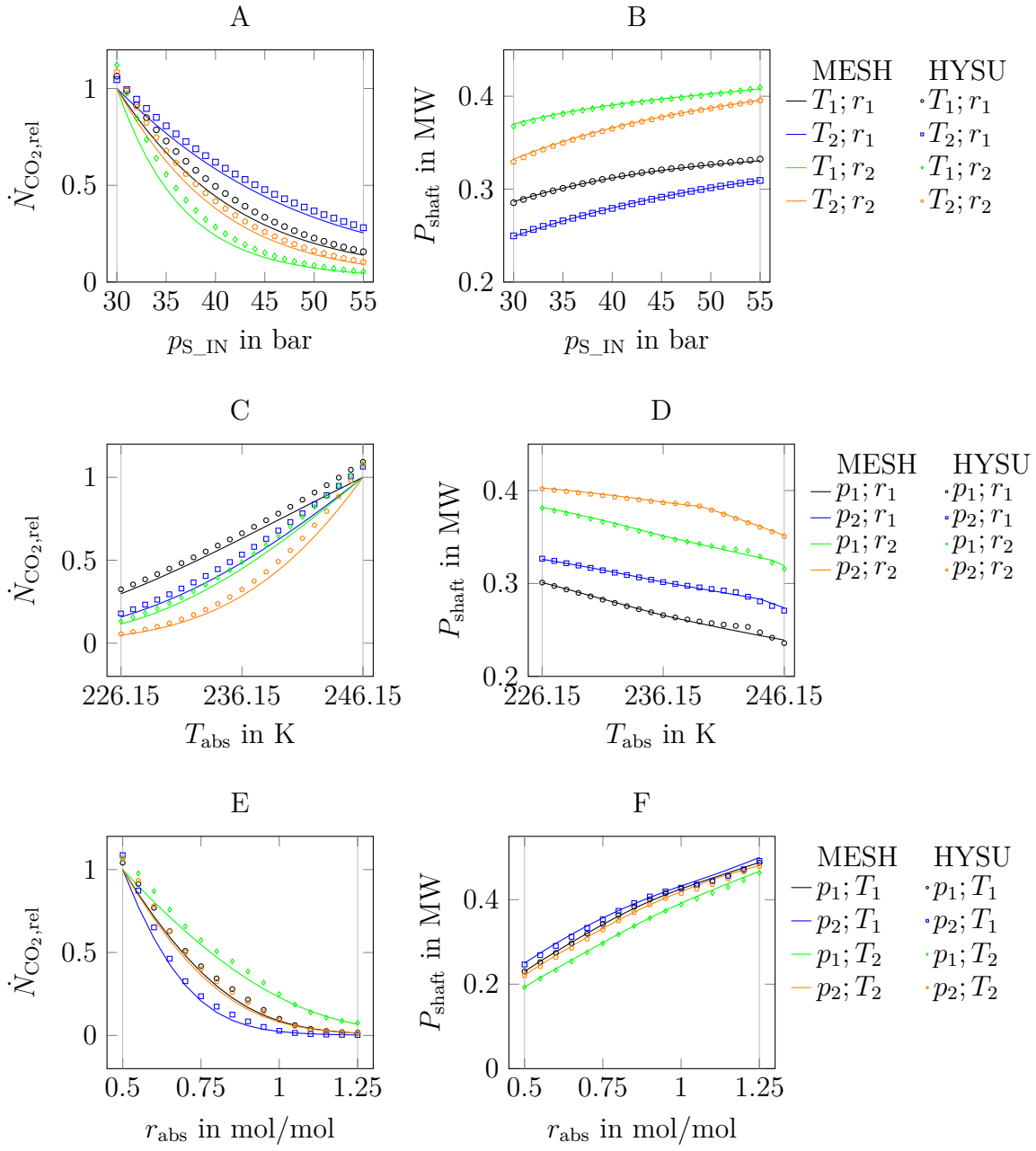

Figure 2.33: Trends for the absorption/desorption hybrid surrogate model;
feed conditions: $y_{CO_2,S\_IN} = 0.2$, $y_{N2,S\_IN} = 0.05$, $y_{C_2H_6,S\_IN} = 0.01$,
$y_{C_3H_8,S\_IN} = 0.001$;
varied process variables $p_1 = 35\,\text{bar}$, $p_2 = 55\,\text{bar}$, $T_1 = 226.15\,\text{K}$,
$T_2 = 246.15\,\text{K}$, $r_{abs,1} = 0.75$, $r_{abs,2} = 1.0$

Please note that the trend plots for other process results are equally accurate. The plots for $\dot{N}_{CO_2,rel}$ in sweet natural gas S_NG are shown because higher maximum relative deviations were oberserved for this output variable compared to other output variables.

The plots for shaft power P_{sh} are shown since the shaft power will be used as part of the objective function in process optimisation.

Small network errors δ_{net} for the training and evaluation data set indicate that the ANN included in HYSU1 and HYSU2 have successfully learned the input/output correlation of the underlying data set (refer to Figure 2.30). As shown in Figure 2.31, relative maximum errors $\delta_{\mathrm{max,rel}}$ are considered to evaluate the fit quality for each data set element.

Significant maximum relative deviations between MESH and hybrid surrogate results occur for the component molar flow of CO_2 in the sweet natural gas. Maximum relative deviations are numerically promoted since they are observed for very small values of $\dot{N}_{\mathrm{CO_2,S\_NG}}$. Further, the data set, which is used to train the ANN in HYSU1, covers a wide range of split fraction $\xi_{\mathrm{CO_2,S\_NG}}$ (10^{-6} to 0.55) and hence $\dot{N}_{\mathrm{CO_2,S\_NG}}$ so that achieving high accuracy in every point is challenging. The accuracy could be improved by using a smaller range of $\xi_{\mathrm{CO_2,S\_NG}}$ or partioning the data set and hence using an additional ANN in HYSU1. However, this would increase the complexity of the hybrid surrogate model.

Maximum relative deviations were found to be moderate for each remaining output variable of HYSU1 and HYSU2. Further, the results for component molar flows in the product streams (calculated with the absorption/desorption module combining HYSU1 and HYSU2) in the parity plots in Figure 2.32 indicate sufficient accuracy.

Figure 2.33 shows that hybrid surrogate and MESH-based results for relative component molar flow $\dot{N}_{\mathrm{CO_2,rel}}$ in sweet natural gas depend on inlet pressure $p_{\mathrm{S\_IN}}$, absorbens temperature T_{abs}, and ratio r_{abs} in a very similar way – despite of comparatively high maximum deviations. Trends for other hybrid surrogate output variables are of similar quality. The trends for shaft power P_{sh} are accurate and particulary interesting since the shaft power will be used in the objective function for process optimisation. Since the reduced module for absorption/desorption is sufficiently accurate and provides sufficient derivative information, it can be used in gradient-based process optimisation.

2.6 Framework for optimisation-based design of industrial processes

In Figure 2.34, the layout of the framework for systematic optimisation-based process design is shown. The framework comprises a task bot, a gradient-based NLP optimiser, and an equation-oriented modelling environment with reduced models and detailed models which are used to build a model of the process. The task bot includes a set of definable specifications such as start values for optimisation variables, constraints such as product purities, tuning factors for the objective function, and different equipment (e.g., membrane areas) or process specifications (e.g., feed conditions).

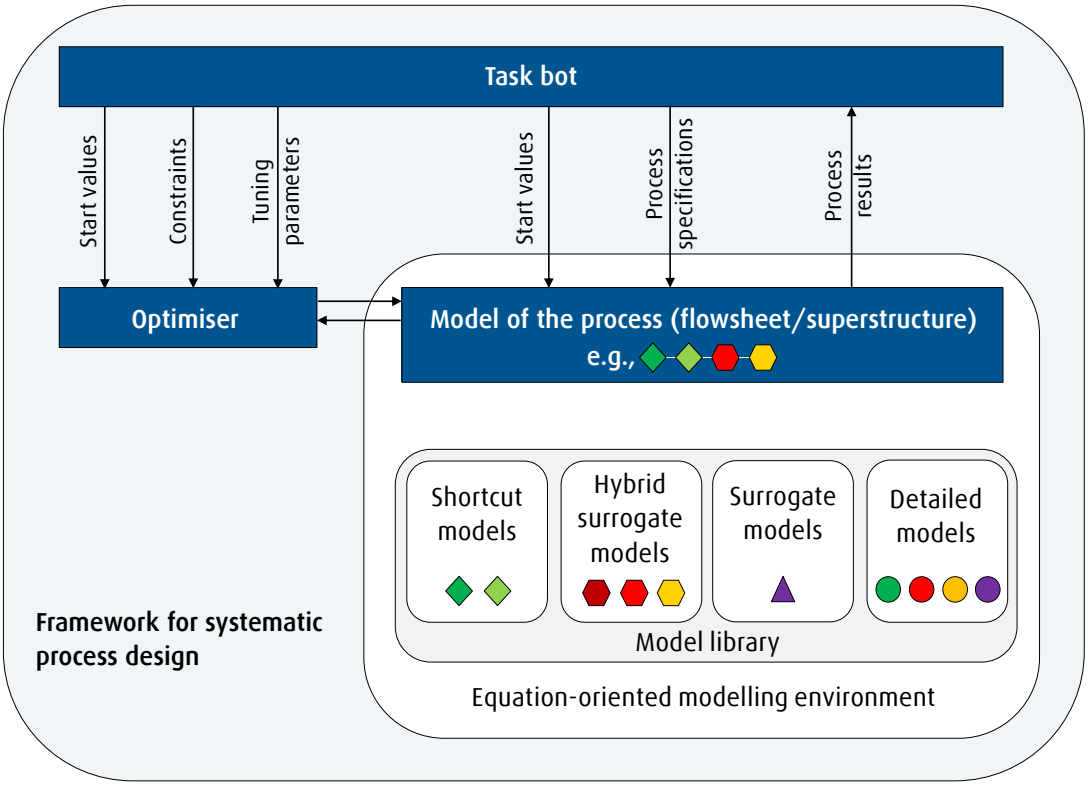

Figure 2.34: Framework for systematic optimisation based process design.

The task bot initialises the process model by performing one steady state simulation and starts process optimisation. After one successful optimisation run, the task bot reads process results from the model and records them.

In Figure 2.35, a procedure for using the framework is shown. After the task bot is specified and the program is started, a process alternative k and a corresponding process model j are selected. $j = 1$ indicates that the process model is based on reduced models. With increasing j, more detailed models are included. The process model can be initialised with the data set pattern i (for $j \geq 1$) or with results from preceeding optimisation with a more reduced process model $j - 1$ (for $j > 1$). The process model is simulated and optimised. The optimisation results are saved. If further data set patterns for process model j of process alternative k are specified in the task bot, the next data set pattern $i + 1$ is selected and the procedure is repeated. The procedure is also repeated for further process models and/or process alternatives before the program is ended. Since optimisation using the framework's reduced models is particularly robust, a large number of optimisation runs can be pre-defined in the task bot and automatically performed in series without convergence issues. However, if a converged solution cannot be reached, error message $err = 1$ is logged so that the optimisation can be checked manually later.

As reduced models, the shortcut for multi-stage compression, the hybrid surrogate for multi-stage cooling, the membrane shortcut, the Adapted Edmister Model, and

different hybrid surrogate models for columns are included. Although the listed reduced models are typically combined with different optimisation algorithms (e.g., surrogate models with gradient-free and shortcut models with gradient-based approaches), they can all be combined in one flowsheet or superstructure which is optimised applying a gradient-based optimiser. This is possible because the hybrid surrogate models include algebraic equations for trained feed forward networks linking input and output information.

The framework is based on the Linde proprietary simulation and optimisation software OPTISIM® (Eich-Soellner et al. 1997) but can be implemented in any other equation-oriented modelling and optimisation environment. For optimisation, the OPTISIM® SQP solver is used. The task bot is implemented using Microsoft Excel, Visual Basic for Applications and available interfaces to Linde OPTISIM®. The reduced models are implemented in OPTISIM's® Dynamic Equation Block (Thomas 2011). The framework can be extended by further reduced models such as models for different unit operations. Apart from shortcut and hybrid surrogate models, surrogate models can be added.

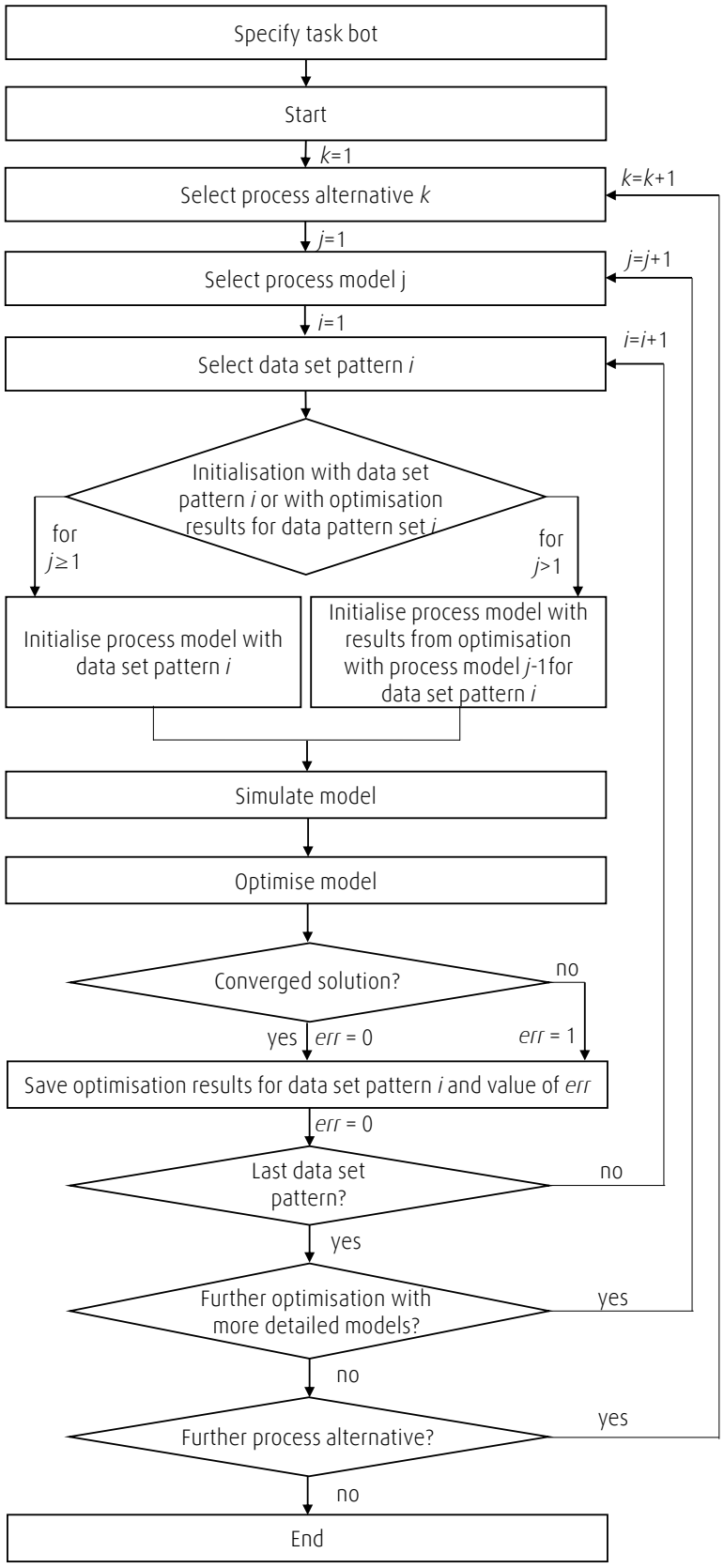

Figure 2.35: Flowchart for automated process optimisation with framework for systematic process design.

3 Optimisation of an air separation double column

An air separation double column is optimised by applying the developed AEM as a column shortcut model. The numbers of column stages in the double column segments are optimised together with process variables such as pressures, temperatures, and split factors. The principle of cryogenic air separation is discussed in detail by Hausen & Linde (1985), Haering (2008) as well as Windmeier & Barron (2013). General modelling specifications are given in Table A.1 in the appendix.

3.1 State of the art: optimisation of column stage numbers and feed and side draw locations

Several approaches to the optimisation of the number of column stages as well as feed and side draw locations using stage-to-stage column models are available in literature. An overview of work on optimal synthesis of complex distillation columns using detailed column models is given by Grossmann et al. (2005).

Sargent & Gaminibandara (1976) provide one of the first approaches to column design based on mathematical programming. A feed or side draw stream is distributed over all or selected column stages. In an NLP problem, the distribution is optimised. Avoiding an MINLP problem formulation, the distribution optimisation problem is solved for every considered number of stages in a separate outer loop.

Visawanathan & Grossmann (1993a) and Visawanathan & Grossmann (1993b) provide an MINLP model for determining optimal feed stage locations and the number of stages required for a separation task simultaneously. A certain number of column stages is modelled, but not all column stages are expected to be needed according to optimisation. Zero phase flows due to modelled conditional but not needed trays can cause numerical problems with solving equilibrium calculations.

Nevertheless, complex design problems have been solved by applying MINLP formulations. For the structural optimisation of distillation processes to separate zeotropic and homogeneous azeotropic mixtures, Bauer & Stichlmair (1998) optimise superstructures with MINLP formulations. Optimal feed stage locations are determined in accordance with Visawanathan & Grossmann (1993b). Dünnebier & Pantelides (1999) optimise multicolumn systems including both conventional and thermally coupled columns (e.g., divided wall columns). Kruber et al. (2021) have developed hybrid optimisation methods to handle complex MINLP based design problems. Their methods integrate a solution strategy based on successively refined NLP problems combined with an upper level metaheuristic for optimisation of discrete variables.

Yeomans & Grossmann (2000a) and Yeomans & Grossmann (2000b) present a generalised disjunctive programming (GDP) solution approach to the MINLP problem of optimising feed tray locations, numbers of trays as well as operating and design parameters. Numerical difficulties are avoided by modelling conditional trays with disjunctions to decide, if equilibrium equations are applied or not. Barttfeld et al. (2003) compare MINLP and GDP formulations for different column representations. They conclude that GDP formulations allow for shorter solution times, are more robust, and not as strongly dependent on good initial guesses as MINLP formulations.

Apart from optimisation of column stage numbers, feed locations, and side draw locations using detailed column models, optimisation approaches with sequential use of shortcut and detailed models can be found in literature. Kraemer et al. (2009) claim that more complex problems regarding optimisation-based column design can only be solved by decomposing the design problem into successive steps with increasing modelling depth.

Kossack et al. (2006) propose a combination of shortcut calculations with the rectification body method (Bausa et al. 1998, von Watzdorf et al. 1999, Brüggemann & Marquardt 2004) and subsequent optimisation with detailed column models. In a shortcut evaluation step, favourable process alternatives are identified and initial values as well as bounds for the optimisation with detailed models are provided. In the subsequent step, the number of column stages and feed locations are determined by optimisation with stage-to-stage column models. Since column stages refer to integer optimisation variables, MINLP problems have to be solved.

However, Kossack et al. (2006) and Kraemer et al. (2009) reformulate the MINLP problem as a continuous NLP problem by relaxing binary variables indicating existing or non-existing stages to continuous decision variables. They assume that, at the optimum, integer values are obtained for the continuous decision variables. Kossack et al. (2006) solve a succession of relaxed MINLP problems with decreasing bounds. Constraints are reformulated with a big-M relaxation. The big-M values of M are subsequently tightend during successive optimisation. Finally, a tight model formulation exhibiting integer solutions for the decision variables is obtained. Kraemer et al. (2009) include a nonlinear Fischer-Burmeister function constraint to force continuous decision variables to zero or one. Kossack et al. (2006) and Kraemer et al. (2009) investigate distillative separation sequences for multi-component azeotropic mixtures. Marquardt et al. (2008) and Kraemer (2012) extend the described approach to hybrid separation sequences.

Kamath et al. (2010) propose a shortcut model based on the Kremser (Kremser 1930) and Edmister group method (Edmister 1943, Edmister 1957). Feed locations are optimised by modelling shortcut-based column segments between the column ends and feeds. Optimising the number of stages in the column segments while constraining the overall number of stages in the column provides the feed location. In a first step, the numbers of stages are relaxed to continuous variables enabling NLP optimisation. In a second step, the resulting numbers of stages are rounded to the nearest integer and

another NLP optimisation with fixed numbers of stages is performed. This approach is referred to as 'rounding heuristic'. It leads to near-optimal solutions.

Dowling & Biegler (2015) note that the approach provided by Kraemer et al. (2009) could lead to infeasibilities since the interior of the relaxed binary variables (between zero and one) is ill-defined. Hence, Dowling & Biegler (2015) propose a MESH-based stage-to-stage model in which a bypass for the liquid and gaseous stream is considered for each equilibrium stage. The ratio of non-bypassed flow to total flow to the column stage is defined by the bypass efficiency of the stage. The number of column stages is determined by the sum of the bypass efficiency for the stages in the column. In a first optimisation step, the rounding heuristic and the shortcut model proposed by Kamath et al. (2010) are applied. In the following optimisation steps, the MESH-based model with stage bypass is used. It is initialised with a number of non-bypassed stages as determined in the first step. A certain number of additional stages are included but initially fully bypassed. This enables increasing the number of column stages by optimisation. In an iterative procedure, the optimised solution is evaluated, additional stages are added or removed so that a fixed number of fully bypassed stages is achieved, and optimisation is performed again. The iterative procedure if stopped, for example, if there is no change in the optimised numbers of stages in comparsion to the previous iteration.

3.2 Problem statement and approach

An air separation double column process providing liquid oxygen as well as liquid and gaseous nitrogen shall be designed using process optimisation. The objective is to minimise the heat which needs to be dissipated from the inlet flow related to the oxygen recovery. This is a measure for energy efficiency. Optimisation variables are one pressure, temperatures, split factors as well as the number of stages in the single column segments. A two-step optimisation approach comprising a first AEM2-based optimisation step and a second MESH-based optimisation step is applied. In the AEM2, the semi-empirical correction approach for air separation as given by eqs. (2.80) to (2.83) with eq. (2.88) is used in each column segment.

The Linde proprietary simulation and optimisation software OPTISIM® is used for flowsheet modelling and optimisation applying the OPTISIM® SQP solver. All calculations are performed with Linde's physical properties.

3.3 Superstructure and optimisation problem

Process description Products of the air separation process in Figure 3.1 are gaseous nitrogen S_GAN1, liquid nitrogen S_LIN, and liquid oxygen S_LOX. The air inlet stream S_AIR1 is specified by

$$\text{S\_AIR1}: \; p = 1.013\,\text{bar}, \; T = 298.15\,\text{K},$$

$$\dot{N}_{\text{N}_2} = 78.084\,\text{mol/s}, \; \dot{N}_{\text{Ar}} = 0.934\,\text{mol/s}, \; \dot{N}_{\text{O}_2} = 20.946\,\text{mol/s}.$$

S_AIR1 is pressurised in two equally performing compression stages with an intermediate and a downstream water cooler. The USP (upstream processing) module represents units between the compressor and the double column, such as the direct contact air cooler, a temperature swing adsorption, and the main heat exchanger. The outlet S_AIR2 of the USP module is cooled dry air at temperature T_{air}. Main components of the flowsheet are high pressure column SEG1, low pressure column SEG2-SEG4, main condenser HX1, and subcooler HX2-HX3.

Flowsheet optimisation The objective is to minimise the required heat flow $\dot{Q}_{\text{cold}}$ related to the oxygen recovery R_{LOX} in stream S_LOX for a constrained total number of column stages $n_{\text{s,tot}}$:

$$\min \;\; obj = \frac{\dot{Q}_{\text{cold}}}{R_{\text{LOX}}} = \frac{\dot{Q}_{\text{cold}}}{\frac{\dot{N}_{\text{LOX}}}{\dot{N}_{\text{O}_2,\text{AIR1}}}}. \tag{3.1}$$

For the calculation of heat flow $\dot{Q}_{\text{cold}}$, it is assumed that the gaseous product streams S_GAN1, S_GAN2, S_IPN are warmed up to 293.15 K in heat integration in the USP module before leaving the air separation plant. Hence, heat flows $\dot{Q}_{\text{GAN1}}$, $\dot{Q}_{\text{GAN2}}$, and $\dot{Q}_{\text{IPN}}$ are determined by assuming single heaters between the colder product streams S_GAN1, S_GAN2, and S_IPN and the corresponding product streams with 293.15 K. In the USP module, $\dot{Q}_{\text{USP}}$ has to be removed from the system in order to achieve the required air stream temperature T_{air}. Heat flow $\dot{Q}_{\text{cold}}$ is then defined by energy balance

$$\dot{Q}_{\text{cold}} = \dot{Q}_{\text{USP}} - \dot{Q}_{\text{GAN1}} - \dot{Q}_{\text{GAN2}} - \dot{Q}_{\text{IPN}}. \tag{3.2}$$

The objective as given in eq. (3.1) is a simplified objective without weighting factors for $\dot{Q}_{\text{cold}}$ and R_{LOX}. The compressor power is not included in the objective function. Although a pressure drop per column stage is considered, the compressor power is not sensitive towards the optimisation variables due to the air inlet flow $\dot{N}_{\text{AIR1}} = 100\,\text{mol/s}$ and the top pressure of the low pressure column $p_{\text{top,SEG4}} = 1.3\,\text{bar}$ being fixed.

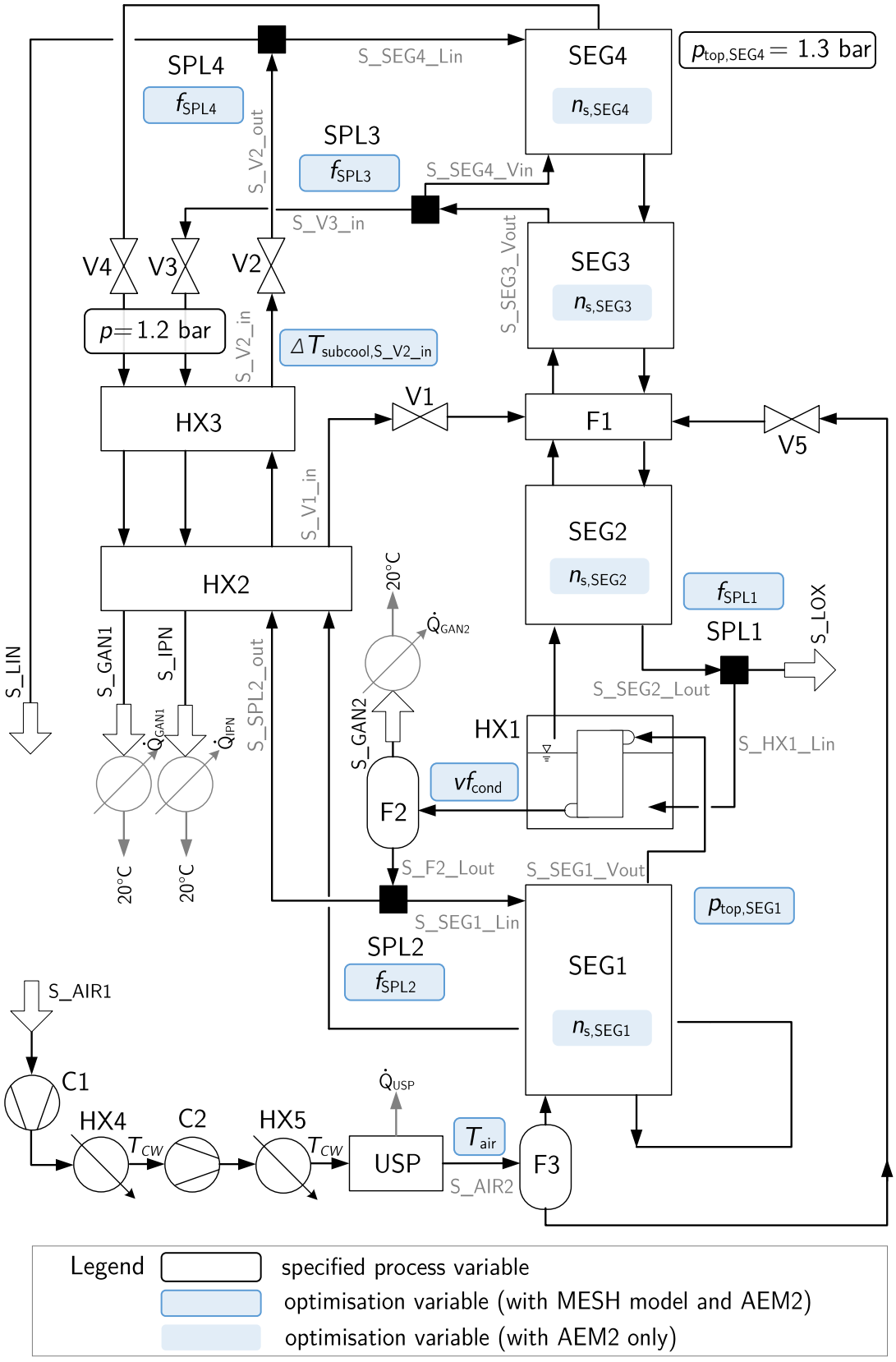

Figure 3.1: Thermally linked double column for separation of air into nitrogen and oxygen products.

During optimisation, the total number of column stages $n_{\mathrm{s,tot}}$ is restricted by an inequality constraint. Since feed flash stage F1 has to be considered as a column stage, the total number of equilibrium stages in the double column is

$$n_{\mathrm{s,tot}} = n_{\mathrm{s,SEG1}} + n_{\mathrm{s,SEG2}} + n_{\mathrm{s,SEG3}} + n_{\mathrm{s,SEG4}} + 1. \tag{3.3}$$

The allowed maximum for the total number of column stages $n_{\mathrm{s,tot,max}}$, which is representing an important part of the investment cost, is systematically varied between 90 and 102. The individual numbers of stages $n_{\mathrm{s,SEG1}}$, $n_{\mathrm{s,SEG2}}$, $n_{\mathrm{s,SEG3}}$, and $n_{\mathrm{s,SEG4}}$ are continuous variables using the AEM2 and are subject to optimisation by the solver. Optimisation of $n_{\mathrm{s,SEG2}}$, $n_{\mathrm{s,SEG3}}$, and $n_{\mathrm{s,SEG4}}$ is equivalent to optimising the feed and side draw location for the low pressure column SEG2-SEG4. Further, typical product purity specifications as well as minimum product recoveries are included as constraints. In this process example, at least 45% of the nitrogen in the air feed shall be recovered as gaseous nitrogen product S_GAN1 and at least 10% of the nitrogen in the air feed shall be recovered as liquid nitrogen product S_LIN:

$$n_{\mathrm{s,tot}} \leq n_{\mathrm{s,tot,max}} \text{ with } n_{\mathrm{s,tot,max}} = 90, 94, 98, 102 \tag{3.4}$$

$$x_{\mathrm{O_2,LIN}}, y_{\mathrm{O_2,GAN}} \leq 10\,\mathrm{ppm} \tag{3.5}$$

$$x_{\mathrm{O_2,LOX}} \geq 0.995 \tag{3.6}$$

$$R_{\mathrm{GAN1}} = \frac{\dot{N}_{\mathrm{GAN1}}}{\dot{N}_{\mathrm{N_2,AIR1}}} \geq 0.45 \tag{3.7}$$

$$R_{\mathrm{LIN}} = \frac{\dot{N}_{\mathrm{LIN}}}{\dot{N}_{\mathrm{N_2,AIR1}}} \geq 0.10. \tag{3.8}$$

Main condenser HX1 is modelled by a disjunct cooler with $\dot{Q}_{\mathrm{HX1,cooling}}$ and heater with $\dot{Q}_{\mathrm{HX1,heating}}$. The necessary condition $\Delta\dot{Q}_{\mathrm{HX1}} = 0$ is met by adjusting temperature T_{air}. According to Haering (2008), a minimal temperature difference of $1 - 2\,\mathrm{K}$ between S_SEG1_Vout and S_HX1_Lin must be maintained to ensure the function of main condenser HX1. This is achieved by adjusting high pressure column pressure $p_{\mathrm{top,SEG1}}$. The subcooling temperature difference $\Delta T_{\mathrm{subcool,S\_V2\_in}}$ is used to ensure minimum temperature difference $\Delta T_{\mathrm{min,HX3}}$. Hence, the following process conditions have to be satisfied:

$$\Delta\dot{Q}_{\mathrm{HX1}} = \dot{Q}_{\mathrm{HX1,heating}} + \dot{Q}_{\mathrm{HX1,cooling}} = 0 \tag{3.9}$$

$$\Delta T_{\mathrm{min,HX1}} = \Delta T_{\mathrm{min,1}} \tag{3.10}$$

$$\Delta T_{\mathrm{min,HX2}}, \Delta T_{\mathrm{min,HX3}} \geq \Delta T_{\mathrm{min,2}}. \tag{3.11}$$

3.4 Process optimisation

Since the AEM2 was pre-tested extensively regarding its applicability in gradient-based NLP process optimisation, it can be used in process optimisation as a standalone model with any available gradient-based NLP solver. A two-step optimisation approach with a first AEM2-based optimisation step and a subsequent MESH-based optimisation step is used. In the two-step approach, stage numbers n_s and process variables (e.g., pressures, temperatures, or split factors) are optimised simultaneously in the first AEM2 NLP optimisation step. The optimised numbers of stages are then rounded to integer variables, applied to a MESH-based column model and maintained constant in the subsequent MESH-based optimisation step.

Optimisation variable start values for the AEM2 and MESH-based optimisation step are determined by systematic start value studies with the AEM2 and are listed in Table 3.1 and Table 3.2. Table 3.1 also includes optimised values for the numbers of stages of the single column segments which are results of the first AEM2-based optimisation step.

While the numbers of stages are optimised using the AEM2 and kept afterwards, the remaining optimisation variables are reset to their original start values. Then, the AEM2 models are exchanged by MESH-based models in the flowsheet. The small differences between start values for AEM2-based and MESH-based optimisation result from active constraints which require minor adjustment to obtain a feasible solution when switching from AEM2 to MESH models. The fact that the flowsheet still satisfies most constraints after switching from AEM2 to MESH models underlines the high accuracy of the AEM2. Hence, the AEM2 is well suited for searching feasible points or optima of flowsheets with MESH column models. This significantly reduces the effort to converge flowsheets with MESH models.

Table 3.1: Start values and AEM2-based optimisation results for the number of stages in each column segment.

	start	result	result	result	result
	$n_{s,tot} = 90$	$n_{s,tot} \leq 90$	$n_{s,tot} \leq 94$	$n_{s,tot} \leq 98$	$n_{s,tot} \leq 102$
$n_{s,SEG4}$	30.0	10.0	10.0	10.0	10.0
$n_{s,SEG3}$	9.0	13.3	15.0	14.7	15.0
n_{F1}	1	1	1	1	1
$n_{s,SEG2}$	15.0	17.3	18.0	18.0	17.9
$n_{s,SEG1}$	35.0	48.4	50.0	54.3	58.2

According to Table 3.1, numbers of stages $n_{s,SEG3}$ and $n_{s,SEG2}$ are increased in each AEM2-based optimisation case. The number of stages $n_{s,SEG4}$ is reduced to its allowed minimum $n_{s,SEG4,min} = 10$ which was set so that purity and recovery specifications of product stream S_GAN1 are ensured. While the optimisation results for the overall

Table 3.2: Start values for AEM2-based (numbers of stages are degrees of freedom) and MESH-based optimisation (numbers of stages are not degrees of freedom).

Optimisation variable	Unit	AEM2	MESH
$f_{\mathrm{SPL1}} = \frac{\dot{N}_{\mathrm{S\_LOX}}}{\dot{N}_{\mathrm{S\_SEG2\_Lout}}}$	-	0.03	0.03
$f_{\mathrm{SPL2}} = \frac{\dot{N}_{\mathrm{S\_SPL2\_out}}}{\dot{N}_{\mathrm{S\_F2\_Lout}}}$	-	0.35	0.35
$f_{\mathrm{SPL3}} = \frac{\dot{N}_{\mathrm{S\_V3\_in}}}{\dot{N}_{\mathrm{S\_SEG3\_Vout}}}$	-	0.51	0.51
$f_{\mathrm{SPL4}} = \frac{\dot{N}_{\mathrm{S\_LIN}}}{\dot{N}_{\mathrm{S\_V2\_out}}}$	-	0.32	0.33
vf_{cond}	-	0.1	0.1
$p_{\mathrm{top,SEG1}}$	bar	5.4	5.4
$\Delta T_{\mathrm{subcool,S\_V2\_in}}$	K	-13.5	-13.5
T_{air}	K	98.5	98.5

number of stages in the low pressure column do not depend strongly on the allowed total number of stages in the double column $n_{\mathrm{s,tot}}$, the number of stages in the high pressure column $n_{\mathrm{s,SEG1}}$ is increased significantly with an increasing maximum for $n_{\mathrm{s,tot}}$.

In Figure 3.2, the optimisation result values for the split factors and for vapour fraction vf_{cond} after AEM2-based and subsequent MESH-based optimisation are plotted. AEM2-based and MESH-based optimisation are performed starting with equal start values for f_{SPL1}, f_{SPL2}, f_{SPL3}, f_{SPL4}, and vf_{cond} (see Table 3.2). Figure 3.2 reveals that both AEM2-based and MESH-based optimisation lead to very similar optimisation results for the four split factors and vapour fraction vf_{cond}. Thus, based on equal start values, optimisation with MESH-based and AEM2-based column segments leads to the same process optimum. While f_{SPL1} and f_{SPL3} are changed insignificantly during optimisation, f_{SPL2} and f_{SPL4} are increased and reduced, respectively. Increasing f_{SPL2} means that less liquid from F2 is led back to the high pressure column SEG1 as reflux. Decreasing f_{SPL4} leads to a smaller fraction of stream S_V2_out being withdrawn as liquid nitrogen product S_LIN. In every optimisation case, stream S_SEG1_Vout is condensed totally ($vf_{\mathrm{cond}} = 10^{-6}$) so that no product S_GAN2 is withdrawn.

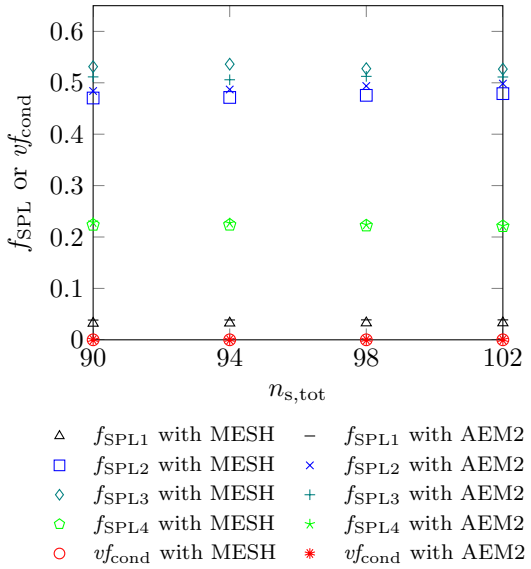

Figure 3.2: Two-step optimisation of thermally linked air separation double column: results for split factors and the vapour fraction vf_{cond} after optimisation with a MESH-based column model and the AEM2.

A higher LOX product flow is achieved because of more liquid reflux through the low pressure column after optimisation. Since S_HX1_Lout is fully liquid, split factor f_{SPL2} is increased and split factor f_{SPL4} is decreased, more liquid nitrogen reflux is sent to the top of the low pressure column.

Although the increased liquid reflux in the low pressure column contains more nitrogen, the specified LOX product purity can be maintained due to two reasons. First, split factor f_{SPL1} remains almost constant during optimisation increasing the boilup ratio of the low pressure column due to the higher liquid reflux. Second, the numbers of stages $n_{\mathrm{s,SEG2}}$ and $n_{\mathrm{s,SEG3}}$ are increased during AEM2-based optimisation.

Since the liquid nitrogen reflux to the low pressure column is increased and the flow of stream S_SEG4_Vin is reduced, the number of stages $n_{\mathrm{s,SEG4}}$ can be significantly reduced in AEM2-based optimisation while the constrained nitrogen product purity is still met. More reflux to the top of the low pressure column means less reflux to the top of the high pressure column SEG1. However, the specified purity of the liquid nitrogen product S_LIN can be maintained due to the number of stages in the high pressure column $n_{\mathrm{s,SEG1}}$ being significantly increased during AEM2-based optimisation.

The trade-off between the objective function obj as defined in eq. (3.1) and the total number of stages in the double column $n_{\mathrm{s,tot}}$ is shown in Figure 3.3. While obj is minimised, $n_{\mathrm{s,tot}}$ is systematically varied as an inequality constraint $n_{\mathrm{s,tot}} \leq n_{\mathrm{s,tot,max}}$. The objective after conventional (one-step) MESH-based optimisation, in which the numbers of column stages are not optimised, is given as a benchmark. The objective values of the two-step approach show a systematic offset between AEM2-based optimisation and subsequent MESH-based optimisation.

Regarding the same point of operation (same values for process variables and parameters), simulation using the AEM2 provides higher LOX flows than simulation using MESH-based column segments (e.g., $\dot{N}_{\mathrm{S\_LOX}} = 20\,\mathrm{mol/s}$ with AEM2 and $\dot{N}_{\mathrm{S\_LOX}} = 18\,\mathrm{mol/s}$ with MESH-based segments). Accordingly, AEM2-based calculation provides higher values for the liquid oxygen recovery R_{LOX} and lower values for objective *obj* than MESH-based calculation. However, the reduction of *obj* for higher numbers of stages $n_{\mathrm{s,tot}}$ is observed for AEM2-based and MESH-based optimisation equally. This is even more appreciable considering that the optimised objective function *obj* numerically depends only slightly on $n_{\mathrm{s,tot}}$ in the evaluated range $90 \leq n_{\mathrm{s,tot}} \leq 102$. Increasing the total number of stages in the double column from $n_{\mathrm{s,tot}} = 90$ and $n_{\mathrm{s,tot}} = 102$ leads to energy savings of 0.77 % which, in practice, is considerable for a highly integrated air separation process.

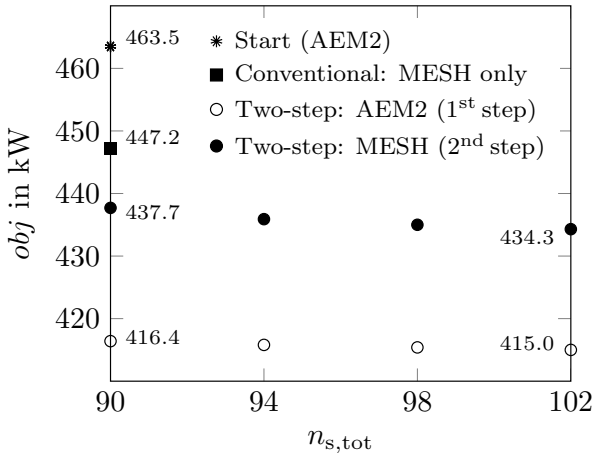

Figure 3.3: Optimisation of thermally linked air separation double column: trade-off between objective function *obj* and total number of column stages n_{tot}.

Flowsheet optimisation could also be performed in one step by only using MESH models. This, however, is accompanied by two drawbacks. First, flowsheet convergence is much harder to obtain with MESH models in comparison to using the AEM2. Second, numbers of stages cannot be optimised in NLP optimisation in OPTISIM®. Further, in practice, MINLP optimisation problems are hard to formulate and to bring to an optimal solution. Based on equal start values (as listed in Table 3.2), one-step optimisation with MESH models would provide an optimal solution with $obj = 447.2\,\mathrm{kW}$ for $n_{\mathrm{s,tot}} = 90$ (number of column stages is not optimised). The two-step optimisation approach results in a minimum which is 2.2% better. This is significant for an air separation process. Here, the AEM2 shows its full potential since optimising the distribution of the number of stages is conveniently possible in NLP optimisation.

4 Optimisation of a natural gas sweeting process

4.1 Natural gas compositions

Natural gas sources vary substantially in composition. Typically, the main component in natural gas is methane. Natural gas also contains ethane, propane, butane, and higher hydrocarbons. Further, raw natural gas contains impurities such as nitrogen, carbon dioxide, hydrogen sulfide, and sometimes helium. Moisture is mostly present, but some gas fields contain no water (Kidnay & Parrish 2006). In the context of this work, the influence of the CO_2 content in raw natural gas on the process to separate CO_2 shall be determined.

4.2 Technology overview for CO_2 bulk separation from natural gas

Since the raw natural gas considered in the context of this thesis does not contain H_2S, separation of H_2S is not regarded in the following paragraphs. In Table 4.1 provides an technology overview for bulk removal of CO_2 from natural gas.

Table 4.1: Technology overview for bulk removal of CO_2

Distillative	**Flash**	**Membranes**	**Absorption**	**Adsorption**
• Cryogenic distillation • Controlled Freeze Zone™ • Ryan/Holmes • SPREX® CO_2 • Dual pressure distillation • Series of cryogenic distillation columns	• Twister • CryoCell® • Condensed rotational separation	Module: • Hollow-fibre • Spiral-wound Material: • Cellulose acetate • Polyimide • Perfluoro polymers silicone rubber	Physical: • Rectisol® • Fluor Solvent™ • Purisol® • Selexol® • Morphysorb® • Genosorb® Chemical: • Amines • Potassium carbonate	Adsorbents: • Zeolites • Activated carbon • Titano-silicates Process: • PSA • TSA • rTSA

Distillative separation Obtaining sharp separation of CO_2 and CH_4 by cryogenic distillation is limited by the mixture's critical pressure. A minimal difference between the vapour and liquid phase densities on every column stage must be respected to guarantee column operation. Further, purification of the CH_4 product in the column top is limited by the CO_2 freezing point. In most cases, a condenser für CH_4 product purification cannot be implemented because the top products condensation temperature (especially if N_2 is included) is below the CO_2 freezing point temperature.

In a Controlled Freeze Zone Tower (CFZ®), two conventional packed column sections enclose a specially designed section for CO_2 freeze out. The top product of the upper packed column section is sweetend natural gas, while the bottom liquid is sprayed into the controlled freeze zone section. Due to increasing temperatures with droplet falling distance, lower boiling components evaporate, the CO_2 concentration increases and pure CO_2 freezes out. In the lower packed column section, CO_2 is withdrawn as a bottom product. Several patents (e.g., Valencia & Denton 1985, Potts & Thomas 1992, Fieler et al. 2010) as well as journal articles (e.g., Thomas & Denton 1988, and Kelley et al. 2011) were published by Exxon Production Research Company or Exxon Mobil Upstream Research Company.

In the Ryan/Holmes Process, a liquid agent is added to the system so that acid gas solids formation is prevented in cryogenic distillation. With a sequence of several distillation columns, CO_2, CH_4, and remaining natural gas components can be withdrawn as products. Further, an agent to prevent the formation of azeotropes between CO_2 and light hydrocarbons can be added. Liquid agents are recovered and recycled in the process. All liquid agents are preferably pure C3-C6 alkanes or mixtures of these. Patents are held by Koch Process Systems, Inc. (e.g., Holmes & Ryan 1982a, Holmes & Ryan 1982b, Holmes & Ryan 1984).

The special pre-extraction method (SPREX®) was patented by IFP Energies nouvelles and further developed in collaboration with TOTAL and Axens Solutions. In a first process step, natural gas with high contents of CO_2 is separated by cryogenic distillation. The liquid CO_2 bottom product can be reinjected. Remainig contents of CO_2 in the top product can be removed by conventional treating (e.g., amine scrubbing) with reduced economical effort due to pre-extraction of CO_2.

With cryogenic dual pressure distillation as patented by Pellegrini (2015), the first distillation column at a higher pressure (e.g., 50 bar) is used for bulk removal of CO_2. The methane enriched top product of the first column is fed into the lower pressure second column (e.g., 40 bar). While the top product of the lower pressure column is high purity methane, the bottom product is recycled to the higher pressure column. The change of pressure is needed since distillative separation is limited by the critical point of the mixture in the higher pressure column. Lowering the pressure shifts the critical point towards pure methane, hence high purity methane products are thermodynamically possible. While solidification does not occur in the higher pressure column (two phase regions vapour/liquid as well as solid/liquid do not intersect in an isobaric diagram), superheating of the expanded feed gas to the lower pressure column

is necessary to avoid solidification lower pressure distillation (Langè et al. 2015). Berstad et al. (2012) use several cryogenic distillation columns in series to reduce the CO_2 content from [50.6]vol − % to LNG specification of [50]ppm.

Flash separation The Twister technology involves a cyclonic fluid separator with a converging inlet section, a vortex generator, a Laval nozzle, a cyclonic separation section, and a diverging outlet section. The Laval nozzle induces adiabatic cooling and causes CO_2, for example, to condense in case of a gaseous feed stream. The swirling motion, which is induced by the vortex generator at the entrance of the Laval nozzle, leads to a strong centrifugal field allowing for cyclonic phase separation. Several patents have been published, e.g., van Veen & Betting (2001), Betting et al. (2002), Betting et al. (2004), Prast et al. (2012), Prast et al. (2013). Older patents were originally assigned to Shell Oil Company, but are now held by Twister B. V.

The CryoCell® was developed by Cool Energy Ltd. It exploits the high solidification temperature of CO_2 in comparison to light natural gas components. Following a typical thermodynamic operating path, the mixture is first cooled at elevated pressure and partly condensed. An isenthalpic flash, e.g., across a Joule-Thomson valve, results in a pure CO_2 solid phase and a vapour and liquid phase still containing CO_2. Based on the described thermodynamic path, Hart & Gnanendran (2009) provide different flow schemes for treating different feed compositions.

The main equipment of a process based on condensed rotational separation is a rotational particle separator patented by Brouwers (1991). The working principle of separating heavy/light phases and particulate matter from fluids by centrifugal forces is explained in detail by Brouwers (2002) and applied to the separation of CO_2 from natural gas by Willems et al. (2010). Bulk separation of CO_2 from methane is achieved by condensing CO_2 into micro-sized droplets and separating the droplet by rotational phase separation.

Absorption The use of physical solvents is facilitated by low temperatures, high pressures and high partial pressures of sour feed components which have to be removed. Low contents of heavy hydrocarbon components are favourable (Elliot et al. 2008). In Table 4.1, some well-known industrially relevant physical solvents are listed. Rectisol® is a physical absorption process developed and patented by Lurgi (Herbert et al. 1958) and Linde (Ranke & Weiss 1982) in which methanol is used to separate CO_2, H_2S, and COS from synthesis gas. In the Flour Solvent™ process, propylene carbonate is used as a physical solvent which does not need heat for regeneration as it is regenerated by flashing at different pressure stages including vaccum. It was patented by Kohl & Miller (1960a) and Kohl & Miller (1960b). The physical solvent in the Purisol® process is N-methyl-2-pyrrolidone (NMP). It was developed and commercialised by Lurgi. The Selexol® process uses a mixture of homologues of the dimethlyether of polyethylen glycols as a physical solvent. It was originally licensed by Allied Chemical Corporation, the current licensor is UOP (Kohl & Nielsen 1997).

With chemical absorbents, CO_2 reacts chemically with the solvent after physical absorption. Solvents can be chosen with respect to partial pressures of acid gas in the feed and in the product. Amines are chosen for low partial pressures in the feed and product (Kidnay & Parrish 2006). Aqueous solutions of various amines are used to remove CO_2 and H_2S. Monoethanolamine, diethanolamine, and methyldiethanolamine are amines of commercial interest (Kohl & Nielsen 1997). Physical solvents are favoured for high partial pressures in the feed in product. In between, hot potassium carbonate is applied (Kidnay & Parrish 2006).

Membranes Suppliers for different membrane module types and materials for CO_2 separation from natural gas are listed in Table 2.1 in section 2.3. Experimental results for innovative and non-commerical membrane materials can be found in literature. Peters et al. (2011) remove CO_2 from natural gas with amine absorption compared to a PVAm/DVA membrane (polyvinyl amine and polyvinylalcohol). For both processes, capital investment and gas processing cost are optimised. While the membrane process cannot reach the same purites as the amine process, it requires lower capital investment. Safari et al. (2009) show the effects of feed pressure, feed temperature, and permeate pressure on permeability and selectivity of a 6FDA-2,6-DAT membrane. They found that the permeate pressure is of significance in process optimisation.

Adsorption After the bulk of acid gases is separated, remaining CO_2 concentrations can be removed from natural gas by adsorption. Substantial CO_2 quantities can be adsorbed even at low CO_2 partial pressures. In the presence of water, applications are limited. Since water adsorbes more strongly than CO_2 and concentrates in the inlet section of the bed, it displaces the CO_2 adsorption zone (Kohl & Nielsen 1997, Kidnay & Parrish 2006). An extensive overview over commercial and novel adsorbents for CO_2 capture is given by Rufford et al. (2012). Commercially used are zeolites, activated carbons, and titanosilicate molecular sieves.

Continuous adsorption process operate with multiple beds of stationary adsorbent which are switched between adsorption and regeneration in turns. Beds are regenerated by increased temperatures in temperature swing adsorption (TSA) or reduced pressures in pressure swing adsorption (PSA). PSA can be operated with shorter cycle durations than TSA. TSA processes entail a high energetic demand, especially if high quantities of impurities have to be removed since regeneration gas has to be heated. rTSA processes reduce this energy demand. Tube bundle adsorbers are heated and cooled indirectly by a fluid heat transfer medium which offers heat integration options. Further, cycle durations are shortened (Schürer & Salazar Duarte 2015, Salazar Duarte et al. 2016).

Studies considering CO_2 capture processes in literature Different studies relating to simulation and optimisation of CO_2 capture processes can be found in literature. Berstad et al. (2012) have proposed a low-temperature process consisting of a series

of distillation columns to reduce the CO_2 content in natural gas from 50.6 vol-% to 50 ppm (LNG specification). Safari et al. (2009) have optimised a one-stage and two-stage membrane process removing CO_2 from a natural gas feed with CO_2 contents of 5 mol-% to 20 mol-%. They have studied the effect of various parameters on the process performance and have found that permeate pressure has a significant effect in optimisation. Peters et al. (2011) have compared a natural gas sweetening process using amine absorption with membrane processes for CO_2 feed contents of 2.9 mol-% and 9.5 mol-%. They have found that the membrane processes yield sweetenend natural gas with higher CO_2 impurities compared to amine absorption but are less expensive with respect to capital investment. Hospital-Benito et al. (2021) have performed a techno-economic assessment of CO_2 separation by chemical absorption with ionic liquids. The feed includes CO_2 contents of 13 mol-% to 40 mol-%. Lee et al. (2018) have described a systematic optimisation framework for automated design of multi-stage membrane processes for CO_2 removal from flue gas. Process structure and operating conditions are determined by superstructure optimisation with a genetic algorithm. Leimbrink et al. (2015) have designed a post-combustion CO_2 capture process considering columns and membrane separation. They propose a multi-stage approach for efficient screening for promising alternatives of hybrid processes using shortcut models. When promising alternatives are identified, modelling detail is increased.

4.3 Problem statement and approach

A sour natural gas feed shall be separated into a sweet natural gas and a CO_2 product. Different process alternatives shall be evaluated for varying feed and natural gas product specifications. The goal is to determine which process is favourable depending on the feed pressure, the feed CO_2 and the allowed natural gas product CO_2 content. The specification of the sour natural gas feed S_FEED as well as the purity requirements on the product streams S_NG and S_CO2 are given in Table 4.2. The natural gas and CO_2 product are compressed to 100 bar.

Table 4.2: Feed and product specifications for the separation of CO_2 from sour natural gas.

S_FEED	$\dot{N} = 100\,{}^{\mathrm{mol}}/_{\mathrm{s}},\ T = 303.15\,\mathrm{K},\ y_{\mathrm{N_2}} = 0.02,\ y_{\mathrm{C_2H_6}} = 0.02,\ y_{\mathrm{C_3H_8}} = 0.01$ $p = 20\,\mathrm{bar} - 80\,\mathrm{bar},\ y_{\mathrm{CO_2}} = 0.4 - 0.8,\ y_{\mathrm{CH_4}} = 1 - \sum_{i=1}^{n_c-1} y_i$
S_NG	$y_{\mathrm{CO_2}} = 0.03 - 50\,\mathrm{ppm},\ p = 100\,\mathrm{bar}$
S_CO2	$y_{\mathrm{CH_4}} = 0.001,\ p = 100\,\mathrm{bar}$

4.4 Process superstructure and optimisation problem

Process optimisation is applied to identify favourable process alternatives depending on feed pressure, feed CO_2 contents, and allowed natural gas product CO_2 contents. The modelled superstructure includes relevant process alternatives as well as corresponding heat integration and recycle options and is shown in Figure 4.1. General modelling specifications are given in Table A.1 in the appendix.

Process alternatives Only process alternatives including two separation units are considered. One unit must separate natural gas to specification, while the other unit must separate CO_2 to specification. For separation of natural gas, either a membrane or an absorption/desorption unit with methanol as a physical solvent is used. For separation of CO_2, either a membrane or a cryogenic distillation unit is used. Hence, eight process alternatives are possible. Table 4.3 lists the possible process alternatives and indicates the further evaluated process alternatives with their corresponding optimisation variables. Unfavourable process alternatives are identified by applying general heuristics and are not further evaluated. In Figures 4.2 to 4.5, the four further evaluated process alternatives are highlighted. Variable w is used as a counting variable and identifier for the four process alternatives.

Table 4.3: Considered process alternatives with their corresponding optimisation variables

ω	**NG**	**CO_2**		**Optimisation variables**
1	MEM01	T01	✓	p_{process}, $p^{\text{P}}_{\text{MEM01}}$, T_{MEM01}, T_{MSE01}, T_{MSE02}, T_{E05}, f_{SPL07}
2	MEM01	MEM02	✓	p_{process}, $p^{\text{P}}_{\text{MEM01}}$, T_{MEM01}, $p^{\text{P}}_{\text{MEM02}}$, T_{MEM02}
	T02/T03	T01	-	
	T02/T03	MEM02	-	
	CO_2	**NG**		**Optimisation variables**
3	T01	MEM02	✓	p_{process}, $p^{\text{P}}_{\text{MEM02}}$, T_{MEM02}, T_{MSE01}, T_{MSE02}, T_{E05}, f_{SPL07}
4	T01	T02/T03	✓	p_{process}, T_{MSE02}, T_{abs}, r_{abs}
	MEM01	MEM02	-	
	MEM01	T02/T03	-	

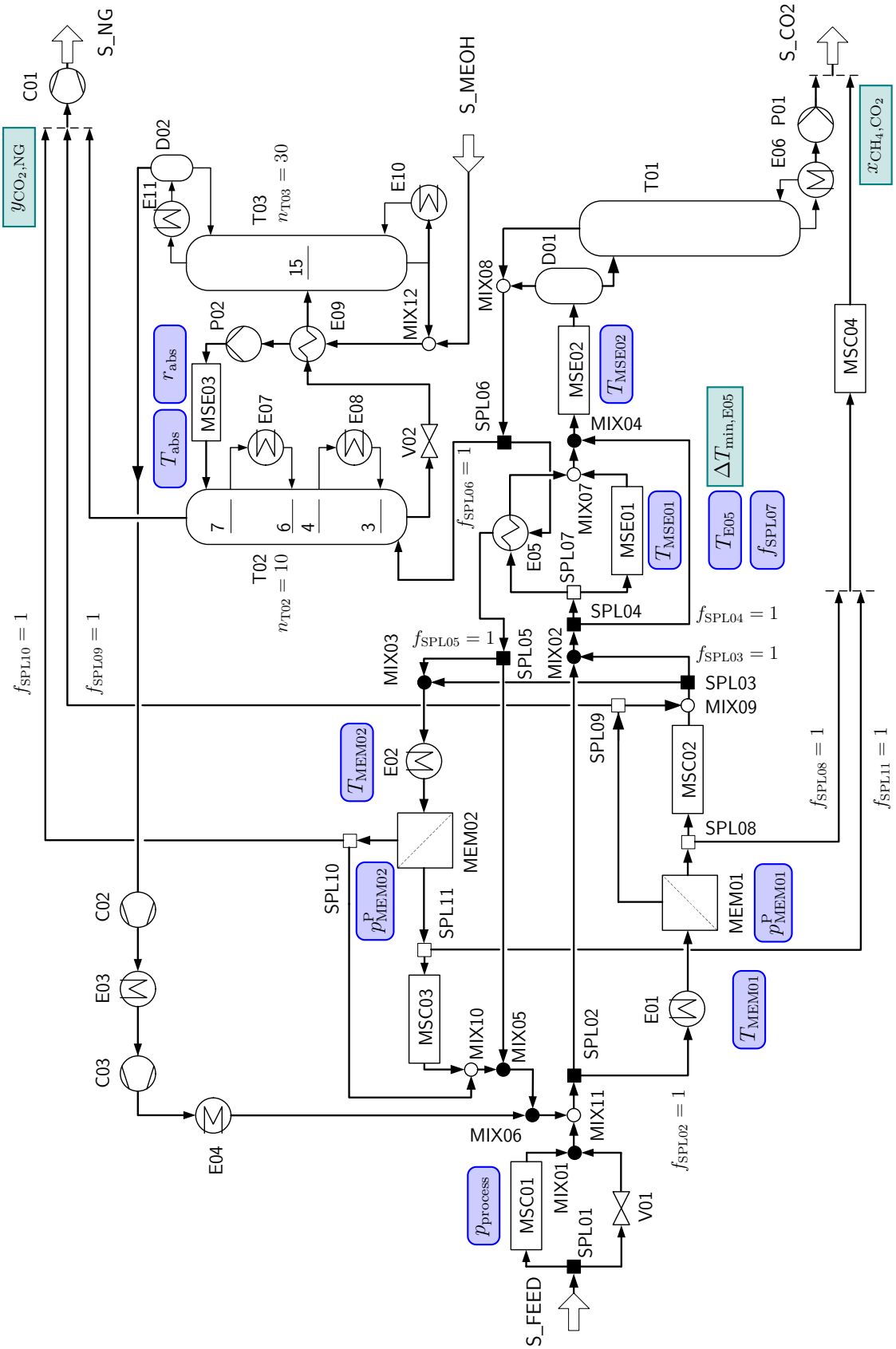

Figure 4.1: Superstructure for CO_2 removal from sour natural gas

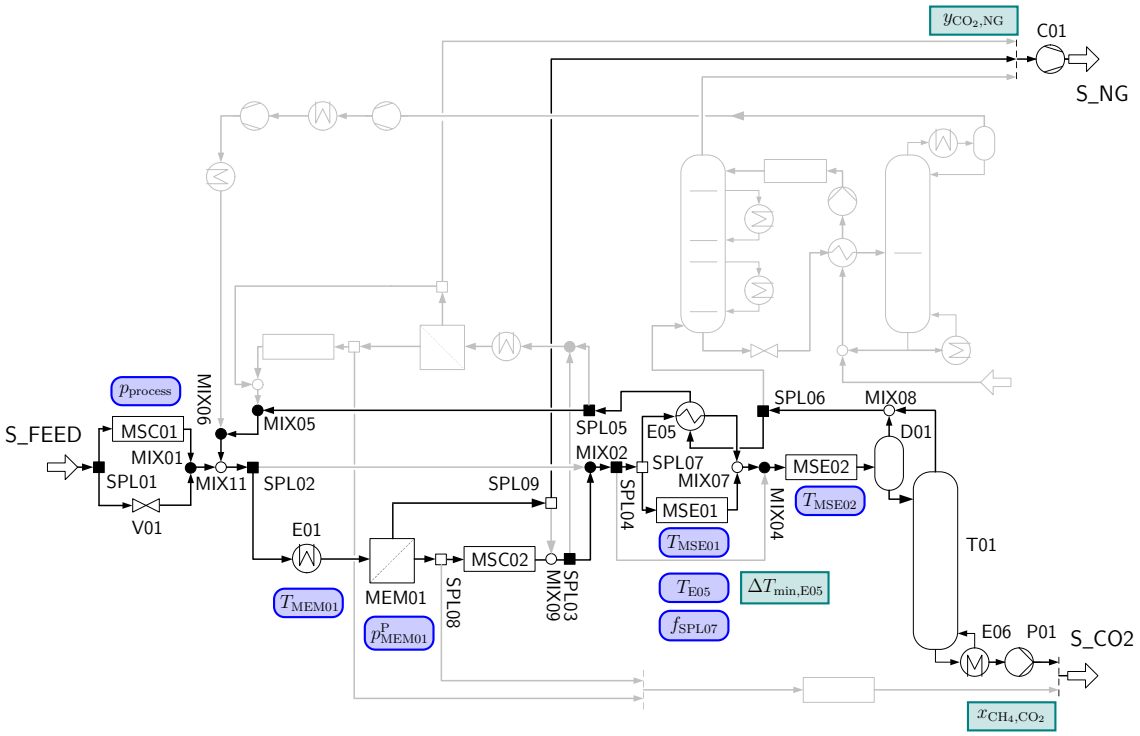

Figure 4.2: Separation of CO_2 from sour natural by gas membrane separation and cryogenic distillation ($\omega = 1$).

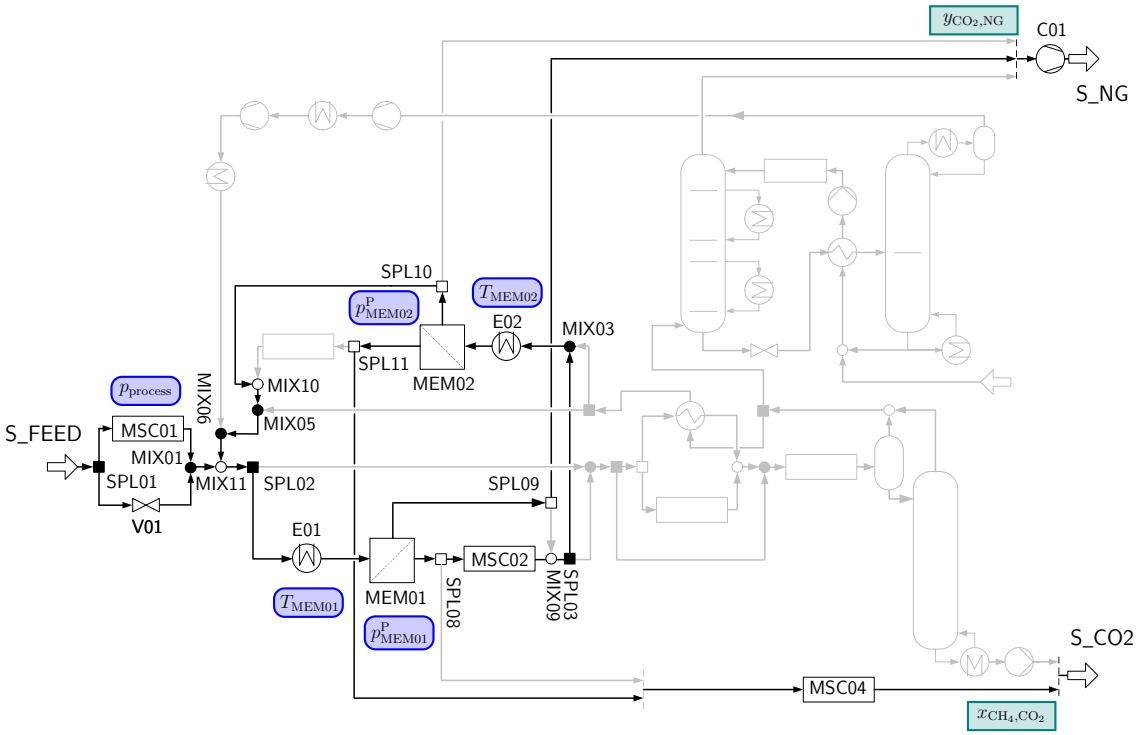

Figure 4.3: Separation of CO_2 from sour natural by one membrane separating natural gas and one membrane separating CO_2 ($\omega = 2$).

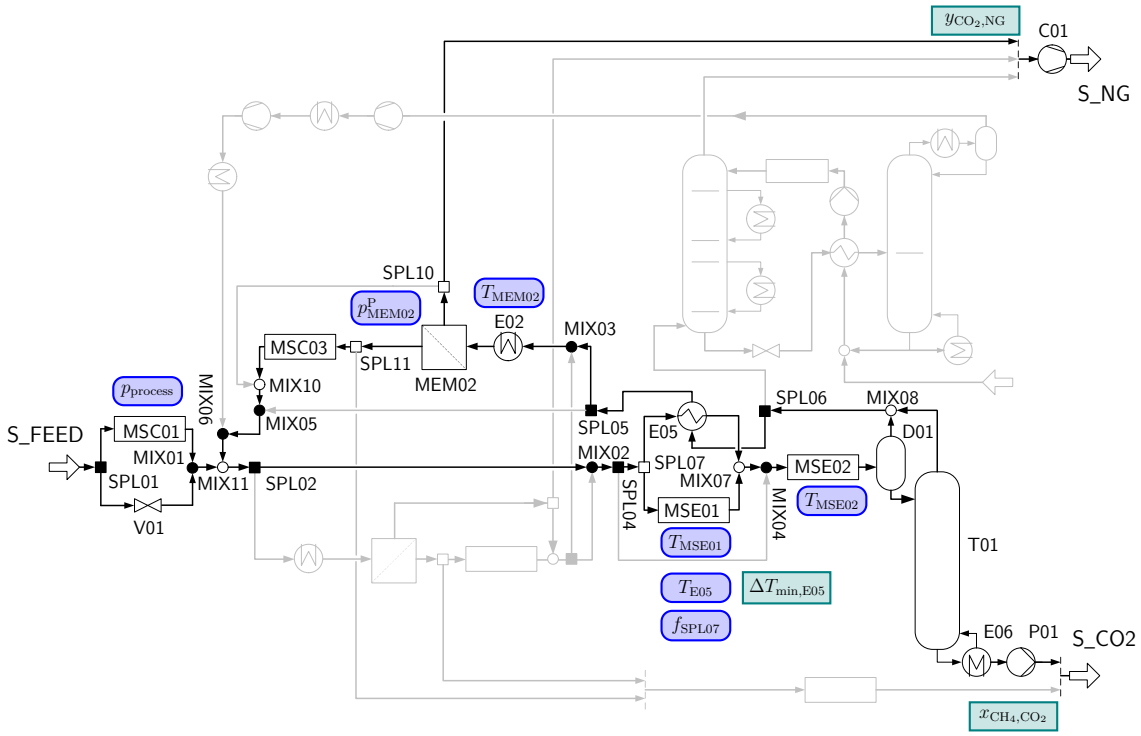

Figure 4.4: Separation of CO_2 from sour natural gas by cryogenic distillation and membrane separation ($\omega = 3$).

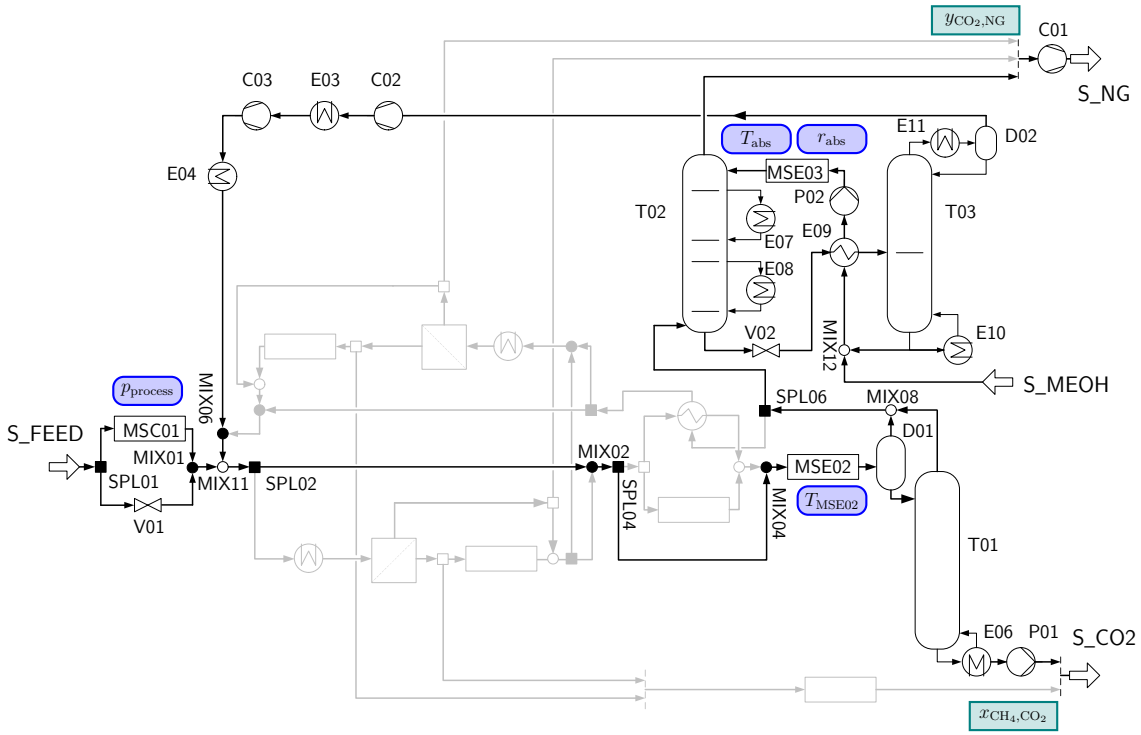

Figure 4.5: Separation of CO_2 from sour natural gas by cryogenic distillation and absorption/desorption ($\omega = 4$).

The absorption/desorption unit is not applied as a first separation step in the process since it would have to separate natural gas from a CO_2 rich feed. The amount of circulated absorbens and the energy requirements for absorbens regeneration are expected to be high. Further, a membrane unit separating CO_2 in the first separation step is not favourable since the CO_2 is permeating through the membrane. Lower membrane areas are needed to meet the required CO_2 product purity x_{CH_4,CO_2} resulting in a low CO_2 product flow.

Models for unit operations The modelled superstructure includes cellulose acetate membrane operations (hollow fibre modules), cryogenic distillation, and an absorption/desorption process part. Since numerous process optimisation calculations are needed for the identification of optimal process alternatives for certain feed and product specifications, the superstructure is modelled based on reduced models. Membrane operations MEM01 and MEM02 are modelled by the shortcut model in section 2.3.2. The cryogenic distillation column T01 is represented by the hybrid surrogate model described in section 2.5.4. The absorption/desorption process T02/T03 is modelled by the hybrid surrogate model given in section 2.5.6. Modules MSC01 to MSC04 are multi-stage compression units according to section 2.1.2. Modules MSE01 to MSE03 are multi-stage cooling units according to section 2.2.2.

Two kinds of split and mix operations are included in the superstructure in Figure 4.1. Splits SPL07 to SPL11 as well as mixes MIX07 to MIX12 are units which physically split or mix streams, respectively. The pairs SPL01/MIX01 to SPL06/MIX06 are used to allow for calculation of unit operations in parallel while preventing zero flow streams and mass balance errors. This concept is shown in Figure 4.6.

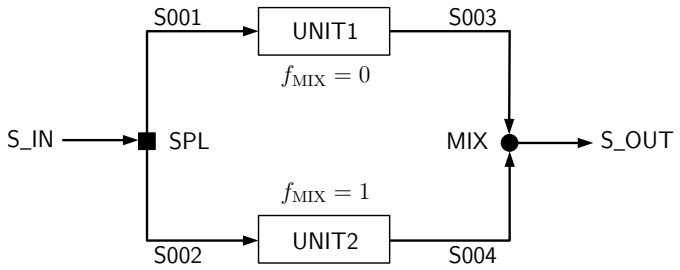

Figure 4.6: Split and mix for parallel calculation of process alternatives.

In the split unit, the split inlet is copied into both split outlets equally:

$$p_{S001} = p_{S002} = p_{S\_IN} \tag{4.1}$$

$$\dot{H}_{S001} = \dot{H}_{S002} = \dot{H}_{S\_IN} \tag{4.2}$$

$$\dot{N}_{i,S001} = \dot{N}_{i,S002} = \dot{N}_{i,S\_IN}. \tag{4.3}$$

In the corresponding mix unit, one of the mix inlets is copied into the mix outlet:

$$p_{\text{S\_OUT}} = (1 - f_{\text{MIX}}) \cdot p_{\text{S003}} + f_{\text{MIX}} \cdot p_{\text{S004}} \tag{4.4}$$

$$\dot{H}_{\text{S\_OUT}} = (1 - f_{\text{MIX}}) \cdot \dot{H}_{\text{S003}} + f_{\text{MIX}} \cdot \dot{H}_{\text{S004}} \tag{4.5}$$

$$\dot{N}_{i,\text{S\_OUT}} = (1 - f_{\text{MIX}}) \cdot \dot{N}_{i,\text{S003}} + f_{\text{MIX}} \cdot \dot{N}_{i,\text{S004}}. \tag{4.6}$$

The dashed lines in the superstructure symbolise modules in which the product stream leaving the active process alternative is selected as the process product stream. Hence, only one of the arriving streams can be the process product at a time so that the process material balance is correct.

Optimisation problem Process optimisation is performed to identify the favourable process alternatives for different combinations of feed and natural gas product specifications. The overall energy requirement – expressed in shaft power – of the examined process alternatives is the optimisation objective *obj*. For each process alternative, the specified natural gas and carbon dioxide product purity have to be respected. The natural gas product purity is systematically varied between $y_{\text{CO}_2,\text{NG,spec}} = 50\,\text{ppm}$ and $y_{\text{CO}_2,\text{NG,spec}} = 0.03$. In case temperature T_{E05} is an optimisation variable, a constraint for the minimum temperature approach in heat exchanger E05 $\Delta T_{\text{min,E05}}$ is included in the optimisation problem. Hence, the optimisation problem is defined by

$$\min \quad obj = P_{\text{tot}} \tag{4.7}$$

$$\text{s.t.} \quad y_{\text{CO}_2,\text{NG}} \leq y_{\text{CO}_2,\text{NG,spec}} \quad \text{with} \quad 50\,\text{ppm} \leq y_{\text{CO}_2,\text{NG,spec}} \leq 0.03 \tag{4.8}$$

$$x_{\text{CH}_4,\text{CO}_2} \leq 0.001 \tag{4.9}$$

$$\Delta T_{\text{min,E05}} \geq 2\,\text{K}. \tag{4.10}$$

Depending on which process alternative ω is active, the components adding to the objective vary. This is considered by including relevant split factors which are either equal to 0 or 1:

$$\begin{aligned} P_{\text{tot}} = & P_{\text{MSC01}} + P_{\text{C01}} + P_{\text{P01}} + f_{\text{SPL02}}(1 - f_{\text{SPL08}})P_{\text{MSC02}} \\ & + f_{\text{SPL05}}(1 - f_{\text{SPL11}})P_{\text{MSC03}} + (f_{\text{SPL08}} + f_{\text{SPL11}})P_{\text{MSC04}} \\ & + f_{\text{SPL03}}((1 - f_{\text{SPL04}})P_{\text{MSE01}} + P_{\text{MSE02}}) \\ & + f_{\text{SPL06}}(P_{\text{C02}} + P_{\text{C03}} + P_{\text{MSE03}} + P_{\text{E07}} + P_{\text{E08}} + P_{\text{E11}} + P_{\text{P02}}). \end{aligned} \tag{4.11}$$

Since the goal of this work is to identify which process alternative is favourable for different combinations of feed and natural gas purity specifications, the superstructure

in Figure 4.1 is optimised for one process alternative at a time. This approach allows to directly compare the energy requirements of the different process alternatives. Hence, relevant split factors are defined as listed in Table 4.4 and kept constant.

Table 4.4: Considered process alternatives with their corresponding split factors.

ω	f_{SPL02}	f_{SPL03}	f_{SPL04}	f_{SPL05}	f_{SPL06}	f_{SPL08}	f_{SPL09}	f_{SPL10}	f_{SPL11}
1	1	1	0	0	0	0	1	0	0
2	1	0	0	1	0	0	1	0	1
3	0	1	0	1	0	0	0	1	0
4	0	1	1	0	1	0	0	0	0

By systematically varying the process options as well as the specifications for p_{feed}, $y_{\mathrm{CO_2,feed}}$, and $y_{\mathrm{CO_2,NG}}$ as shown in Table 4.5, at least 520 optimisation calculations are performed. For each of these optimisation calculations, optimality tolerances are lowered until the found minimum does not change anymore.

Table 4.5: Varied process specifications.

ω	p_{feed} in bar	$y_{\mathrm{CO_2,feed}}$	$y_{\mathrm{CO_2,NG}}$
1	20, 40, 60, 80	0.4, 0.5, 0.6, 0.7, 0.8	0.03, 0.02, 0.01, 0.005, 0.001
2	20, 40, 60, 80	0.4, 0.5, 0.6, 0.7, 0.8	0.03, 0.02, 0.01, 0.005, 0.001
3	20, 40, 60, 80	0.4, 0.5, 0.6, 0.7, 0.8	0.03, 0.02, 0.01, 0.005, 0.001
4	20, 40, 60, 80	0.4, 0.5, 0.6, 0.7, 0.8	0.03, 0.01, 0.001, 0.0001, 50ppm

The bounds for the optimisation variables are given in Table 4.6. The process pressure p_{process} is limited to a maximum of 55 bar to ensure appropriate density differences between the liquid and gaseous phase in column `T01` on every column stage. Membrane permeate pressures do not have fixed upper bounds, but are limited by the membrane feed pressure. Temperature T_{E05} is naturally constrained by the corresponding inlet temperatures. For process option $\omega = 4$ (cryogenic distillation and absorption/desorption), the bounds for temperature $T_{\mathrm{MSE02}} \leq 240\,\mathrm{K}$, temperature T_{abs}, and ratio r_{abs} are defined according to the valid intervals of the hybrid surrogate model.

Table 4.6: Bounds of optimisation variables.

ω	Variable	Min	Max
1-4	p_{process} in bar	30	55
1, 2	$p^{\text{P}}_{\text{MEM01}}$ in bar	1.013	-
2, 3	$p^{\text{P}}_{\text{MEM02}}$ in bar	1.013	-
1, 2	T_{MEM01} in K	283.15	303.15
2, 3	T_{MEM02} in K	283.15	303.15
1, 3	T_{E05} in K	226	-
1, 3	T_{MSE01} in K	226.15	293.15
1, 3, 4	T_{MSE02} in K	226.15	293.15
4	T_{abs} in K	226.15	236.15
4	r_{abs}	0.5	1.25
1,3	f_{SPL07}	0.20	0.99

4.5 Process optimisation

In the first subsection, results for process optimisation with reduced models are presented and discussed. In the second subsection, results obtained with reduced models are compared to results obtained with detailed models.

4.5.1 Comparison of different process alternatives

In Figure 4.7, the trade-off between remaining CO_2 content in the natural gas product $y_{CO_2,NG}$ and the optimised required shaft power *obj* is plotted. The optimisation problem is given in eqs. (4.7) to (4.11). The optimisation variables for the different process alternatives are given in Table 4.3. The six diagrams account for six combinations of feed pressures $p_{\text{feed}} = 40\,\text{bar}$ and $p_{\text{feed}} = 60\,\text{bar}$ with CO_2 feed contents $y_{CO_2,\text{feed}} = 0.4$, $y_{CO_2,\text{feed}} = 0.6$ and $y_{CO_2,\text{feed}} = 0.8$.

In Figure 4.8, the influence of the feed CO_2 content $y_{CO_2,\text{feed}}$ and the feed pressure p_{feed} on the minimised required shaft power *obj* for the different process alternatives is shown. The four diagrams in Figure 4.8 are valid for a natural gas purity specification of $y_{CO_2,NG} = 0.1$.

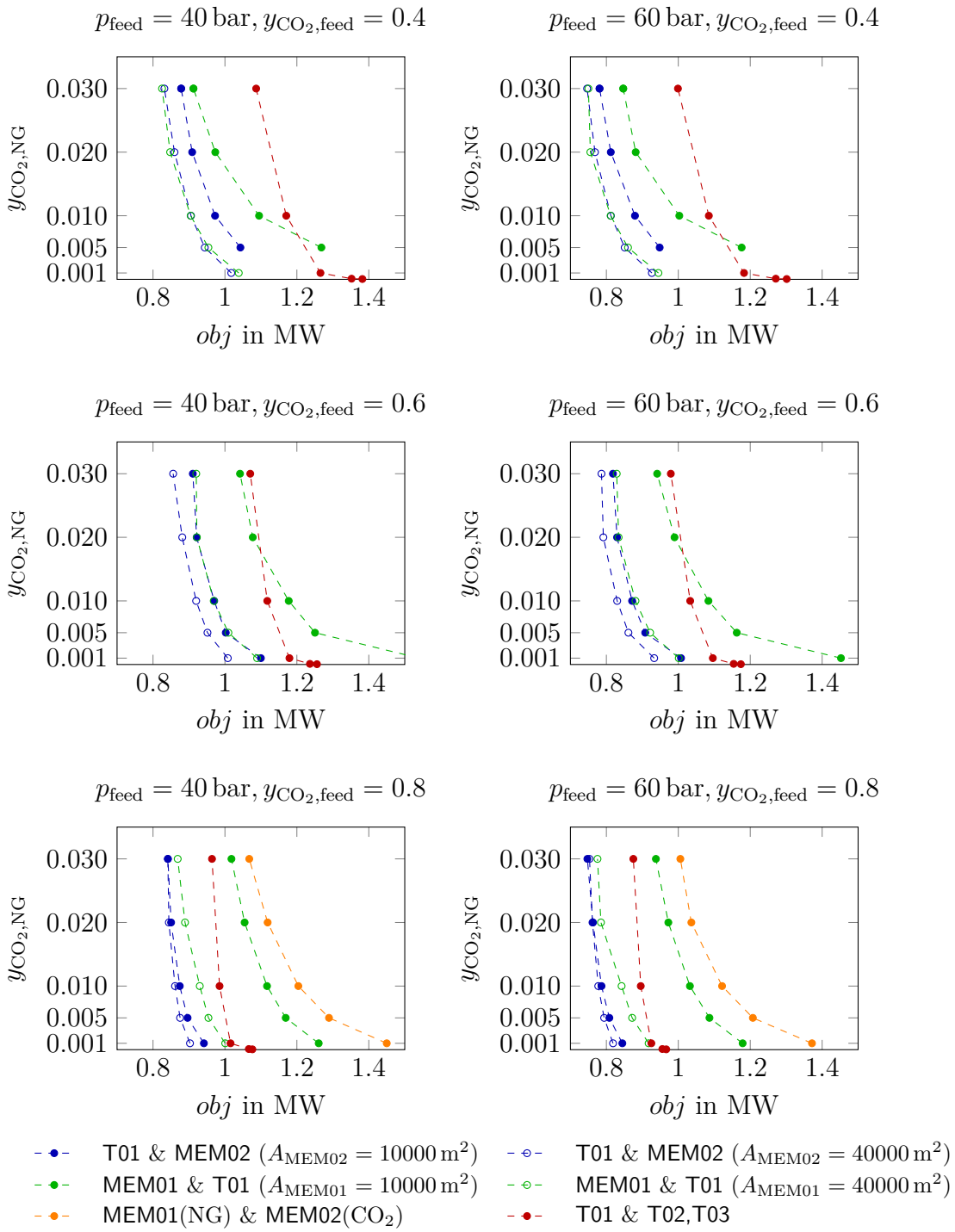

Figure 4.7: Optimisation results for different process alternatives depending on the natural gas impurity specification $y_{\text{CO}_2,\text{NG}}$ ($x_{\text{CH}_4,\text{CO}_2} = 0.001$).

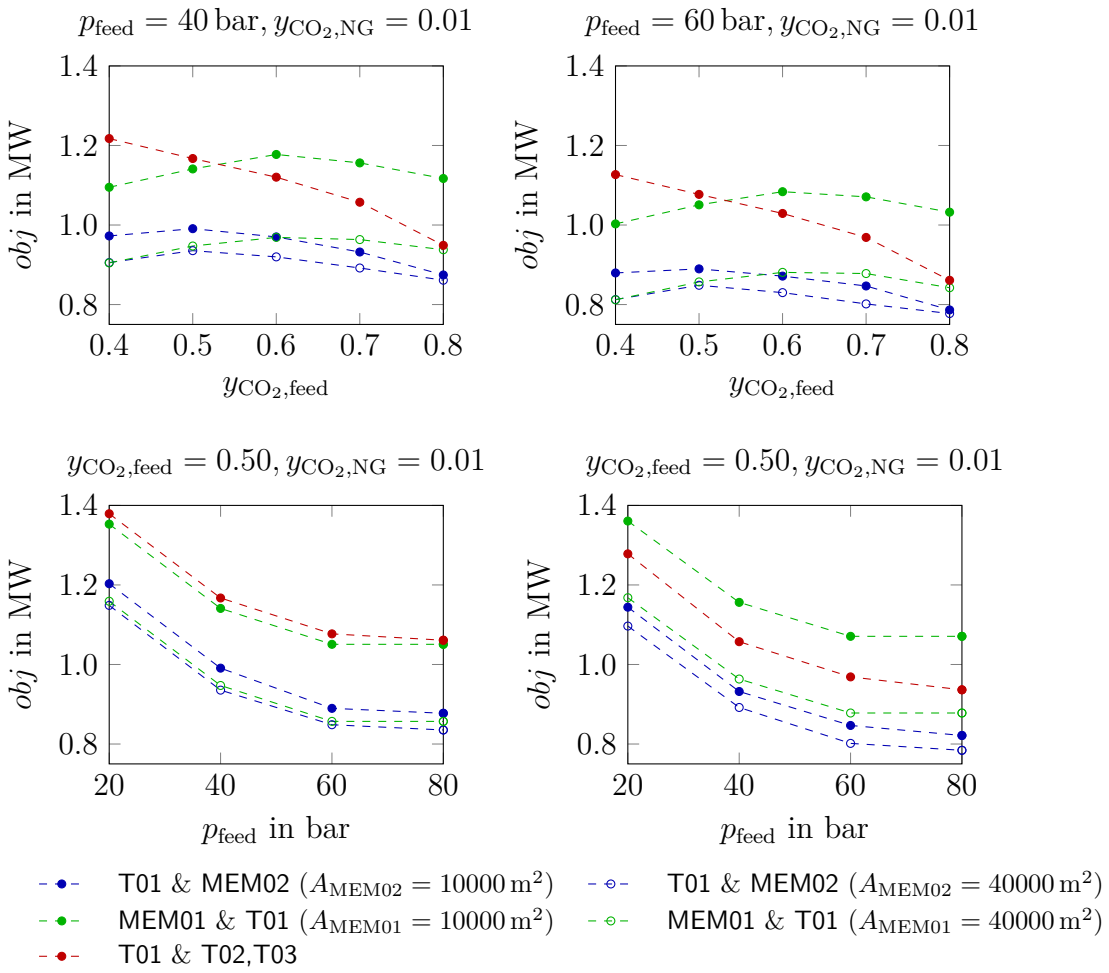

Figure 4.8: Optimisation results for different process alternatives depending on the feed specifications p_{feed} and $y_{\text{CO}_2,\text{feed}} = 0.50$.

According to Figures 4.7 and 4.8, higher feed pressures result in lower shaft power requirements for each process alternative. Varying the feed pressures does not influence which process alternative is favourable.

For a CO_2 content of $y_{\text{CO}_2,\text{feed}} = 0.4$ in the feed, the order of cryogenic distillation and membrane separation does not make a difference in shaft power requirements as long as the membrane area is large enough. For smaller membrane areas, cryogenic distillation before membrane separation is favoured. Since the product purity of $y_{\text{CO}_2,\text{NG}} = 0.001$ cannot be achieved with smaller membrane areas, the corresponding data points are missing in the diagrams. The combination of cryogenic distillation and absorption/desorption is the energetically most expensive alternative for $y_{\text{CO}_2,\text{NG}} \geq 0.01$, but also the only alternative which is able to reach product purities of $y_{\text{CO}_2,\text{NG}} \leq 0.0001$.

For higher CO_2 contents $y_{\text{CO}_2,\text{feed}}$ in the feed, the order of cryogenic distillation and membrane separation becomes more important. Even with a smaller membrane area, process alternative T01/MEM02 is advantageous in comparison to MEM01/T01 with a

larger membrane area. MEM01/T01 with a smaller membrane area is energetically more expensive than the combination of cryogenic distillation and absorption/desorption. The process of two membrane units requires the most shaft power. Data points for the combination MEM01/MEM02 are only included in the diagrams for $y_{CO_2,feed} = 0.8$. For any other combination of feed pressure and feed CO_2 content, the optimisation results for this process alternative are even further away from the other process alternatives.

In Figure 4.8, the optimised objective is plotted in dependence of the CO_2 content $y_{CO_2,feed}$ in the feed. For the process alternatives including heat exchanger E05, maxima are observed for medium values of $y_{CO_2,feed}$. The correlations between $y_{CO_2,feed}$ and energy requirements of the single process alternatives as described in the two paragraphs above are confirmed.

To explain and discuss the energy requirements of the different process alternatives, Figure 4.9 and Figure 4.10 show the superstructure including detailed results for optimisation variables and shaft power components.

It was found that varying feed pressure p_{feed} does not determine which process alternative is favourable because the values for the optimised process pressure $p_{process}$ are in a similar range for each process alternative. This is partly caused by limiting $p_{process}$ to 55 bar in order to ensure appropriate density differences between the liquid and gaseous phase in column T01 on every column stage. For higher process pressures, cryogenic distillation might not be operating correctly. For process alternative MEM01/MEM02, allowing higher process pressures does not improve the results. Although process alternative MEM01/MEM02 is not cryogenic, it features the highest shaft power requirements. Membrane MEM02 cannot separate a high enough CO_2 product flow (CO_2 is permeating) so that the process recycle flow is significantly higher than for process alternatives including cryogenic distillation. Hence, re-compression in multi-stage compression unit MSC02 is energetically expensive. This effect is enhanced for lower CO_2 partial pressures in the process.

Regarding the comparison of alternatives T01/MEM02 and MEM01/T01, including cryogenic distillation as a first and membrane separation as a second operation leads to lower shaft power requirements for the re-compression of the permeate stream although trans-membrane pressure differences are similiar. Permeate re-compression is energetically less expensive for T01/MEM02 because CO_2 is partly removed in the column and hence a smaller permeate flow needs to be re-compressed. In case membrane separation is performed before cryogenic distillation, the required shaft power of multi-stage cooling units MSE01 and MSE02 is lower since a smaller and also CO_2 enriched permeate flow is cooled and temperature T_{MSE02} can remain higher. Overall, process T01/MEM02 is energetically less expensive than MEM01/T01. For membrane areas of 40000 m^2 and $y_{CO_2,feed} = 0.4$, the higher shaft power for re-compression with MEM01/T01 and the higher shaft power for cooling with T01/MEM02 compensate one another and both T01/MEM02 and MEM01/T01 are equally favourable.

Regardless of the order of cryogenic distillation and membrane separation, solutions with smaller membrane areas are energetically more expensive. Higher transmembrane pressure differences are necessary to achieve a specified natural gas product purity $y_{CO_2,NG}$ and hence permeate re-compression requires higher shaft powers. However, for T01/MEM02 and a CO_2 feed content of $y_{CO_2,feed} = 0.8$, applying a membrane area of $A_{MEM02} = 10000\,m^2$ results in almost equally favourable process results as applying $A_{MEM02} = 40000\,m^2$. In this case, the higher re-compression shaft power $\dot{W}_{MSC03}$ for $A_{MEM02} = 10000\,m^2$ is compensated by a lower required cooling shaft power $\dot{W}_{MSE01} + \dot{W}_{MSE02}$. The required cooling shaft power is lower for $A_{MEM02} = 10000\,m^2$ because the process pressure $p_{process}$ is higher making condensation in MSE02 easier. Further, for $A_{MEM02} = 40000\,m^2$, the stream combining the process feed and the recycled permeate from membrane MEM02 (stream leaving MIX11) has a flow of $165\,{}^{mol}/_{s}$ with a CO_2 content of $y_{CO_2} = 0.75$. For $A_{MEM02} = 10000\,m^2$, the same stream has a flow of $135\,{}^{mol}/_{s}$ with a CO_2 content of $y_{CO_2} = 0.80$ making condensation easier in MSE02.

For process alternatives including cryogenic distillation and membrane separation, non-intuitive maxima of the optimised objective are observed for varying CO_2 contents $y_{CO_2,feed}$ in the feed. Two opposing effects cause the observed maxima. First, the shaft power required by multi-stage cooling unit MSE01 is higher for higher values of $y_{CO_2,feed}$ because more flow is directed to MSE01 (higher values for f_{SPL07}). The capacity of heat exchanger E05 is limited since condensation of streams with a higher CO_2 content limits temperature decrease of the warm stream (higher values for T_{E05}) and the minimum temperature difference $\Delta T_{E05} = 2\,K$ has to be respected. Second, although the inlet temperature to multi-stage cooling unit MSE02 is slightly higher for higher values of $y_{CO_2,feed}$, the shaft power requirements of MSE02 are lower since condensing a stream with higher CO_2 contents requires less cooling duty and allows for higher outlet temperatures T_{MSE02}. While increased shaft power requirements for MSE01 dominate for lower CO_2 contents in the feed, this effect is compensated by savings regarding the shaft power requirements of MSE02 for higher CO_2 contents in the feed.

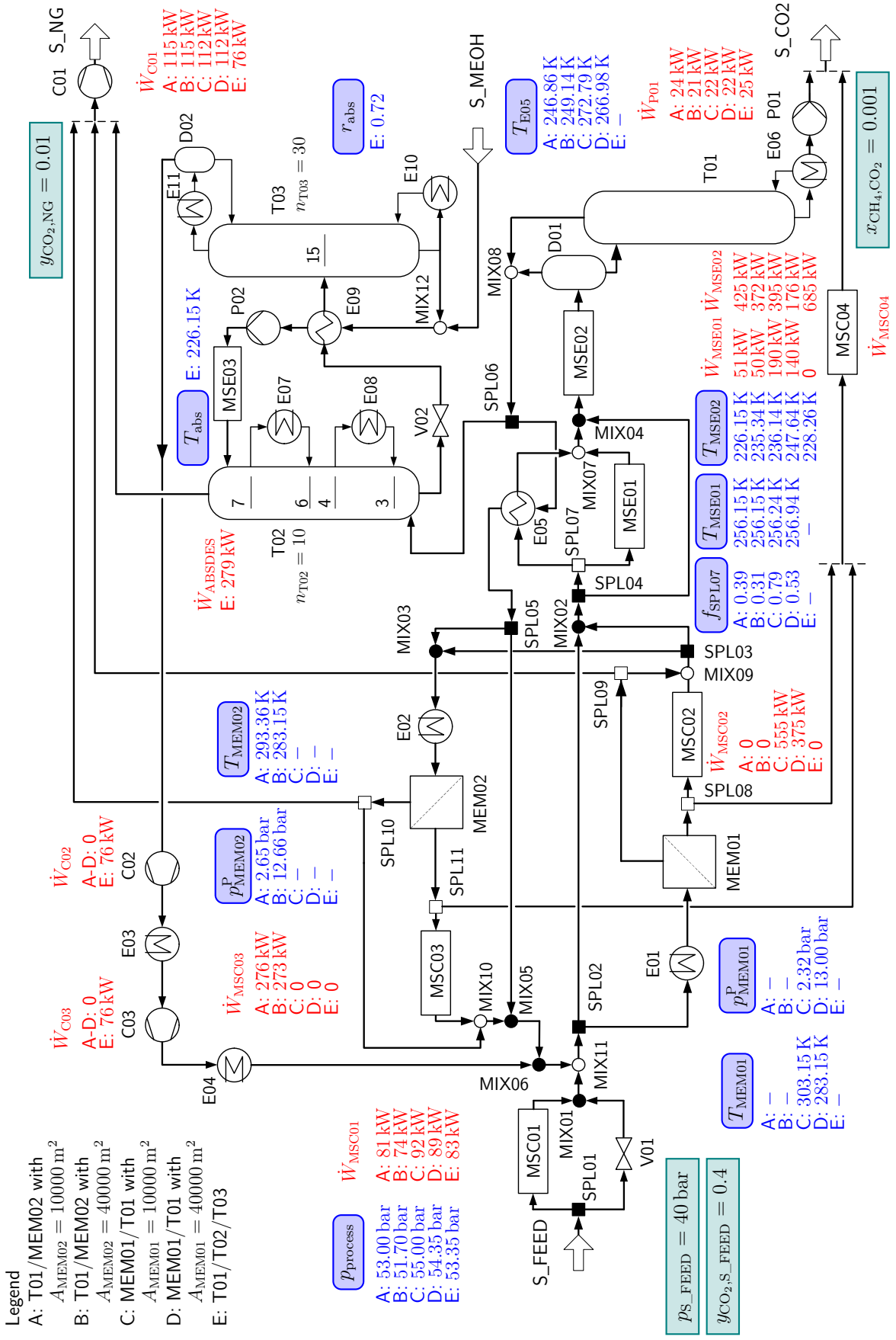

Figure 4.9: Results for optimisation of CO_2 removal from sour natural gas for $p_{S\_FEED} = 40\,bar$, $y_{CO_2,S\_FEED} = 0.4$, and $y_{CO_2,NG} = 0.01$.

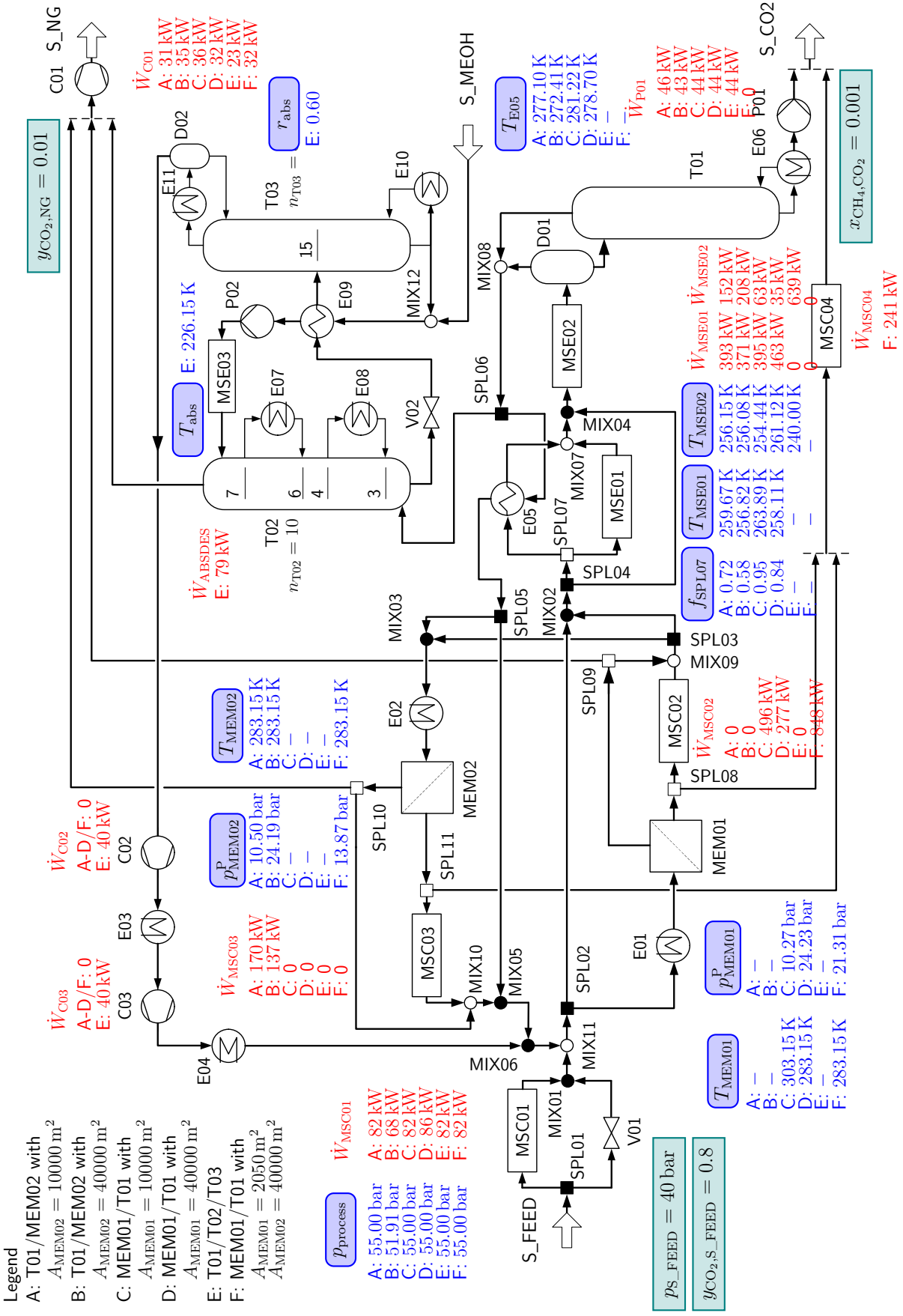

Figure 4.10: Results for optimisation of CO_2 removal from sour natural gas for $p_{S\_FEED} = 40\,bar$, $y_{CO_2,S\_FEED} = 0.8$, and $y_{CO_2,NG} = 0.01$.

4.5.2 Comparison of results based on reduced and detailed models

Combination of distillation and absorption/desorption Exemplary results for process T01/T02/T03 are given in Table 4.7. Based on equal start values, optimisation with reduced (columns 'R, opt.') and detailed models (column 'D, opt.') is performed. In both cases, the start value for ratio r_{abs} is adjusted so that the desired natural gas purity of $y_{\text{CO}_2,\text{NG}}$ is achieved. No other process variable or parameter is changed.

Table 4.7: Process T01/T02/T03: comparison of results obtained with detailed and reduced models ($p_{\text{feed}} = 40\,\text{bar}$, $y_{\text{CO}_2,\text{feed}} = 0.8$).

		$y_{\text{CO}_2,\text{NG}} = 0.0001$		$y_{\text{CO}_2,\text{NG}} = 0.01$	
	Unit	R, opt.	D, opt.	R, opt.	D, opt.
p_{process}	bar	54.97	54.77	55.00	54.48
T_{MSE02}	K	240.00	236.10	240.00	235.98
T_{abs}	K	226.15	226.15	226.15	226.15
r_{abs}	-	1.038	1.144	0.603	0.704
obj	MW	1.013	1.044	0.949	0.985

In Figure 4.11, optimisation results obtained with reduced and detailed models for process T01/T02/T03 are compared. The difference between optimised process energy requirements calculated with reduced and detailed models is between 2.7 % and 3.3 %. Subsequent optimisation with detailed models provides slightly higher process energy requirements than optimisation with reduced models.

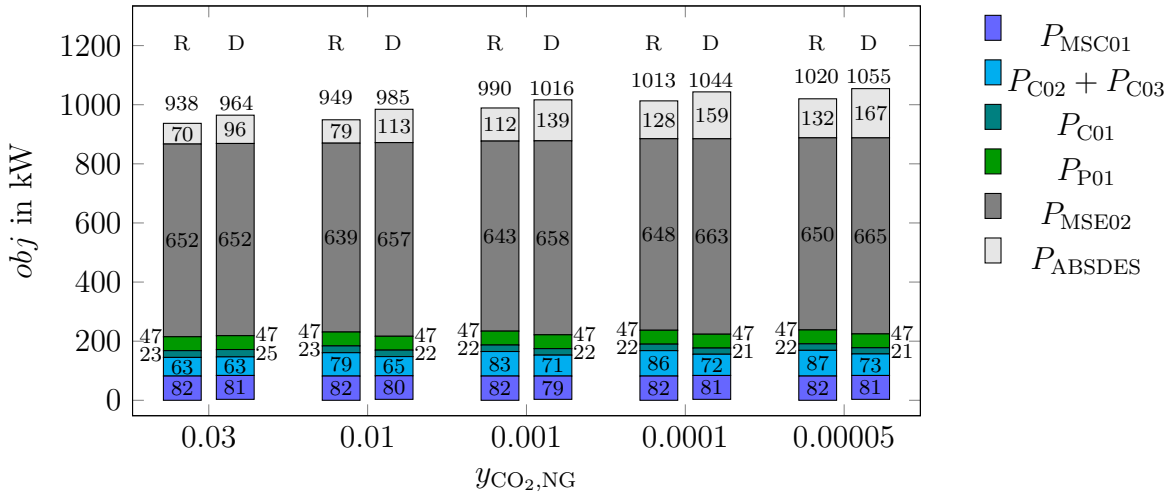

Figure 4.11: Process T01/T02/T03: comparison of optimisation results obtained with reduced or detailed models ($p_{\text{feed}} = 40\,\text{bar}$, $y_{\text{CO}_2,\text{feed}} = 0.8$).

The energy requirements in multi-stage compression unit MSC01, natural gas compressor C01, and CO_2 pump P01 are similar after optimisation with reduced and

detailed models. Differences occur for multi-stage cooling unit MSE02, recycle compressors C02/C03 and the shaft power requirement in the absorption/desorption unit T02/T03.

For both optimisation with reduced and detailed models, the optimised absorbens temperature T_{abs} is at the lower bound of 226.15 K. Using detailed models, the desired natural gas purity is achieved by increasing ratio r_{abs} leading to higher energy requirements in multi-stage cooling unit MSE03 and hence higher shaft power requirements in the absorption/desorption unit T02/T03. The increase in r_{abs} is limited by reducing T_{MSE02} below 240 K which has three effects making natural gas purification easier: the stream entering the absorption column is colder, has a lower flow and a lower CO_2 content. The lower flow of the absorption column gas inlet also results in a lower recycle and hence in lower shaft power requirements of recycle compressors C02/C03.

However, optimisation with reduced and detailed models was performed based on equal start values and results in similar process optima (see Table 4.7 and Figure 4.11). In the two-step optimisation approach, optimisation with reduced models can be used to identify the process optimum, while subsequent optimisation with detailed models can be used to ensure high accuracy.

Combination of distillation and membrane Reduced models provide similar simulation and optimisation results compared to detailed models. Exemplary results for process T01/MEM02 are given in Table 4.8. After optimisation with reduced models (columns 'R, opt.'), the reduced models are replaced by corresponding detailed models (columns 'D, start'). Permeate pressure $p^{\mathrm{P}}_{\mathrm{MEM02}}$ is adjusted so that the desired natural gas purity of $y_{\mathrm{CO_2,NG}}$ is achieved. Temperature T_{E05} is adjusted so that the minimum temperature approach in heat exchanger E05 is respected. Apart from $p^{\mathrm{P}}_{\mathrm{MEM02}}$ and T_{E05}, no process variable or parameter is changed. Based on the start values for detailed models, optimisation is performed using detailed models (column 'D, opt.').

Table 4.8: Process T01/MEM02: comparison of results obtained with detailed and reduced models ($p_{\text{feed}} = 40\,\text{bar}$, $y_{\text{CO}_2,\text{feed}} = 0.4$, $A_{\text{MEM02}} = 40000\,\text{m}^3$).

		$y_{\text{CO}_2,\text{NG}} = 0.001$			$y_{\text{CO}_2,\text{NG}} = 0.03$		
	Unit	R, opt.	D, start	D, opt.	R, opt.	D, start	D, opt.
p_{process}	bar	52.10	52.10	52.01	52.29	52.29	52.29
$p^{\text{P}}_{\text{MEM02}}$	bar	8.77	8.74	8.79	16.25	16.25	16.25
T_{MEM02}	K	283.15	283.15	283.15	283.15	283.15	283.15
T_{MSE01}	K	255.99	255.99	255.99	254.23	254.23	254.23
T_{MSE02}	K	229.78	229.78	227.94	236.18	236.18	236.18
T_{E05}	K	245.78	245.80	244.71	249.63	249.61	249.61
f_{SPL07}	-	0.3178	0.3178	0.3220	0.3048	0.3048	0.3047
obj	MW	1.018	1.034	1.033	0.832	0.840	0.840

Although the constraints for the natural gas CO_2 content $y_{\text{CO}_2,\text{NG}}$ and the minimum temperature approach $\Delta T_{\text{min,E05}}$ are active after optimisation with reduced models, variables $p^{\text{P}}_{\text{MEM02}}$ and T_{E05} are only slightly adjusted after switching from reduced models to detailed models. This indicates that the reduced model flowsheet is very accurate.

Optimisation results obtained with reduced (referring to column 'R, opt.') and detailed models (referring to column 'D, opt.') for process T01/MEM02 are compared in Figure 4.12. Relative deviations of 1.0 % to 1.6 % occur between the optimised objective *obj*.

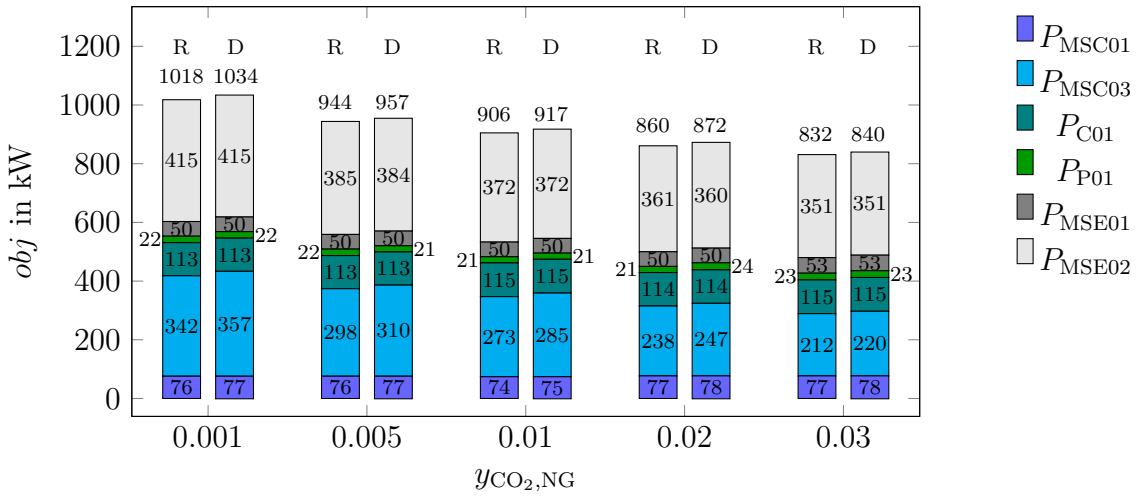

Figure 4.12: Process T01/MEM02: comparison of optimisation results obtained with reduced (R) or detailed (D) models ($p_{\text{feed}} = 40\,\text{bar}$, $y_{\text{CO}_2,\text{feed}} = 0.4$, $A_{\text{MEM02}} = 40000\,\text{m}^3$).

These differences are solely caused by multi-stage compression units MSC01 and MSC03. The inlet flows, the inlet temperatures and the recompression ratios are equal in the optimisation results with reduced and detailed models. Hence, the differences occur due to differences in unit modelling. In the reduced multi-stage compression unit, the compression ratios of each stage are assumed equal in order to approximate equal stage shaft powers. This leads to slight differences in compressor power consumption. In the detailed multi-stage compression unit, the shaft powers of the compression stages are assumed equal since each compression stage is connected to the compressor's bull gear (not considering specialist designs).

However, considering Table 4.8, optimisation calculations with reduced models and with detailed models provide the same process optimum. In the two-step optimisation approach, optimisation with reduced models can be used to identify the process optimum, while subsequent optimisation with detailed models can be used to ensure high accuracy.

5 Summary, conclusion, and outlook

Process synthesis and design by simulatenously optimising separation sequences, recycle and heat integration options as well as process design variables is a systematic, practical, and hence powerful approach. However, industrial application of simultaneous process optimisation can result in large-scale and complex optimisation problems. The goal of this work is to facilitate simultaneous optimisation of process structure and design in early development phases of industrial process synthesis by diminishing the complexity of the arising optimisation problem.

The complexity of the arising optimisation problem is diminished by applying reduced models for unit operations. In the context of this work, several reduced models for use in gradient-based process optimisation are developed and validated: a multi-stage compression unit, a multi-stage cooling unit, a membrane shortcut model, a column shortcut model as well as hybrid surrogate models for columns. Each reduced model is accurate and can be used in process optimisation. For reduced models to be applicable in gradient-based process optimisation, the Karush-Kuhn-Tucker conditions of the reduced and the corresponding detailed model must be similar (Biegler et al. 2014). This ensures that gradient-based optimisation algorithms are provided with correct derivative information. The reduced models have been successfully evaluated with respect to criteria derived from the Karush-Kuhn-Tucker conditions.

To reduce the complexity of a unit operation model, the number of equations introducing nonlinearities such as equilibrium calculations is decreased. In particular, hard to solve stage-to-stage column models are successfully substituted by the Adapted Edmister Model, a newly developed shortcut model, as well as hybrid surrogate models. Both the Adapted Edmister Model and the hybrid surrogate models are based on column segments in which column stages are grouped together. Another important way to reduce optimisation problem complexity is to enable integer-free NLP optimisation instead of harder to solve MINLP optimisation. Design variables which would typically be degrees of freedom in process optimisation such as column stage numbers and the number of compression stages are included as continuous variables in the developed reduced models.

Two industrial process examples are used to demonstrate the great potential of the developed reduced models. The application of the newly developed shortcut model for distillation columns is demonstrated by designing a thermally coupled double column for separation of air into nitrogen and oxygen products based on process optimisation. The number of column stages in the high pressure column, side draw and feed locations of the low pressure column as well as further design variables such as split factors, pressures, and temperatures are optimised simultaneously in a nonlinear programming problem using the new shortcut model. Optimisation is performed to show the trade-off between the plant's energy efficiency related to liquid oxygen production and the overall number of stages in the double column.

With a second process example, systematic design of hybrid separation processes for removal of CO_2 from natural gas considering different combinations of distillation, membrane separation, and absorption is demonstrated. The presented framework using different shortcut and hybrid surrogate models is applied for automated performance of an extensive series of optimisation calculations minimising operational energy requirements. As a result, an overview for identification which process topology is optimal for which combination of natural gas feed and natural gas product specification is provided.

Satisfying industrial standards of simulation and optimisation accuracy, a two-step optimisation approach can be applied. This two-step approach consists of a first optimisation step using reduced models and a second optimisation step using detailed models which can be initialised using results from the first step. However, the second optimisation step is not obligatory since the reduced models were found to provide very similar optima to the detailed models. Further, using reduced models shortens calculation times and improves convergence behaviour significantly.

In the context of this thesis, the reduced models are based on steady-state assumptions. If the reduced models are extended to dynamic simulation, they can be used for new applications, for example, in advanced process control or as soft senors for production plants. In this case, calculation times and robustness are of even more importance than for process design. The Adapted Edmister Model, for example, has been modified for dynamic optimisation. It has been applied successfully in model reduction of a high accuracy digital twin of air separation processes by Kender et al. (2022). Further, it is going to be used in the control model and state estimator of a new nonlinear model predictive controller for air separation units. The available set of reduced models can be extended for application to other processes. The reduced models have been implemented in Linde OPTISIM® but can be migrated to any equation-oriented environment for use in different frameworks, if required.

A Appendix

A.1 General modelling specifications

In Table A.1, general modelling specifications are listed. They apply to each chapter of this thesis unless stated otherwise.

Table A.1: General modelling specifications.

Unit	Assumption
Heat exchanger	$\Delta p = 0.2\,\text{bar}$ (no phase change)
	$\Delta p = 0.1\,\text{bar}$ (condensing/boiling)
	$\Delta T_{\text{min}} = 1 - 2\,\text{K}$
Cooling water cooler	$\Delta T_{\text{CW}} = 303.15\,\text{K}$ (process side)
Separator	$\Delta p = 0$
Column	$\Delta p_{\text{tray}} = 0.001\,\text{bar}$
Compressor	$\eta_{\text{adia}} = 0.8$
Pump	$\eta_{\text{adia}} = 0.5$

A.2 Annotations to artificial neural networks architectures

Table A.2 summarises common architectures of artifical neural networks and provides information about their application as well as network examples.

Table A.2: Overview of network architectures (according to da Silva et al. (2017)).

Architecture	**Description**	**Application**	**Examples**
Single-layer feed forward network	Network with only one layer which is the output layer	Pattern classification, function approximation, linear filtering problems	Perceptron (Rosenblatt 1961), ADALINE (Widrow & Hoff 1960)

Multi-layer feed forward network	Network with one or more hidden layers and an output layer	Pattern classification, function approximation, process control, optimisation, robotics	Multi-layer perceptron (Rosenblatt 1961), radial basis function network (Broomhead & Lowe 1988)
Recurrent network	Network in which neuron outputs are used as feedback inputs for other neurons	Time series prediction, optimisation, process control	Hopfield (Hopfield 1982), perceptron with feedback (Rosenblatt 1961)
Mesh network	Spatial neuron localisation and connection depend on the training process	Pattern recognition, data clustering, system optimisation	Kohonen network (Kohonen 1982)

A.3 Annotations to feed forward artificial neural network training

In Figures A.1 and A.2, exemplary plots for feed forward network training progress with backpropagation and different constant and dynamic learning rates are shown. The training progress is quantified by decreasing network errors δ_{net} as defined in eq. (2.115). Both figures include plots for the training and the evaluation data set which are generated randomly in a size ratio of 3:1 from the original data set.

Figure A.1 for constant learning rates illustrates two aspects:

- If the constant learning rate is too small, the network error δ_{net} is not decreased fast enough at the beginning of the training. Hence, the training result after 10^5 epochs is not sufficient.
- If the constant learning rate is too large, the network error δ_{net} is decreased sufficiently at the beginning of the training. However, the network error does not converge to a stable value towards the end of the training.

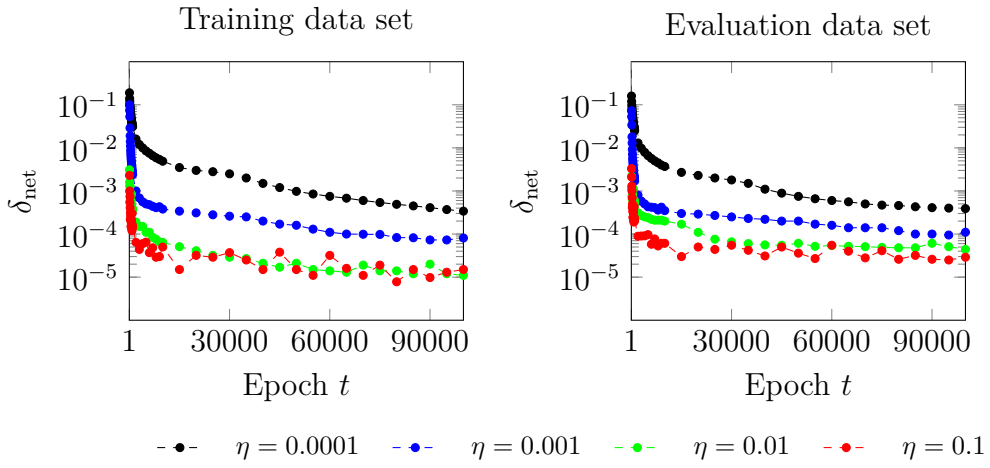

Figure A.1: Training progress for constant learning rates.

In Figure A.2, the training progress for different ranges of dynamic learning rates is shown. While the network error δ_{net} remains stable towards the end of the training in all four cases, the learning progress at the beginning of the training is better for higher start learning rates.

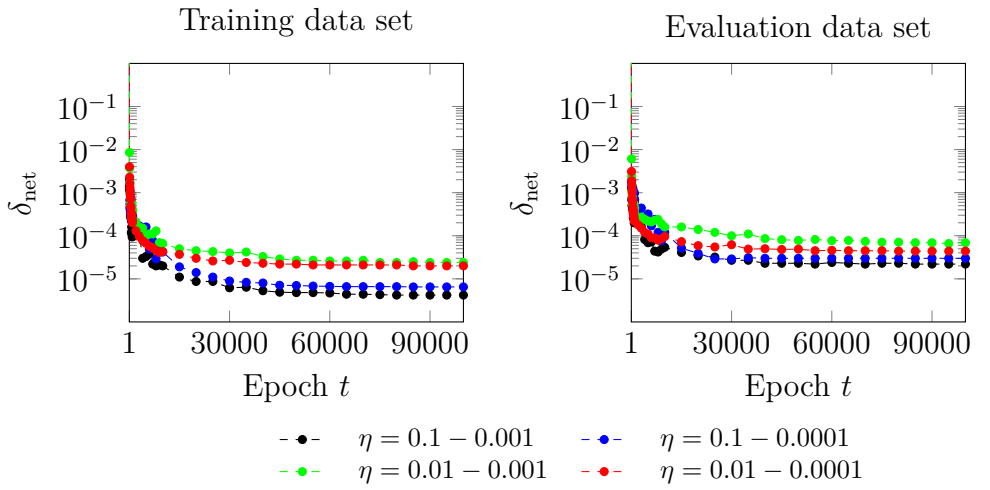

Figure A.2: Training progress for dynamic learning rates.

A.4 Annotations to the implementation of the Adapted Edmister Model

The reduced models which are presented in this thesis are implemented in the Linde proprietary simulation and optimisation software OPTISIM® (Eich-Soellner et al. 1997) using the Dynamic Equation Block as a process unit modelling framework (Thomas 2011). In this section, modelling strategies for improved convergence of the Adapted Edmister Model are pointed out.

As described in section 2.4.2, the effective absorption and stripping factors are determined by eqs. (A.1) and (A.2):

$$Ae_i = \sqrt{A_{i,n_\mathrm{s}}(A_{i,1}+1)+0.25} - 0.5 \qquad \text{for } i = 1, ..., n_\mathrm{c} \tag{A.1}$$

$$Se_i = \sqrt{S_{i,1}(S_{i,n_\mathrm{s}}+1)+0.25} - 0.5 \qquad \text{for } i = 1, ..., n_\mathrm{c}. \tag{A.2}$$

Before solving these equations, they are transformed into a different form by OPTISIM® internally:

$$0 = Ae_i - \exp\left(\frac{1}{2}\ln(A_{i,n_\mathrm{s}}(A_{i,1}+1)+0.25)\right) - 0.5 \qquad \text{for } i = 1, ..., n_\mathrm{c} \tag{A.3}$$

$$0 = Se_i - \exp\left(\frac{1}{2}\ln(S_{i,1}(S_{i,n_\mathrm{s}}+1)+0.25)\right) - 0.5 \qquad \text{for } i = 1, ..., n_\mathrm{c}. \tag{A.4}$$

The (uncorrected) performance factors are determined by

$$\phi_{\mathrm{A},i} = \frac{Ae_i - 1}{Ae_i^{(n_\mathrm{s}-2)+1} - 1} \qquad \text{for } i = 1, ..., n_\mathrm{c} \tag{A.5}$$

$$\phi_{\mathrm{S},i} = \frac{Se_i - 1}{Se_i^{(n_\mathrm{s}-2)+1} - 1} \qquad \text{for } i = 1, ..., n_\mathrm{c} \tag{A.6}$$

with the terms $Ae_i^{(n_\mathrm{s}-2)+1}$ and $Se_i^{(n_\mathrm{s}-2)+1}$ being transformed to

$$Ae_i^{(n_\mathrm{s}-2)+1} = \exp\left(((n_\mathrm{s}-2)+1)\ln(Ae_i)\right) \qquad \text{for } i = 1, ..., n_\mathrm{c} \tag{A.7}$$

$$Se_i^{(n_\mathrm{s}-2)+1} = \exp\left(((n_\mathrm{s}-2)+1)\ln(Se_i)\right) \qquad \text{for } i = 1, ..., n_\mathrm{c}. \tag{A.8}$$

Hence, it is beneficial to consider that Ae_i and Se_i are ln-arguments and cannot be zero within the implemented modelling equations (before OPTISIM® transforms the modelling equations internally). However, the solution of $\phi_{\mathrm{A},i} = 1$ and $\phi_{\mathrm{S},i} = 1$ is not obtainable, if Ae_i and Se_i cannot reach zero. This is why a linear substitute function for $\phi_{\mathrm{A},i}$ and $\phi_{\mathrm{S},i}$ for values of Ae_i and Se_i between zero and a very small number ε is introduced. In eqs. (A.9) to (A.12), the implemented cases are given:

$$Ae_i = \begin{cases} \sqrt{A_{i,1}(A_{i,n_\mathrm{s}}+1)+0.25} - 0.5 & \text{for } A_{i,1}(A_{i,n_\mathrm{s}}+1) > \varepsilon \\ \sqrt{\varepsilon+0.25} - 0.5 & \text{for } A_{i,1}(A_{i,n_\mathrm{s}}+1) \leq \varepsilon \end{cases} \tag{A.9}$$

$$Se_i = \begin{cases} \sqrt{S_{i,n_\mathrm{s}}(S_{i,1}+1)+0.25} - 0.5 & \text{for } S_{i,n_\mathrm{s}}(S_{i,1}+1) > \varepsilon \\ \sqrt{\varepsilon+0.25} - 0.5 & \text{for } S_{i,n_\mathrm{s}}(S_{i,1}+1) \leq \varepsilon. \end{cases} \tag{A.10}$$

The slope of the linear substitute function for $\phi_{\mathrm{A},i}$ and $\phi_{\mathrm{S},i}$ for $0 \leq Ae_i, Se_i \leq \varepsilon$ is assumed to be -1:

$$\phi_{\mathrm{A},i} = \begin{cases} \frac{Ae_i - 1}{Ae_i^{(n_\mathrm{s}-2)+1} - 1} & \text{for } Ae_i > \varepsilon \\ -Ae_i + 1 & \text{for } 0 \leq Ae_i \leq \varepsilon \end{cases} \tag{A.11}$$

$$\phi_{\mathrm{S},i} = \begin{cases} \frac{Se_i - 1}{Se_i^{(n_\mathrm{s}-2)+1} - 1} & \text{for } Se_i > \varepsilon \\ -Se_i + 1 & \text{for } 0 \leq Se_i \leq \varepsilon. \end{cases} \tag{A.12}$$

Implementing the cases given in eqs. (A.9) to (A.12) improves the convergence of the implemented Adapted Edmister Model significantly, especially for its application in process optimisation.

A.5 Derivation of the equations for permeate pressure drops in hollow fibres

The following derivations are made to develop an equation for the pressure drop inside the hollow fibres of a hollow fibre membrane module. It is assumed that a low pressure permeate is passed through the hollow fibres. Hagen-Poiseuille equations describe laminar flow through a pipe/hollow fibre of uniform cross section and relate the pressure drop $\frac{\partial p^\mathrm{P}}{\partial z}$ along the length of a pipe/hollow fibre L_fibres to the average flow velocity u_av in the pipe/hollow fibre. They can be derived from the Navier-Stokes equation for coordinate z in cylindrical coordinates:

$$\begin{aligned} &\rho \left(\frac{\partial u_z}{\partial t} + u_r \frac{\partial u_z}{\partial r} + \frac{u_\theta}{r} \frac{\partial u_z}{\partial \theta} + u_z \frac{\partial u_z}{\partial z} \right) = \\ &- \frac{\partial p}{\partial z} + \mu \left(\frac{1}{r} \frac{\partial}{\partial r} \left(r \frac{\partial u_z}{\partial r} \right) + \frac{1}{r^2} \frac{\partial^2 u_z}{\partial \theta^2} + \frac{\partial^2 u_z}{\partial z^2} \right) + \rho f_z \ . \end{aligned} \tag{A.13}$$

As shown in Fig. 2.9, the membrane area, the feed side and the permeate side of the membrane can be discretised into n_fv finite volumes. Within one finite volume, the following assumptions can be made for the flow inside the fibres:

- steady flow ($\frac{\partial u_z}{\partial t} = 0$),
- axisymmetric flow ($\frac{\partial}{\partial \theta} = 0$),
- zero radial and swirl velocity components ($u_r = u_\theta = 0$),
- fully developed flow ($\frac{\partial u_z}{\partial z} = 0$),
- body accelerations acting on the continuum (e.g., gravity) are negleted ($f_z = 0$).

Hence, eq. (A.13) is reduced to eq. (A.14). Eq. (A.14) is valid within one finite volume of the permeate flow on the inside of the fibres. A premise for fully developed flow is that

the molar flow is constant within the finite volume. Consequently, for the pressure drop calculation, the complete trans-membrane stream of one finite volume is accounted for at the inlet of the respective finite volume instead of being considered distributed over Δz. This provides a conservative solution for the pressure drop over the finite volume on the permeate side since maximum flow is assumed over the length Δz. Eq. (A.14) is not applied to the whole length of the hollow fibres L_{fibres} because the flow on the permeate side increases due to permeation along the fibre ($\frac{\partial u_z^{\text{P}}}{\partial z} \neq 0$).

$$\frac{\partial p^{\text{P}}}{\partial z} = \mu^{\text{P}} \frac{1}{r} \frac{\partial}{\partial r} \left(r \frac{\partial u_z^{\text{P}}}{\partial r} \right) \tag{A.14}$$

The Navier-Stokes equation for coordinate r provides $\frac{\partial p^{\text{P}}}{\partial r} = 0$, hence $p^{\text{P}} = p^{\text{P}}(x)$. Since $\frac{\partial u_z^{\text{P}}}{\partial z} = \frac{\partial u_z^{\text{P}}}{\partial \theta} = 0$ is assumed, $u_z^{\text{P}} = u_z^{\text{P}}(r)$ follows. Thus, both sides of eq. (A.14) are constant. Integration of the right side provides:

$$\mu^{\text{P}} \frac{1}{r} \frac{\partial}{\partial r} \left(r \frac{\partial u_z^{\text{P}}}{\partial r} \right) = c_1 \tag{A.15}$$

$$\frac{\partial}{\partial r} \left(r \frac{\partial u_z^{\text{P}}}{\partial r} \right) = \frac{c_1}{\mu^{\text{P}}} \cdot r \quad \text{with } \mu^{\text{P}} \neq 0 \tag{A.16}$$

$$r \frac{\partial u_z^{\text{P}}}{\partial r} = \frac{1}{2} \frac{c_1}{\mu^{\text{P}}} r^2 + c_2 \tag{A.17}$$

$$u_z^{\text{P}}(r) = \frac{1}{4} \frac{c_1}{\mu^{\text{P}}} r^2 + c_2 \ln(r) + c_3 \tag{A.18}$$

with

$$\frac{\partial p^{\text{P}}}{\partial z} = c_1 \tag{A.19}$$

$$\frac{\partial u_z^{\text{P}}}{\partial r}|_{r=0} = 0 : \quad c_2 = 0 \tag{A.20}$$

$$u_z^{\text{P}}(r = \frac{d_{\text{fibres}}}{2}) = 0 : \quad c_3 = -\frac{1}{4} \frac{1}{\mu^{\text{P}}} \frac{\partial p^{\text{P}}}{\partial z} \frac{d_{\text{fibres}}^2}{4}. \tag{A.21}$$

In the hollow fibres, laminar flow is assumed. The parabolic velocity is described by

$$u_z^{\text{P}}(r) = \frac{1}{4\mu^{\text{P}}} \frac{\partial p^{\text{P}}}{\partial z} \left(r^2 - \frac{d_{\text{fibres}}^2}{4} \right). \tag{A.22}$$

In order to relate the permeate flow velocity $u_z^{\text{P}}(r)$ along the z-axis to the permeate volume flow $\dot{V}^{\text{P}}$ in one hollow fibre, $u_z^{\text{P}}(r)$ is integrated over the fibre cross section A_{fibre}.

$$\dot{V}^{\text{P}} = \int_0^{A_{\text{fibre}}} u_z^{\text{P}}(r) \cdot 2\pi r \cdot dr = \int_0^{\frac{d_{\text{fibres}}}{2}} u_z^{\text{P}}(r) \cdot 2\pi r \cdot dr = -\frac{(d_{\text{fibres}})^4 \pi}{128\mu^{\text{P}}} \frac{\partial p^{\text{P}}}{\partial z} \tag{A.23}$$

Based on the assumption of ideal gas conditions, the permeate molar flow $\dot{N}^{\mathrm{P}}$ is related to the permeate volume flow $\dot{V}^{\mathrm{P}}$ by

$$\dot{V}^{\mathrm{P}} = \frac{\dot{N}^{\mathrm{P}} \cdot R \cdot T^{\mathrm{P}}}{p^{\mathrm{P}}}. \tag{A.24}$$

On the permeate side of one finite volume, a linear pressure profile is assumed. Hence, combination of eqs. (A.23) and (A.24) provides:

$$\frac{\partial p^{\mathrm{P}}}{\partial z} = \frac{\Delta p^{\mathrm{P}}}{\Delta z} = -\frac{128 \mu^{\mathrm{P}} R T^{\mathrm{P}}}{(d_{\mathrm{fibres}})^4 \pi} \frac{\dot{N}^{\mathrm{P}}}{p^{\mathrm{P}}}. \tag{A.25}$$

Applying eq. (A.25) to the permeate side of one finite volume ($j \leftarrow j+1$) as shown in Fig. 2.9 results in eq. (A.26). The molar flow on the permeate side of one finite volume is assumed to be constant at $N^{\mathrm{P}}_{j,\mathrm{fibres}}$. This is equivalent to applying the complete trans-membrane flow of the finite volume to the inlet of the respective finite volume. The permeate flow of the membrane module is determined from the permeate flow in each fibre and the number of fibres as given in eq. (A.27):

$$\left(p^{\mathrm{P}}_j - p^{\mathrm{P}}_{j+1}\right) \frac{n_{\mathrm{fv}}}{L_{\mathrm{fibres}}} = -\frac{128 \mu^{\mathrm{P}} R T^{\mathrm{P}}}{(d_{\mathrm{fibres}})^4 \pi} \frac{\dot{N}^{\mathrm{P}}_{j,\mathrm{fibres}}}{p^{\mathrm{P}}_{j+1}} \tag{A.26}$$

$$\dot{N}^{\mathrm{P}}_j = \dot{N}^{\mathrm{P}}_{j,\mathrm{fibres}} \cdot n_{\mathrm{fibres}} = \dot{N}^{\mathrm{P}}_{j,\mathrm{fibres}} \cdot \frac{A_{\mathrm{mem}}}{d_{\mathrm{fibres}} \pi \cdot L_{\mathrm{fibres}}}. \tag{A.27}$$

Combination of eqs. (A.26) and (A.27) provides a quadratic equation in p_{j+1}:

$$\left(p^{\mathrm{P}}_{j+1}\right)^2 - p^{\mathrm{P}}_j \cdot p^{\mathrm{P}}_{j+1} - \frac{128 \mu^{\mathrm{P}} R T^{\mathrm{P}} \dot{N}^{\mathrm{P}}_j L^2_{\mathrm{fibres}}}{(d_{\mathrm{fibres}})^3 A_{\mathrm{mem}} n_{\mathrm{fv}}} = 0 \tag{A.28}$$

$$p^{\mathrm{P}}_{j+1} = \frac{1}{2} \left(p^{\mathrm{P}}_j \pm \sqrt{(p^{\mathrm{P}}_j)^2 + 4 \cdot \frac{128 \mu^{\mathrm{P}} R T^{\mathrm{P}} \dot{N}^{\mathrm{P}}_j L^2_{\mathrm{fibres}}}{(d_{\mathrm{fibres}})^3 A_{\mathrm{mem}} n_{\mathrm{fv}}}} \right). \tag{A.29}$$

Since the fraction is positive, it follows:

$$\sqrt{(p^{\mathrm{P}}_j)^2 + 4 \cdot \frac{128 \mu^{\mathrm{P}} R T^{\mathrm{P}} \dot{N}^{\mathrm{P}}_j L^2_{\mathrm{fibres}}}{(d_{\mathrm{fibres}})^3 A_{\mathrm{mem}} n_{\mathrm{fv}}}} \geq p^{\mathrm{P}}_j. \tag{A.30}$$

To guarantee physically reasonable solutions for p_{j+1}, the equation is solved by:

$$p^{\mathrm{P}}_{j+1} = \frac{1}{2} \left(p^{\mathrm{P}}_j + \sqrt{(p^{\mathrm{P}}_j)^2 + 4 \cdot \frac{128 \mu^{\mathrm{P}} R T^{\mathrm{P}} \dot{N}^{\mathrm{P}}_j L^2_{\mathrm{fibres}}}{(d_{\mathrm{fibres}})^3 A_{\mathrm{mem}} n_{\mathrm{fv}}}} \right). \tag{A.31}$$

List of Tables

List of Figures

Bibliography

Agrawal 1996
Agrawal, R.: *Synthesis of Distillation Column Configurations for a Multicomponent Separation*. Industrial & Engineering Chemistry Research 35.4 (1996), pp. 1059–1071.

Agrawal 2003
Agrawal, R.: *Synthesis of Multicomponent Distillation Column Configurations*. AIChE Journal 49.2 (2003), pp. 379–401.

Ahsan & Hussain 2016
Ahsan, M. ; Hussain, A.: *Mathematical modelling of membrane gas separation using finite difference method*. Pacific Science Review A: Natural Science and Engineering 18.1 (2016), pp. 47–52.

Baker & Lokhandwala 2008
Baker, R. W. ; Lokhandwala, K.: *Natural Gas Processing with Membranes: an Overview*. Industrial & Engineering Chemistry Research 47.7 (2008), pp. 2109–2121.

Barbosa & Doherty 1988a
Barbosa, D. ; Doherty, M. F.: *Design and minimum-reflux calculations for double-feed multicomponent reactive distillation columns*. Chemical Engineering Science 43.9 (1988), pp. 2377–2389.

Barbosa & Doherty 1988b
Barbosa, D. ; Doherty, M. F.: *Design and minimum-reflux calculations for single-feed multicomponent reactive distillation columns*. Chemical Engineering Science 43.7 (1988), pp. 1523–1537.

Barttfeld et al. 2003
Barttfeld, M. ; Aguirre, P. A. ; Grossmann, I. E.: *Alternative representations and formulations for the economic optimization of multicomponent distillation columns*. Computers & Chemical Engineering 27.3 (2003), pp. 363–383.

Bauer & Stichlmair 1998
Bauer, M. H. ; Stichlmair, J.: *Design and economic optimization of azeotropic distillation processes using mixed-integer nonlinear programming*. Computers & Chemical Engineering 22.9 (1998), pp. 1271–1286.

Bausa et al. 1998
Bausa, J. ; von Watzdorf, J. R. ; Marquardt, W.: *Shortcut methods for nonideal multicomponent distillation: 1. Simple columns*. AIChE Journal 44.10 (1998), pp. 2181–2198.

Bekiaris et al. 1996
Bekiaris, N.; Meski, G. S.; Morari, M.: *Multiple Steady States in Heterogenous Azeotropic Distillation.* Industrial & Engineering Chemistry Research 35.1 (1996), pp. 207–227.

Bekiaris et al. 1993
Bekiaris, N.; Meski, G. S.; Radu, C. M.; Morari, M.: *Multiple Steady States in Homogenous Azeotropic Distillation.* Industrial & Engineering Chemistry Research 32.9 (1993), pp. 2023–2038.

Bekiaris & Morari 1996
Bekiaris, N.; Morari, M.: *Multiple Steady States in Distillation: ∞/∞ Predictions, Extensions, and Implications for Design, Synthesis, and Simulation.* Industrial & Engineering Chemistry Research 35.11 (1996), pp. 4264–4280.

Beneke & Linninger 2011
Beneke, D. A.; Linninger, A. A.: *Graphical Design and Analysis of Thermally Coupled Sidestream Columns Using Column Profile Maps and Temperature Collocation.* AIChE Journal 57.9 (2011), pp. 2406–2420.

Berstad et al. 2012
Berstad, D.; Neksa, P.; Anantharaman, R.: *Low-temperature CO_2 Removal from Natural Gas.* Energy Procedia 26 (2012), pp. 41–48.

Betting et al. 2004
Betting, M.; van Holten, T.; Prast, B.: "Cyclonic fluid separator with vortex generator in inlet section". US20040262218A1. Twister BV. 2004.

Betting et al. 2002
Betting, M.; van Holten, T.; van Veen, J. M. H. M.: "Supersonic separator apparatus and method". US20020194988A1. Twister BV. 2002.

Biegler 2014
Biegler, L. T.: *Recent Advances in Chemical Process Optimization.* Chemie Ingenieur Technik 86.7 (2014), pp. 943–952.

Biegler et al. 1999
Biegler, L. T.; Grossmann, I. E.; Westerberg, A. W.: *Systematic Methods of Chemical Process Design.* Prentice Hall PTR, Upper Saddle River, 1999.

Biegler et al. 2014
Biegler, L. T.; Lang, Y.; Lin, W.: *Multi-scale optimization for process systems engineering.* Computers & Chemical Engineering 60 (2014), pp. 17–30.

Biegler 2017
Biegler, L. T.: *New nonlinear programming paradigms for the future of process optimization*. AIChE Journal 63.4 (2017), pp. 1178–1193.

Bounaceur et al. 2006
Bounaceur, R.; Lape, N.; Roizard, D.; Vallieres, C.; Favre, E.: *Membrane processes for post-combustion carbon dioxide capture: A parametric study*. Energy 31.14 (2006), pp. 2556–2570.

Broomhead & Lowe 1988
Broomhead, D. S.; Lowe, D.: *Multivariable Functional Interpolation and Adaptive Networks*. Complex Systems 2 (1988), pp. 321–355.

Brouwers 1991
Brouwers, J. J. H.: "Rotational particle separator". US5073177A. Romico Hold AVV. 1991.

Brouwers 2002
Brouwers, J. J. H.: *Phase separation in centrifugal fields with emphasis on the rotational particle separator*. Experimental Thermal and Fluid Science 26.2-4 (2002), pp. 325–334.

Brüggemann & Marquardt 2004
Brüggemann, S.; Marquardt, W.: *Rapid screening of design alternatives for nonideal multiproduct distillation processes*. Computers & Chemical Engineering 29.1 (2004), pp. 165–179.

Bryson & Ho 1969
Bryson, A. E.; Ho, Y.-C.: *Applied optimal control: optimization, estimation, and control*. Blaisdell Publishing Co., Waltham, 1969.

Bubel et al. 2021
Bubel, M.; Ludl, P. O.; Seidel, T.; Asprion, N.; Bortz, M.: *A modular approach for surrogate modeling of flowsheets*. Chemie Ingenieur Technik 93.12 (2021), pp. 1987–1997.

Burger & Hasse 2013
Burger, J.; Hasse, H.: *Multi-objective optimization using reduced models in conceptual design of a fuel additive production process*. Chemical Engineering Science 99 (2013), pp. 118–126.

Caballero 2008
Caballero, J. A.: *An Algorithm for the Use of Surrogate Models in Modular Flowsheet Optimization*. AIChE Journal 54.10 (2008), pp. 2633–2650.

Caballero & Grossmann 2001
Caballero, J. A.; Grossmann, I. E.: *Generalized Disjunctive Programming Model for the Optimal Synthesis of Thermally Linked Distillation Columns.* Industrial & Engineering Chemistry Research 40.10 (2001), pp. 2260–2274.

Cardella et al. 2017
Cardella, U.; Decker, L.; Sundberg, J.; Klein, H.: *Process optimization for large-scale hydrogen liquefaction.* International Journal of Hydrogen Energy 42.17 (2017), pp. 12339–12354.

Carroll 2010
Carroll, J.: *Acid Gas Injection and Carbon Dioxide Sequestration.* Salem, Massachusetts: Scrivener Publishing, 2010.

Chen & Chen 1995
Chen, T.; Chen, H.: *Approximation Capability to Functions of Several Variables, Nonlinear Functionals, and Operators by Radial Basis Function Neural Networks.* IEEE Transactions on Neural Networks 6.4 (1995), pp. 904–910.

Chowdhury et al. 2005
Chowdhury, M. H. M.; Feng, X.; Douglas, P.; Croiset, E.: *A New Numerical Approach for a Detailed Multicomponent Gas Separation Membrane Model and AspenPlus Simulation.* Chemical Engineering & Technology 28.7 (2005), pp. 773–782.

Coker et al. 1998
Coker, D. T.; Freeman, B. D.; Fleming, G. K.: *Modeling multicomponent gas separation using hollow-fiber membrane contactors.* AIChE Journal 44.6 (1998), pp. 1289–1302.

Colmenares & Seider 1989
Colmenares, T. R.; Seider, W. D.: *Synthesis of cascade refrigeration systems integrated with chemical processes.* Computers & Chemical Engineering 13.3 (1989), pp. 247–258.

Couper et al. 2010
Couper, J. R.; Penney, W. R.; Fair, J. R.; Walas, S. M.: *Chemical Process Equipment. Selection and Design.* Butterworth-Heinemann, Burlingtion/Oxford, 2010.

Cybenko 1989
Cybenko, G.: *Approximation by Superpositions of a Sigmoidal Function.* Mathematics of Control, Signals, and Systems 2 (1989), pp. 303–314.

da Silva et al. 2017
da Silva, I. N.; Spatti, D. H.; Andrade Flauzino, R.; Bartocci Liboni, L. H.; dos Reis Alves, S. F.: *Artificial neural networks. A practical course*. Springer International Publishing, Cham, 2017.

Dowling & Biegler 2015
Dowling, A. W.; Biegler, L. T.: *A framework for efficient large scale equation-oriented flowsheet optimization*. Computers & Chemical Engineering 72 (2015), pp. 3–20.

Drud 1994
Drud, A. S.: *CONOPT - a large-scale GRG code*. ORSA Journal on Computing 6.2 (1994), pp. 107–220.

Duch & Jankowski 2001
Duch, W.; Jankowski, N.: *Transfer functions: hidden possibilities for better neural networks*. ESANN'2001 proceedings - European Symposium on Artificial Neural Networks. 2001, pp. 81–94.

Dünnebier & Pantelides 1999
Dünnebier, G.; Pantelides, C. C.: *Optimal Design of Thermally Coupled Distillation Columns*. Industrial & Engineering Chemistry Research 38.1 (1999), pp. 162–176.

Ecker et al. 2022
Ecker, A.; Klein, H.; Peschel, A.: *Systematic and efficient optimisation-based design of a process for CO_2 removal from natural gas*. Chemical Engineering Journall 445 (2022), p. 136178.

Ecker et al. 2019
Ecker, A.-M.; Thomas, I.; Häfele, M.; Wunderlich, B.; Obermeier, A.; Ferstl, J.; Klein, H.; Peschel, A.: *Development of a new column shortcut model and its application in process optimisation*. Chemical Engineering Science 196 (2019), pp. 538–551.

Edmister 1943
Edmister, W. C.: *Design for Hydrocarbon Absorption and Stripping*. Industrial and Engineering Chemistry 35.8 (1943), pp. 837–839.

Edmister 1957
Edmister, W. C.: *Absorption and Stripping-factor Functions for Distillation Calculation by Manual- and Digital-computer Methods*. A.I.Ch.E. Journal 3.2 (1957), pp. 165–171.

Eich-Soellner et al. 1997
Eich-Soellner, E. ; Lory, P. ; Burr, P. ; Kroener, A.: *Stationary and dynamic flowsheeting in the chemical engineering industry*. Surveys on Mathematics for Industry 7 (1997), pp. 1–28.

Elliot et al. 2008
Elliot, D. ; Kuo, J. C. ; Nasir, P.: *Plant Processing of Natural Gas*. The University of Texas, Petroleum Extension Service, Austin, 2008.

Eschenbacher 2016
Eschenbacher, A.: *Process Synthesis of Hybrid Separation Sequences for the Removal of CO_2 from Sour Natural Gas*. Master's Thesis. Technical University of Munich, 2016.

Fenske 1932
Fenske, M. R.: *Fractionation of Straight-Run Pennsylvania Gasoline*. Industrial and Engineering Chemistry 24.5 (1932), pp. 482–485.

Fernandes 2006
Fernandes, F. A. N.: *Optimization of Fischer-Tropsch synthesis using neural networks*. Chemical Engineering Technology 29.4 (2006), pp. 449–453.

Fidkowski et al. 1993
Fidkowski, Z. T. ; Doherty, M. F. ; Malone, M. F.: *Feasibility of Separations for Distillation of Nonideal Ternary Mixtures*. AIChE Journal 39.8 (1993), pp. 1303–1321.

Fieler et al. 2010
Fieler, E. R. ; Grave, E. J. ; Northrop, P. S. ; Yeh, N. K.: "Controlled Freeze Zone Tower". US20100018248A1. Exxon Mobil Upstream Research Company. 2010.

Funahashi 1989
Funahashi, K.-I.: *On the approximate realization of continuous mappings by neural networks*. Neural Networks 2.3 (1989), pp. 183–192.

Geankoplis 2003
Geankoplis, C. J.: *Transport processes and separation process principles (includes unit operations)*. Fourth Edition. Prentice Hall, Upper Saddle River, 2003.

Gilliland 1940
Gilliland, E. R.: *Multicomponent Rectification. Estimation of the Number of Theoretical Plates as a Function of the Reflux Ratio*. Industrial and Engineering Chemistry 32.9 (1940), pp. 1220–1223.

Graupe 2013
Graupe, D.: *Principles of Artificial Neural Networks. Advanced Series in Circuits and Systems*. Ed. by W.-K. Chen ; D. A. Mlynski. Third Edition. 7. World Scientific Publishing, Singapore, 2013.

Grossmann et al. 2005
Grossmann, I. E. ; Aguirre, P. A. ; Barttfeld, M.: *Optimal Synthesis of Complex Distillation Columns Using Rigorous Models*. Computers & Chemical Engineering 29.6 (2005), pp. 1203–1215.

Haering 2008
Haering, H.-W., ed.: *Industrial gases processing*. Wiley-VCH, 2008.

Hart & Gnanendran 2009
Hart, A. ; Gnanendran, N.: *Cryogenic CO_2 Capture in Natural Gas*. Energy Procedia 1.1 (1 2009). Part of special issue: Greenhouse Gas Control Technologies 9, pp. 697–706.

Hausen & Linde 1985
Hausen, H. ; Linde, H.: *Tieftemperaturtechnik. Erzeugung sehr tiefer Temperaturen, Gasverflüssigung und Zerlegung von Gasgemischen*. Second edition. Springer-Verlag, Berlin, Heidelberg, 1985.

Henao & Maravelias 2011
Henao, C. A. ; Maravelias, C. T.: *Surrogate-based Superstructure Opitmization Framework*. AIChE Journal 57.5 (2011), pp. 1216–1232.

Herbert et al. 1958
Herbert, W. ; Kohrt, H.-U. ; Becker, R. ; Danulat, F.: "Process for the purification of gases". US2863527A. Metallgesellschaft AG. 1958.

Hertz et al. 1991
Hertz, J. ; Krogh, A. ; Palmer, R. G.: *Introduction to the Theory of Neural Computation*. Addison-Wesley Publishing Company, Redwood City, 1991.

Holmes & Ryan 1982a
Holmes, A. S. ; Ryan, J. M.: "Cryogenic distillative separation of acid gas from methane". US4318723A. Koch Process Systems, Inc. 1982.

Holmes & Ryan 1982b
Holmes, A. S. ; Ryan, J. M.: "Distillative separation of carbon dioxide from light hydrocarbons". US4350511A. Koch Process Systems, Inc. 1982.

Holmes & Ryan 1984
Holmes, A. S.; Ryan, J. M.: "Distillative separations of gas mixtures containing methane, carbon dioxide and other components". US4462814A. Koch Process Systems, Inc. 1984.

Hopfield 1982
Hopfield, J. J.: *Neural networks and physical systems with emergent collective computational abilities*. Proceedings of the National Academy of Sciences of the United States of America 79.8 (1982), pp. 2554–2558.

Hornik et al. 1989
Hornik, K.; Stinchcombe, M.; White, H.: *Multilayer Feedforward Networks are Universal Approximators*. Neural Networks 2.5 (1989), pp. 359–366.

Horton & Franklin 1940
Horton, G.; Franklin, W. B.: *Calculation of Absorber Performance and Design. Improved Methods*. Industrial and Engineering Chemistry 32.10 (1940), pp. 1384–1388.

Hospital-Benito et al. 2021
Hospital-Benito, D.; Lemus, J.; Moya, C.; Santiago, R.; Ferro, V. R.; Palomar, J.: *Techno-economic feasibility of ionic liquids-based CO_2 chemical capture processes*. Chemical Engineering Journal Advances 407 (2021), p. 127196.

Huellen 2017
Huellen, G.: *Untersuchung künstlicher neuronaler Netze zur Erzeugung von Ersatzmodellen für Rektifikationskolonnen*. Forschungspraktikum. Technical University of Munich, 2017.

Janus & Engell 2021
Janus, T.; Engell, S.: *Iterative process design with surrogate-assisted global flowsheet optimization*. Chemie Ingenieur Technik 93.12 (2021), pp. 2019–2028.

Julka & Doherty 1990
Julka, V.; Doherty, M. F.: *Geometric Behavior and Minimum Flows for Nonideal Multicomponent Distillation*. Chemical Engineering Science 45.7 (1990), pp. 1801–1822.

Kaldis et al. 2000
Kaldis, S. P.; Kapantaidakis, G. C.; Sakellaropoulos, G. P.: *Simulation of multicomponent gas separation in a hollow fiber membrane by orthogonal collocation – hydrogen recovery from refinery gas*. Journal of Membrane Science 173.1 (2000), pp. 61–71.

Kamath et al. 2010
Kamath, R. S.; Grossmann, I. E.; Biegler, L. T.: *Aggregate models based on improved group methods for simulation and optimization of distillation systems.* Computers & Chemical Engineering 34.8 (2010), pp. 1312–1319.

Karuppiah et al. 2008
Karuppiah, R.; Peschel, A.; Grossmann, I. E.; Martín, M.; Martinson, W.; Zullo, L.: *Energy Optimization for the Design of Corn-Based Ethanol Plants.* AIChE Journal 54.6 (2008), pp. 1499–1525.

Karush 1939
Karush, W.: *Minima of functions of several variables with inequalities as side conditions.* Master's Thesis. University of Chicago, Department of Mathematics, 1939.

Kawajir & Laird 2015
Kawajir, Y.; Laird, C.: *Introduction to IPOPT: a tutorial for downloading, installing, and using IPOPT.* Ed. by S. Vigerske; A. Wächter. 2015. url: `https://projects.coin-or.org/Ipopt/browser/stable/3.11/Ipopt/doc/documentation.pdf?format=raw`.

Kelley et al. 2011
Kelley, B. T.; Valencia, J. A.; Northrop, P. S.; Mart, C. J.: *Controlled Freeze Zone^{TM} for developing sour gas reserves.* Energy Procedia 4 (2011). Part of special issue: 10th International Conference on Greenhouse Gas Control Technologies, pp. 824–829.

Kender et al. 2022
Kender, R.; Stops, L.; Wunderlich, B.; Pottmann, M.; Ecker, A.-M.; Rehfeldt, S.; Klein, H.: *Development of a Model Reduction Approach for a Pressure-Driven Column Model Using Digital Twin Technology.* American Institute of Chemical Engineers (AIChE) 2022 Spring Meeting and 18th Global Congress on Process Safety. San Antonio, Texas, 2022.

Kidnay & Parrish 2006
Kidnay, A. J.; Parrish, W. R.: *Fundamentals of Natural Gas Processing.* CRC Press, Taylor & Francis Group, Boca Raton, 2006.

Koehler et al. 1991
Koehler, J.; Aguirre, P.; Blass, E.: *Minimum Reflux Calculations for Nonideal Mixtures using the Reversible Distillation Model.* Chemical Engineering Science 46.12 (1991), pp. 3007–3021.

Kohl & Miller 1960a
Kohl, A. L.; Miller, F. E.: "Organic carbonate process for carbon dioxide". US2926751A. The Fluor Corporation, Ltd. 1960.

Kohl & Miller 1960b
Kohl, A. L.; Miller, F. E.: "Process for carbon dioxide absorption". US2926753A. The Fluor Corporation, Ltd. 1960.

Kohl & Nielsen 1997
Kohl, A. L.; Nielsen, R. B.: *Gas Purification*. Gulf Publishing Company, Houston, 1997.

Kohonen 1982
Kohonen, T.: *Self-organized formation of topologically correct feature maps*. Biological Cybernetics 43.1 (1982), pp. 59–69.

Kossack et al. 2006
Kossack, S.; Kraemer, K.; Marquardt, W.: *Efficient optimization based design of distillation columns for homogeneous azetropic mixtures*. Industrial & Engineering Chemistry Research 45.25 (2006), pp. 8492–8502.

Kovvali et al. 1994
Kovvali, A. S.; Vemury, S.; Admassu, W.: *Modeling of Multicomponent Countercurrent Gas Permeators*. Industrial & Engineering Chemistry Research 33.4 (1994), pp. 896–903.

Kraemer 2012
Kraemer, K.: *Optimization-based Synthesis of Hybrid Separation Processes*. PhD thesis. RWTH Aachen, 2012.

Kraemer et al. 2009
Kraemer, K.; Kossack, S.; Marquardt, W.: *Efficient optimization-based design of distillation processes for homogenous azeotropic mixtures*. Industrial & Engineering Chemistry Research 48.14 (2009), pp. 6749–6764.

Kremser 1930
Kremser, A.: *Theoretical Analysis of Absorption Process*. National Petroleum News 22.21 (1930), pp. 43–49.

Kruber et al. 2021
Kruber, K. F.; Grueters, T.; Skiborowski, M.: *Advanced hybrid optimization methods for the design of complex separation processes*. Computers & Chemical Engineering 147 (2021), p. 107257.

Kuhn & Tucker 1951
Kuhn, H. W.; Tucker, A. W.: *Nonlinear Programming*. Proceedings of the Second Berkeley Symposium on Mathematical Statistics and Probability 2 (1951), pp. 481–492.

Landes & Bell 1960
Landes, S. H.; Bell, F. W.: *Absorber Design – Fast Yet Rigorous*. Petroleum Refiner 39.6 (1960), pp. 201–206.

Langè et al. 2015
Langè, S.; Pellegrini, L. A.; Vergani, P.; Savio, M. L.: *Energy and Economic Analysis of a New Low-Temperature Distillation Process for the Upgrading of High-CO_2 Content Natural Gas Streams*. Industrial & Engineering Chemistry Research 54.40 (2015), pp. 9770–9782.

Lapedes & Farber 1988
Lapedes, A.; Farber, R.: *How Neural Networks Work*. Evolution, Learning and Cognition. Ed. by Y. C. Lee. World Scientific Publishing, Singapore, 1988, pp. 331–346.

Lasdon & Waren 1981
Lasdon, L.; Waren, A.: *GRG2: an all FORTRAN general purpose nonlinear optimizer*. ACM SIGMAP Bulletin 30 (1981), pp. 10–11.

LeCun 1985
LeCun, Y.: *Learning Processes in an Asymmetric Threshold Network*. Proceedings of Cognitiva 85. 1985, pp. 599–604.

LeCun 1986
LeCun, Y.: *Learning process in an asymmetric threshold network*. Disordered systems and biological organization. Ed. by E. Bienenstock; F. Fogelman; G. Weisbuch. Springer-Verlag, Les Houches, 1986, pp. 233–240.

LeCun 1988
LeCun, Y.: *A Theoretical Framework for Back-Propagation*. Proceedings of the 1988 Connectionist Models Summer School. Ed. by D. Touretzky; G. Hinton; T. Sejnowski. Carnegie-Mellon University. 1988.

LeCun et al. 1998
LeCun, Y. A.; Bottou, L.; Orr, G. B.; Mueller, K.-R.: *Efficient BackProp*. Neural networks: tricks of the trade. Ed. by G. Montavon; G. B. Orr; K.-R. Mueller. Second Edition. Springer-Verlag, Berlin, Heidelberg, 1998. Chap. *Efficient BackProp*, pp. 10–48.

Lee et al. 2018
Lee, S.; Binns, M.; Kim, J.: *Automated process design and optimization of membrane-based CO_2 capture for a coal-based power plant*. Journal of Membrane Science 563 (2018), pp. 820–834.

Leimbrink et al. 2015
Leimbrink, M.; Kunze, A.-K.; Hellmann, D.; Górak, A.; Skiborowski, M.: *Conceptual Design of Post-Combustion CO2 Capture Processes - Packed Columns and Membrane Technologies. 12th International Symposium on Process Systems Engineering and 25th European Symposium on Computer Aided Process Engineering*. Ed. by K. V. Gernaey; J. K. Huusom; R. Gani. 37. Computer Aided Chemical Engineering. Elsevier, 2015, pp. 1223–1228.

Levy et al. 1985
Levy, S. G.; Dongen, D. B. V.; Doherty, M. F.: *Design and Synthesis of Homogeneous Azeotropic Distillations. 2. Minimum Reflux Calculations for Nonideal and Azeotropic Columns*. Industrial & Engineering Chemistry Fundamentals 24.4 (1985), pp. 483–474.

Linninger 2009
Linninger, A.: *Industry-wide energy saving by complex separation networks*. Computers & Chemical Engineering 33 (2009), pp. 2018–2027.

Lucia et al. 2008
Lucia, A.; Amale, A.; Taylor, R.: *Distillation pinch points and more*. Computers & Chemical Engineering 32 (2008), pp. 1342–1364.

Maqsood et al. 2014
Maqsood, K.; Mullick, A.; Ali, A.; Kargupta, K.; Ganguly, S.: *Cryogenic carbon dioxide separation from natural gas: a review based on conventional and novel emerging technologies*. Reviews in Chemical Engineering 30.5 (2014), pp. 453–477.

Marquardt et al. 2008
Marquardt, W.; Kossack, S.; Kraemer, K.: *A Framework for the Systematic Design of Hybrid Separation Processes*. Chinese Journal of Chemical Engineering 16.3 (2008), pp. 333–342.

Mehrotra et al. 2000
Mehrotra, K.; Mohan, C. K.; Ranka, S.: *Elements of Artificial Neural Networks*. Second Edition. MIT Press, Cambridge, 2000.

Melin & Rautenbach 2004
Melin, T.; Rautenbach, R.: *Membranverfahren. Grundlagen der Modul- und Anlagenauslegung*. 2nd edition. Springer-Verlag, Berlin, Heidelberg, 2004.

Mitchell et al. 2018
Mitchell, M.; Muftakhidinov, B.; Winchen, T.; Jedrzejewski-Szmek, Z.; Badger, T. G.; badshah400: *Engauge Digitizer Software*. Feb. 2018. doi: https://zenodo.org/badge/latestdoi/26443394. url: http://markummitchell.github.io/engauge-digitizer.

Ohlrogge & Ebert 2006
Ohlrogge, K.; Ebert, K.: *Membranen. Grundlagen, Verfahren und industrielle Anwendungen*. Wiley-VCH Verlag, Weinheim, 2006.

Owens & Maddox 1968
Owens, W. R.; Maddox, R. N.: *Short-cut Absorber Calculations*. Industrial and Engineering Chemistry 60.12 (1968), pp. 14–28.

Palmer & Realff 2002
Palmer, K.; Realff, M.: *Metamodeling Approach to Optimization of Steady-State Flowsheet Simulations. Model Generation*. Chemical Engineering Research and Design 80.7 (2002), pp. 760–772.

Pan 1986
Pan, C. Y.: *Gas Separation by High-Flux, Asymmetric Hollow-Fiber Membrane*. AIChE Journal 32.12 (1986), pp. 2020–2027.

Papalexandri & Pistikopoulos 1996
Papalexandri, K. P.; Pistikopoulos, E. N.: *Generalized modular representation framework for process synthesis*. AIChE Journal 42.4 (1996), pp. 1010–1032.

Parker 1985
Parker, D. B.: *Learning Logic: Casting the Cortex of the Human Brain in Silicon*. Sloan School of Management, MIT, Cambridge, 1985.

Peer et al. 2008
Peer, M.; Mahdyarfar, M.; Mohammadi, T.: *Evaluation of a mathematical model using experimental data and artificial neural network for prediction of gas separation*. Journal of Natural Gas Chemistry 17.2 (2008), pp. 135–141.

Pellegrini 2015
Pellegrini, L. A.: "Process for the removal of CO_2 from acid gas". US20150276308A1. Stamicarbon B.V. acting under the name of MT Innovation Center. 2015.

Peschel et al. 2012
Peschel, A.; Jörke, A.; Sundmacher, K.; Freund, H.: *Optimal reaction concept and plant wide optimization of the ethylene oxide process*. Chemical Engineering Journal 207-208 (2012), pp. 656–674.

Peters et al. 2011
Peters, L.; Hussain, A.; Follmann, M.; Melin, T.; Hägg, M.: *CO_2 removal from natural gas by employing amine absorption and membrane technology – a technical and economical analysis*. Chemical Engineering Journal 172.2-3 (2011), pp. 952–960.

Petlyuk & Aventyan 1971
Petlyuk, F. B.; Aventyan, V. S.: *Investigation of the rectification of three-component mixtures with infinite reflux*. Theoretical Foundations of Chemical Engineering 5.4 (1971), pp. 499–507.

Pettersen & Lien 1994
Pettersen, T.; Lien, K. M.: *A new robust design model for gas separating membrane modules, based on analogy with counter-current heat exchangers*. Computers & Chemical Engineering 18.5 (1994), pp. 427–439.

Pirrung et al. 2017
Pirrung, S. M.; van der Wielen, L. A. M.; van Beckhoven, R. F. W. C.; van de Sandt, E. J. A. X.; Eppink, M. H. M.; Ottens, M.: *Optimization of Biopharmaceutical Downstream Processes Supported by Mechanistic Models and Artifical Neural Networks*. Biotechnology Progress 33.3 (2017), pp. 696–707.

Plaut & Hinton 1987
Plaut, D. C.; Hinton, G. E.: *Learning sets of filters using backpropagation*. Computer Speech & Language 2.1 (1987), pp. 35–61.

Poellmann et al. 1994
Poellmann, P.; Glanz, S.; Blass, E.: *Calculating Minimum Reflux of Nonideal Multicomponent Distillation using Eigenvalue Theory*. Computers & Chemical Engineering 18, Supplement 1 (1994), S49–S53.

Potts & Thomas 1992
Potts, W. A.; Thomas, E. R.: "Method for separating a multi-component feed stream using distillation and controlled freezing zone". US5120338A. Exxon Production Research Company. 1992.

Prast et al. 2012
Prast, B.; Langerak, J. A. C.; Betting, M.; Willink, C. A. T.: "Method of removing carbon dioxide from a fluid stream and fluid separation assembly". US20120017638A1. Twister BV. 2012.

Prast et al. 2013
Prast, B.; Langerak, J. A. C.; Betting, M.; Willink, C. A. T.: "Method of removing and solidifying carbon dioxide from a fluid stream and fluid separation assembly". US8475572B2. Twister BV. 2013.

Proios et al. 2005
Proios, P.; Goula, N. F.; Pistikopoulos, E. N.: *Generalized modular framework for the synthesis of heat integrated distillation column sequences*. Chemical Engineering Science 60.17 (2005), pp. 4678–4701.

Quirante et al. 2015
Quirante, N.; Javaloyes, J.; Caballero, J. A.: *Rigorous Design of Distillation Columns Using Surrogate Models Based on Kriging Interpolation*. AIChE Journal 61.7 (2015), pp. 2169–2187.

Raman & Grossmann 1994
Raman, R.; Grossmann, I. E.: *Modelling and computational techniques for logic based integer programming*. Computers & Chemical Engineering 18.7 (1994), pp. 563–578.

Ranke & Weiss 1982
Ranke, G.; Weiss, H.: "Separation of gaseous components from a gaseous mixture by physical scrubbing". US4324567A. Linde GmbH. 1982.

Riedmiller 1994
Riedmiller, M.: *Advanced supervised learning in multi-layer perceptrons – From backpropagation to adaptive learning algorithms*. Computer Standards & Interfaces 16 (3 1994), pp. 265–278.

Rooks et al. 1996
Rooks, R. E.; Malone, M. F.; Doherty, M. F.: *A Geometric Design Method for Side-Stream Distillation Columns*. Industrial & Engineering Chemistry Research 35.10 (1996), pp. 3653–3664.

Rosenblatt 1961
Rosenblatt, F.: *Principles of Neurodynamics. Perceptrons and the Theory of Brain Mechanisms*. Cornell Aeronautical Laboratory, Inc., Cornell University, New York, 1961.

Rufford et al. 2012
Rufford, T. E.; Smart, S.; Watson, G. C. Y.; Graham, B. F.; Boxall, J.; Diniz da Costa, J. C.; May, E. F.: *The removal of CO_2 and N_2 from natural gas: a review of conventional and emerging process technologies.* Journal of Petroleum Science and Engineering 94-95 (2012), pp. 123–154.

Ruiz et al. 2010
Ruiz, G. J.; Kim, S. B.; Moon, J.; Zhang, L.; Linninger, A. A.: *Design and optimization of energy efficient complex separation networks.* Computers & Chemical Engineering 34.9 (2010), pp. 1556–1563.

Rumelhart et al. 1985
Rumelhart, D. E.; Hinton, G. E.; Williams, R. J.: *Learning internal representations by error propagation.* Parallel distributed processing: explorations in the microstructure of cognitio. Ed. by D. E. Rumelhart; J. L. McClelland. 1: Foundations. Bradford Books / MIT Press, Cambridge, 1985.

Ryll et al. 2012
Ryll, O.; Blagov, S.; Hasse, H.: *∞/∞-Analysis of homogeneous distillation processes.* Chemical Engineering Science 84 (2012), pp. 315–332.

Ryll et al. 2014
Ryll, O.; Blagov, S.; Hasse, H.: *Thermodynamic analysis of reaction-distillation processes based on piecewise linear models.* Chemical Engineering Science 109 (2014), pp. 284–295.

Safari et al. 2009
Safari, M.; Ghanizadeh, A.; Montazer-Rahmati, M. M.: *Optimization of membrane-based CO_2-removal from natural gas using simple models considering both pressure and temperature effects.* International Journal of Greenhouse Gas Control 3 (1 2009), pp. 3–10.

Salazar Duarte et al. 2016
Salazar Duarte, G.; Schürer, B.; Voss, C.; Bathen, D.: *Modeling and simulation of a tube bundle adsorber for the capture of CO_2 from flue gases.* Chemie Ingenieur Technik 88.3 (2016), pp. 336–345.

Sargent & Gaminibandara 1976
Sargent, R. W. H.; Gaminibandara, K.: *Optimum design of plate distillation columns.* Optimisation in action. Ed. by L. W. C. Dixon. Academic Press, London, 1976, pp. 267–314.

Schaul et al. 2010
Schaul, T.; Bayer, J.; Wierstra, D.; Sun, Y.; Felder, M.; Sehnke, F.; Rückstiess, T.; Schmidhuber, J.: *PyBrain*. Journal of Machine Learning Research 11 (2010), pp. 743–746.

Schöneberger et al. 2021
Schöneberger, J. C.; Aker, B.; Fricke, A.: *Explaining and integrating machine learning models with rigorous simulation*. Chemie Ingenieur Technik 93.12 (2021), pp. 1998–2009.

Schürer & Salazar Duarte 2015
Schürer, B.; Salazar Duarte, G.: "Verfahren zur Abscheidung einer Komponente eines Gasgemischs unter Verwendung einer Temperaturwechseladsorption". EP2902087A1. Linde AG. 2015.

Schweidtmann & Mitsos 2019
Schweidtmann, A. M.; Mitsos, A.: *Deterministic global optimization with artifical neural networks embedded*. Journal of Optimization Theory and Applications 180 (2019), pp. 925–948.

Seider et al. 2004
Seider, W. D.; Seader, J. D.; Lewin, D. R.: *Product & Process Design Principles*. John Wiley & Sons, Inc., New York, 2004.

Senftl 2016
Senftl, A.: *Superstrukturoptimierung bei der CO_2-Abtrennung bei Oxyfuel-Prozessen*. Bachelor's Thesis. Technical University of Munich, 2016.

Shelton & Grossmann 1985
Shelton, M. R.; Grossmann, I. E.: *A shortcut procedure for refrigeration systems*. Computers & Chemical Engineering 9.6 (1985), pp. 615–619.

Shelton & Grossmann 1986
Shelton, M. R.; Grossmann, I. E.: *Optimal synthesis of integrated refrigeration systems - I: Mixed integer programming model*. Computers & Chemical Engineering 10.5 (1986), pp. 445–459.

Shindo et al. 1985
Shindo, Y.; Hakuta, T.; Yoshitome, H.: *Calculation Methods for Multicomponent Gas Separation by Permeation*. Separation Science and Technology 5&6 (1985), pp. 445–459.

Smith & Linnhoff 1988
Smith, R.; Linnhoff, B.: *The design of separators in the context of overall processes*. Chemical Engineering Research and Design 66.3 (1988), pp. 195–228.

Sounders & Brown 1932
Sounders, M.; Brown, G. G.: *IV Fundamental Design of Absorbing and Stripping Columns for Complex Vapors*. Industrial and Engineering Chemistry 24.5 (1932), pp. 519–522.

Stookey 2006
Stookey, D. J.: *Gas-separation membrane applications*. Membrane technology in the chemical industry. Ed. by S. P. Nunes; K. Peinemann. Wiley VCH, Weinheim, 2006, pp. 119–150.

Sundberg et al. 2017
Sundberg, J.; Rehfeldt, S.; Peschel, A.; Klein, H.: *Prozessoptimierung am Beispiel der Methanolsynthese mithilfe verschiedener lokaler Optimierungsalgorithmen*. Chemie Ingenieur Technik 89.5 (2017), pp. 675–685.

Tessendorf et al. 1999
Tessendorf, S.; Gani, R.; Michelsen, M. L.: *Modeling, simulation and optimization of membrane-based gas separation systems*. Chemical Engineering Science 54 (7 1999), pp. 943–955.

Thomas & Denton 1988
Thomas, E.; Denton, R.: *Conceptual studies for CO_2/natural gas separation using the controlled freeze zone process (CFZ)*. Gas Separation & Purification 2 (2 1988), pp. 84–89.

Thomas 2011
Thomas, I.: *A Process Unit Modeling Framework within a Heterogeneous Simulation Environment. 21st European Symposium on Computer Aided Process Engineering*. Ed. by E. N. Pistikopoulos; M. C. Georgiadis; A. C. Kokossis. 29. Computer Aided Chemical Engineering. Elsevier, 2011, pp. 31–35.

Thundyil & Koros 1997
Thundyil, M. J.; Koros, W. J.: *Mathematical modeling of gas separation permeators - for radial crossflow, countercurrent, and cocurrent hollow fiber membrane modules*. Journal of Membrane Science 125.2 (1997), pp. 275–291.

Underwood 1932
Underwood, A. J. V.: *The Theory and Practice of Testing Stills*. Transactions. Institution of Chemical Engineers 10 (1932), pp. 112–158.

Underwood 1946a
Underwood, A. J. V.: *Fractional distillation of multi-component mixutres - Calculation of minimum reflux ratio.* Journal of the Institute of Petroleum 32 (1946), pp. 614–626.

Underwood 1946b
Underwood, A. J. V.: *Fractional distillation of ternary mixtures. Part II.* Journal of the Institute of Petroleum 32 (1946), pp. 598–613.

Vaidyaraman & Maranas 1999
Vaidyaraman, S.; Maranas, C. D.: *Optimal Synthesis of Refrigeration Cycles and Selection of Refrigerants.* AIChE Journal 45.5 (1999), pp. 997–1017.

Valencia & Denton 1985
Valencia, J. A.; Denton, R. D.: "Method and Apparatus for Separating Carbon Dioxide and Other Acid Gases from Methane by the Use of Distillation and a Controlled Freezing Zone, Patent US 4533372". US4533372A. Exxon Production Research Company. 1985.

Van Dongen & Doherty 1985
Van Dongen, D. B.; Doherty, M. F.: *Design and synthesis of homogeneous azeotropic distillations. 1. Problem formulation for a single column.* Industrial & Engineering Chemistry Fundamentals 24.4 (1985), pp. 454–463.

van Veen & Betting 2001
van Veen, J. W. H. M.; Betting, M.: "Removing solids from a fluid". US6280502B1. Twister BV. 2001.

Villarrubia et al. 2018
Villarrubia, G.; De Paz, J. F.; Chamoso, P.; De la Prieta, F.: *Artificial neural networks used in optimization problems.* Neurocomputing 272 (2018), pp. 10–16.

Visawanathan & Grossmann 1993a
Visawanathan, J.; Grossmann, I. E.: *An alternative MINLP model for finding the number of trays required for a specified separation objective.* Computers & Chemical Engineering 17.9 (1993), pp. 949–955.

Visawanathan & Grossmann 1993b
Visawanathan, J.; Grossmann, I. E.: *Optimal Feed Locations and Number of Trays for Distillation Columns with Multiple Feeds.* Industrial & Engineering Chemistry Research 32.11 (1993), pp. 2942–2949.

von Stosch et al. 2014
von Stosch, M.; Oliveira, R.; Peres, J.; de Azevedo, S. F.: *Hybrid semi-parametric modeling in process systems engineering: past, present, and future*. Computers & Chemical Engineering 60 (2014), pp. 86–101.

von Watzdorf et al. 1999
von Watzdorf, R.; Bausa, J.; Marquardt, W.: *Shortcut methods for non-ideal multicomponent distillation: 2. complex columns*. AIChE Journal 45.8 (1999), pp. 1615–1628.

Werbos 1974
Werbos, P. J.: *Beyond Regression: New Tools for Prediction and Analysis in the Behavioral Sciences*. PhD thesis. Harvard University, Cambridge, 1974.

Widrow & Hoff 1960
Widrow, B.; Hoff, M. E.: *Adaptive Switching Circuits*. Stanford Electronics Laboratories, Stanford University, 1960.

Willems et al. 2010
Willems, G. P.; Golombok, M.; Tesselaar, G.; Brouwers, J. J. H.: *Condensed Rotational Separation of CO_2 from Natural Gas*. AIChE Journal 56.1 (2010), pp. 150–159.

Windmeier & Barron 2013
Windmeier, C.; Barron, R. F.: *Cryogenic Technology*. Ullmann's Encyclopedia of Industrial Chemistry. 2013, pp. 1–71.

Wu & Zhu 2002
Wu, G.; Zhu, X. X.: *Design of Integrated Refrigeration Systems*. Industrial & Engineering Chemistry Research 41.3 (2002), pp. 553–571.

Yeomans & Grossmann 1999
Yeomans, H.; Grossmann, I. E.: *A systematic modeling framework of superstructure optimization in process synthesis*. Computers and Chemical Engineering 23.6 (1999), pp. 709–731.

Yeomans & Grossmann 2000a
Yeomans, H.; Grossmann, I. E.: *Disjunctive Programming Models for the Optimal Design of Distillation Columns and Separation Sequences*. Industrial & Engineering Chemistry Research 39.6 (2000), pp. 1637–1648.

Yeomans & Grossmann 2000b
Yeomans, H. ; Grossmann, I. E.: *Optimal Design of Complex Distillation Columns Using Rigorous Tray-by-Tray Disjunctive Programming Models*. Industrial & Engineering Chemistry Research 39.11 (2000), pp. 4326–4335.

Zhang & Xu 2011
Zhang, J. ; Xu, Q.: *Cascade refrigeration system synthesis based on exergy analysis*. Computers & Chemical Engineering 35.9 (2011), pp. 1901–1914.

Zhang & Linninger 2004
Zhang, L. ; Linninger, A. A.: *Temperature Collocation Algorithm for Fast and Robust Distillation Design*. Industrial & Engineering Chemistry Research 43.12 (2004), pp. 3163–3182.